Studies on the Late Rhodopsin Activation Steps

Dissertation

zur Erlangung des akademischen Grades

doctor rerum naturalium
(Dr. rer. nat.)

im Fach Biophysik

eingereicht an der

Mathematisch-Naturwissenschaftlichen Fakultät I

der Humboldt-Universität zu Berlin

von

Dipl.-Biophys. Bernhard Knierim
geboren in Bad Hersfeld am 1.12.1978

Präsident der Humboldt-Universität zu Berlin
Prof. Dr. Christoph Markschies

Dekan/Dekanin der Mathematisch-Naturwissenschaftlichen Fakultät I
Prof. Dr. Christian Limberg

GutachterInnen:
1. Prof. Dr. Klaus-Peter Hofmann
2. Prof. Dr. Andreas Herrmann
3. Prof. Dr. Annette Beck-Sickinger

Tag der mündlichen Prüfung: 12.3.2008

8.10.2007

Abstract in German

Rhodopsin ist der Photorezeptor der Stäbchenzellen in der Retina von Vertebraten und wird als Prototyp für die gesamte Gruppe der GPCRs (= G-Protein gekoppelte Rezeptoren) beforscht, deren gemeinsames Merkmal der Aufbau aus sieben transmembranen Helices ist. Trifft ein Photon auf das Protein, so wird der über eine Schiffbase kovalent gebundene Chromophor Retinal von seiner 11-*cis*- in die All-*trans*-Konfiguration isomerisiert und setzt infolgedessen den Aktivierungsprozess in Gang. Dieser mündet in der aktiven Rezeptorkonformation, die das G-Protein Transducin aktivieren kann und dadurch eine Kaskade von weiteren Aktivierungsschritten einleitet, die letztlich ein Nervensignal verursachen.

Das Ziel dieser Arbeit war die Aufklärung der späten Aktivierungsschritte und ihrer Ursache-Wirkungs-Beziehungen. Zu diesem Zweck wurden Blitzlichtphotolyse, Elektronenspinresonanz (EPR) mit ortsgerichteter Mutagenese und Spinlabeling (SDSL), UV/vis-Spektroskopie, FTIR-Spektroskopie und Fluoreszenzspektroskopie angewandt. Kinetische Messungen wurden unter identischen Bedingungen durchgeführt, um die Abfolge der mit den unterschiedlichen Techniken zugänglichen Aktivierungsschritte aufzuklären.

Nach der Bildung des absorptionsspektroskopisch definierten Metarhodopsin-II-Zustands (Meta-II) bewegt sich die Helix TM6 in einem späteren Schritt als ganzes nach außen und markiert damit den Übergang von Meta-IIa zu Meta-IIb. Dadurch wird die in der ganzen Rezeptorgruppe konservierte und bis dahin in der Membran verborgene D(E)RY-Region für das Umgebungsmedium zugänglich und nimmt ohne Zeitverzögerung ein Proton auf, wodurch der Meta-IIb·H^+-Zustand gebildet wird.

Das in der Rezeptorgruppe hochkonservierte D(E)RY-Motiv spielt eine doppelte Rolle – sowohl bei der Stabilisierung der TM6-Position als auch bei der Aktivierung des Transducins. Die Stabilisierung erfolgt insbesondere durch eine Wasserstoffbrücke zwischen dem D(E)RY-Motiv in Helix TM3 und dem Residuum Glu^{247} in Helix TM6, die wiederum durch eine Salzbrücke zwischen Glu^{134} und Arg^{135} im D(E)RY-Motiv ermöglicht wird. In der nativen Membranumgebung scheint im inaktiven Zustand ein Phosphatidylserinmolekül an das Motiv zu binden und könnte so ebenfalls zur Stabilisierung beitragen. Ein weiteres konserviertes und für die Aktivierung zentrales Motiv, das NPxxY$(x)_{5,6}$F-Motiv am Übergang zwischen der Helix TM7 und der zur Membranoberfläche parallelen Helix H8, ist mit dem D(E)RY-Motiv schwach verbunden. Auch in dieser Region findet eine strukturelle Änderung statt, allerdings mit einer von TM6 unabhängigen Kinetik.

Die verfügbaren Daten sprechen dafür, dass das D(E)RY-Motiv bei der Aktivierung des Transducins sowohl die γ- als auch die α-Untereinheit desselben bindet. Die Bindung von zu Transducin-Abschnitten analogen Peptiden kann dann erfolgen, wenn die Helix TM6 im nach außen bewegten Zustand ist, und führt zur Abgabe von bis zu zwei Protonen vom aktivierten Rhodopsin. Sowohl das D(E)RY- und das NPxxY$(x)_{5,6}$F-Motiv als auch die beiden Zustände Meta-IIb und Meta-IIb·H^+ könnten relevant für den sequenziellen Transducin-Aktivierungsmechanismus sein.

Abstract in English

Rhodopsin is the photoreceptor in the rod cells of the vertebrate retina. It is considered as a prototype of the whole group of GPCRs (= G protein couplec receptors), whose common feature is the composition of seven transmembrane helices. Upon absorption of a photon the chromophore retinal, which is covalently bound through a Schiff base, is isomerized from its 11-*cis* into the all-*trans* configuration. This initiates the activation process and finally results in the active receptor conformation which is capable of activating the G protein transducin and thereby triggers a cascade of further activation steps which finally cause a nerve signal.

The aim of this work was the clarification of the late activation steps and their cause-and-effect chain. For this purpose flash photolysis, electron paramagnetic resonance (EPR) with site-directed mutagenesis and spin labeling (SDSL), UV/vis spectroscopy, FTIR spectroscopy and fluorescence spectroscopy were applied. Kinetic measurements were executed under identical conditions in order to elucidate the sequence of activation steps, which are accessible with the different techniques.

After formation of the spectroscopically defined Metarhodopsin-II (Meta-II) state helix TM6 moves outward as a rigid body, thereby marking the transition from Meta-IIa to Meta-IIb. Therefore the D(E)RY region, which is conserved throughout the whole receptor group and until then buried in the membrane, gets accessible to the surrounding solution. It consequently takes up a proton without delay, thus forming the Meta-IIb·H^+ state.

The D(E)RY motif, which is highly conserved in this group of receptors, plays a double role – both for stabilization of the inward TM6 state and for activation of transducin. The stabilization especially results from a hydrogen bond between the D(E)RY motif in helix TM3 and the residue Glu^{247} in helix TM6. This bond is itself enabled by a salt bridge between Glu^{134} and Arg^{135} in the D(E)RY motif. In the native membrane environment a phostphatidylserine molecule appears to bind to the motif in the inactive state and could thus also be involved in stabilization. A further conserved motif which is central for activation is the NPxxY$(x)_{5,6}$F motif at the interface between helix TM7 and helix H8, which is a helix parallel to the membrane. It is weakly connected to the D(E)RY motif. In this region another structural transition occurs, though with kinetics which are independent of TM6.

Available data argue for the D(E)RY motif binding both the γ and the α subunit of transducin during activation of the latter. The binding of peptides which are analogous to sections of transducin is possible when helix TM6 is in the outward position. It causes the release of up to two protons from the activated rhodopsin. Both the D(E)RY motif and the NPxxY$(x)_{5,6}$F motif as well as both the states Meta-IIb and Meta-IIb·H^+ are potentially relevant for the sequential transducin activation mechanism.

Contents

List of figures

If figures are not prepared by the author, the sources are mentioned in the underline. Molecular graphics are – except for Fig. 89 – prepared with the software PyMol 0.99 (DeLano Scientific) using the PDB data set 1GZM. All graphs are prepared with the software Microcal Origin 6.0. For schemes the software Micrografx Designer 2.0 has been used.

List of tables

Abbreviations

9-dm	9-demethyl (see Fig. 21)
Abu	amino butyric acid
ATP	adenosinetriphosphate
β_2-AR	β_2-adrenoreceptor (a GPCR)
Batho	bathorhodopsin
BCP	bromocresol purple (see Fig. 6)
BTP	bis-tris-propane
Ca^{2+}	calcium
cGMP	cyclic guanosinemonophosphate
CR	cresol red (see Fig. 7)
CW	continuous wave
D(E)RY	conserved motif at the cytoplasmic end of TM3 in class I GPCRs
DTT	dithiothreitol (see Fig. 27)
DM	n-dodecyl-β-D-maltoside (detergent, see Fig. 29)
E_A	activation energy
EDC	1-Ethyl-3-[3-dimethylaminopropyl]carbodiimide hydrochloride
EDTA	ethylendiamine-tetraacetic acid
EPR	electron paramagnetic resonance
ERY	D(E)RY motif in rhodopsin, consisting of Glu^{134}, Arg^{135} and Tyr^{136}
ESR	electron spin resonance (different expression for EPR)
far	farnesyl
FTIR	Fourier-transform infrared spectroscopy
GDP	guanosinediphosphate
GMP	guanosinemonophosphate
GPCR	G-protein coupled receptor
G_t	transducin (G-protein of the vertebrate rod cell)
GTP	guanosinetriphosphate
HA	high affinity
HPLC	high performance liquid chromatography
IMPB	Institute for Medical Physics and Biophysics at Charité Berlin
IR	infrared
Lumi	lumirhodopsin
Meta-I	metarhodopsin I
Meta-II (a/b)	metarhodopsin II (a/b)
Meta-III	metarhodopsin III
MOPS	3-(N-Morpholino)-propanesulfonic acid (buffer)
MTSSL	(1-oxyl-2,2,5,5 tetramethylpyrroline-3-methyl)methanethiosulfonate
NEM	N-ethylmaleimide (see Fig. 26)

NMR	nuclear magnetic resonance
OG	n-Octyl-b-D-glucopyranoside
OPO	optical parametric oscillator
PBS	phosphate buffered saline
4,4'-PDS	4,4'-dithiopyridine (see Fig. 23)
PCR	polymerase chain reaction
PMSF	phenylmethylsulfonylfluorid (inhibitor for Serine- and Cysteine-proteases)
POPC	1-Palmitoyl-2-Oleoyl-*sn*-Glycero-3-Phosphocholine (see Fig. 30)
POPE	1-Palmitoyl-2-Oleoyl-*sn*-Glycero-3-Phosphoethanolamine (see Fig. 30)
POPS	1-Palmitoyl-2-Oleoyl-*sn*-Glycero-3-Phospho-L-Serine (see Fig. 30)
PS	phosphatidylserine (independent of the fatty acid chains, e.g. POPS)
R*	activated rhodopsin
Rho	rhodopsin
ROS	rod outer segments
SB	Schiff base (at the retinal, sometimes referred to as RSB)
SDSL	site-directed spin labeling
TM	transmembrane helix (numbered TM1 – TM7)
TTL	transistor-transistor-logic
UV/vis	absorption spectroscopy in UV/visible range (usually 250 - 650 nm)
WT	wild type
YAG	yttrium-aluminium-garnet

Amino acids have been abbreviated according to the standard one- and three-letter code, respectively.

Acknowledgments

I want to thank the following people for supporting me with this dissertation. I am especially grateful to PROF. DR. KLAUS PETER HOFMANN for his guidance over the past years encouraging this work in his lab especially with a lot of ideas and helpful discussions. Equal thanks to DR. HABIL. OLIVER P. ERNST who directly supervised me and developed a lot of ideas thereby making this dissertation possible. Special thanks also to PROF. WAYNE L. HUBBELL, PHD for giving me the opportunity to perform a part of the experiments in his lab at UCLA, supporting me during these times and for helpful discussions.

Many people in the HOFMANN lab at Charité also supported me: DR. MARTIN HECK gave useful aid and feedback concerning kinetic analysis and spent a lot of time on this. DR. SIGURD MAGNUS was an invaluable support during construction of the flash photolysis setup. Thanks also to THOMAS PENCZOK and ANDREAS VON GARNIER who constructed technical parts and were great helpers for any technical problem. DR. HABIL. FRANZ J. BARTL supported me with performing and analysing the FTIR data. DR. EGLOF RITTER helped me with the FTIR experiments and also was a great support for general questions. DR. ROLF HERRMANN gave useful ideas concerning the peptide experiments. CHRISTINE KOCH and JANA ENGELMANN took care of the tissue culture and also helped me with protein purifications, while HELENA SEIBEL did the genetic work.

Special thanks also to the people who helped me during my working periods in the HUBBELL lab: DR. CHRISTIAN and RUTH ALTENBACH very kindly hosted me twice much better than any hotel. DR. CHRISTIAN ALTENBACH also supported me with discussions and technical help with the EPR spectrometer. CHERIE HUBBELL always had an open ear for me and greatly helped me with organizing my visits. NED VAN EPS, PHD and ANAKARIN KUSNETZOW, PHD were great partners for discussions and helped me with the lab work. SHIRLEY OKA also helped me with a lot of laboratory technique.

Very special thanks to SIMONE HOLZWARTH who read the manuscript of this work and was my greatest support during the whole time. Also big thanks to VERENA GRAMSE who carefully read the manuscript and suggested important corrections.

Special thanks to the Boehringer Ingelheim Fonds for Basic Research in Medicine for financially supporting this work over two years and four months. Thanks also to CLAUDIA WALTHER, MONIKA BEUTELSPACHER and DR. HERMANN FRÖHLICH from the Boehringer Ingelheim Fonds who organized interesting seminars and the fonds as a great scientific family. Another big thank to the ‘Studienstiftung des Deutschen Volkes’ (German National Academic Foundation) who supported me ideally over the whole period of this work and financially during the last months.

Published journal articles

Parts of this thesis are published in the following journal articles:

1. Bernhard Knierim, Klaus Peter Hofmann, Wolfgang Gärtner, Wayne L. Hubbell, and Oliver P. Ernst (2008): Rhodopsin and 9-demethyl Retinal Analog: Effect of a Partial Agonist on Displacement of Transmembrane Helix 6 in Class A GPCRs. *J. Biol. Chem.*, **283**, 4967-4974.
2. Bernhard Knierim, Klaus Peter Hofmann, Oliver P. Ernst, and Wayne L. Hubbell (2007): The Sequence of Late Molecular Events in the Activation of Rhodopsin. *Proc. Natl. Acad. Sci. USA*, **104** (51), 20290-20295.
3. Bernhard Knierim, Franz J. Bartl, Oliver P. Ernst, and Klaus Peter Hofmann (2008): Role of the Conserved ERY Motif in the Rhodopsin Ground State and During Activation. In preparation.

Poster presentations

The work was presented and discussed on the following conference posters:

1. Conference of the Biophysical Society, 2004 (Baltimore, USA):
   B. Knierim, O. P. Ernst: W. L. Hubbell, K. P. Hofmann: Interactions of the 9–methyl Group and β-ionone Ring of Retinal in Rhodopsin studied with Site-directed Spin Labeling.
2. Rhodopsin – Advances and Perspectives, 2006 (Fort Lauderdale, USA):
   B. Knierim, K. P. Hofmann, O. P. Ernst: Role of the ERY motif for rhodopsin activation.
3. International Conference for Retinal Proteins, 2006 (Awaji Island, Japan):
   B. Knierim, K. P. Hofmann, W. L. Hubbell, O. P. Ernst: Sequence of Rhodopsin Activation Steps.
4. Conference of the Biophysical Society, 2007 (Baltimore, USA):
   B. Knierim, K. P. Hofmann, W. L. Hubbell, O. P. Ernst: Sequence of Rhodopsin Activation Steps.
5. Conference of the Biophysical Society, 2008 (Long Beach, USA):
   B. Knierim, K. P. Hofmann, O. P. Ernst, W. L. Hubbell: Sequence of Late Intermediates in the Activation of Rhodopsin.

1 Introduction

1.1 Rhodopsin and the visual cascade

1.1.1 Location of rhodopsin

Rhodopsin is a retinal protein with a molecular weight of about 40 kD. It is located in the rod cells (see Fig. 1), which are part of the retina in the eye of vertebrates. Rhodopsin is an integral membrane protein of the disc and plasma membrane of the rod cells. In disc membranes it can freely move laterally and rotationally. Discs are separate membrane vesicles with a thickness of about 16 nm [Chabre and Worcester, 1982]. Each rod cell contains approximately 1000 discs with approximately 70,000 rhodopsin molecules per disc. Each disc has a life span of about one month. New discs are constantly pinched off from the cell membrane of the basal end of the outer segment. The dismantling of packages of discs at the apical end of the outer segment is done via phagocytosis once every 24 hours.

The inner segment of the rod cells is connected to the outer segment through a thin, immobile cilium. It is filled with the nucleus, mitochondria, and ribosomes which are important for the synthesis of rhodopsin. The production of ATP is located in the mitochondria. For signal transduction ATP is used to generate GTP through the enzyme diphosphatekinase.

At the basal end of the inner segment, the synaptic vesicles are located. They are filled with the neurotransmitter Glutamate. In the case of light activation of the rod cell, the constant release of glutamate is decreased, leading to the excitation of downstram located neurons (see chapter 1.1.5). Rod cells only enable black-and-white vision. In cone cells, which enable mammals to distinguish between different colors, similar opsin molecules are present. They show an adaption of their maximal absorption to three different wavelengths (λ_{max} = 426 nm, 530 nm and 560 nm) [Imai et al., 2005]. Cone cells, however, are not as sensitive as rod cells, which can be activated by a single photon [Baylor et al., 1979].

In vertebrates, the light first shines through the nerve cells and the inner segment before hitting the discs in the outer segment.

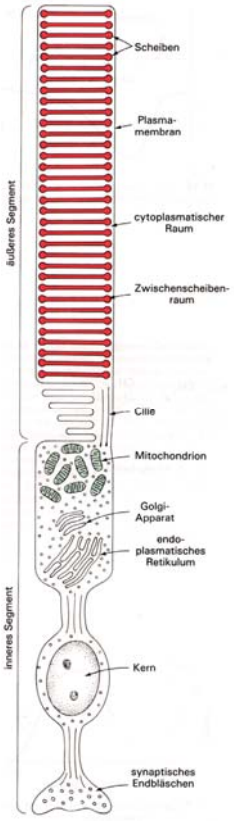

Fig. 1: *Scheme of a rod cell (taken from [Stryer, 1996]).*

1.1.2 Protein family

Rhodopsin belongs to the important family of G-Protein coupled receptors (GPCRs). It is part of the biggest class of these, called GPCR class I, and it is also studied as a model system for other GPCRs, including receptors for neurotransmitters and hormone receptors.

The distinctive and name-giving mark of GPCRs is their ability to activate a so-called G-protein through an exchange of GDP by GTP. This G-protein itself activates further proteins which affect the concentration of second messengers. Chapter 1.1.5 (signal transduction) describes this for rhodopsin. All GPCRs, which are also referred to as seven-helix-receptors, have seven transmembrane helices as their basic structure. They also carry several other highly conserved motifs, which therefore seem to play an important role for activation of these proteins [Mirzadegan et al., 2003].

GPCRs of the rhodopsin family have a prosthetic group, which often is a biogenic amine ligand with a cationic ammonium group at one end and a ring-like structure at the other. The transition from the ground state to the active state, which can activate the G-protein, shows similarities for all these receptors [Okada et al., 2001].

1.1.3 Molecular structure of rhodopsin

The 3D-structure of rhodopsin has first been shown by G. SCHERTLER and coworkers [Schertler et al., 1993] and solved at atomic detail in the lab of K. PALCZEWSKI [Palczewski et al., 2000] using x-ray diffraction. It has been refined in later works [Li et al., 2004; Okada et al., 2004]. The structure is shown in Fig. 2: Rhodopsin consists of opsin as a 348 amino acid protein and retinal as a prosthetic group, which acts as chromophore and absorbs the light energy.

Like all GPCRs, opsin contains seven transmembrane α-helices (TM1 to TM7) and in addition to those a short peripheral intercellular helix (H8). These transmembrane helices are connected by three intracellular (C-I to C-III) and three extracellular (E-I to E-III) loops. The fourth intracellular loop (C-IV) connects TM7 with a membrane anchor formed by two palmitoylated cysteines. C-IV has the structure of a short amphiphilic α-helix and is therefore referred to as helix H8. H8 is part of the binding site for the G protein [Fritze et al., 2003]. TM6 has a kink in its middle, which is close to the retinal and caused by the helix-breaking Pro^{267} residue.

The binding site for retinal is Lys^{296} in TM7, to which it is connected via a protonated Schiff base. Retinal is an aldehyde derivative of vitamin A. It has a β-ionone ring on one end, which is part of a linear conjugated polyene. The result is a coupled π-electron system, which is suited for the absorption of UV/visible light.

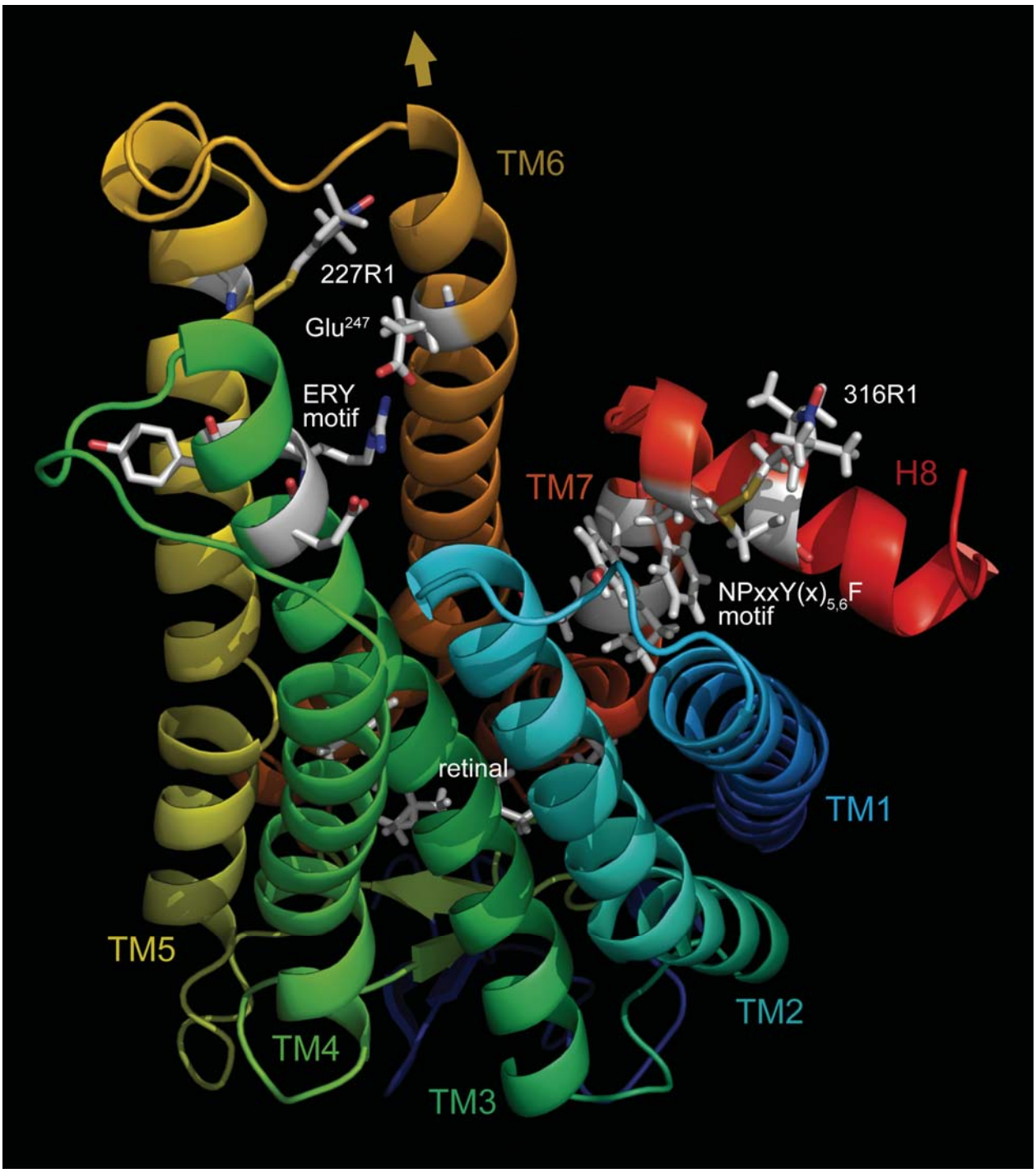

Fig. 2: *Structure of a rhodopsin molecule. The picture is based on the PDB molecule 1GZM [Li et al., 2004] and was prepared with PyMol (DeLano Scientific). The view onto the molecule is angular from the cytoplasmic side. The seven transmembrane helices are labeled TM with their respective numbers. H8 is the eighth helix which is parallel to the membrane surface. The retinal is only partially visible in the molecule due to the helices in the front.*
The important motifs ERY and NPxxY(x)$_{5,6}$F (see chapters 4.2.3 and 4.2.4) and the residue Glu^{247} which is connected to the ERY motif are colored according to the atoms. The movement of TM6 is shown with a brown arrow at the top. The two spinlabel positions used in this study to detect movements inside the molecule are drawn as cysteines with MTSSL spin labels (see Fig. 15) and labeled 227R1 and 316R1, respectively.

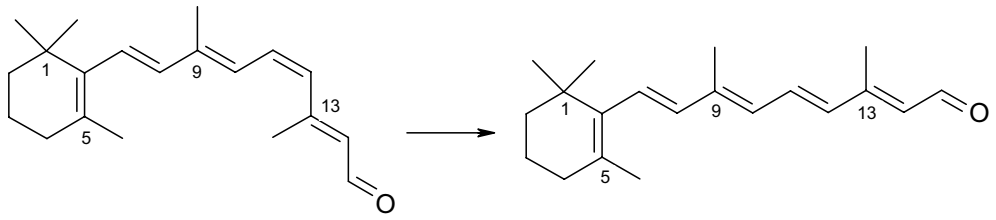

Fig. 3: Cis-trans *isomerization of retinal upon light absorbance.*

The other end in unbound retinal contains an aldehyde group, which forms the Schiff base with Lys^{296} when retinal is bound to opsin. With the exception of the *cis* configured bond between C_{11} and C_{12}, all double bonds are in *trans* configuration. The C_{11}-C_{12} bond isomerizes to *trans* configuration upon light activation (Fig. 3). Free retinal has an absorption maximum in the near UV (λ_{max} = 380 nm). Several interactions between protein and retinal shift this absorption maximum to a wavelength of approximately 498 nm. This phenomenon is called opsin-shift and results mainly from the presence of the protonated Schiff base in the ground state, which influences the π-electron system. Moreover, there are hydrophobic interactions with the β-ionone ring and with further amino acid side chains. The different absorption maxima in the three cone opsins for color vision result from different interactions because of a changed primary structure [Stenkamp et al., 2002].

The protonated Schiff base connecting opsin and retinal would normally be unstable, but Glu^{113}, which is deprotonated in ground-state rhodopsin, together with Glu^{181} acts as a complex counter ion. The formation of a salt bridge between the Schiff base and Glu^{113}/Glu^{181} results in high stability of rhodopsin in the dark state [Cohen et al., 1992; Ludeke et al., 2005]. Several other salt bridges and hydrogen bonds between different helices help to stabilize the ground state [Palczewski et al., 2000], many of the being highly conserved throughout the GPCR family.

One of the most conserved motifs is the D(E)RY motif, which has the sequence ERY in rhodopsin (see Fig. 2). It is composed of the amino acids Glu^{134}, Arg^{135} and Tyr^{136} and located at the cytoplasmic end of TM3. There are several interactions between the ERY motif and amino acid side chains in TM6, which are supposed to result in the stabilization of the position of TM6 [Li et al., 2004] – together with the side chain Trp^{265} that interacts with the β-ionone ring. Furthermore, there is evidence that Glu^{134} is involved in a proton uptake process that occurs during activation of rhodopsin [Arnis et al., 1994]. The ERY motif is also supposed to be a binding site for the G-protein [Franke et al., 1990].

Another equally conserved motif is the NPxxY$(x)_{5,6}$F motif at the transition between TM7 and H8 (see Fig. 2). It seems to play an important role during activation, probably in terms of stabili-

zation of the H8 position [Fritze et al., 2003]. Like the D(E)RY motif it is furthermore thought to be a G-protein binding site [Ernst et al., 2000b; Fritze et al., 2003].

Because of the described stabilizations, rhodopsin has an extremely low dark activity. statistically, a rod cell containing $1.4 \cdot 10^8$ rhodopsin molecules is activated spontaneously once every 160 s at body temperature (37 °C). Therefore activation without absorption of a photon statistically happens once in 760 years for any given molecule [Rodieck, 1998]. Nevertheless, a single photon suffices to start the activation cascade, and therefore the signal to noise ratio is extremely high [Hofmann and Ernst, 2001].

A short antiparallel β-sheet, which is part of the extracellular loop E-II, is located next to the retinal. A highly conserved disulfide bridge between Cys^{110} and Cys^{187}, the only native disulfide bridge in rhodopsin, holds it close to the polyene chain of the retinal [Okada et al., 2001].

1.1.4 Light activation of rhodopsin

The retinal absorbs the energy of a photon. Because of the absorbed energy the double bond between the carbon atoms C_{11} and C_{12} of the retinal isomerizes from its *cis* - into the *trans* configuration. This isomerization process is complicated and seems to include not only a rotation around the C_{11}-C_{12}-bond but as well a partial twisting of the C_9-C_{10}-bond (about 40°, which is limited by steric interactions) and other bonds. A simple isomerization only around the C_{11}-C_{12}-bond would lead to collisions of the retinal with the protein [Warshel, 1982].

The molecule is pushed from its stable energy minimum via the short-lived intermediate *Photorhodopsin* to the intermediate *Bathorhodopsin*, which happens on a ps timescale. During this transition the protonated Schiff base is moved to a nonpolar region of the protein and a large amount of the steric energy seems to be converted to electrostatic energy [Warshel, 1982]. The counterion Glu^{113} remains deprotonated and forms a weaker salt bridge with the Schiff base. Because of steric constraints (especially with the side chain Ser^{186}), the Bathorhodopsin state is not stable. Due to this tension a thermal relaxation of the retinal-protein complex occurs: The next intermediate, which is formed on a ns timescale, is *Lumirhodopsin*. Up to Lumirhodopsin, the structural transitions in the protein remain small [Borhan et al., 2000; Spooner et al., 2003].

Then, rhodopsin merges into an equilibrium between *Metarhodopsin-I* (Meta-I) and *Metarhodopsin-II* (Meta-II). In Meta-I the retinal has a similar configuration as in Lumirhodopsin, but rearrangements have occurred in the protein [Okada et al., 2001]. Contrary to assumptions based on photoaffinity labeling [Borhan et al., 2000], NMR experiments have suggested that the β-ionone ring stays in the same place until the Meta-I state [Patel et al., 2004; Spooner et al., 2003].

In the Meta-I state the Schiff base is still protonated and the counterion Glu^{113} is deprotonated, whereas the Schiff base is deprotonated and Glu^{113} therefore protonated in the Meta-II state [Jäger et al., 1994a]. This results in a loss of the stabilizing salt bridge between the Schiff base and Glu^{113} together with Glu^{181} [Ludeke et al., 2005; Martinez-Mayorga et al., 2006], so that the opsin-shift does not occur. The absorption maximum of the Meta-II state is therefore displaced to 380 nm. This means that the transition between Meta-I and Meta-II, which occurs on a ms-timescale, can be observed using UV/visible spectroscopy.

During the transition from Meta-I to Meta-II several helices are moving. This accompanies formation of the active state, which is capable of activating the G-protein transducin via a GDP-GTP exchange (see chapter 1.1.5). An active rhodopsin molecule has a catalytic activity towards transducin, which is by a factor 10^{10} higher than the activity of ground state rhodopsin [Okada et al., 2001]. In addition to that one active rhodopsin molecule can activate hundreds of transducin molecules, which means an amplification of the signal [Hofmann and Ernst, 2001]. Binding of the transducin to rhodopsin stabilizes the Meta-II state [Emeis et al., 1982].

As spin-labeling techniques with EPR on detergent solubilized rhodopsin (see chapter 1.3.4) have shown, the most important movement is that of the cytoplasmatic part of TM6, with the before-mentioned Pro^{267} as pivotal point [Farrens et al., 1996]. This finding is supported by the structure, as there is much free space around TM6, it is not strongly bound to other helices, and the third intracellular loop is very flexible and has only few tertiary interactions [Hubbell et al., 2003; Palczewski et al., 2000]. To make this movement possible, the neighbouring helices TM2, TM3 and TM7 undergo minor conformational changes [Hubbell et al., 2003]. The sequence of these movements is still under discussion. The rhodopsin structure in Fig. 2 gives an overview.

The Meta-II state can be further divided into *Meta-IIa* und *Meta-IIb*. In Meta-IIa the Schiff base is already deprotonated and Glu^{113} is protonated. As a result of the protonation of Glu^{113}, another residue (probably Glu^{134}), which is part of the highly conserved D(E)RY-motif, is protonated, too. According to the current nomination, this marks the transition from Meta-IIa to Meta-IIb, the catalytically active state [Arnis and Hofmann, 1993]. This nomination will be changed in the work at hand (chapter 4.1). Glu^{134} forms a salt bridge with the neighboring Arg^{135}, which interacts with Glu^{247} and Thr^{251} in TM6 [Palczewski et al., 2000]. These proton-transfer reactions are only possible if the participating side chains are well aligned [Okada et al., 2001].

Meta-I and -II form an equilibrium that is pH- and temperature-dependent [Matthews et al., 1963; Parkes and Liebman, 1984]. Meta-II has a lifetime of several minutes. The late photoproducts can be depicted as follows:

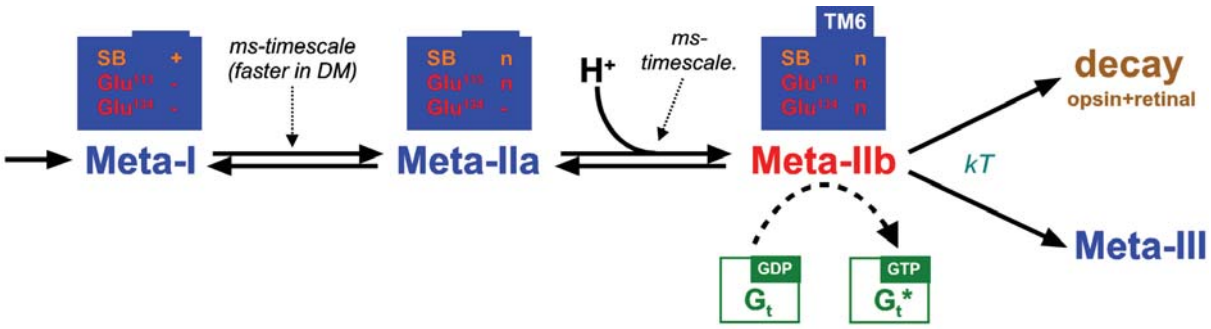

Fig. 4: *Scheme of the late photoproducts of rhodopsin according to the current nomination. '+' means a residue with a positive charge, '-' one with a negative charge and 'n' a neutral one at the respective location. The outward rigid body movement of TM6 is symbolized by the blue bar, but the exact time of occurrence is not known so far. Residues change their charge state by proton uptake or release, respectively. Meta-IIb is capable of catalyzing the GDP-GTP exchange in G_t.*

1.1.5 Signal transduction

The G-protein which is activated by rhodopsin is named transducin (G_t). It is activated through an exchange of bound GDP with GTP. The activated G_t can now in turn bind to a further effector protein, which is a cGMP-specific phosphodiesterase. Upon activation, this phosphodiesterase catalyzes the reaction from cGMP (cyclic guanosinmonophosphate) to 5'-GMP. Consequently, the amount of the second messenger cGMP in the ROS cell decreases which results in the closure of cation channels in the ROS plasma membrane. This lead to a hyperpolarization of the cell and consequently decreasing release of Glutamate into the synaptic cleft compared to the inactive ground state. Thus, the result of the light detection is a negative signal at the synapse that is forwarded to the brain via further neurons.

Such a signal cascade with several steps has two advantages: Firstly, the initial signal can be amplified several times through these steps, so that the effect is enormously increasing. Secondly, these steps make regulation of this signal pathway possible at several positions.

1.1.6 Deactivation

To deactivate the signal cascade, all the activating steps shown above have to be switched off again. Active rhodopsin is deactivated by rhodopsin kinase und arrestin [Dolph et al., 1993]. The GTP bound to G_t is hydrolyzed to GDP by G_t itself, but this intrinsic GTPase activity is enhanced by further proteins [Burns and Arshavsky, 2005]. The effect is a loss of binding ability of G_t towards phosphodiesterase.

Finally, the concentration of cGMP as a second messenger has to be raised to the resting state again: As a result of the closure of the cGMP-dependent cation channels, the influx of Na^+ and

Ca^{2+} decreases. The decreased intracellular concentration of free Ca^{2+} activates the enzyme guanylatecyclase via gCAP [Burns and Arshavsky, 2005] which catalyzes the reaction of 5'-GMP to cGMP. The increase of the cGMP level results in binding to and re-opening of the cGMP-dependent cation channels and therefore in depolarization of the cell and increased release of Glutamate at the synaptic cleft. Finally, the initial state before light activation is reached again and the cell is prepared for another activation process.

1.1.7 Blue light state

The illumination of the active Meta-IIb state with blue light ($\lambda < 420$ nm) creates another photoproduct. It was first described by ARNIS and HOFMANN [Arnis and Hofmann, 1995] based on work by EBREY [Ebrey, 1968], and it has been closer investigated by BARTL and coworkers [Bartl et al., 2001; Ritter et al., 2007; Ritter et al., 2004; Zimmermann et al., 2004].

While the photoproduct formed after milliseconds has been called P_{500} due to its absorption maximum close to 500 nm, the final product is identical to Metarhodopsin-III [Ritter et al., 2004] which is also generated as a normal decay product of Meta-II parallel to the Schiff base hydrolysis to opsin and all-*trans* retinal (see Fig. 5).

The absorption maximum of Meta-III in the 470 nm region suggests that the Schiff base is reprotonated as it is in the ground state. The behaviour of Meta-III is also similar to the ground state.

The striking difference between Meta-III and the ground state is a FTIR difference band around 1349 cm^{-1}, which is connected to the retinal and observable for Meta-III but not for the ground state [Bartl et al., 2001]. This cannot be explained by an isomerization of the all-*trans* retinal to 11-*cis*, 9-*cis*, or 7-*cis* retinal (B.

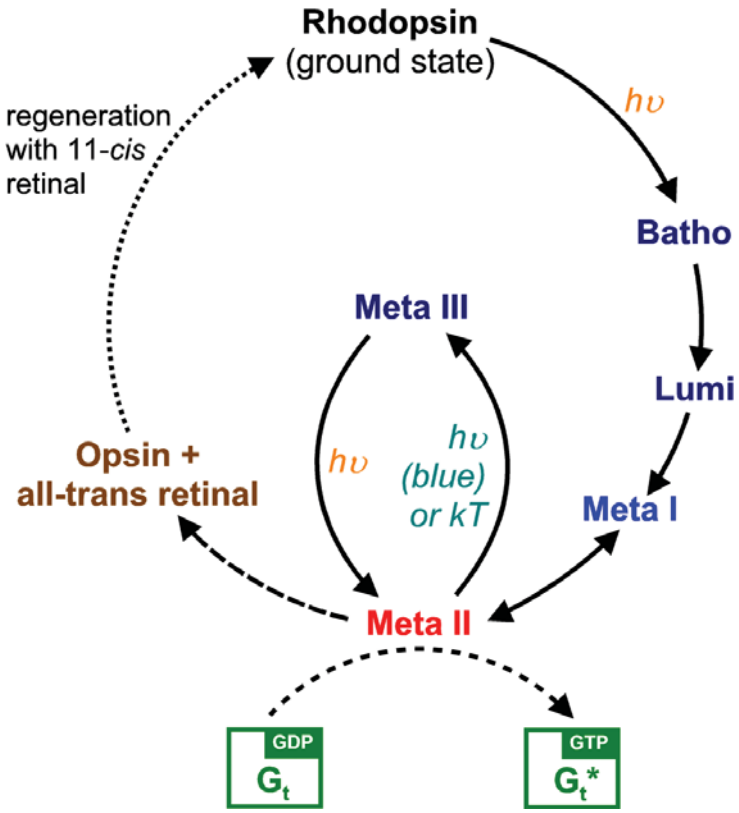

Fig. 5: *Activation scheme for rhodopsin including the Meta-III state.*

KNIERIM, Studienjahresarbeit). It has been shown that retinal isomerizes at the Schiff base C=N double bond and therefore Meta-III contains the retinal in an all-*trans* 15-*syn* configuration [Vogel et al., 2003].

The full reaction scheme for rhodopsin including the Meta-III state is shown in Fig. 5. The current state of research is that the transition between the photoproducts can only go clockwise with the exception of the equilibrium between Meta-I and Meta-II, but the ground state can not be recreated from the active state. The Meta-III state is thought to be a storage form during the presence of high light intensities in order to save on the permanent energy consuming regeneration of rhodopsin (Fig. 5, left arrow) [Ritter, 2006].

1.2 Flash photolysis

Flash photolysis can be used to monitor the kinetics of Meta-II formation parallel to proton uptake into the rhodopsin molecule. This is done at fixed wavelenghts in the UV/visible range. In addition to that, light scattering measurements are performed concurrently.

1.2.1 General considerations

The formation of Meta-II can be followed kinetically by monitoring either the increase of the absorption at 380 nm (λ_{max} of Meta-II) or the decrease of absorption at 500 nm (λ_{max} of dark state rhodopsin). Absorption at 380 nm is used when a pH-dependent dye is present in the sample (see below), which itself has absorption changes at 500 nm. However, when measuring absorption changes at 380 nm, the measuring light has an influence on rhodopsin itself: The illumination of the active state of rhodopsin with $\lambda < 400$ nm leads to formation of Meta-III [Ritter et al., 2004; Zimmermann et al., 2004]. Therefore illumination with 380 nm has to be kept minimal and the effect has to be taken into account.

A pH indicator dye is needed to optically follow the light-induced proton uptake reaction by rhodopsin. This marks the transition from Meta-IIa to Meta-IIb. Typically, bromocresol purple (pH range 5-7) and cresol red (pH range 7-9) were used. The structures of these dyes is shown in Fig. 6 and Fig. 7. The pH dependent changes in their absorption spectra are shown in Fig. 8. pH changes can be followed by observing the absorption at 595 nm or 575 nm, respectively. In order

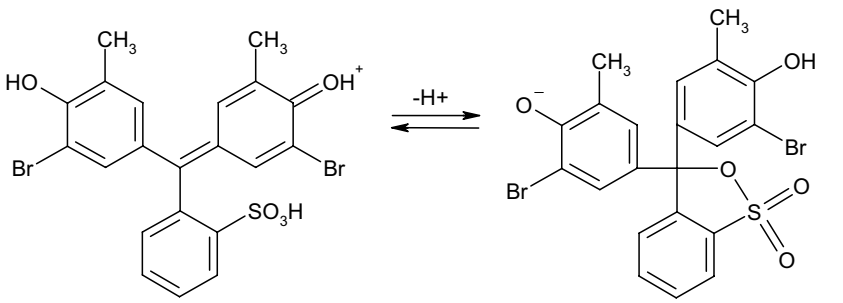

Fig. 6: *Bromocresol purple (BCP) and the reaction between the proton-bound and proton-unbound state.*

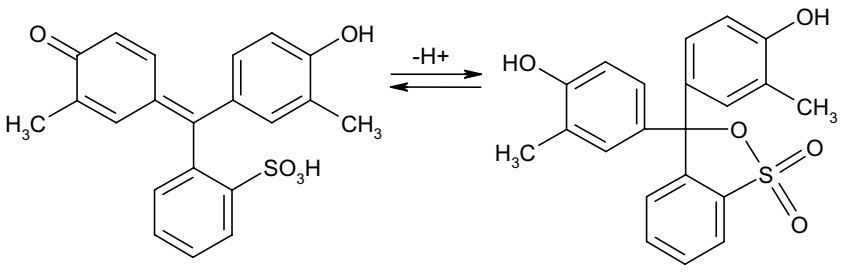

Fig. 7: *Cresol red (CR) and the reaction between the proton-bound and proton-unbound state.*

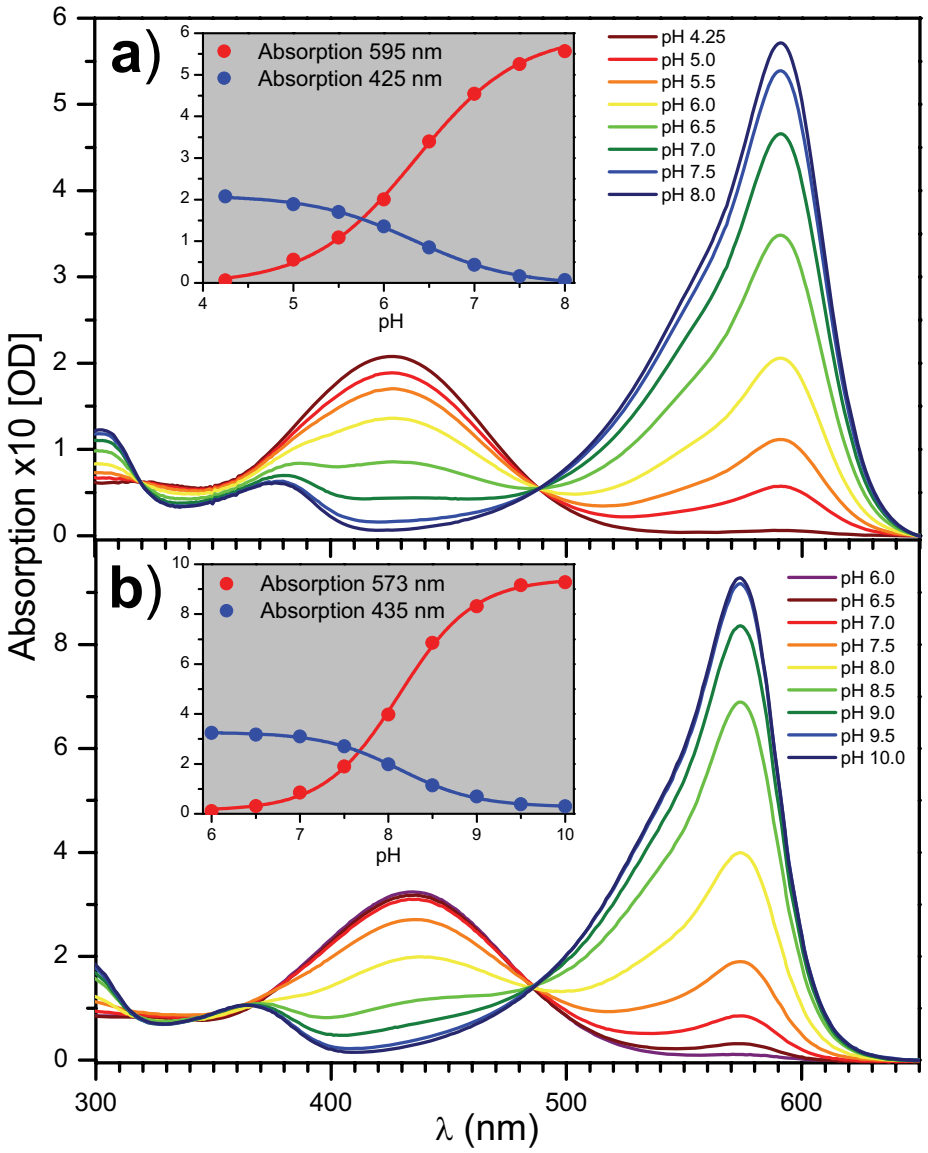

Fig. 8: *pH dependent absorption changes of the two dyes used. a) Bromocresol purple (BCP) is usable in the pH range between 5.0 and 7.0, showing absorption maxima at 425 and 595 nm. The inset shows the plot of the two absorption maxima against the pH. b) Cresol red (CR) can be used in the pH range between 7.0 and 9.0, showing absorption maxima at 435 and 573 nm. The inset shows the pH dependent plot.*

to get a good signal to noise ratio, the detectable pH change in solution has to be maximized. To obtain this, the buffering capacity of the sample must be low, which means that buffers are usually absent in the measured samples. As a result, the pH value of the sample is very sensitive to environmental influences. Therefore the pH of the sample is determined right in the cuvette that is used during measurements. This cannot be done reliably with a pH electrode due to the small size of the cuvette. I take advantage of the dye present in the sample and measure the pH using the quotient of the two absorption peaks as shown in Fig. 8.

At the wavelengths used to follow the pH changes during rhodopsin activation (595 or 575 nm, respectively), there is also a small spectral contribution from rhodopsin. To eliminate this effect, two samples are measured, one sample without buffer as described above and a second identical sample which contains buffer in addition. The measurement of the latter sample will only show

the contribution of Meta-II formation and can be subtracted from the former to receive the pure pH signal. This process is shown in Fig. 9. To determine how many protons are taken up per activated rhodopsin molecule, it is necessary to calibrate the indicator dye for each measurement, because the sample itself buffers the pH significantly so that the response might be different for each sample (see below).

1.2.2 Near infrared kinetic light scattering

Light scattering enables the observation of changes in the size of disc membrane samples or rhodopsin containing vesicles [Ernst et al., 2000a; Heck et al., 2000; Schleicher and Hofmann, 1987]. This is done in the near infrared range at λ = 840 nm. In order to only measure the change in scattered light, the direct light beam into the sample is blocked during detection and all the light scattered with an angle above 5° is collected and observed. This can also be done in an an-

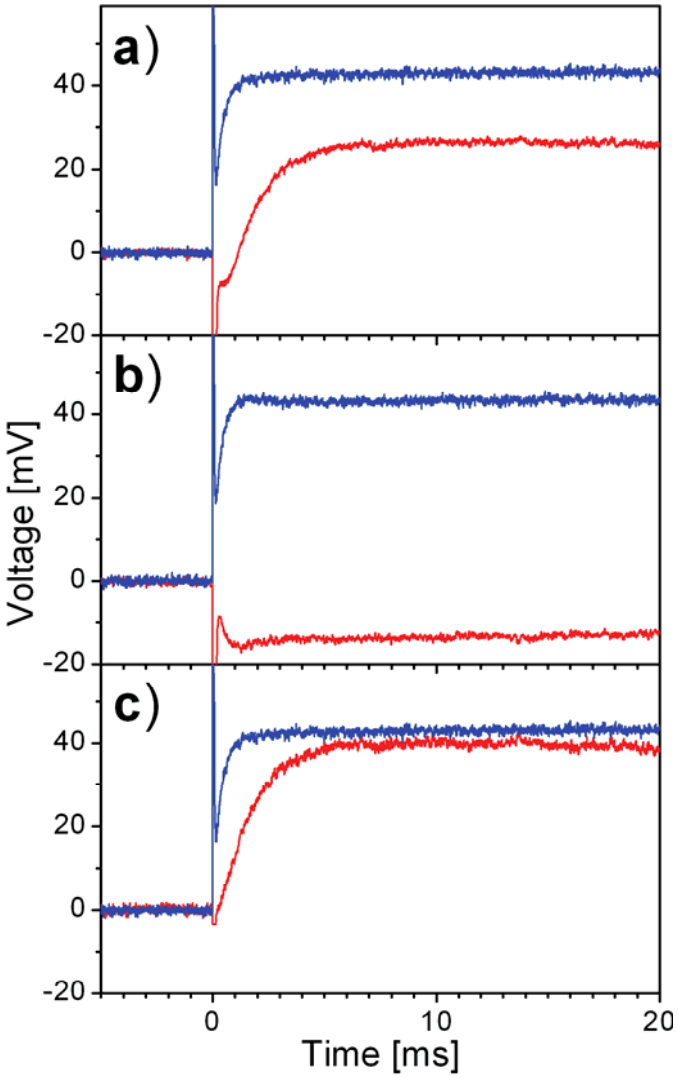

Fig. 9: *A typical flash photolysis experiment with rhodopsin in dodecyl maltoside (DM) as detergent. The blue trace represents the 380 nm channel (Meta-II formation), the red trace the 595 nm channel (bromocresol purple (BCP) with a contribution from the rhodopsin ground state). The samples were flash excited at 500 nm (0 ms).* a) *rhodopsin and BCP in an unbuffered solution at pH 6.3.* b) *rhodopsin and BCP in a buffered solution at pH 6.3.* c) *difference of the two 595 nm signals representing the pure pH signal as described in the text.*

gular dependent manner [Heck et al., 2000]. In the here described setup, the angular range from 5°-23° is selected in favor of a higher signal to noise ratio for measuring interactions of rhodopsin with G_t or other signaling proteins [Heck et al., 2000].

1.2.3 Instrumentation

The experimental setup is shown in Fig. 10. It is based on a home-made two-wavelength spectrophotometer described before [Hofmann and Emeis, 1981; Meyer and Hofmann, 2000]. It enables parallel time-resolved absorption measurements at two wavelengths and simultaneous detection of light scattering changes, all with a time resolution below one millisecond. Light from a 150 W halogen light source is sent through two monochromators (HR 460, Jobin-Yvon, USA). One of them is usually set to 380 nm to detect the formation of Meta-II while the other one is used to detect pH changes and is set to 595 nm or 575 nm for measuring changes of the dyes bromocresol purple or cresol red, respectively. Both refocussed beams pass the sample at an angle of approximately 35 ° relative to each other. After passing the sample the beams are refocused by fresnel lenses and then lead through a dielectric filter of the desired wavelength with ±2 nm aperture (Dr. Hugo Anders, Nabburg, Germany). Dielectric filters are stacked with an additional heat protection filter (Schott) to block all infrared light. Photodiode light detectors (UV-444BQ, EG&G) are used to convert light signals into electrical signals. To avoid unnecessary

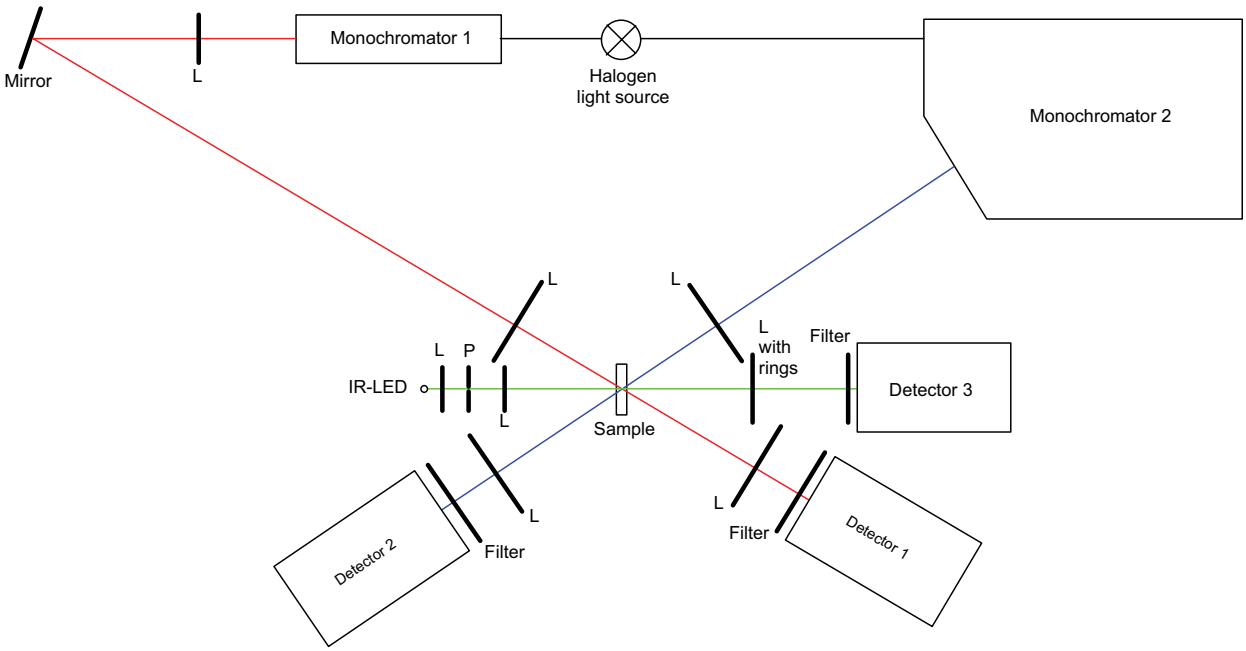

Fig. 10: *Scheme of the flash photolysis apparatus used in this work. Abbreviations: L: lens; P: pinhole. The filters are chosen according to the respective wavelength.*

bleaching of the samples, shutters are placed in both beampaths, and the sample is only exposed to light during the measurement.

The infrared light beam for light scattering measurements is generated by an infrared LED (Hitachi HLP 60R, λ = 840 nm) and first focused onto a pinhole and from there into the sample. After the sample, a 10 cm diameter fresnel lens collects the scattered light and focuses it onto the photodiode detector which is equipped with a dielectric filter (λ = 800-860 nm, Dr. Hugo Anders, Nabburg, Germany). To block direct light, the center of the fresnel lens is covered with a conical piece of metal that absorbs the light scattered at an angle < 5°.

The signals from the photodiodes are amplified with operation amplifiers (AD743, Analog Devices) and then recorded in a four channel digital oscilloscope (Accura 100, Nicolet).

The sample volume is 100 µl. Small custom-made sealable quartz cuvettes (Hellma, Müllheim, Germany) are used, which are 0.4 mm wide and 0.2 mm deep (inner dimensions). To control the temperature of the sample, the cuvette is tightly attached onto an insulated heat block, which is temperature controlled through a water cooling system and an additional piezo cooler; the latter is used for temperatures below 10 °C. With a micro temperature sensor (HH506R, Omega, Stamford, USA) the temperature in the middle of the cuvette can be checked.

For illumination several systems are used sequentially or alternatively: A laser (λ = 532 nm, Orion Nd:YAG), a regular flash lamp (PerkinElmer Optoelectronics) and a UV flash (Dr. Rapp Optoelectronics, Hamburg, Germany) equipped with dielectric bandpass filters (480-540 nm or 380-480 nm, respectively; Dr. Hugo Anders, Nabburg, Germany). The timing of the experiment is controlled electronically through a computer that transmits TTL signals to the shutters, the oscilloscope and the flashes.

1.2.4 Characterisation of the instrument

The time resolution of the instrument is limited by the used electronics and is 200 µs for the described setup.

The conventional flash bleaches 11 % of the rhodopsin molecules present in a solubilized rhodopsin sample and about 8% in a disk membrane sample depending on the scattering conditions. Higher bleaching rates could be achieved with a more intense flash. However, this is not desirable because a flash duration of about 300 µs would also increase reisomerization of the chromophore. The used laser, which generates 17 mJ per 5 ns flash, bleaches up to 32 % of the rhodopsin molecules in the sample.

Upon flash excitation an artefact is observable on both optical channels which lasts for about 300 µs – both with the conventional flash and with the laser (probably due to oversaturation of the

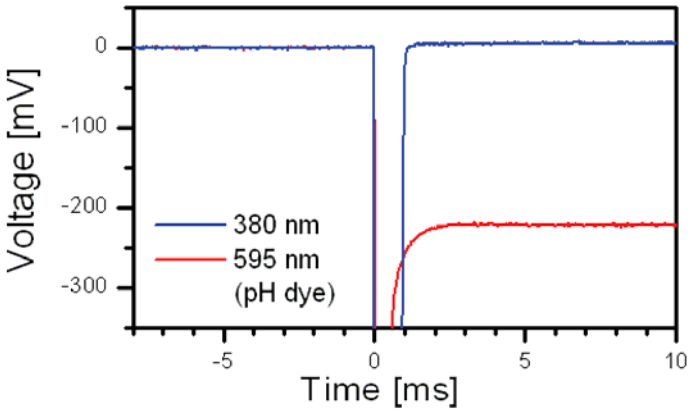

Fig. 11: *In this experiment only bromocresol purple as pH dependent dye and a caged proton compound were present. Protons were released upon a UV flash (time 0) resulting in a long flash artefact on the 380 nm channel and a shorter one on the 595 nm channel. The pH signal on the 595 nm channel shows an instantaneous acidification.*

detecting diode). Therefore the first 300 µs of each experiment cannot be observed which makes very fast experiments impossible. The artefact caused by the UV flash is even longer (600 µs on the 595 nm channel and 1 ms on the 380 nm channel which is directly illuminated).

Examining the formation of Meta-IIa and Meta-IIb, one could argue that the apparent later formation of Meta-IIb [Arnis and Hofmann, 1993] might be due to the fact that either diffusion of the protons or the reaction of the dye might be rate limiting. To exclude this possibility I have examined the behaviour of the bromocresol purple dye upon microsecond proton concentration jumps due to UV flash photolysis of caged protons (caged GTP, purchased from Merck Calbiochem) [Janko and Reichert, 1987]. The result is shown in Fig. 11 and reveals that the absorption change of the dye happens instantaneously and the time course is not observable due to the flash artifact. The half lifetime of the process must therefore be very fast and can not account for the delay of the proton uptake by Meta-II which is in the millisecond range. The speed of proton diffusion in the samples has been discussed in MEYER et al. [Meyer and Hofmann, 2000].

1.2.5 Experiments in detergent

For each experiment two samples are prepared: In the first sample the pigment is diluted with the same buffer-free solution to 5-10 µM, in the second sample it is diluted to the same concentration with BTP buffer for pH > 6 and acetate buffer for pH < 6. 50 µM bromocresol purple or cresol red (depending on the desired pH) is added to both samples. The buffer-free sample is adjusted to the desired pH by adding small amounts of 1 mM HCl or NaOH, respectively. Accordingly, the buffered sample is adjusted to the same pH using 100 mM HCl and NaOH solutions. A pH-microelectrode (A157, Schott, Germany) is used to measure pH. After transfer into the cuvette and sealing to prevent gas diffusion, the pH has to be checked again for the unbuffered sample. As mentioned before, this cannot be done reliably with a pH electrode due to the small size of the cuvette. However, the dye present in the sample allows convenient meas-

urement of pH by using the quotient of the two absorption peaks as shown in Fig. 8 and correcting for the absorption contribution from rhodopsin. Typical traces for buffer-free and buffered rhodopsin samples, which are activated by a single flash, are shown in Fig. 9 A and B. The pure proton uptake signal can be calculated by subtracting the trace measured with the buffered sample from the trace measured with the unbuffered sample and is shown in Fig. 9 C. At pH < 6, each activated rhodopsin molecule takes up about one proton, at more basic pH less. The recordings of Meta-II formation (blue trace) and proton uptake (red trace) show that the latter process is clearly slower, allowing to distinguish between Meta-IIa and Meta-IIb [Arnis and Hofmann, 1993].

1.2.6 Experiments with disc membranes

When disc membranes or purified rhodopsin reconstituted into vesicles are used, light scattering changes due to rhodopsin activation can be recorded on a third additional channel. When working with membranes or vesicles, the signal to noise ratio for the two optical channels is worse than in detergent solutions due to the scattering of the membranes. The signal on the light scattering channel has to be adjusted to 0 before the start of the experiment as every sample scatters differently. The countervoltage used for this adjustment is recorded because it represents the basic scattering to which the amplitude change has to be referred. Typical traces reflecting Meta-II formation, proton uptake and light scattering were measured simultaneously and are shown in Fig. 12. The kinetics observed with membranes are usually slower by one order of magnitude compared to measurements in detergent solution. The difference between Meta-II formation and

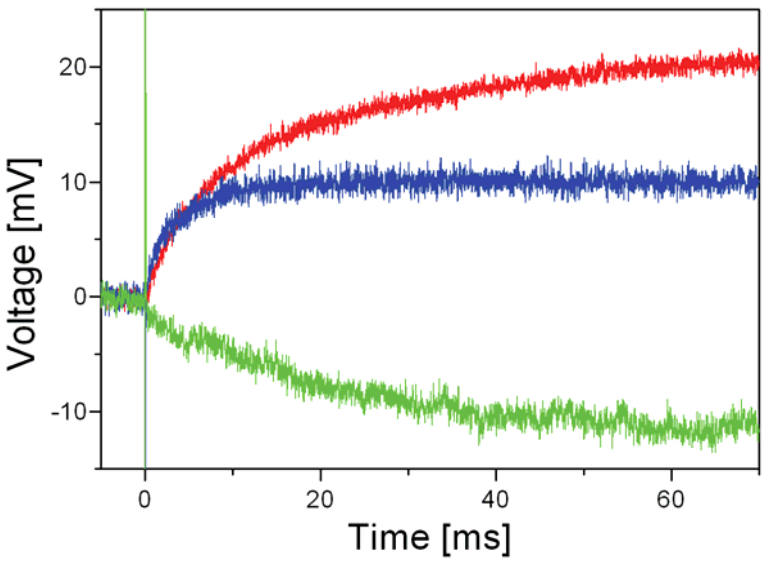

Fig. 12: *A kinetic rhodopsin experiment in native membranes (difference as shown in Fig. 9c), raw data. The blue trace represents the 380 nm channel (Meta-II formation); the red trace the 595 nm channel (BCP), and the green trace the light scattering signal (N-signal). The sample was flash excited at 500 nm (0 ms), and the 595 nm already represents the difference of the buffered and the unbuffered sample as described.*

proton uptake is clearly smaller here, indicating that the difference in activation enthalpy between both processes is smaller. The observed light scattering change represents the so-called N-signal [Schleicher and Hofmann, 1983]. This signal is kinetically similar to the EPR signal assigned to TM6 movement (see 3.1.2). In disc membrane samples, the light-induced binding of G_t and other signaling proteins such as arrestin or rhodopsin kinase to activated rhodopsin can be investigated as well [Heck et al., 2000; Herrmann et al., 2004]. The here described instrumental setup allows simultaneous measurement of Meta-II formation, changes of proton concentration in the bulk phase and interactions which are observable through scattering changes.

1.2.7 Calibration of the indicator dye response

To calibrate the response of the indicator dye, 100 µM HCl is titrated into the unbuffered sample in steps of 1 µl and quickly stirred while the absorbance at 595 or 575 nm is recorded. Differences in pH response of unilluminated and illuminated samples measured directly after the experiment are negligible. The amount of protons taken up per activated molecule can then be calculated as follows:

$$\frac{H^+}{R^*} = \frac{c_{HCl}}{\Delta I_{HCl}} \cdot \frac{\Delta I_{flash} \cdot \frac{100}{b\%}}{c_{Rho}} \qquad \text{(I)}$$

with c_{HCl} and c_{Rho} being the concentrations of the titrated HCl and rhodopsin in the sample, respectively, ΔI_{HCl} and ΔI_{flash} being the intensity changes detected and b% representing the percentage of rhodopsin bleached with one flash. For a detailed derivation see [Meyer and Hofmann, 2000].

1.3 Electron Paramagnetic Resonance (EPR)

1.3.1 General principle of EPR spectroscopy

EPR, which is also refered to as ESR (electron spin resonance), is the absorption of electromagnetic radiation in the microwave frequency domain, which causes a transition between different energy levels of the electron spins. Therefore the most important prerequisite for EPR spectroscopy are molecules with unpaired electrons. These may be natively present transition metals, which occur in some proteins, free radicals, which appear as intermediate stages in some bio-

chemical reactions, or special spin probes, which are usually stable organic radicals covalently bound to biomolecules.

An electron can have two different spin states concerning its own rotation, which are usually named $m_S = +½$ ("parallel") and $m_S = -½$ ("antiparallel") (for $S = \frac{1}{2}$). The energy levels of these two spin states are usually degenerated, but split up in the presence of an external magnetic field. This phenomenon is called *Zeeman effect*.

The energy difference can be calculated as follows:

The magnetic moment of an electron consists of the magnetic moment of the orbital rotation and of the rotation of the electron around itself, which is called electron spin:

$$\vec{\mu}_{total} = \vec{\mu}_L + \vec{\mu}_S \tag{II}$$

(μ_L: magnetic moment of the orbital rotation; μ_S: magnetic moment of the electron spin)

The absolute value of the magnetic moment is composed as follows:

$$\left|\vec{\mu}_{total}\right| = g \cdot \mu_B \cdot \left|\vec{J}\right| \tag{III}$$

(g: Landé-factor; μ_B: Bohr Magneton; J: quantum number)

The *Landé-factor* g is dependent on the quantum numbers of the considered electron:

$$g = 1 + \frac{J(J+1) + S(S+1) - L(L+1)}{2J(J+1)} \tag{IV}$$

(J, S, L: quantum numbers of the considered electron)

The *Bohr Magneton* is a constant value, which is defined as follows:

$$\mu_B = \frac{e \cdot \hbar}{m_e \cdot c} \approx 0.92 \cdot 10^{-23} \frac{J}{T}; \quad \hbar = \frac{h}{2\pi} \tag{V}$$

(e: elementary charge; h: Planck constant; m_e: mass of the electron; c: speed of light)

Normally it suffices to consider an electron without its orbital rotation, so that equation I can be simplified as follows using equation II:

$$\left|\vec{\mu}_{total}\right| = \left|\vec{\mu}_S\right| = -g \cdot \mu_B \cdot \left|\vec{S}\right| \tag{VI}$$

The minus sign indicates that the magnetic moment and electron spin have opposite directions. Resulting from equation III the Landé-factor then has a fixed value of $g = 2.00232 \cong 2$ (considering quantum mechanics).

The energy of a magnetic dipole in a magnetic field can generally be calculated as:

$$E = -\vec{\mu}_S \cdot \vec{B}_0 = -\left|\vec{\mu}_S\right| \cdot \left|\vec{B}_0\right| \cdot \cos\delta \tag{VII}$$

(E: energy, B_0: flux density of the magnetic field; δ: angle between magnetic field and magnetic moment)

Considering equation V this results in:

$$E = g \cdot \mu_B \cdot \left|\vec{S}\right| \cdot \left|\vec{B}_0\right| \cdot \cos\delta \tag{VIII}$$

The cosine of the angle between magnetic field and magnetic moment can be calculated as:

$$\cos\delta = \frac{m_S}{\left|\vec{S}\right|} \tag{IX}$$

Using this formula we can modify equation VII as follows:

$$E = g \cdot \mu_B \cdot \left|\vec{B}_0\right| \cdot m_S \tag{X}$$

As the spin of the electron can be $m_S = \pm\frac{1}{2}$, there are two different energy levels for the electron in presence of a magnetic field:

$$\begin{aligned} E_+ &= +\tfrac{1}{2} \cdot g \cdot \mu_B \cdot \left|\vec{B}_0\right| \\ E_- &= -\tfrac{1}{2} \cdot g \cdot \mu_B \cdot \left|\vec{B}_0\right| \end{aligned} \tag{XI}$$

The difference between these energy levels is consequently:

$$\Delta E = g \cdot \mu_B \cdot \left|\vec{B}_0\right| \tag{XII}$$

If exactly this energy ΔE is brought into the system in terms of electromagnetic radiation, the electron can absorb this energy and be switched between the two energy levels E_- and E_+, which is then called *resonance* (see Fig. 13):

$$\Delta E = h \cdot \nu = g \cdot \mu_B \cdot \left|\vec{B}_0\right| \tag{XIII}$$

(h: Planck constant; ν: frequency of the electromagnetic radiation)

If we consider a magnetic flux density of B_0 = 0.1 to 1 T, which is common for EPR measurements, the wavelength λ of the electromagnetic radiation has to be several centimetres, which means microwave radiation is needed.

The number of electrons in either energy level E_+ and E_- in the equilibrium state is given by a Boltzman distribution:

$$n(E_+) = n(E_-) \cdot e^{\frac{\Delta E}{-k_B \cdot T}} \tag{XIV}$$

($n(E_x)$: number of electrons in the energy level x; k_B: Boltzman constant; T: absolute temperature)

In thermal equilibrium the number of electrons in the lower energy level is bigger than the number in the higher energy level ($n(E_-) > n(E_+)$). When electromagnetic radiation is absorbed in the system, the distribution of electrons between the two energy levels is changed. Finally there should be as many electrons in the higher as in the lower energy level, and one would not see an EPR signal any longer. But there are two relaxation mechanisms which make electrons change

from the higher to the lower energy level again, so that the distribution between the two energy levels will not be equal but pushed towards the direction of the Boltzman distribution:

Spin-lattice relaxation means that the spin system interacts with its environment (called lattice). The lost energy is absorbed by the environment as thermal energy. The time, which is needed to reconstitute the Boltzman distribution to the value $\frac{1}{e}$, is called spin-lattice relaxation time T_1. T_1 is usually shorter in solid objects than in fluids, because the interactions are stronger. If the relaxation time is too long or the power of excitation is too big, saturation is obtained, which can reveal information about the environment.

Spin-spin relaxation means the exchange of spins between two adjacent spin systems. This does not change the distribution of electrons in the energy levels but the lifetime of the spin states. The product of energy fuzziness and lifetime τ has a lower limit according to the Heisenberg uncertainty relation:

$$\Delta E \cdot \tau \geq \frac{\hbar}{2} \tag{XV}$$

Therefore the energy uncertainty is big if the lifetime of the state is short. As a result the width of the resonance line broadens. Because spin-spin relaxation is much more important than spin-lattice relaxation in fluids, the line width is mainly determined by the spin-spin relaxation time T_2, to which it is anti-proportional.

In general the line width can be calculated as:

$$\Delta H = \frac{1}{2T_1} + \frac{1}{T_2} \tag{XVI}$$

The shape of resonance lines can generally be described by a Lorentzian function.

According to this theory, an EPR spectrum would contain only one line. But there is another phenomenon called *hyper fine coupling*, which describes the interaction of the electron with the magnetic moment of the nucleus, wherefore the effective magnetic field taking effect on the electron is different from the outer magnetic field. This interaction results from Fermi- or contact-interactions as well as from dipole-dipole-interactions. For a nuclear spin of $I = 1$ like for nitrogen there are three possible directions of the nuclear spin (+1, 0 and -1) and hence three possible local magnetic orientations. One third of all unpaired electrons are associated each with nitrogen nuclei in one of the three spin states, which means that we receive three EPR lines instead of one. In general, the number of EPR lines because of hyper fine coupling is given by the equation:

$$n_{lines} = 2S \cdot (2I + 1) \tag{XVII}$$

Additional hyperfine coupling can be detected because of interactions of the unpaired electron with ^{13}C and ^{15}N nuclei, but these signals are weak and therefore imperceptible in most spectra, because these isotopes have a low natural abundance (1.1 % and 0.37 % respectively).

The sample in an EPR spectrometer is arranged in the middle of a strong electromagnet, which creates the constant magnetic field $\vec{B}_0$. The microwave radiation is produced by a klystron with a frequency ν of about 10 GHz. It is conveyed to the sample through a cavity, which is adjusted so that a linearly polarized standing wave forms in its interior. The constant outer magnetic field

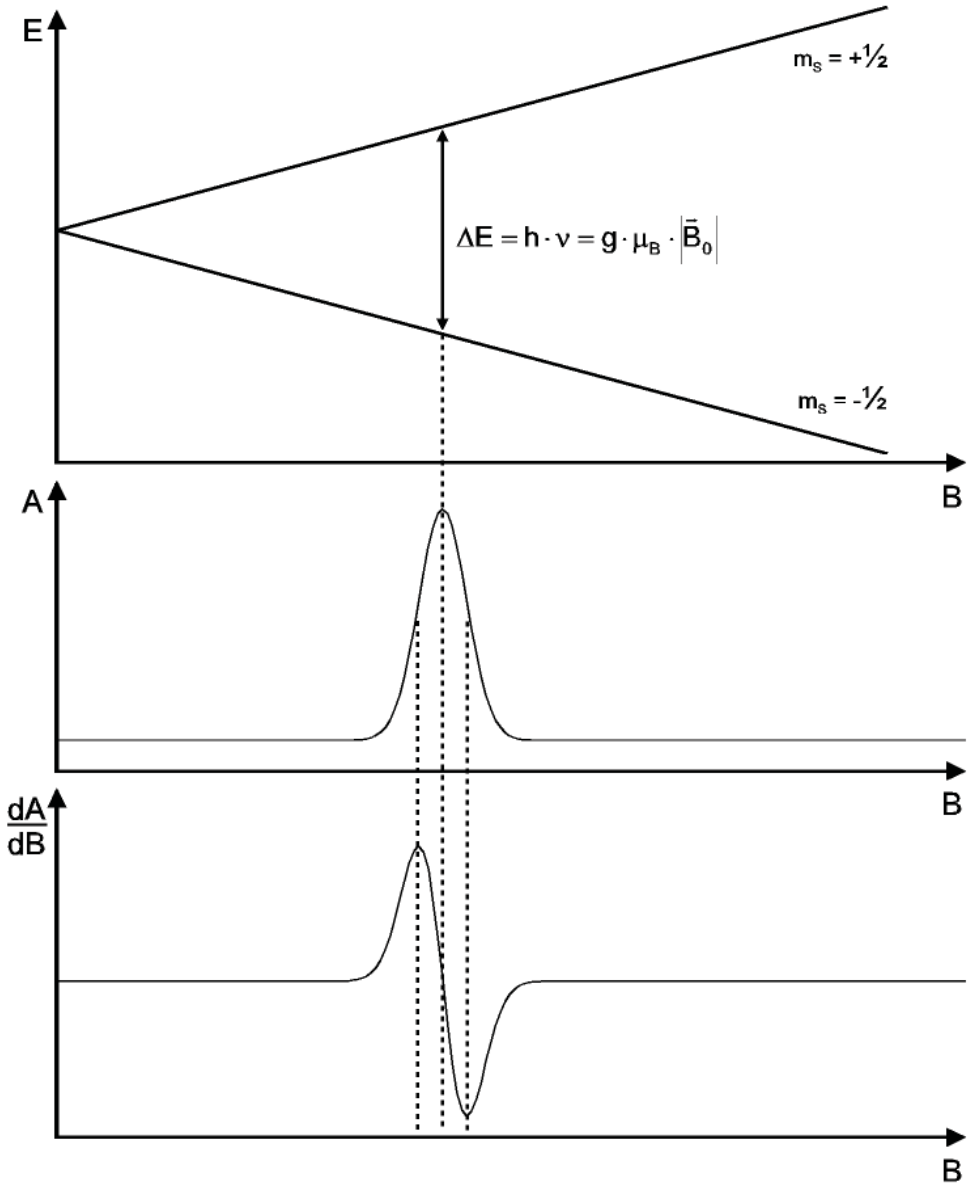

Fig. 13: *Energy difference between the two spin states (upper panel) and the resulting EPR spectrum at the position where resonance is obtained (middle panel). Due to modulation the first derivative of the EPR spectrum is measured (lower panel).*

and the changing magnetic field from the klystron are perpendicular to each other. Usually the frequency of the microwaves, which is determined by the shape of the klystron, is held constant and the outer magnetic field $\vec{B}_0$ is changed. The absorption of microwave energy in dependence of the outer magnetic field results in the EPR-spectrum (see Fig. 13).

As the absorption is usually weak, it is necessary to increase the signal to noise ratio. Therefore the magnetic field is modulated in a sinusoidal shape with the help of additional electromagnets at a frequency of 100 kHz. The resulting alternating voltage at the detector can be recorded with less noise. The amplitude of the field modulation can usually be chosen, but it must not be broader than the absorption signal, because otherwise the lines of the EPR spectrum cannot be resolved any more. What is measured because of this modulation is the gradient of the microwave absorbance, which means that the resulting signal is the first derivative of the EPR spectrum.

Different frequencies of microwaves make it possible to detect changes on different timescales. In these studies only X-band EPR is used, but the other frequency regions of are shown in the table below.

Region	Frequency	Magnetic flux density
L-Band	1.1 GHz	390 G
S-Band	4.0 GHz	1430 G
X-Band	9.75 GHz	3480 G
Q-Band	34.0 GHz	21 100 G
W-Band	94.0 GHz	33 500 G

Table 1: *EPR frequency regions.*

1.3.2 Orientation and motion in EPR samples

The unpaired electron in a paramagnetic sample has a certain orientation. Thus, the interaction of the spin label with the external magnetic field $\vec{B}_0$ depends on their relative orientation to each other. The orientation of the molecules in a sample is usually random (if one does not orient the membranes where the molecules are located, which is also possible), so that the hyperfine splitting has a wide range of values, which is usually called a *powder spectrum*. The superposition of these spectra results in a spectrum with broadened peaks on both sides and a huge peak in the middle, because this peak is not influenced by hyperfine coupling.

In a liquid sample the paramagnetic molecules are moving, too. If the movement is slow compared to the characteristic time of the EPR spectrometer, a normal powder spectrum will be ob-

tained. But if the movement is fast (with a rotational correlation time equal or shorter than 10^{-9} s for X-band), only one single value for hyperfine splitting is observed, which is the weighted average of splittings according to the various orientations. Such a spectrum, which is equal to the spectrum of a sample in which all molecules have one direction, is then called *isotropic* (or "fast tumbling").

In a fluidic sample it is usually possible to measure the spectrum at two different temperatures. At room temperature the spectrum is homogenously broadened because of relaxation effects, in the frozen state it is inhomogeneously broadened due to static dipolar interactions.

These different motions can be simulated to understand the contributions of different factors [Budil, 1996].

1.3.3 Nitroxide spin labels

As mentioned in the last chapter one of the most important prerequisites for an EPR measurement is the presence of unpaired electrons. As they usually do not occur in biomolecules, it is necessary to attach labels to molecules of interest. Nitroxide spin labels are commonly used mainly because of their chemical stability, as free radicals are highly reactive species in general. The best-known nitroxide spin label is TEMPO (2,2,6,6-tetramethylpiperidin-1-oxid, Fig. 14), which can easily be inserted into membranes to examine their dynamic properties.

Nitroxide contains an unpaired electron and is therefore a stable radical and thus paramagnetic. This electron is located in a p orbital, which has an orientation perpendicular to the axis of the N-O bond.

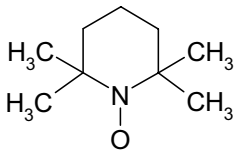

Fig. 14: *TEMPO (2,2,6,6-Tetramethyl-piperidine-1-oxyl).*

If nitroxides are chemically reduced (the oxygen becomes a hydroxide group then), they lose their unpaired electron and hence their paramagnetic properties. It is therefore necessary to conserve non-reducing conditions in the spin labeled sample [Humphries, 1982]. The methyl groups attached to adjacent carbons increase the stability of the nitroxide group greatly by isolating it sterically from potentially reactive environment [Humphries, 1982].

A general advantage of spin labels is the possibility to observe one specified position in the molecule without seeing any disturbances by other atoms, because they simply do not interact with microwaves. The disadvantage is that in order to detect changes in several locations within one molecule, every position of interest has to be labelled separately.

1.3.4 Side-directed spin labeling (SDSL)

SDSL means that a spin label – usually a nitroxide spin label – is attached to a specific site in a protein. This is done by site-directed mutagenesis of an amino acid at the site, which is to be examined, into a cysteine (details in chapter 2.1.3). A sulfhydryl-specific nitroxide reagent can then be coupled to the newly generated cystein residue. Other reactive cysteines present in the native protein have to be mutated into different amino acids (e.g. Ser) to prevent the spin label from attaching to several different sites.

The most commonly used spin label for SDSL experiments is methanethiosulfonate (MTSSL) which generates the nitroxide side chain R1. This reaction is shown in Fig. 15.

The R1 spin label which was used for all samples in this study has several advantages:

1) The labeling reaction can be performed under physiological conditions without changing the chemical environment of the considered protein.
2) The reaction is highly specific to sulfhydryl groups, and there are no side reactions at other sites. Native cysteines, which are connected through a disulfide bridge, normally do not react with methanethiosulfonate, so that they do not necessarily have to be removed. This is useful, because they might be important for the native structure of the protein.
3) The R1 spin label is well tolerated at many different positions in the protein, as it has a similar structure to native amino acids (volume and polarity are comparable to tryptophane). Thermal stability of the protein is rarely affected.
4) A big advantage of SDSL in general is the small protein amount required for these measurements: 50 to 100 pmol are sufficient.

A general disadvantage of SDSL measurements is a small possibility that the attachment of the R1 side chain might perturb the protein structure causing artefacts during measurements. However, the used spin label is relatively small and it has been shown in several studies that the x-ray structures of labeled and unlabeled proteins are almost identical [Langen et al., 2000].

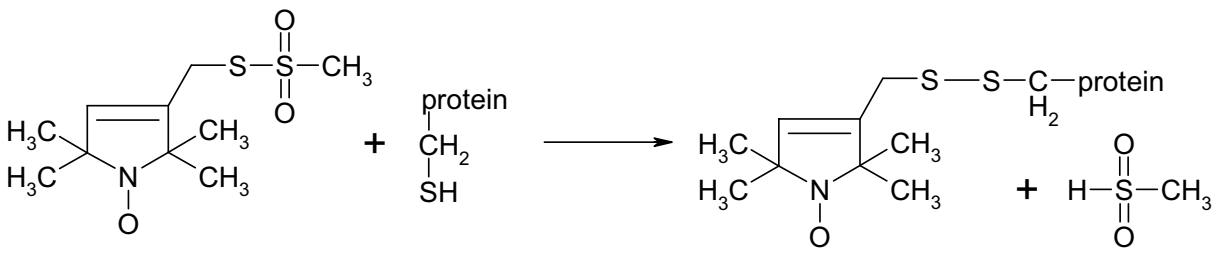

Fig. 15: *Reaction of methanethiosulfonate spin label (MTSSL) with a cysteine side chain, generating the side chain R1.*

1.3.5 Mobility measurements with SDSL

The mobility of a spin labeled side chain can be derived from the spectral line shape as explained in chapter 1.3.2. The measured quantities for mobility are the inverse linewidth of the nitroxide central resonance and the spectral second moment [Oh et al., 2000]. A comparison of linewidths for free spin label at different temperatures is shown in Fig. 16 to illustrate the influence of mobility on the spectral line shape. If the spin label becomes less mobile (decreasing temperature), the spectrum is broadened. The same effect is visible for spin labels attached to proteins.

The motion of a nitroxide site chain is the result of three contributing factors:

1) the rotational correlation time for the entire protein, τ_R;
2) the effective correlation time because of local backbone flexibility, τ_B;
3) the effective correlation time of isomerizations of the nitroxide-backbone bond, τ_S.

In the EPR spectrum, one sees the sum of these three processes. They can only be distinguished if one simulates the spectra with a computer [Budil, 1996].

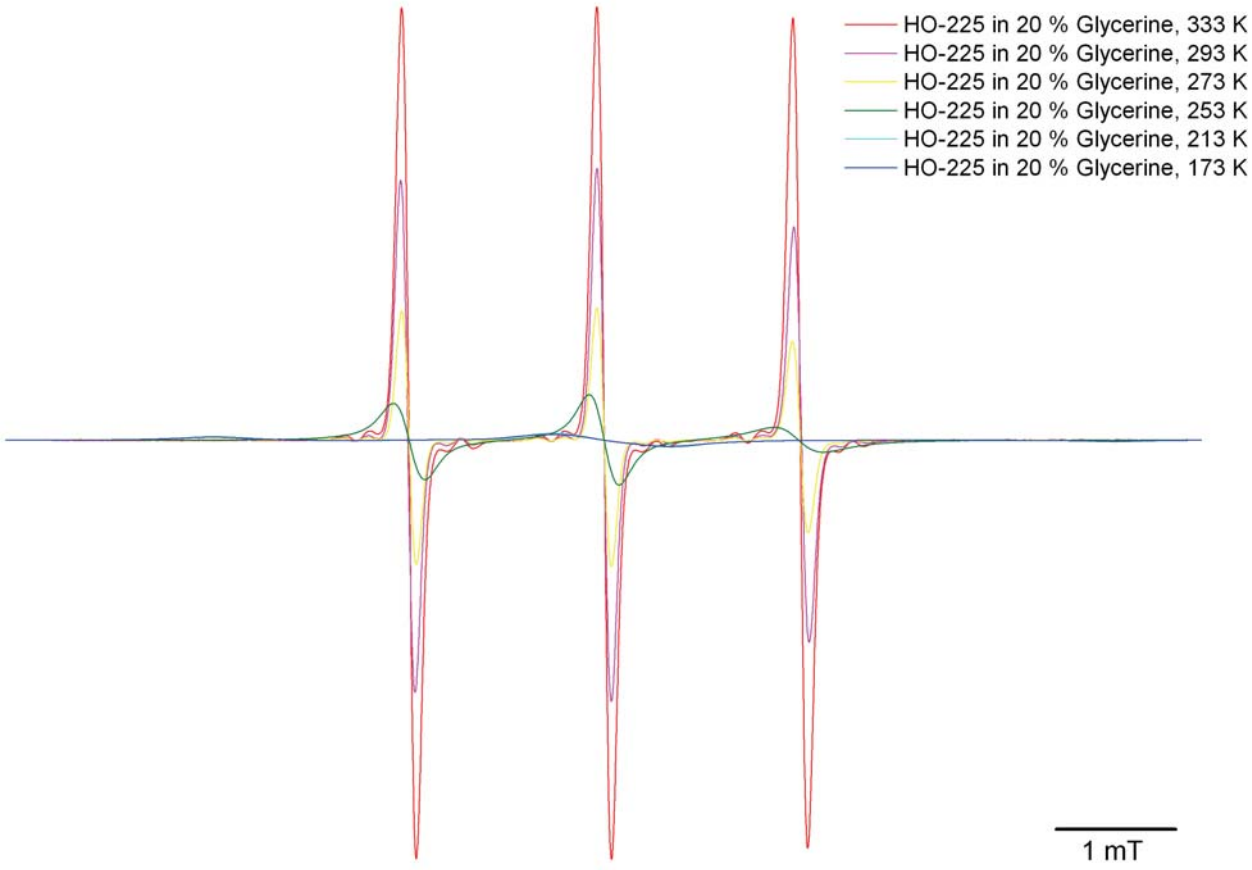

Fig. 16: *Free spin label MTSSL (= HO-225, see Fig. 15) in water (+ 20 % Glycerol) at different temperatures to illustrate the change in the line shape. At lower temperatures the line shape extremely broadens due to the reduced mobility of the spin label.*

The mobility of R1 is strongly modulated by both tertiary interactions in the protein and by local segmental motion. Hence it is possible to determine from mobility alone if the spin labeled site is located on the surface of the protein, in the interior, at a tertiary contact site, or in a flexible loop [Oh et al., 2000].

The time resolution for changes in mobility is in the millisecond time scale.

The value for mobility is the *scaled mobility* M_S, which is calculated from the linewidth of the central resonance δ as follows:

$$M_S = \frac{\delta^{-1} - \delta_i^{-1}}{\delta_m^{-1} - \delta_i^{-1}} \qquad \text{(XVIII)}$$

(δ: linewidth of central resonance; δ_m: linewidth of R1 at the most mobilized site; δ_i: linewidth of R1 at the most immobilized site)

This method has been used to detect the conformational changes in rhodopsin, which are described in chapter 1.1.4 [Hubbell et al., 2003; Hubbell et al., 2000]. These changes have been shown to coincide with activation of rhodopsin [Farahbakhsh et al., 1993].

1.3.6 Other applications of SDSL

Besides the here described application, SDSL is a powerful method with a huge variety of possibilities:

1. It is possible to conclude the solvent accessibility from the collision frequency of the nitroxide side chain with paramagnetic reagents in solution (usually O_2 and NiEDDA = Ni(II)ethylenediaminediacetic acid). This is usually done by progressive power saturation [Oh et al., 2000]. A change in solvent accessibility for a given site can also be used to detect changes in protein conformations.
2. The distance between two nitroxide side chains (or a nitroxide and a paramagnetic metal ion) can be measured by means of the interactions between these two residues [Altenbach et al., 2001c]. This measured value can also be used do detect conformational changes or the binding of other proteins (e.g. transducin).
3. Electrostatic potentials at biological surfaces (e.g. membranes) can be determined from the collision frequency of a charged nitroxide in solution with a nitroxide which is fixed on the point of interest [Shin and Hubbell, 1992].
4. Considering the solvent accessibility and side chain mobility (see chapter 1.3.5) for many different sites, it is even possible to determine the static structure of a protein [Humphries, 1982].

1.4 FTIR spectroscopy

1.4.1 Classical Infrared Spectroscopy

Infrared (IR) spectroscopy is the absorption spectroscopy with infrared light at wavelenghts between 2.5 und 250 μm. In this region – different from UV/visible spectroscopy – no electronic transitions occur due to the lower energy of infrared light (about 400 $\frac{kJ}{mol}$ would be necessary for this), but only molecular vibrations with an energy of 40 $\frac{kJ}{mol}$ and molecular rotations with an energy of 4 $\frac{kJ}{mol}$ are observable. Both intra- and intermolecular vibrations can be detected, if the dipolar moment of the molecule or molecule part is changed.

Instead of the wavelength the reciprocal wavenumber $\tilde{\nu}$, which is proportional to the energy (the unit is $\frac{1}{cm}$), is shown on the abscissa of an IR spectrum. On the ordinate of the spectrum the transmission is shown.

The energy can be calculated from the wavenumber as follows:

$$E = h \cdot \nu = h \cdot \frac{c}{\lambda} = h \cdot c \cdot \tilde{\nu} \qquad \text{(XIX)}$$

(h: Planck constant, ν: frequency, c: speed of light in vacuum, λ: wavelength)

Excitation is observable, if the molecule is excited from one vibrational state into a higher one through uptake of a photon. The energy difference of this excitation must be equal to the energy of the absorbed photon:

$$\Delta E = E_{i+1} - E_i = h \cdot \nu \qquad \text{(XX)}$$

(ΔE: energy difference, E_{i+1}: energy of the higher excited state, E_i: energy of the ground state)

Normally, excitation into the higher excited state follows the selection rules. The transition into other not favoured higher excited states is possible, but less probable.

In classical IR spectroscopy, light emitted by an IR light source (usually oxides or siliciumcarbide) is filtered through a monochromator (usually a lattice or a prism) to obtain the desired wavelengths before it passes trough the sample.

Absorption can be described with the LAMBERT-BEER law:

$$I = I_0 \cdot 10^{-\varepsilon \cdot c \cdot d} \qquad \text{(XXI)}$$

(I_0: input intensity, I: output intensity, ε: extinction coefficient, c: concentration: d: layer thickness)

There are different kinds of molecular vibrations: *Valence* or *stretching vibrations* change the length of a chemical bond. *Deformation* or *bending vibrations* are those vibrations with a remaining bond length but a change in the bond angle. Both vibrations can be either symmetrical

or asymmetrical. Many chemical groups can be excited into stretching and bending vibrations. Therefore several absorption bands for the same chemical group are possible.

For the optics in IR spectroscopy no conventional glass can be used, because it absorbs IR radiation. Mineral salts such as NaCl, KBr, NaF, BaF_2 or CaF_2 are usually used instead. After transition through the sample the transmitted light is detected. This is usually done with a semiconductor diode which needs to be cooled down to liquid nitrogen temperature.

1.4.2 Fourier-transform Infrared Spectroscopy

Today usually Fourier-transform Infrared Spectrosopy (FTIR) is used. Instead of changing the wavelengths with a monochromator, which is slow, all frequencies are measured simultaneously. They can then be stripped down using the mathematical technique of Fourier-transformation and the spectrum does not differ from that one obtains with a monochromator. The FTIR technique is much faster and has a better spectral resolution than the classical IR spectroscopy.

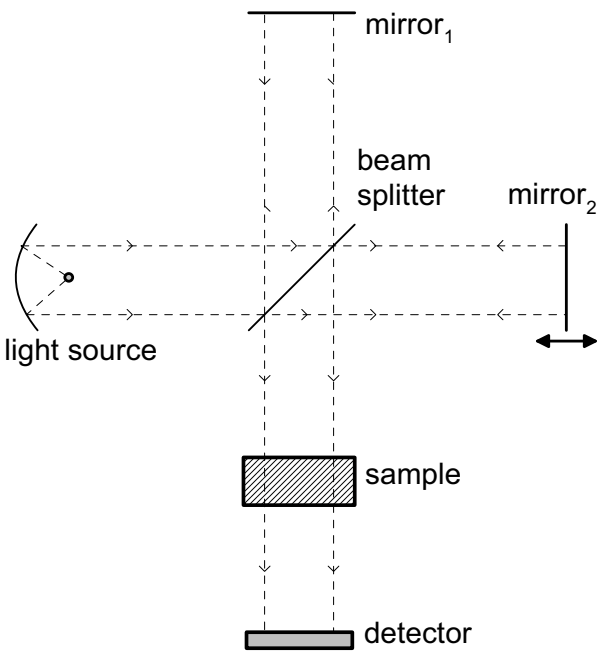

Fig. 17: *Scheme of a FTIR spectrometer with a Michelson interferometer. Mirror 1 is fixed, while mirror 2 is moved back and forth to create the interferogram as described in the text.*

The heart of an FTIR spectroscope consists of the Michelson interferometer which is shown schematically in Fig. 17. The IR beam falls onto a beam splitter (usually a semipermeable mirror) and is devided into two equal beams. One beam goes onto a fixed mirror, the other one onto a moving mirror. When both beams are merged again, there is obliterative and strengthening interference due to the changing path length of the beam that is reflected by the moving mirror. The interferogram that is created that way contains all wavelenghts in parallel.

To extract the single wavelenghts in order to recreate the classical IR spectrum (see 1.4.1), a Fourier transformation is performed. The intensity of the interferogram can be described as follows:

$$I(x) = \int_R I(\tilde{\nu}) \cdot \cos(2\pi\tilde{\nu}x) \cdot d\tilde{\nu} \qquad \text{(XXII)}$$

(I(x): intensity in dependence of the mirror position, R: range, x: mirror position, $\tilde{\nu}$:wavenumber)

The Fourier cosinus transition can be performed as follows and results in the IR spectrum:

$$I(\tilde{\nu}) = \int_{-\infty}^{\infty} I(x) \cdot D(\tilde{\nu}) \cdot \exp(i2\pi\tilde{\nu}x) \cdot dx \qquad \text{(XXIII)}$$

1.4.3 Difference spectroscopy

IR spectroscopic differences on rhodopsin upon light activation are very small and hard to interpret. Therefore one usually uses difference spectra, which only show the changes between the dark and the illuminated state. Those show that vibrations are stimulated in addition (positive peaks) or discontinued (negative peaks), respectively.

For rhodopsin experiments the spectrum of the dark state is usually subtracted from the spectrum of the illuminated state. A typical difference spectrum of the Meta-II state is shown in Fig. 19. The interesting range for rhodopsin experiments is between 1800 cm^{-1} und 900 cm^{-1}. The difference spectra are interpreted according to [Siebert, 1995]. Table 2 shows a composition of the most important IR-sensitive ranges.

Wavenumber [cm^{-1}]	Functional group(s)	Vibration
1780 - 1700	C = O (protein)	Stretching of protonated carboxyl groups
1700 - 1620	Amid-I (protein)	C = O -stretching
1657	C = N (protein-retinal)	Stretching vibration of the Schiff base
1570 - 1500	Amid-II (protein)	C = O -stretching
1570 - 1500	C = C (retinal)	Stretching of the double bonds in the retinal
1300 - 1050	C – C, CH (retinal)	C – C -stretching und CH-binding vibration
< 1000	C = C (retinal)	HOOP vibration (hydrogen-out-of-plane)

Table 2: *Important ranges for FTIR spectroscopy on rhodopsin [Siebert, 1995].*

1.4.4 Time resolved FTIR spectroscopy

Because of the fast movement of the mirror an acquisition of spectra with a time delay of about 100 ms is possible.

As this time resolution is usually not high enough, modern FTIR spectrometers offer a function called step-scan: The wavelength is fixed at a certain position where one expects a change. Upon light activation with a laser one can follow the time resolved change of IR absorption at this position.

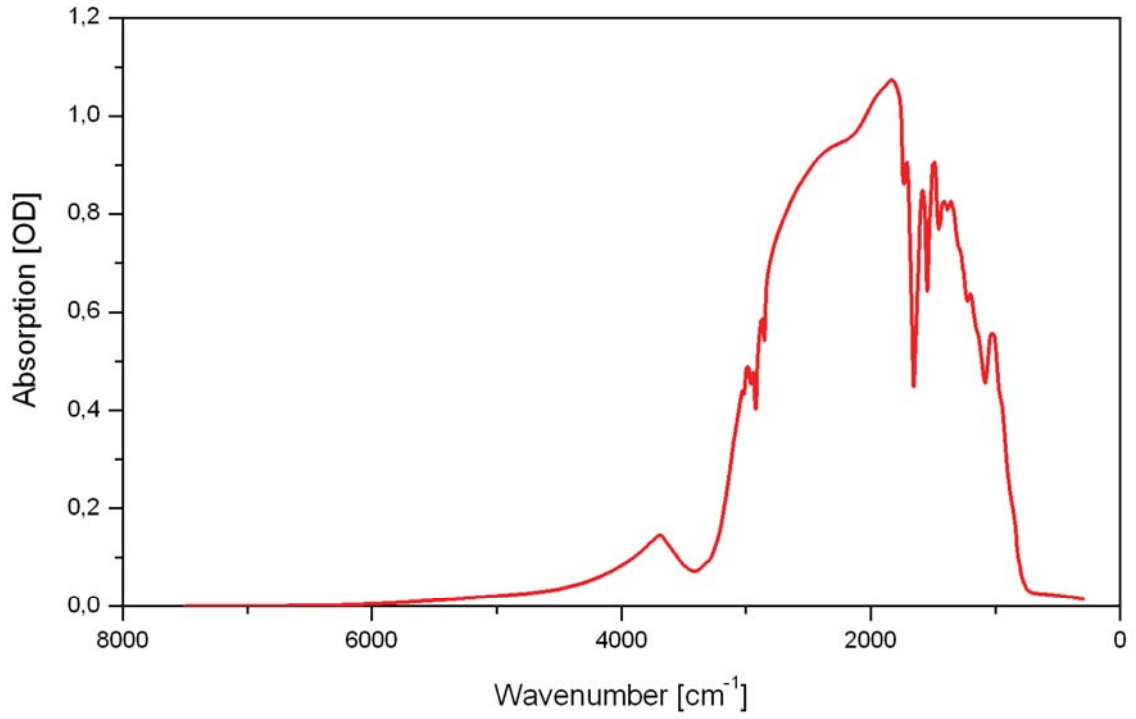

Fig. 18: *Pure IR spectrum (one channel) of rhodopsin*

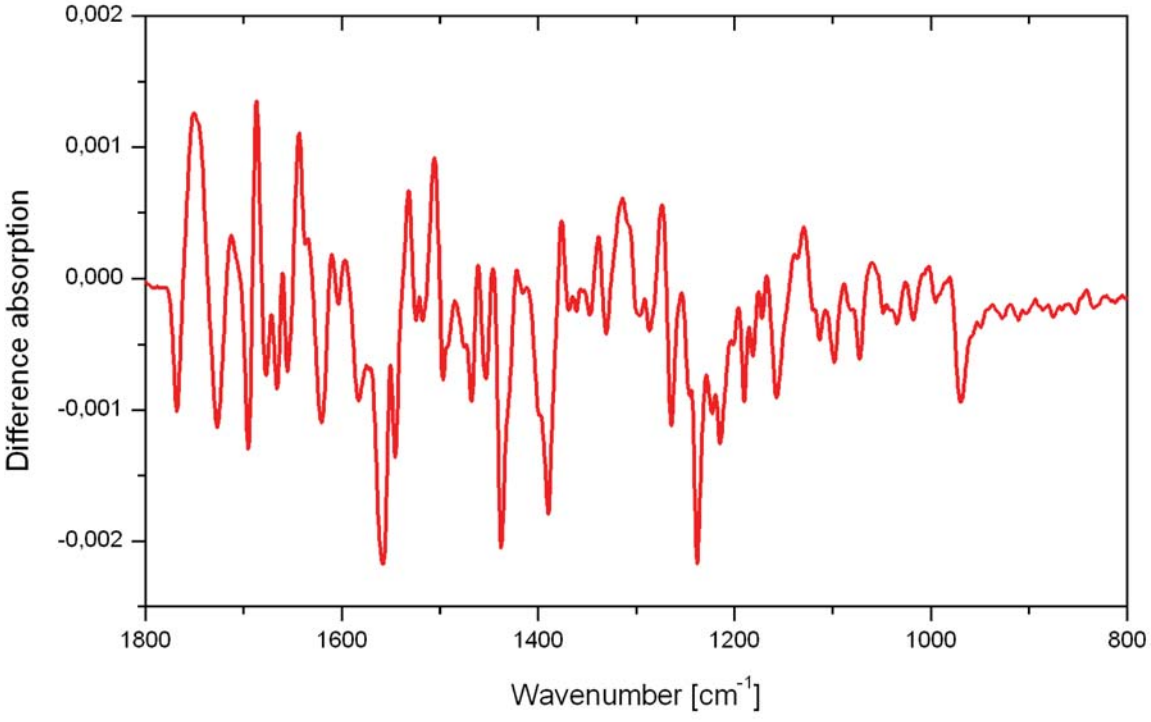

Fig. 19: *IR difference spectrum of rhodopsin activation into Meta-II (light minus dark).*

1.5 Aims of this work

The current state of research on the activation of rhodopsin has been presented above (see chapter 1.1.4). Particularly it has been shown that both a proton uptake and the motion of TM6 are involved in activation, without knowing the sequence of these and other activation steps. The aim of this work is to get further insight into the activation mechanism.
First I want to answer the question how the different activation steps are interconnected and in which causal relationship the late activation steps stand to each other. The second question is how these activation steps work in detail and how the different protein regions are involved. I especially focus my work on the highly conserved D(E)RY region. Further foci are the NPxxY$(x)_{5,6}$F region, the formation of Metarhodopsin-III, the binding of the G protein G_t to rhodopsin and the lipid environment. Finally, I present a model for the complex activation process leading from the extremely stable rhodopsin dark state to the highly G_t-active receptor state.

This doctoral thesis is structured as follows: Chapter 2 (page 47 ff.) describes the methods that were used. Chapter 3 (page 67 ff.) presents the pure experimental results, starting with the sequence of the activation steps (chapter 3.1, page 67 ff.) followed by a detailed examination of the D(E)RY region (chapter 3.2, page 78 ff.) and other rhodopsin regions that are important for activation (chapter 3.3, page 87 ff.). Furthermore, some experiments on rhodopsin with partial agonists are presented (chapter 3.4, page 94 ff.). The formation of Metarhodopsin-III and rhodopsin ground state upon illumination with blue light is investigated (chapter 3.5, page 96 ff.), followed by the examination of G_t binding to rhodopsin (chapters 3.6 and 3.7, page 109 ff.). Recent results on the involvement of lipids in the activation mechanism are presented (chapter 3.8, page 124 ff.).
In chapter 4 (page 131 ff.) the experimental results are discussed and interconnected, starting with the sequence of the activation steps (chapter 4.1, page 131 ff.). Thereafter, the regions which are important for activation, namely the D(E)RY motif, the NPxxY$(x)_{5,6}$F motif and connecting amino acids are discussed (chapter 4.2, page 135 ff.), followed by the mechanism of G_t activation (chapter 4.3, page 153 ff.). Finally, the importance of the lipid environment is investigated (chapter 4.4, page 160 ff.). The thesis closes with the attempt of deriving a coherent activation scheme for rhodopsin (chapter 4.5, page 168 ff.).

2 Methods and applications

2.1 Sample production

2.1.1 Rod outer segments (ROS)

Rod outer segments (ROS) were extracted from frozen bovine retinas following the protocol of PAPERMASTER and DREYER [Papermaster and Dreyer, 1974] and considering the modifications of MCDOWELL and KÜHN [Kuhn and Wilden, 1982]. Unless noted differently, all steps were carried out under red light and at 4 °C.

Bovine retinae were thawed and solvated in KB buffer (70 mM Potassiumphosphate, pH 6.0, 1 mM MgOAc, 0.1 mM PMSF, and 5 mM Mercaptoethanol freshly added) containing 30 % sucrose (conc.: 0.6 ml/retina). To break the ROS off the retina, the solution was vortexed for several minutes. Then the homogenate was centrifuged (6 min at 5,000 rpm), and the supernatant was set aside. The remaining pellet was reextracted in the same way with the same buffer.

The two supernatants were then put together, and 1 volume of KB buffer without sucrose was added carefully while stirring to prevent lysis of the ROS. The crude ROS were pelleted (10 min at 10,000 rpm, SW-28 rotor) and resuspended to 0.5 ml/retina in KB buffer containing 15 % sucrose. The solution was homogenized copiously. After that, 12.5 ml each of the solution were underplayed with a cushion of 0.64 M sucrose in KB and centrifuged (10 min at 10,000 rpm, SW-28 rotor). The pellet was again resuspended and homogenized to 0.4-0.45 ml/retina in 0.64 ml sucrose in KB and then loaded onto a sucrose step gradient with one third each of 0.78 M, 1 M and 1.2 M sucrose in KB buffer. The step gradient was centrifuged (30 min at 25,000 rpm, SW-28 rotor) and the purified ROS fraction was removed from the layer between 0.78 M and 1 M sucrose. This fraction was then diluted in 3 volumes of KB and sedimented again (30 min at 20,000 rpm, SW-28 rotor). The pellet was again resuspended.

2.1.2 Washed membranes (WMs)

To produce washed membranes devoid of peripheral proteins, the ROS were then washed three times with urea solution following the method of SHICHI and SOMERS [Shichi and Somers, 1978]: The ROS were first diluted in 4 M urea, 70 mM $NaPO_4$, and 10 mM EDTA to a concentration of 0.2 - 0.5 mg rhodopsin per ml. Then they were pelleted again (30 min at 40,000 rpm, SW-28 rotor). After three of these wash steps, the ROS were washed four times in KB buffer to

remove all urea. The concentration of rhodopsin was determined by UV/vis analysis (ε_{Rho} = 42,700 $M^{-1}cm^{-1}$ at 498 nm [Ernst et al., 2007]). ROS solutions were stored at -80 °C.

2.1.3 Rhodopsin mutants

For the experiments different rhodopsin mutants were studied. The purified mutants were provided by HELENA SEIBEL, CHRISTINE KOCH and JANA ENGELMANN (IMPB).

Mutants are labeled with the original amino acid, the position and the replacement amino acid. X1Y means that amino acid X at position 1 is replaced by amino acid Y. In those mutants used for SDSL, reactive Cys^{140} and Cys^{316} were replaced by serine. Sites for spin label attachment were created by the V227C or V250C mutation, respectively.

The list of mutants and amino acid substitutions is given in Table 3.

Purified rhodopsin mutants were prepared in a degassed 10 mM BTP buffer (pH 6.0) with a concentration of 0.03 % DM as detergent. Briefly, COS cells expressing rhodopsin were harvested from the tissue culture flasks (850 cm² roller flasks) with PBS and 0.2 Vol.% EDTA and a complete protease inhibitor cocktail tablet (Roche). Retinal dissolved in ethanol was added to the cells to a concentration of 30 µM and the mixture was incubated for 4 - 6 h on a nutator. DM was added to a concentration of 1 %, and after 4 h incubation the cell debris was removed by centrifugation.

The supernatant was mixed with washed 1D4 sepharose resin (approx. 1 µg rhodopsin per µl resin binding capacity). The mixture was incubated over night and then the resin was washed twice with PBS and 0.03 % DM. The resin was then washed with 5 mM MES, pH 6.0 including 0.03 % DM and diluted up to 30 to 50 ml with the same buffer.

For mutants used with SDSL, the spinlabel (MTSL, purchased from Toronto Research Chemicals and dissolved to a 50 mM solution in acetonitrile) was added to the solution to a final concentration of 100 µM. After a 3 h incubation at room temperature on a nutator, the resin was spun down and the supernatant was discarded. The resin was washed four times with 5 mM MES, pH 6.0, 0.03 % DM and three times with 5 mM BTP, pH 6.0, 0.03 % DM. For elution, 10 mM BTP buffer (pH 6.0) with 0.03 % DM and 100 µM 1D4-peptide (equivalent to amino acids 330-348 of rhodopsin) was used. Rhodopsin was eluted three times with 1000 µl, 800 µl and 500 µl and stored at -30 °C.

For EPR measurements, samples were concentrated to 40 - 80 µM using Microcon™ filters (30 kDa exclusion size).

For measurements at different pHs, the pH was adjusted directly prior to the experiment by addition of a 100 mM BTP solution (pH 7.5 and pH 5.0, respectively).

Mutant	Amino acid substitution(s)
D83N (HB1)	D83N
D83N/ E134Q (HB1H)	D83N + E134Q
N73D (XB1)	N73D
N73A (XB3)	N73A
E113Q (HC6)	E113Q
E113A (HC16)	E113A
E122A (HC9)	E122A
E112A/E134Q (HC9H)	E122A + E134Q
E134R/R135E (HC3)	E134R + R135E (“charge reversal”)
E134Q (HC4)	E134Q
R135K (XC1)	R135K
R135L (XC2)	R135L
R135K/E134Q (XC3)	E134Q + R135K
R135K/E247Q (XC4)	R135K + E247Q
R135K/E247A (XC5)	R135K + E247A
R134R/R135E/V227C (MC20)	R134R + R135 E + C140S + V227C + C316S
R135K/V227C (MC21)	R135K + C140S + V227C + C316S
R135L/V227C (MC22)	R135L + C140S + V227C + C316S
V227C (MC11)	C140S + V227C + C316S
H211F (XE1)	H211F
E247Q (XF2)	E247Q
E249Q (XF3)	E249Q
V250Y (XF4)	V250Y
E247A (XF7)	E247A
E249A (XF8)	E249A
Y306A (FM2)	Y306A
P303A (FM3)	P303A
N302A (FM4)	N302A
F313A (FM6)	F313A
AA310-321 β_2-AR (CTr2)	aa 310-321 replaced with β_2-adren. receptor sequence (see Table 6)
AA310-312 β_2-AR (CTr4)	aa 310-312 replaced with β_2-adren. receptor sequence (see Table 6)
AA307-321 β_2-AR (CTr6)	aa 307-321 replaced with β_2-adren. receptor sequence (see Table 6)

Table 3: *Rhodopsin mutants used in this study.*

2.1.4 Retinal analogs

Two different modified retinals either lacking the 9-methyl group (9-demethyl-11-*cis*-retinal) or lacking half of the β-ionone ring (diethyl-acyclic-9-*cis*-retinal) were used in this study. Both act as partial agonists and therewith shift the equilibrium between Meta-I and Meta-II towards Meta-I [Bartl et al., 2005; Jäger et al., 1994b; Meyer et al., 2000]. The chemical structures are shown below.

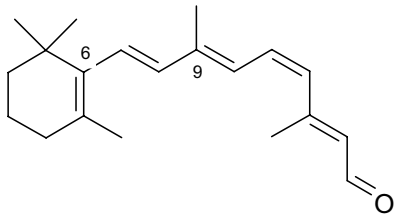

Fig. 20: *11*-cis-*retinal (native chromophore).*

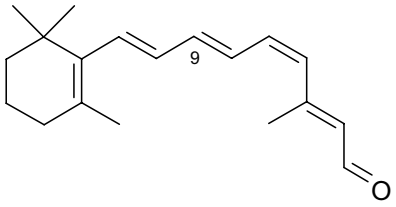

Fig. 21: *9-demethyl-11*-cis-*retinal (9-dm-retinal).*

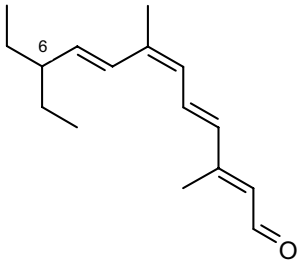

Fig. 22: *Diethyl-acyclic-9*-cis-*retinal (acyclic retinal)*

The chromophore analogs were added to the COS-1 cells in the same way as the 11-*cis* retinal (described in chapter 2.1.3) but usually incubated for a longer time because of the slower binding kinetics.

2.1.5 Bacteriorhodopsin

Bacteriorhodopsin was used in this study mainly to test and align the experimental setup for the time-resolved measurements. It was extracted from cultures of *Halobacterium halobium* following the instructions of OESTERHELT and STOECKENIUS [Oesterhelt and Stoeckenius, 1974].

Halobacterium halobium was grown in a media of 4.28 M NaCl, 81.1 mM $MgSO_4$ (anhydrous), 26.8 mM KCl, 93.5 mM NH_4Cl, 10.2 mM sodium citrate · 2 H_2O, 0.1 Vol. % glycerol; 0.735 mM KH_2PO_4, 1.4 mM $CaCl_2$ (anhydrous), and 10 g/l bacteriological peptone. Reagents were added in the order above and always dissolved completely before adding the next reagent. The pH was adjusted to 7.2 and the media autoclaved (20 min at 121.1 °C, AOP cycle).

First, a preculture was grown on an agar plate containing media described above and 15 g/l agar noble. The frozen culture of *Halobacterium halobium* was defrosted, and 3 drops were diluted with 100 µl of autoclaved 4 M NaCl. Then the culture was streaked out onto a plate with a sterilized loop. The plates were then stored upside down and taped for sealing. The cultures were grown in a 40 °C incubator for about two weeks.

The large-scale cultures were then grown in 2 l flasks as follows: A colony was picked from the plates and put into 10 ml of broth. This was then added to the flasks with 2 l of autoclaved media. The flasks were kept in an incubator at 40 °C while shaking them permanently. The growing was followed by daily UV/vis analysis (the amount of bR is visible at 570 nm wavelength), and after 5 days there was no more growth of the culture and it was harvested.

The cells were collected by centrifugation (10-15 min at 5000 rpm). The supernatant was discarded, and the cells were scraped out with a rubber policeman. The remaining cells were rinsed out with distilled water, and after that the total volume was brought up to 500 ml with distilled water. This lyses the membrane and the cell wall, because the bacteria are halophiles. Then 0.075 g DNAse I type IV and 4.2 mM $MgSO_4$ (anhydrous) were added, and the solution was stirred gently overnight.

After that the cell debris was spun down again (10 min at 5000 rpm), and the supernatant was kept. The pellet containing the cell debris was discarded. The purple membranes were concentrated by spinning them down (30 min at 32,000 rpm) and saving the purple part of the pellet (the white part containing other proteins was discarded). The pellet was resuspended in a buffer of 20 mM MES and 100 mM NaCl (pH 6.0) using a Pasteur pipette. This was repeated three times to wash out other proteins.

The concentration of bacteriorhodopsin was determined by UV/vis analysis ($\varepsilon_{BR} = 63{,}000\ M^{-1}cm^{-1}$).

Spin labeling of the purple membranes was performed as described in 2.2.1.

In these studies mutant V101C was used, which binds a single spin label at position 101.

2.2 Sample preparation

Sample preparation for rhodopsin was done under dim red light conditions ($\lambda_{max} > 660$ nm), to make sure that rhodopsin remains in its ground state.

2.2.1 Spin labeling

The spin labeling for bacteriorhodopsin and wild type rhodopsin was done by adding the spin label (MTSSL, see Fig. 15) in acetonitrile solution in a three to ten fold excess compared to the protein. The pH was always held close to 6.0 for spin labeling. This solution was stored on a nutator at room temperature for several hours, after which the free spin label was removed by four centrifugation (30 min at 35,000 rpm) and resuspension cycles. After the last washing step, the sample was concentrated to a final concentration of about 400 μM.

2.2.2 Selective spin labeling of Cys^{316}

The following reaction was performed in a buffer of 100 mM MOPS and 100 mM NaCl at pH 6.7. The initial concentration of urea-washed rhodopsin was 10 µM.

The labeling kinetics of 4,4'-PDS are shown in Fig. 24. 5 µM rhodopsin in urea-washed membranes was labelled with 950 µM 4,4'-PDS, and the reaction was examined in a Olis DW-2 absorption spectrometer. The reaction of the 4,4'-PDS with Rhodopsin can be followed by an absorption peak at 324 nm corresponding to 4-thiopyridone which is the side product of the labeling reaction (Fig. 25). The kinetics clearly show two components, most likely corresponding to two Cysteines in rhodopsin being labeled. The half lifetimes of the two components are 1.2 and 17 min, respectively. This corresponds to the rates determined by YONG SHIAU CHEN [Chen and Hubbell, 1978].

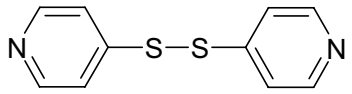

Fig. 23: *4,4'-dithiopyridine (4,4'-PDS)*

For selective labeling, first 4,4'-PDS was added to the sample to a final concentration of 950 µM and incubated for 8 min. According to the kinetics measured above this should result in a labeling of 27.8 % at Cys^{140} and 99.0 % of Cys^{316}. This reaction was again monitored absorption spectroscopically using the absorption at 324 nm as explained above.

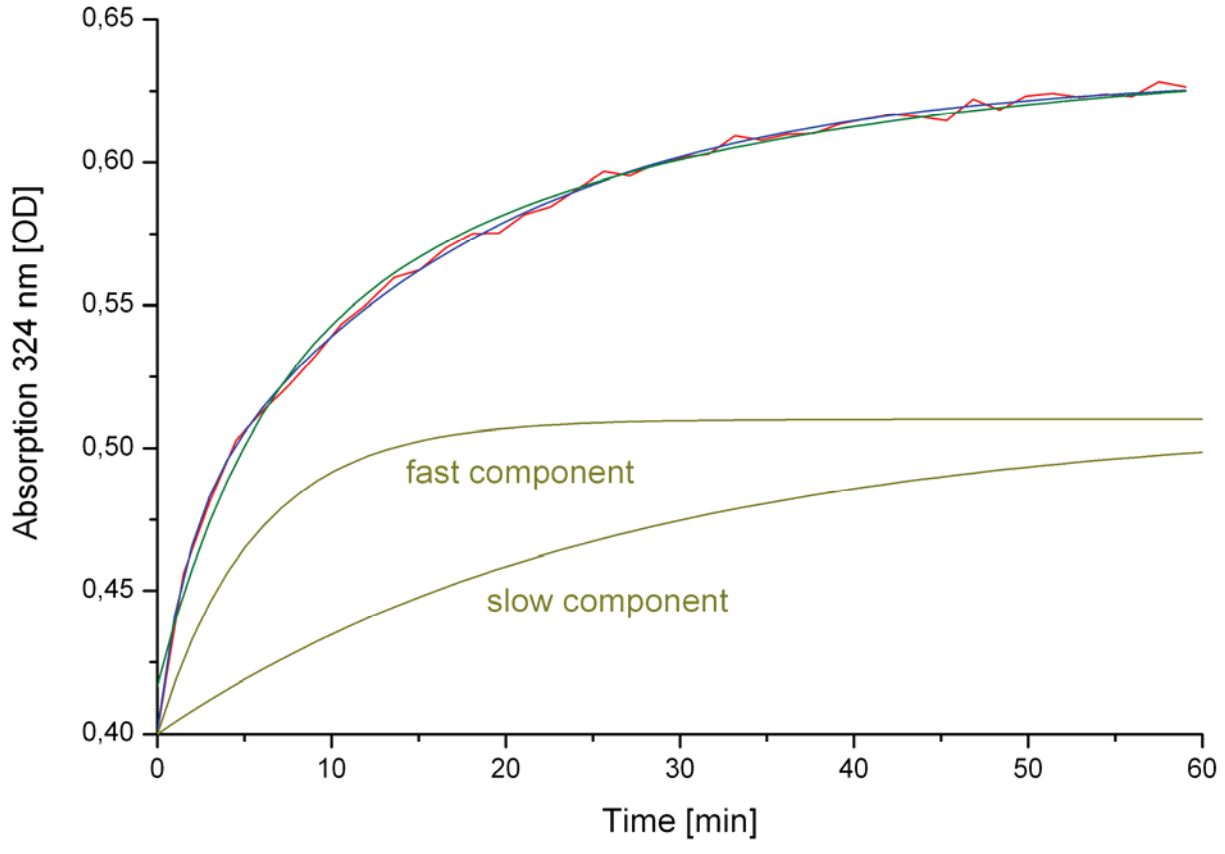

Fig. 24: *Reaction of 4,4'-PDS with a Cysteine side chain.*

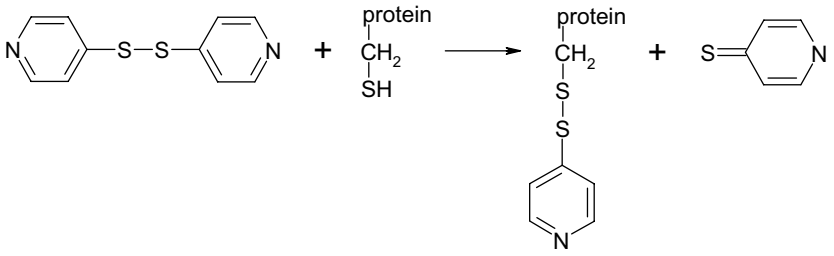

Fig. 25: *Reaction of 4,4'-PDS with a Cysteine side chain. The side product, 4-thiopyridone, has an absorption of λ_{max} = 324 nm enabling absorption spectroscopic control.*

After the labeling time, the sample was diluted with 25 ml of the same buffer at ice temperature and pH 6.0 to stop the reaction. The sample was then spun down 15 min at 20,000 rpm and washed with buffer three times.

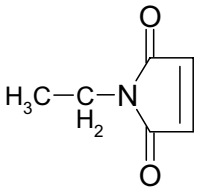

Fig. 26: *N-ethylmaleimide (NEM).*

Then the PDS-labeled rhodopsin was labelled with N-Ethylmaleimide in a 10fold excess for 8 h. This reaction induces a covalent bond with sulfhydryl bonds forming a thioether and thereby labels all the unlabeled Cys[140] (the product is S-(N-ethylsuccinimido)-L-cysteine [Smyth et al., 1960]). Then the sample was again spun down 15 min at 20,000 rpm and washed with buffer three times to remove all excess ethylmaleimide.

After that Dithiothretiol (DTT) was added to the sample to cleave the 4-thiopyridone from the Cys[316]. DTT cleaves only the 4-pyridone, but not the N-ethylmaleimide. DTT was incubated with the sample for 1 h, and the cleavage reaction was again followed using the 324 nm absorption peak which determines the amount of cleaved 4-thiopyridone.

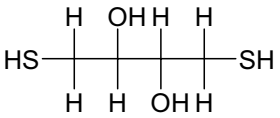

Fig. 27: *Dithiothreitol (DTT).*

The DTT was washed off carefully to ensure that there is no significant amount of DTT present during the spin labeling reaction. The membranes were washed 5 times with the same buffer and spun down 15 min at 40,000 rpm.

Then spin label MTSSL (see section 2.2.1) was added to the sample in a 10fold excess and incubated over night. This should result in a labling of the free Cys[316] close to 100 %. The spin label was washed off by 5 more washing steps with buffer A.

2.2.3 Selective spin labeling of Cys[140]

The protocol to label Cys[140] selectively is similar to the protocol for the selective labeling of Cys[316] (see section 2.2.2): After labeling with 4,4'-PDS the sample is not labeled with N-Ethylmaleimide but directly with the spinlabel instead. After that the spin label is washed off by 5 washing steps with the same buffer A. The pyridone is left on the sample.

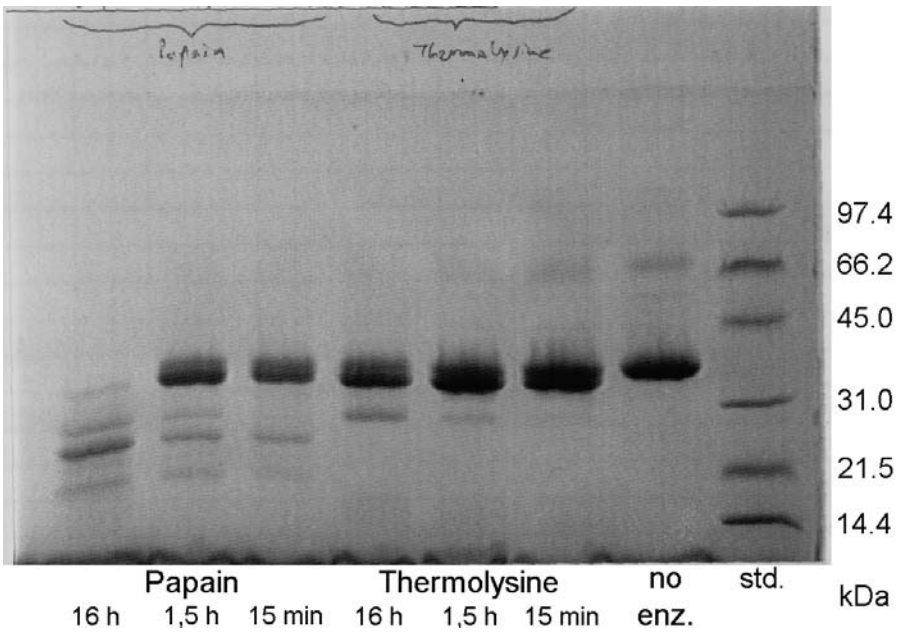

Fig. 28: *Typical rhodopsin cleavage experiment: rhodopsin was incubated with papain and thermolysine, respectively, for 15 min, 1.5 hours and 16 hours. Cleavage into two parts is already visible after 15 min; after longer times cleavage into more smaller parts takes place.*

2.2.4 Analysis of selective spin labeling

To make sure that Rhodopsin is really labelled in the right way rhodopsin was cleaved using papain and thermolysin (Calbiochem Corp.; LaJolla, CA, USA). The buffer used for papain was 10 mM MOPS, 10 mM NaCl, 10 mM cysteine and 1 mM EDTA, pH 7.0. The buffer used for thermolysin was 10 mM MOPS, 10 mM NaCl, 1 mM $CaCl_2$ at pH 7.5. Rhodopsin concentration was 35 µM with 0,22 µM papain or 1,3 µM thermolysin, respectively. A typical experiment comparing both enzymes is shown in Fig. 28. After 15 min incubation, rhodopsin is already cleaved into two parts: helix 8 including the C-terminus and the rest of the protein (thermolysin cleaves between residues 240 and 241 and cuts some smaller pieces from the C-terminus [Findlay et al., 1984; Papac et al., 1992]). Thus the smaller part contains Cys^{316} while the larger part contains Cys^{140}. The cleavage reaction was stopped with addition of EDTA or iodacetamide, respectively.

The cleavage reaction can be performed in the same way while rhodopsin is bound to a ConA column. Upon illumination the cleaved small part with helix 8 comes off, and the large part can be eluted with methyl-α-D-mannopyranoside. Then both parts can be seperately measured in the EPR spectrometer and the amount of spin labeling can be quantified.

2.2.5 Fluorescence labeling

For time resolved fluorescence experiments, labeling was performed similar to spin labeling as described above. The pigment V227C was incubated for three hours with a ten-fold excess of the

fluorescence dye Alexa-594 (purchased from Molecular Probes/Invitrogen, Karslruhe, Germany) while bound to the 1D4 column that was used for purification of the sample.

To label the native cysteine Cys^{316}, the dye was added to the membranes in a 2.5fold excess and incubated for 15 h at room temperature. The reaction was then stopped by addition of 35 µl of 55 mM glutathione and kept on ice to stop the reaction as described before [Imamoto et al., 2000]. After that the labeled pigment was purified as described in 2.2.6. An absorption spectroscopic analysis of the sample ($\varepsilon_{Alexa,\ 594\ nm}$ = 96 000) showed that it was labeled with 1.2 molecules Alexa-594 per rhodopsin molecule, so that one can conclude that only a small part of the molecules was also labeled at position Cys^{140}.

The Alexa dye has been shown before to be pH independent [Imamoto et al., 2000] and is not hydrophobic so that it does not lead to a different hydrophobicity of the sample.

2.2.6 Purification of rhodopsin from ROS

For measurements on wild type rhodopsin (preparation: see 2.1.1) in detergent solution, dodecyl maltoside (DM, stored frozen as a 10 % solution) was used. To make sure that the lipids, which are still present in DM-solubilized ROS solutions, do not influence the rhodopsin activation, these lipids were removed using an immunoaffinity column as follows:

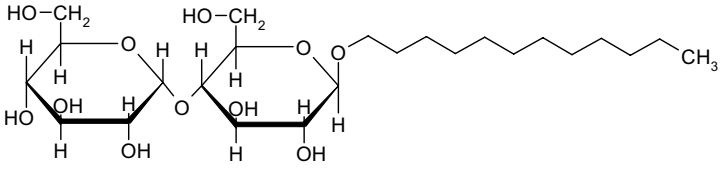

Fig. 29: *Dodecyl maltoside (DM).*

Rhodopsin was spun down (1 h at 100,000 g) and washed in a buffer of 20 mM MES and spun down again twice. Then the sample was added to a ConA resin (2 mg rhodopsin per ml resin) and filled up to 50 ml with a buffer of 20 mM MES and 1 % DM. This was incubated for 2 h. The resin with the bound rhodopsin was then filled into a 10 ml column and washed three times with 20 mM BTP buffer containing 0.03 % DM to remove all lipids.

After that the elution buffer containing 20 mM BTP, 0.03 % DM, and α-D-mannopyranosid was added to the column and incubated overnight. Rhodopsin was eluted from the column in three elutions (8 ml, 5 ml and 3 ml) with the same buffer. After that the elutions were pooled and concentrated up to 600 µM using Microcon™ concentrators (30 kDa exclusion size).

2.2.7 Addition of Peptides to samples

Peptides have been used for a long time in rhodopsin research to mimic certain parts of G_t [Hamm et al., 1988]. The peptides used here either mimic the α or the γ subunits of G_t, partly

Sequence	Function	Amino acid sequence
$G_t\alpha(340\text{-}350)$	native α peptide, [Ern-10]	NH_2-IKENLKDCGLF-COOH
Ac-$G_t\alpha(340\text{-}350)$	acetylated α peptide, [Ern-10-Ac]	Ac-NH-IKENLKDCGLF-COOH
$G_t\alpha(340\text{-}350)$ E342N	α peptide w/o Glutamate [Ern-27]	NH_2-IK**N**NLKDCGLF-COOH
$G_t\alpha(340\text{-}350)$ D346M	α peptide w/o Aspartate [Ern-102]	NH_2-IKENLK**M**CGLF-COOH
$G_t\alpha(340\text{-}350)$ C347S	α peptide w/o Cysteine [Ern-13]	NH_2-IKENLKD**S**GLF-COOH
$G_t\alpha(340\text{-}350)$ K341L	HAα peptide [Ern-87]	NH_2-I**L**ENLKDCGLF-COOH
Ac-$G_t\alpha(340\text{-}350)$ K341L	HAα peptide [Ern-87Ac]	Ac-NH-I**L**ENLKDCGLF-COOH
$G_t\alpha(340\text{-}350)$ HAA	HAα peptide [Ern-4]	NH_2-**VL**E**D**LK**S**CGLF-COOH
$G_t\alpha(340\text{-}350)$ HAA K345A	HAα peptide w/o Lysine [Ern-37]	NH_2-**VL**E**D**L**AS**CGLF-COOH
$G_t\alpha(340\text{-}350)$ HAA C347S	HA α peptide w/o Cysteine [Ern-14]	NH_2-**VL**E**D**LK**SS**GLF-COOH
$G_t\alpha(340\text{-}350)$ HAA C347M	HA α peptide w/o Cysteine [Ern-44]	NH_2-**VL**E**D**LK**SM**GLF-COOH
$G_t\alpha(340\text{-}350)$ C347Abu	α peptide w/o Cysteine [Ern-165]	NH_2-IKENLKD-Abu-GLF-COOH
$G_t\alpha(340\text{-}350)$ HAA K341L/C347Abu	HA α peptide w/o Cysteine [Ern-166]	NH_2-I**L**ENLKD-Abu-GLF-COOH
$G_t\alpha(340\text{-}350)$ L349A	nonbinding α peptide [Ern-101]	NH_2-IKENLKDCG**A**F-COOH
$G_t\gamma(60\text{-}71)$far	native γ-peptide [Ern-6far]	NH_2-DKNPFKELKGGC-$CONH_2$ far
$G_t\gamma(60\text{-}71)$	γ peptide without farnesyl [Ern-78]	NH_2-DKNPFKELKGGC-$CONH_2$

Table 4: *C-terminal peptides derived from $G_t\alpha$ and $G_t\gamma$ used in this study. The amino acids are represented according to their one-letter codes. 'Abu' means amino butyric acid.*

with certain modifications such as farnesylation. The peptides signed 'HAA' have been shown before to have a high affinity towards activated rhodopsin [Martin et al., 1996].

The peptides used in this work are shown in Table 4, the modifications compared to the native G_t sequence marked with fat letters. They were synthesized by PETER HENKLEIN and coworkers at the Institut für Biochemie at Charité Berlin.

Peptides were added to the sample as aqueous solutions of different concentrations. The peptide stock solutions (usually 10 mM) were usually adjusted to a neutral pH by addition of NaOH before using them for experiments.

2.2.8 Addition of lipids to DM samples

To determine the role of certain lipids for the Rhodopsin activation mechanism those lipids were added to solutions of rhodopsin in DM. The lipids used here were phosphatidylserine (PS), phos-

phatidylcholine (PC) and phosphatidylethanolamine, all with palmitoyl acid (P, 16:0) and oleoyl acid (O, 18:1) as side chains. The lipids were purchased from Avanti Polar lipids (Alabaster, Alabama, USA). For preparation of the lipid stock solution the solvent chlorophorm was evaporated and the lipids were dissolved in 0.03 % DM.

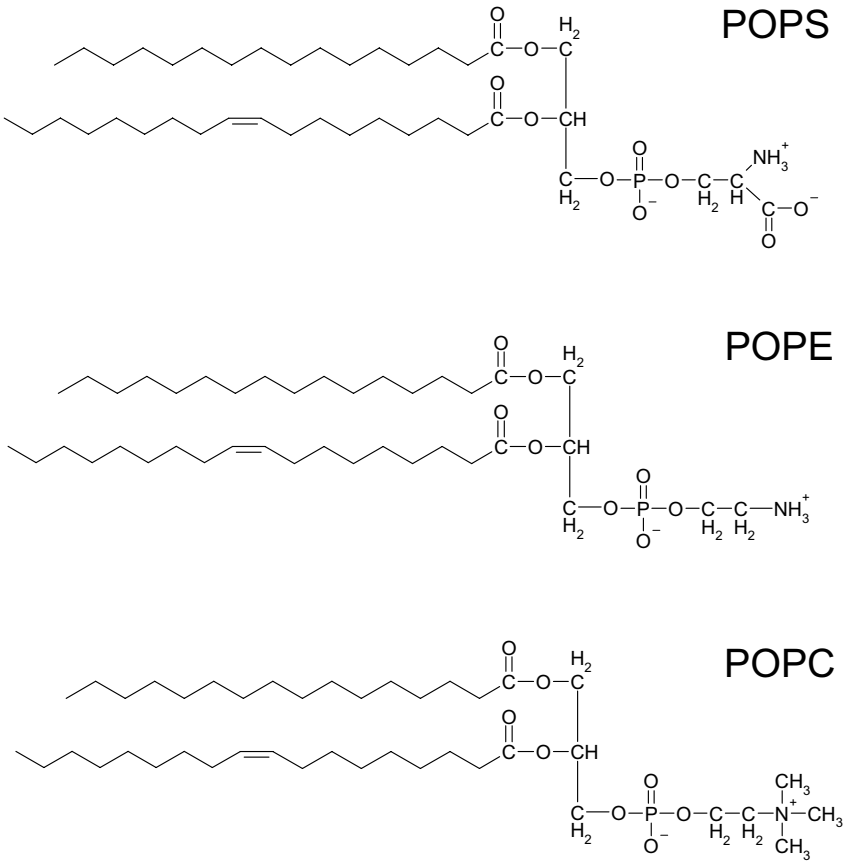

Fig. 30: *Structures of the Phospholipids used in this study.*

Lipids were added to the samples at relatively high concentrations (up to 4 mM). The resulting concentrations of lipids effectively interacting with rhodopsin are probably lower, but this could not be determined.

2.2.9 Cross-linking

For cross-linking salt bridges to form covalent bonds the compound EDC (1-Ethyl-3-[3-dimethylaminopropyl]carbodiimide hydrochloride) was used.

EDC was added to the samples in a concentration of 5 mM with 5 mM Sulfo-NHS, which acts as a catalysator. The reaction was allowed to proceed for 15 min, and then Glycine was added to the samples (100 mM) to stop it. The sample was then

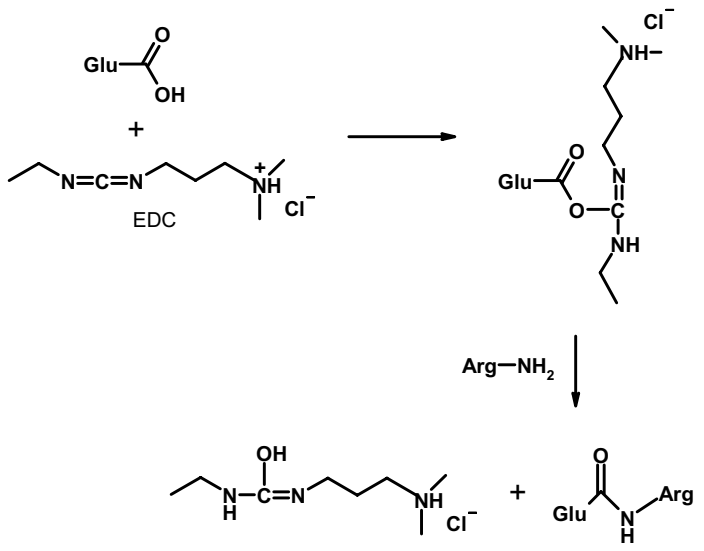

Fig. 31: *The reaction of EDC with a Glutamate and an Arginine residue as examples.*

dialysed for several hours against pure buffer to remove the reaction products. The cross-linking reaction works for carboxyl groups with amino groups. It is shown in Fig. 31 and results in a stable amide bond.

2.2.10 Extraction of retinal and HPLC analysis

To determine the existence of the different retinal isoforms 11-*cis*, 9-*cis*, 7-*cis*, all-*trans* and 13-*cis* retinal in the rhodopsin photoproducts the retinal can be extracted from the sample and then analysed using high performance liquid chromatography (HPLC).

To extract the retinal, the sample is solvated in a high ethanol concentration (25 Vol-%). This leads to degeneration of the protein and thereby solvation of the retinal. The sample has to be vortexed several times and to be kept cold at the same time to avoid thermal isomerization of the extracted retinals.

After that the ethanol solution is mixed thoroughly with heptane, and then centrifuged to separate the heptane layer from the ethanol layer. The retinal sample is then taken from the heptane layer using a syringe and applied to a size exclusion column using a HPLC (HP 1050 Series).

The HPLC runs were performed with heptane and 5 % diethyl ether as medium at 20 to 30 bar. After the size exclusion gel column (LiChrosorb Si 60, 5 µM; Merck, Darmstadt, Germany) the sample runs through a monochromatic spectrometer. Because the different retinals have different retention times they are detected at different elution times. First 13-*cis* retinal is eluted, then 11-*cis*, 9-*cis* and 7-*cis* retinal and at the end all-*trans* retinal followed by a small fraction of retinols. The retention times have to be calibrated using a known mixture of all retinals. Typical chromatograms are shown in Fig. 57.

The area under the curves corresponds to the total amount of the different retinals so that the percentage of each retinal can be calculated if referenced to the total area. Thereby it has to be taken into account that some thermal isomerization between the different retinal isoforms always occurs.

2.3 Measurement technique

2.3.1 Flash photolysis

Flash photolysis was performed on a custom built spectrometer as described in 1.2.3. The usual sample size was 100 µl at a 10 µM concentration in DM or a 5 µM concentration in membranes, respectively. The dye (BCP or CR) was added to a 50 µM concentration. Usually no buffer was present in the samples (see 1.2.1), and the pH was adjusted by carefully adding small amounts of diluted HCl and NaOH (10 mM). After adjustment of the pH the sample was filled into a quartz cuvette, sealed, and the pH was checked again optically using the absorption peaks of the dye.
The experiments were performed automatically as described (see 1.2.3), after adjusting the temperature for 10 minutes. At temperatures below 10 °C dry, temperature adjusted air was blown over the cuvette in order to prevent condensation at the outside of the cuvette.
Samples were illuminated by either a conventional flash with a 480-540 nm dielectric bandpass filter or a laser at 532 nm (for details see 1.2.3). After several flashes the sample was totally bleached using a laser at 543 nm and then illuminated with several blue flashes at 380 – 480 nm (for details see 1.2.3).
The signals were recorded at 380 nm for Meta-II formation and 595 or 575 nm for the dye response. Normal recording times were several ms to s depending on the temperature. In membrane samples the light scattering signal was recorded at 840 nm. If G_t was present in the sample, the light scattering signal was recorded over 100 s to obtain a binding signal.

2.3.2 EPR spectroscopy

EPR measurements were performed on a Bruker E-580 spectrometer. Continuous wave (cw) measurements were made using the X-EPR software. The temperature was controlled by the flow of N_2 gas of the desired temperature and was usually stabilized at 298 K for room temperature or at 310 K for high temperature measurements.
All spectra were measured in X-band using a high-sensitivity resonator with a dewar with nitrogen flow for temperature stabilization manufactured by Bruker. 10 to 20 µl of the sample were filled into a flat cell made of Suprasil™ quartz of approximately 250 µm thickness, which was used for optimizing illumination in the sample. Normally the following EPR parameters were used: 100 G scan width; 10.24 ms time-constant; 4 G modulation at 100 kHz; 10 mW microwave-power; receiver gain 70 to 80 dB.

First a dark spectrum was taken (16 to 32 scans), then the sample was illuminated for approx. 20 s using a halogen light source with a long pass filter (515 nm cutoff), and after that a second spectrum was taken (16 to 32 scans again). A part of the illuminated states was measured as 2D-experiments acquiring 40 single spectra in a row to observe spectral changes after illumination.

2.3.3 Time-resolved Electron Paramagnetic Resonance (EPR)

For time-resolved measurements, samples were concentrated up to 400 - 800 µM, and 20 µl each were filled into the same flat cells used for cw spectroscopy.

As the software of the used spectrometer was not suitable for transient measurements, data acquisition was done using an oscilloscope (LeCroy Waverunner 2). For illumination a tuneable laser (Opotek Vibrant, YAG-Laser with an OPO) was used, which expels single flashes of 10 ns duration and an energy of about 38 mJ (at 500 nm). The wavelength was always adjusted to 500 nm, and the laser light was directly exposed to the sample through a window in the resonator. Coordination of the timing was done using a pulse generator (Berkeley Nucleonics), which gave TTL pulses to the laser flashlamp (at 10 Hz rate permanently), the Q-switch of the laser and the oscilloscope for data acquisition.

Most of the measurements were performed in a newly developed rectangular loop-gap resonator [Piasecki et al., 1998], some experiments were done in a Bruker dielectric resonator and a Bruker high-sensitivity cavity, which had a worse signal-to-noise-ratio but a more reliable temperature stabilization. The EPR-parameters were the same as for the cw measurements (see chapter 2.3.1), but the time-constant was adjusted for each temperature, and the receiver gain was lowered to 50 to 65 dB due to the higher sample concentration.

First a cw spectrum (1 scan) was taken to make sure that the sample was in the right position and to detect the peak positions (see Fig. 32A, black spectrum). Then the field position was usually fixed at the position of the central negative peak (3362 ± 1.5 G for the high-sensitivity cavity, marked with a black arrow and ‘a’ in Fig. 32A) and the sample was illuminated with at least three single laser-shots while the time courses were recorded (Fig. 32B). Usually about 70 % of the sample was bleached by the first shot. After illumination a second cw spectrum was taken to ensure total bleaching (see Fig. 32A, red spectrum).

All time resolved measurements show a huge artefact of approx. 150 µs duration at the time when the laser light hits the cavity (Fig. 32 B, at time 0). The reason for this might be an ionization of air in the resonator. As the artefact is short on the timescale of the transients (ms-range) it was left in the curves.

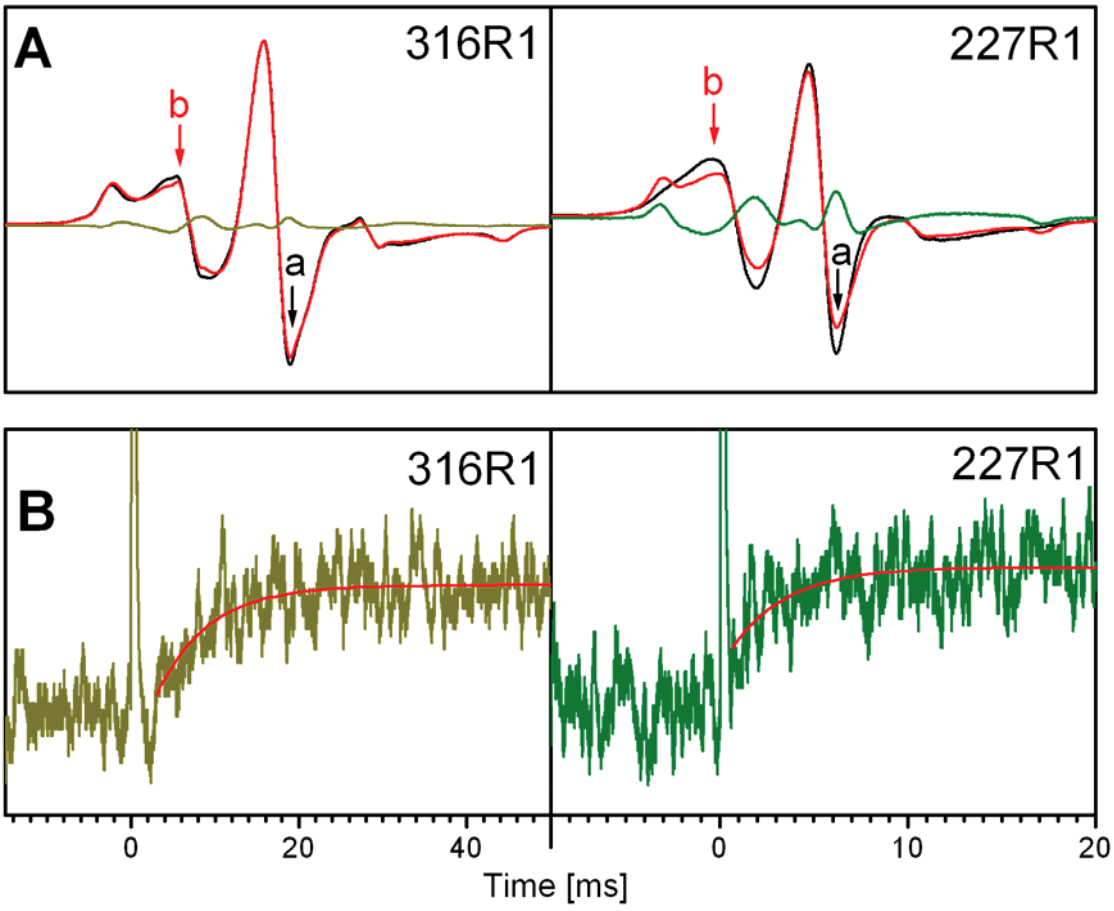

Fig. 32: A *EPR spectra of rhodopsin. Left: The spectrum of the V316R1 dark state (black) reflects a slightly higher mobility of the spin label than in the illuminated state (red). The difference spectrum is shown in yellow, and the two spectral positions used for time resolved experiments are marked with a and b. Right: Spectra of V227R1 in the dark and illuminated state, the difference spectrum shown in green. The mobility of V227R1 is reduced upon light activation of rhodopsin.* **B** *Kinetics of V316R1 (left) and V227R1 (right) EPR changes at 20 °C (both at spectral position a).*

2.3.4 FTIR spectroscopy

FTIR spectroscopy was performed on a Bruker IFS-66 v/S spectrometer. Spectra were measured on transmitted samples, the sample chamber being flooded with dry air to minimize the disturbances by water onto the spectra.

Samples in DM were dried onto BaF_2 windows and then resolvated with 1 µl buffer of the desired pH. The samples were then squeezed with a second BaF_2 window to obtain a final sample thickness of approximately 5 µm. Membranes samples were first centrifuged for 30 min at high speed (60,000 rpm), then the excess solvent was removed, and the membrane pellet was put onto the BaF_2 window and squeezed to approximately 5 µm thickness, too.

Temperature control of the experiments was assured with an ethanol cooling system. Samples were illuminated with a 150 W cold light source that was coupled into the sample chamber via fiber optics. Filters used were 495 nm for 11-*cis* pigments and 475 nm for 9-dm pigments. Illumination time was usually 15 s.

Spectra were recorded using the Opus NT software from Bruker. Usually 32 scans were performed of the dark and the illuminated state, and then the difference spectra were calculated as described (see 1.4.3).

2.3.5 UV/vis absorption spectroscopy

UV/vis spectroscopy (Varian Cary 50, Varian Cary 100) was used for absorption measurements. It was also used for determining the concentration of rhodopsin as well as for final checking of the sample prior to other experiments. Pigments with a protonated Schiff base (in the ground state) show an absorption peak at 498 nm (11-*cis* retinal), 466 nm (9-demethyl retinal) or 459 nm (acyclic retinal), respectively, while pigments with a deprotonated Schiff base (in the MII state) show an absorption peak at 380 nm.

Quartz cuvettes with a sample size of 100 µl and a pathlength of 1 cm were used. Data were recorded with the software belonging to the spectrometer (Cary Win-UV). A scan with pure buffer in the same cuvette was used as baseline, which was automatically subtracted. The wavelength range was usually 250 to 650 nm, and one scan was taken before and one after illumination (20 s with a 515 nm longpass filter or a 475 nm longpass filter for 9-dm retinal). Data were compared and plotted with the software Origin 6.1.

For concentration determination of rhodopsin the extinction coefficient at 498 nm of ε_{Rho} = 42,700 $M^{-1}cm^{-1}$ was used.

2.3.6 Time resolved UV/vis spectroscopy

Time resolved UV/vis spectroscopy was used to determine the reaction kinetics of the different sulfhydryl reagents used for selective spin labeling of rhodopsin (see 2.2.2). An Olis DW-2 Spectrometer was used for this purpose with cuvettes of 1 cm pathlenght and 1 ml sample volume. The sample was excited with a 500 µs flash, and absorption changes were recorded over several minutes (see Fig. 24).

2.3.7 G_t activation measurements

G_t activation measurements were done via fluorescence spectroscopy taking advantage of the intrinsic tryphtophan fluorescence [Farrens and Khorana, 1995]. Measurements were performed

on a Spex Fluorolog 2 spectrometer (Spex Industries, Metuchen, NJ). The fluorescence was excited at 300 nm (3 mm slit), and the emission was measured at 345 nm (4 mm slit).
Protein concentrations in the sample were 2 nM pigment and 250 nM G_t in 20 mM BTP (pH 7.5), 130 mM NaCl, 1 mM $MgCl_2$, and 0.01 % DM in a final volume of 650 µl. Bovine G_t (250 nM) and guanosine 5'-[γ-thio]triphospate (GTP[γS]; 5 µM) were incubated with the sample in a stirring cuvette for 2 min at 20 °C. Then, initial fluorescence intensity was recorded for 1 min, followed by illumination of the pigment through a 150 W halogen light source with a 495 nm filter (GG495, Schott, Mainz, Germany). For determination of the rates of G_t activation, traces were normalized to the fluorescence intensity before illumination, and initial slopes of the first 30 – 60 s of data after illumination were fitted by linear regression. Samples were measured at least in triplicates.

2.3.8 Time resolved fluorescence spectroscopy

Time resolved fluorescence spectroscopy was performed in the same flash photolysis setup described in chapter 1.2. One beam was used at 380 nm to detect formation of Meta-II as for the flash photolysis experiments. The sample was additionally illuminated at 594 nm, the absorption maximum of the used Alexa-594 dye (for the labeling protocol see 2.2.5), and the emission from the fluorescence was measured at 620 – 680 nm, using an adequate dielectric filter (Dr. Hugo Anders, Nabburg, Germany). Illumination was done as described in 2.3.1.

2.4 Analysis of spectra

2.4.1 cw-EPR spectra

Cw spectra were recorded using the software Bruker X-EPR. They were converted to ASCII and aligned to the center peak using the program "Convert & align" by CHRISTIAN ALTENBACH. Spectra showing strong free-spin peaks (usually those at pH 7.5) were corrected using the software "Subtract mobile component" by CHRISTIAN ALTENBACH (used parameters: Modulation: 3.68; A_0: 16.22; dHpp for low field: 0.80; dHpp for center field: 0.74; dHpp for high field: 1.10). After that all spectra were normalized, baseline-corrected and smoothed using the software "EPR baseline correction" by the same author.
Spectra were aligned and compared to each other using the software Origin Professional 7.0. Spectra are always shown without a scaling because the scale is changed during normalization and the important information is included in the line shape. The scan width is always 100 G (= $1 \cdot 10^{-2}$ T).

Difference spectra were calculated from the spectra for the illuminated minus those for the dark state and not scaled after that, so that the total amplitude corresponds to the absolute change.

2.4.2 FTIR measurements

FTIR spectra were exported from the Bruker Opus software as ASCII files and plotted and analyzed using the software Microcal Origin. To compare spectra they were plotted above each other, and the bands were compared, taking into account the accuracy of 2 cm^{-1}.

2.4.3 Time-resolved mesurements

Time courses were exported from the transient recorder as single column ASCII files. They were then converted to usable ASCII files with a time axis, normalized and subtracted using a special software programmed for this purpose in Borland Delphi. To deduce reaction speeds from these time courses they were overlayed with either single or double exponentials functions in the form

$$y = y_0 \cdot e^{-k \cdot t} + b \qquad \text{(XXIV)}$$

(y: signal amplitude; t: time; k: reaction constant; b: displacement in y-direction)

This is the solution for a simple first order reaction $A \xrightarrow{k} P$. The transition between two protein states can usually be assumed to be such a first order reaction. The rate is proportional to the concentration of the reactant:

$$\frac{d[A]}{dt} = -k \cdot [A] \qquad \text{(XXV)}$$

([A]: concentration of the reactant; k: reaction constant)

This simple differential equation is solved as:

$$[A] = [A]_0 \cdot e^{-k \cdot t} \qquad \text{(XXVI)}$$

($[A]_0$: initial concentration of the reactant)

If the transition between protein states is reversible (such as the equilibria between Meta-I and Meta-IIa or between Meta-IIa and Meta-IIb), an equilibrium emerges, and equation XXV has to be replaced by:

$$-\frac{d[A]}{dt} = \frac{d[P]}{dt} = k_+[A] - k_-[P] \qquad \text{(XXVII)}$$

([P]: concentration of the reaction product; k_+: reaction constant of the forward reaction; k_-: reaction constant of the backward reaction)

The solution is again an exponential equation [Schmidt and Sapunov, 1982]:

$$[A] = [A]_\infty + ([A]_0 - [A]_\infty) \cdot e^{-(k_+ + k_-)t} \qquad \text{(XXVIII)}$$

($[A]_\infty$: concentration of the reactant in equilibrium)

This equation is similar to equation XXIV and explains the assumption that the signals can be overlayed with single exponential kinetics. Thus the observed reaction rate k contains $k_+ + k_-$, and the factor y_0 contains $[A]_0 - [A]_\infty$.

2.4.4 Bimolecular reactions

If several reactants take part in the reaction, the solution of the equation gets more complex. The equations for this case have been derived by SCHLEICHER et al. [Schleicher et al., 1989].

A simple example for such a reaction is the reaction of rhodopsin with G_t or a peptide that mimics G_t. For the reaction type $A + B \longleftrightarrow P$ the rate is determined by:

$$-\frac{d[A]}{dt} = -\frac{d[B]}{dt} = \frac{d[P]}{dt} = k_+[A]\cdot[B] - k_-[P] \qquad \text{(XXIX)}$$

(k_+: reaction constant of the forward reaction; k_-: reaction constant of the backward reaction)

If a reaction like that is reversible it finally reaches an equilibrium. The equilibrium constant K_d which is increased by the concentrations of the reactants and decreased by the concentration of the product is a measure for this equilibrium:

$$K_d = \frac{k_+}{k_-} = \frac{[A]\cdot[B]}{[P]} \qquad \text{(XXX)}$$

If both reactants react in a 1:1 ratio and both components have to be assumed to undergo depletion while reacting, the total concentrations of both components can be written as:

$$\begin{aligned} [A]_t &= [A] + [P] \\ [B]_t &= [B] + [P] \end{aligned} \qquad \text{(XXXI)}$$

Setting these constraints into equation (XXX) gives:

$$K_d = \frac{([A]_t - [P])\cdot([B]_t - [P])}{[P]} \qquad \text{(XXXII)}$$

Multiplication and conversion of this equation leads to a quadratic equation:

$$0 = [P]^2 - [P]\cdot(K_d + [A]_t + [B]_t) + [A]_t \cdot [B]_t \qquad \text{(XXXIII)}$$

This is solved as:

$$[P] = \frac{(K_d + [A]_t + [B]_t) - \sqrt{(K_d + [A]_t + [B]_t)^2 - 4\cdot[A]_t \cdot [B]_t}}{2} \qquad \text{(XXXIV)}$$

This equation can now be used to obtain the K_d of a reaction knowing the total concentration of one component $[A]_t$, varying the total (= starting) concentration of the other component $[B]_t$ and measuring the amount of the product [P].

2.4.5 Calculation of activation energies

Reaction constants in dependence on the temperature are expressed by the Arrhenius equation:

$$k = A \cdot e^{-\frac{E_A}{RT}} \qquad \text{(XXXV)}$$

(k: reaction constant; A: Arrhenius factor; E_A: activation energy, R: universal gas constant, T: temperature)

This equation can be linarized by logarithmizing both sides:

$$\ln(k) = \ln(A) - \frac{E_A}{R} \cdot \frac{1}{T} \qquad \text{(XXXVI)}$$

This is a linear equation with $\ln(k)$ as the ordinate, $\frac{1}{T}$ as the abszissa, $-\frac{E_A}{R}$ as slope and $\ln(A)$ as y-axis intersect. A plot with these properties is called an Arrhenius plot, and the activation energy can consequently be deduced from the slope of a line in this plot.

The activation energy E_A is not identical with the enthalpy. The reaction enthalpy can be calculated from the activation energy:

$$\Delta H^{\ddagger} = E_A - R \cdot T \qquad \text{(XXXVII)}$$

($H^{\ddagger}$: reaction enthalpy; R: universal gas constant, T: temperature)

The Gibbs free enthalpy can in turn be calculated from the enthalpy, if the entropy is known:

$$\Delta G^{\ddagger} = \Delta H^{\ddagger} - T \cdot \Delta S^{\ddagger} \qquad \text{(XXXVIII)}$$

($G^{\ddagger}$: free enthalpy; $S^{\ddagger}$: entropy)

These values have been deduced for the Meta-I/Meta-II equilibrium by PARKES and LIEBMAN [Parkes and Liebman, 1984].

3 Results

3.1 Time resolved measurements and Metarhodopsin-IIa/b

3.1.1 Separation of Metarhodopsin-IIa and b

The existence of two Meta-II subspecies has been discovered through parallel flash photolysis measurements of Meta-II formation and uptake of a proton from the surrounding solution [Arnis and Hofmann, 1993]. However, so far it was unknown how these two subspecies are connected to the formation of the G_t activating form of rhodopsin and especially to the rigid body movement of TM6 [Farrens et al., 1996].

To gain an insight into these processes, the following approach was chosen: performance of experiments both with flash photolysis and with time resolved EPR on samples prepared under identical conditions. The aim was to be able to decide whether TM6 moves parallel to the formation of Meta-IIa, Meta-IIb or independently.

A typical kinetic experiment of Meta-IIa and b formation in dodecyl maltoside (DM) is shown in Fig. 9. The proton uptake was observed using bromocresol purple as pH dependent dye (Fig. 6), and the proton uptake clearly lagged behind the formation of Meta-II.

Calibration of the proton uptake signals was performed as described (see chapter 1.2.7) and yielded an uptake of one proton per rhodopsin molecule.

3.1.2 Kinetic EPR experiments on conformational changes of TM6

To determine the kinetics of TM6 movement, the reaction shown in Fig. 15 was used to attach spin labels attached to position 227 after replacing Val^{227} with Cysteine and the normally reactive side chains Cys^{140} and Cys^{316} with Serine (see chapter 1.3.4). Typical EPR spectra of the labeled pigment V227R1, in the dark and in the illuminated state as well as a typical time course at 20 °C are shown in Fig. 32 (right).

3.1.3 Kinetic EPR experiments on conformational changes of helix 8

In addition to this, a spin label at the native Cys^{316} was used. It is possible to either label Cys^{316} along with the other reactive Cys^{140} or to label either of them separately (see chapter 2.2.2 and 2.2.3), using the same spin label reaction as before (Fig. 15). While the spin label at position 140 does not show any change in EPR lineshape at all [Farahbakhsh et al., 1993] the spin label at

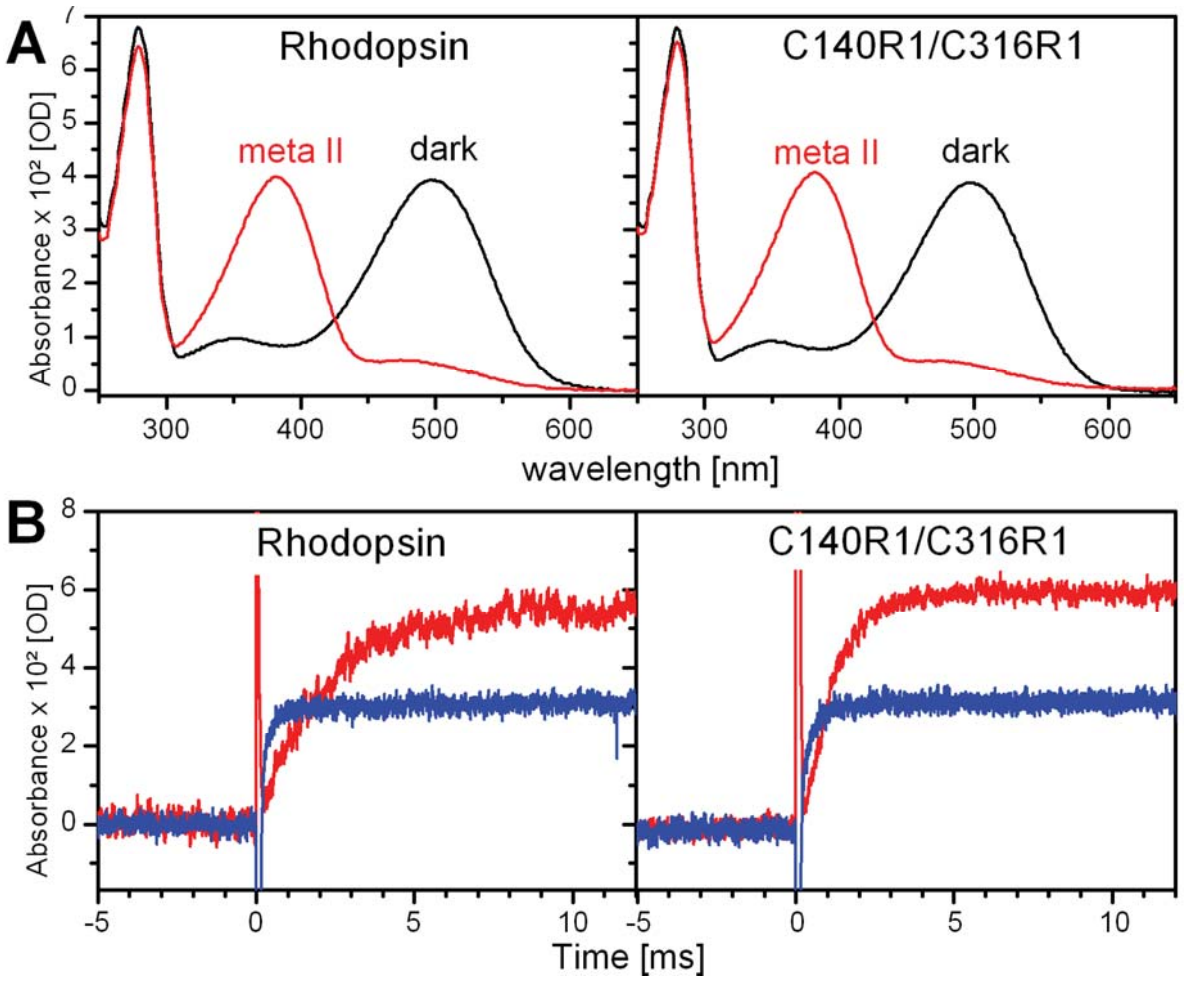

Fig. 33: A *UV/vis spectra of WT rhodopsin and spin labeled rhodopsin (positions* Cys^{140} *and* Cys^{316}*). There is no difference between both spectra.* **B** *Kinetics of Meta-II formation (blue) and proton uptake (red). For the spin labeled sample (right) both processes are slightly accelerated. The same behaviour is observable for the V227R1 pigment (data not shown).*

position 316 shows a distinct change [Kusnetzow et al., 2006]. Therefore it did not matter if both positions or only position 316 was selectively labeled.

UV/vis spectra of rhodopsin and rhodopsin with spin labels attached to Cys^{140} and Cys^{316} are shown in Fig. 33A (black: dark state; red: illuminated state). The kinetics of both samples are shown in Fig. 33B. Attachment of the spin label to rhodopsin accelerated both processes slightly but had no effect on the delay between Meta-II formation and the proton signal.

The change in the continuous wave EPR spectrum upon light activation of rhodopsin (black to red) along with the difference spectrum between the light-activated and the dark-adapted state (dark yellow) is shown for C316R1 in Fig. 32 (left). A typical time course is shown in Fig. 32B (left).

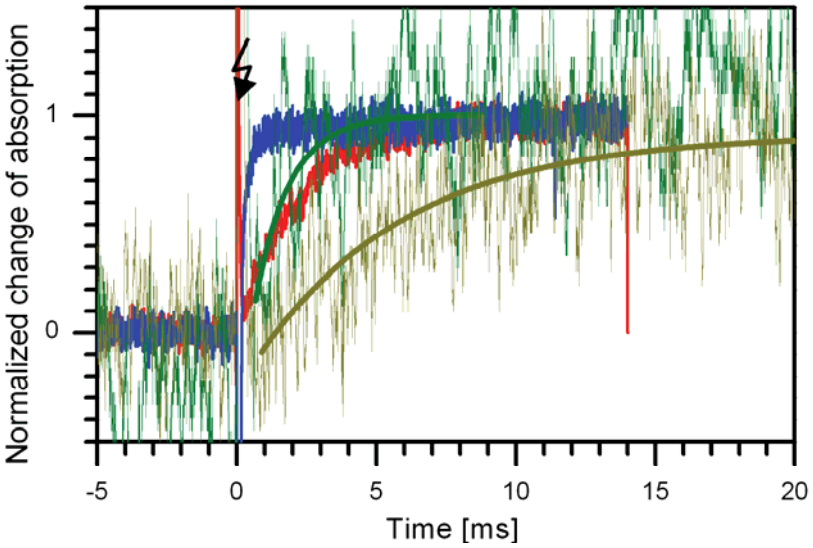

Fig. 34: *Direct comparison of processes in DM solution at 20 °C reveals that the movement of TM6 (green) occurs concomitant with the proton uptake (red line) and clearly after Meta-II formation (blue line). The movement of H8 (yellow) appears to happen in a third, slower step. The laser excitation (time 0) is marked with a flash symbol.*

3.1.4 Overlay and analysis of the kinetics

An overlay of all processes described is shown in Fig. 34 and reveals the following:

1. Proton uptake is slower that Meta-II formation.
2. The kinetics of TM6 movement are similar to kinetics of the proton uptake.
3. The available data show that change in mobility of the spin label for 316R1 or 140R1/316R1 (not shown) is slower than Meta-II formation and proton uptake.

The measurements of Meta-II formation and proton uptake (both measured in parallel) and changes in spin label mobility have been performed as described above under identical conditions at different temperatures and fitted with single exponential kinetics. The data for Meta-II formation and proton uptake are summarized in an Arrhenius plot showing the observed rates (Fig. 35A). This reproduces earlier findings [Arnis and Hofmann, 1993]. Since the attachment of the spin labels can have an effect on rhodopsin structure and kinetics, the same set of Meta-II and proton uptake measurements was repeated with spin-labeled rhodopsin C140R1/C316R1 Fig. 35B. The proton uptake is slightly faster here, but the slope in the Arrhenius plot and therefore the activation energy remains the same.

The EPR data are shown in Fig. 35B with olive stars representing data for the movement of TM6 (V227R1) and the dark yellow triangles representing data for structural changes in the H8 region (V316R1 or V140R1/V316R1). The EPR data and the measurements of Meta-II formation have also been performed with buffer-free samples used for monitoring proton uptake (see 1.2.1). Removal of the buffer had no effect on the various measurements (data are overlayed with data from buffered samples).

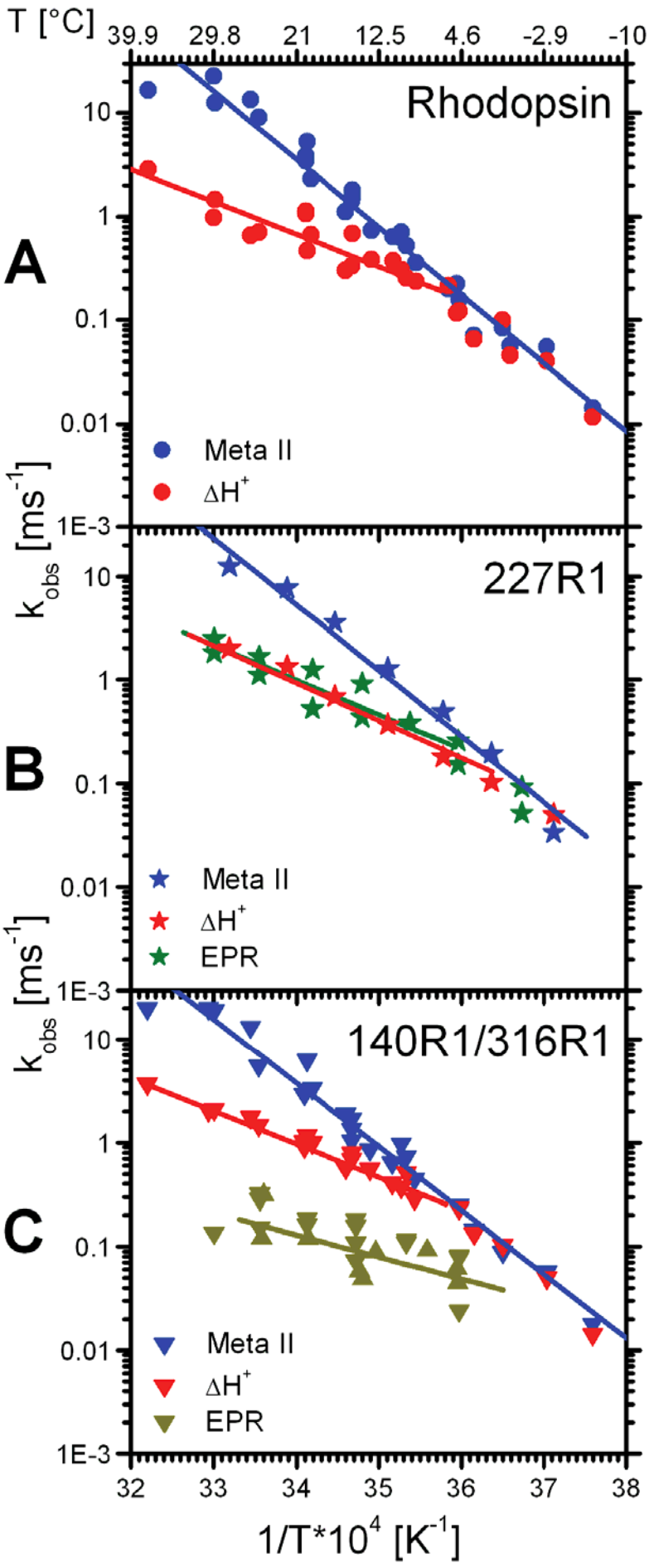

Fig. 35: *Arrhenius plots of the rate constants determined for different temperatures. Blue symbols represent the formation of Meta-II, red symbols proton uptake, green stars the movement of TM6 (spin label at position 227) and yellow triangles the movement of helix 8 (spin label at position 316).* **A** *Unlabeled rhodopsin in DM.* **B** *Pigment V227R1 in DM.* **C** *Spin labeled rhodopsin in DM. The native cysteines Cys^{140} and Cys^{316} are labeled. For a part of the samples only Cys^{316} was labeled selectively (see 2.2.2), obtaining the same kinetics (distinguished for the EPR data with the yellow triangles pointing up).*
Activation energies deduced from the plots are shown in Table 5.

Data of all four processes in the Arrhenius plot in Fig. 35 can be fit with straight lines which are for the Meta-II formation and the proton uptake comparable to data obtained in an earlier study [Arnis and Hofmann, 1993]. Meta-II formation (blue line) shows the steepest slope and therewith has the largest activation energy. Proton uptake (red line) displays a shallower temperature profile and goes parallel with TM6 movement (olive line). The change in H8 (dark yellow line) is more difficult to interpret, due to the poor quality of the EPR signals (Fig. 34). Available data are consistent with a generally slower reaction, and the Arrhenius representation shows a similar slope as seen for TM6 movement and proton uptake. At low temperatures the formation of Meta-II becomes rate limiting and therefore all four processes go parallel with formation of Meta-II.

3.1.5 Dependence on pH

The kinetic data reported above show that, as a consequence of Meta-II formation and dissocia-

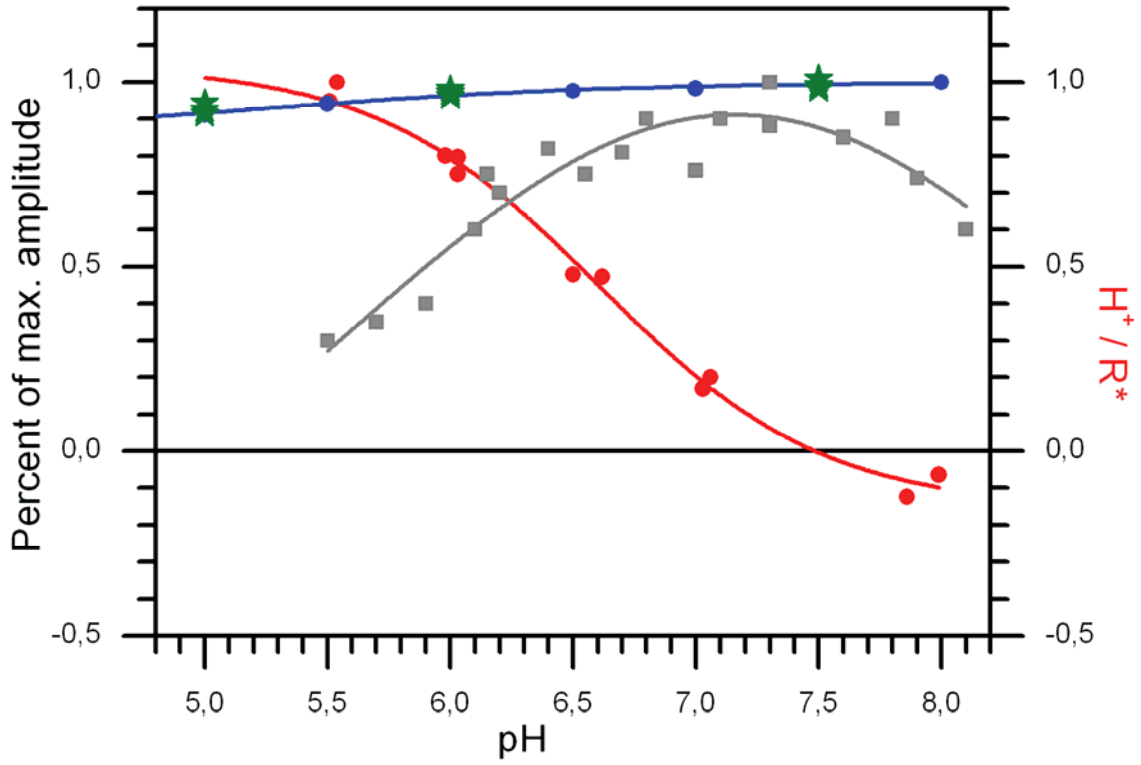

Fig. 36: *pH dependent plot of characteristics for the different activation steps. Meta-II formation (blue circles) is nearly independent of pH, only being slightly reduced at acidic pH due to the formation of Meta-II-PSB (see [Knierim et al., 2007]). The movement of TM6 (green stars, 227R1) shows the same behavior, while the proton uptake (red circles) is one proton per activated rhodopsin (see scale on the right side) at pH 5.5 and goes down to zero proton uptake at pH 7.5 with a pK around 6.5. The G_t acivation rate (grey boxes, data taken from [Kisselev et al., 1999]) is from light scattering dissociation signals [Heck and Hofmann, 2001; Kühn et al., 1981].*

tion of the proton from the retinal SB, the protein adopts a conformation in which helix motion and proton uptake can occur. Does the conformational change require or result in proton uptake? Fig. 36 shows pH dependent data allowing to decide this question.

The EPR signal from spin-labeled pigment 227R1 has a broad pH profile (Fig. 36, green stars) and stays constant within the whole accessible range of pH. The same is seen for Meta-II formation (blue circles). The slight decrease of the amplitude at acidic pH is most likely due to a Meta-II product with a reprotonated Schiff base [Bartl et al., 2005; Meyer et al., 2000; Vogel et al., 2000]. The dominant effect is that the proton uptake signal drops with a titration curve reflecting a pK of about 6.5.

To test the different pH trends with another method, fluorescence spectroscopy and labeled rhodopsin with the Alexa-594 dye (see 2.2.5) was applied. Labeling was done at the native Cys^{316} position and at position 227 taking advantage of the V227R1 pigment that was also used

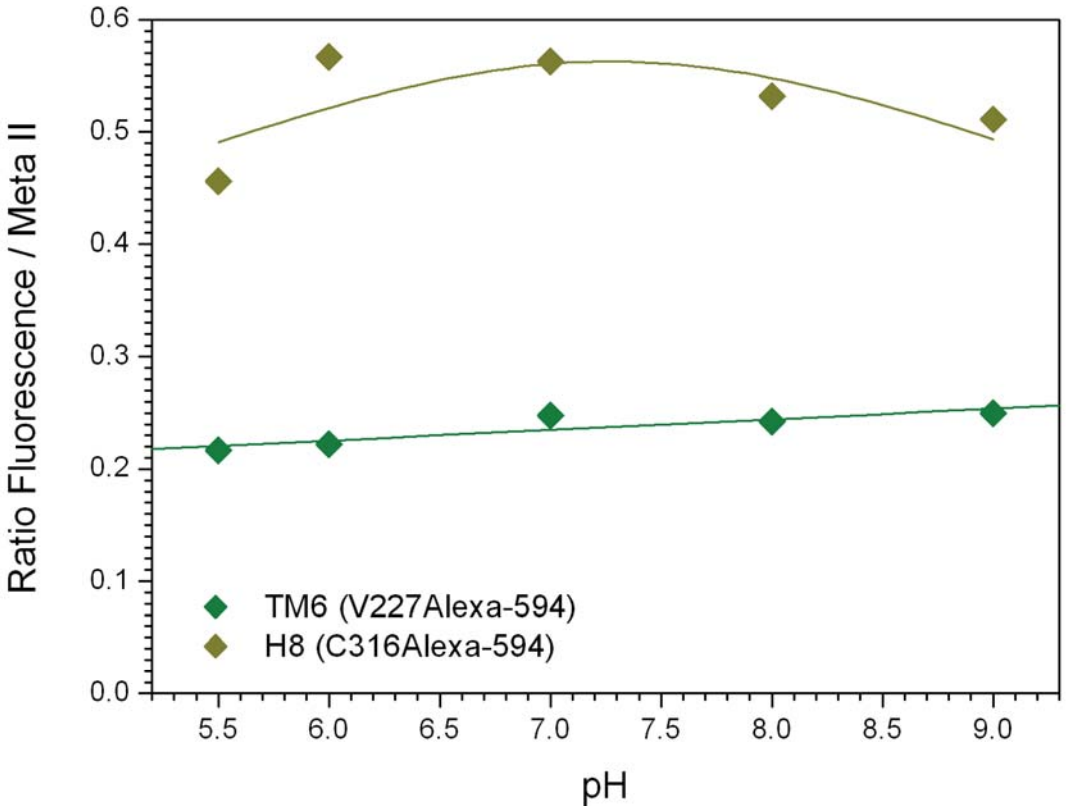

Fig. 37: *pH dependent plot of the fluorescence change. Pigment concentration was 10 µM, measurements were performed at 20 °C. The ratio of the change in fluorescence upon activation and Meta-II formation is shown. Pigments were either labeled at position 227 (V227C mutation labeled with Alexa-594) or at position 316 (native rhodopsin labeled with Alexa-594). The movement of TM6 (green diamonds, V227Alexa-594) is almost pH independent with a small trend towards less fluorescence at acidic pH. The movement of H8 (yellow diamonds, 316Alexa-594) is also only slightly pH dependent with a trend towards a bigger change at acidic pH but a drop at pH 5.5.*

for spin labeling as described above. Fig. 37 shows a plot of the relative fluorescence change (related to the amount of Meta-II formation) plotted against the pH. Upon rhodopsin activation the fluorescence increases with the label at either position. Interestingly, the fluorescence change at position 316 is about twice as big as the fluorescence change at position 227. This is the opposite behaviour compared to spin labeling at these positions. EPR experiments show that the spin label 227R1 shows a bigger change than the spin label 316 R1 (see Fig. 32A). This is a hint that the relatively small spin label and the relatively large Alexa dye sense different environments and that the results obtained with both techniques can be different.

Nevertheless the pH dependencies support the findings above: For the 227 position sensing TM6 movement the fluorescence change is pH independent with a little decrease at acidic pH. For the 316 position there is no distinct pH dependence observable either. Fluorescence is only slightly higher at acidic pH with a peak at pH 6.0 but is decreased at more acidic pH (pH 5.5).

Therefore we can conclude that both TM6 and the H8 movement are independent of proton uptake, because the proton uptake shows a distinct pH dependence as shown in Fig. 36.

3.1.6 Comparison of detergent environment with membranes

The behaviour of Meta-II formation, proton uptake and helix movement in detergent has been described in the chapters above. But how are these activation steps related in membranes, rhodopsin's native environment?

To answer this question, the same experiments as described above in hypotonically washed native disk membranes (for the preparation protocol see 2.1.2) were performed. Data for the movement of TM6 could not be obtained here, because this can only be determined using the pigment V227C (with spin labeling) which can only be heterologously expressed and prepared. Vesicles are sometimes regarded to be an equivalent system, but especially the kinetics are different.

However, an additional experiment could be performed in membranes: The light scattering change can be measured parallel to the formation of Meta-II and the proton uptake using the same flash photolysis setup (for a description see 1.2.3). The light scattering signal is called 'N-signal' because of its negative amplitude. The signal has been described before, but its origin is not yet clear [Hofmann and Reichert, 1985; Hofmann et al., 1981; Hofmann et al., 1976; Hofmann and Emeis, 1981; Kühn et al., 1981; Uhl et al., 1985; Uhl et al., 1977; Uhl et al., 1980].

A typical flash photolysis experiment measuring all three signals in parallel is shown in Fig. 38. Like in the DM environment, Meta-II formation precedes the proton uptake as well as the 'N-signal', but the kinetic difference is much smaller than in DM. The signal intensity is weaker than in DM due to the light scattering caused by the membranes.

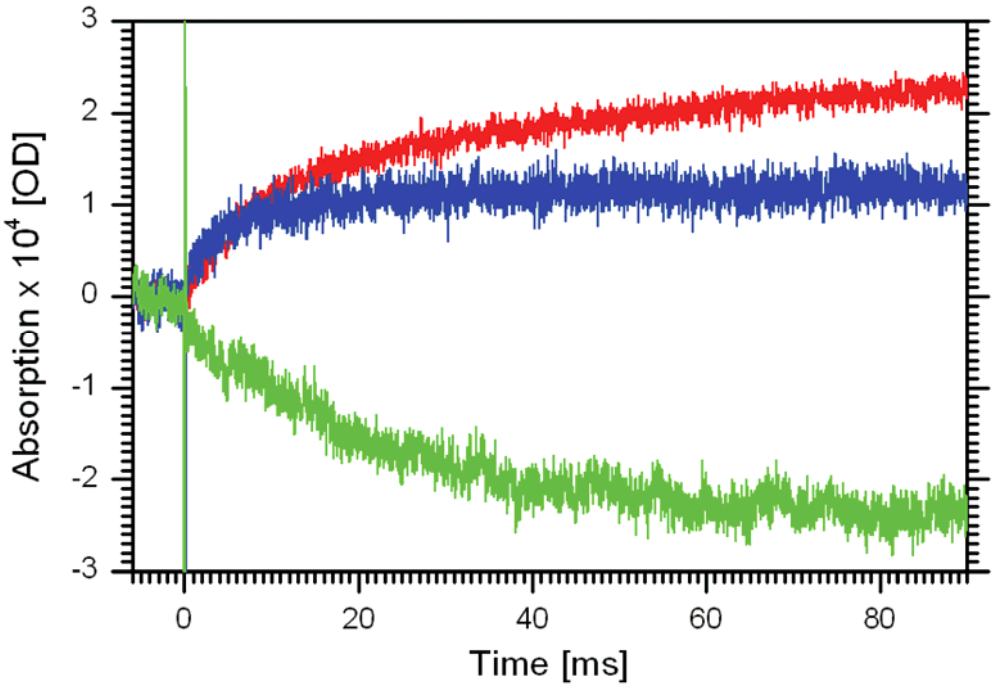

Fig. 38: *Typical flash photolysis experiment on washed disk membranes using three channels at 20 °C and pH 6.0. The blue line represents the formation of Meta-II (measured at 380 nm), the red line the proton uptake measured with BCP as a pH dependent dye (595 nm) and the green line the light scattering signal (840 – 860 nm, scattering > 5°) which is called 'N-signal' due to the negative amplitude. The kinetics are slower than in DM, the proton uptake and the 'N-signal' lagging behind Meta-II formation.*

The data are shown in an Arrhenius plot in Fig. 39 (comparable to Fig. 35 for the DM data). Panel A shows the kinetics of the activation steps in native disk membranes without spinlabel. Formation of Meta-II (blue line) is the fastest process, followed by proton uptake (red line) and the 'N-signal' (green line). The latter two processes show the same kinetics. The difference between Meta-II formation and proton uptake with the parallel 'N-signal' is small compared to the DM environment and is less than a factor of 10 even at 40 °C. At low temperatures (< 0 °C) all three processes have identical kinetics.

Panel B shows the data for spin labeled washed disk membranes (same color scheme as above). Both the formation of Meta-II and the proton uptake – again parallel with the 'N-signal' – are accelerated by roughly a factor of three compared to the non spin labeled system. The EPR signals (dark yellow triangles) that represent H8 movement [Kusnetzow et al., 2006; Resek et al., 1993] were acquired under identical conditions. They also roughly coincide with proton uptake and the 'N-signal', but unfortunately scatter widely.

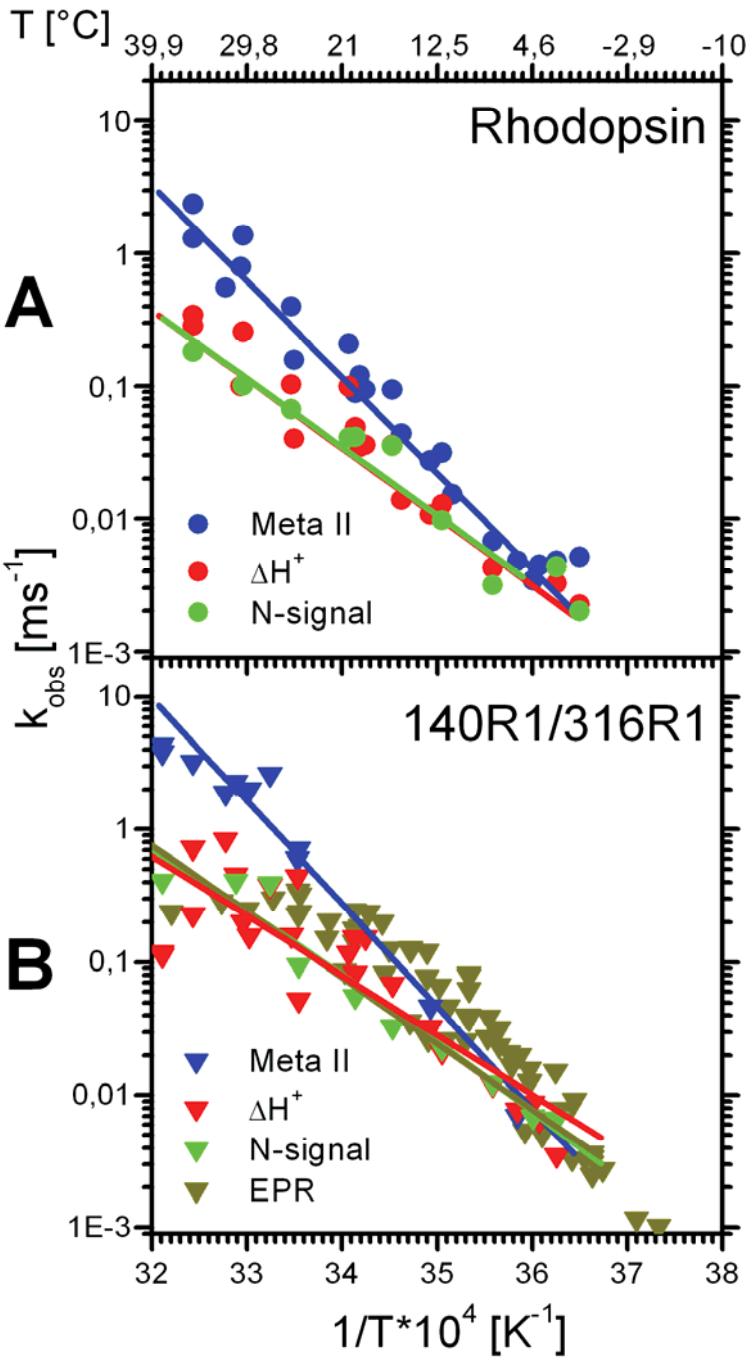

Fig. 39: *Arrhenius plots of the rate constants determined for different temperatures. Blue symbols represent the formation of Meta-II, red symbols proton uptake, green symbols the light scattering 'N-signal' and yellow triangles the movement of helix 8 (spin label at position 316).* **A** *Unlabeled rhodopsin in native membranes.* **B** *Spin labeled rhodopsin in native membranes. Both native cysteines Cys^{140} and Cys^{316} were labeled. For a part of the samples only Cys^{316} was labeled selectively (see 2.2.2), obtaining the same kinetics.*
The calculated activation energies deduced from the plot are shown in Table 5.

3.1.7 Meta-IIa and -IIb in 2D crystals

Besides the detergent and the native membrane environment, rhodopsin can exist in a further form, which is rather uncommon: in crystals. In this study, 2D crystals designed for structure determination via electron scattering [Mielke et al., 2002b] were tested as well. The crystals were prepared by ALEXA GREUBE and THORSTEN MIELKE.

In 2D crystals Meta-II formation is favoured at high temperatures and basic pH. Typical signals are shown in Fig. 40. The signals are weak due to the massive light scattering of the crystals.

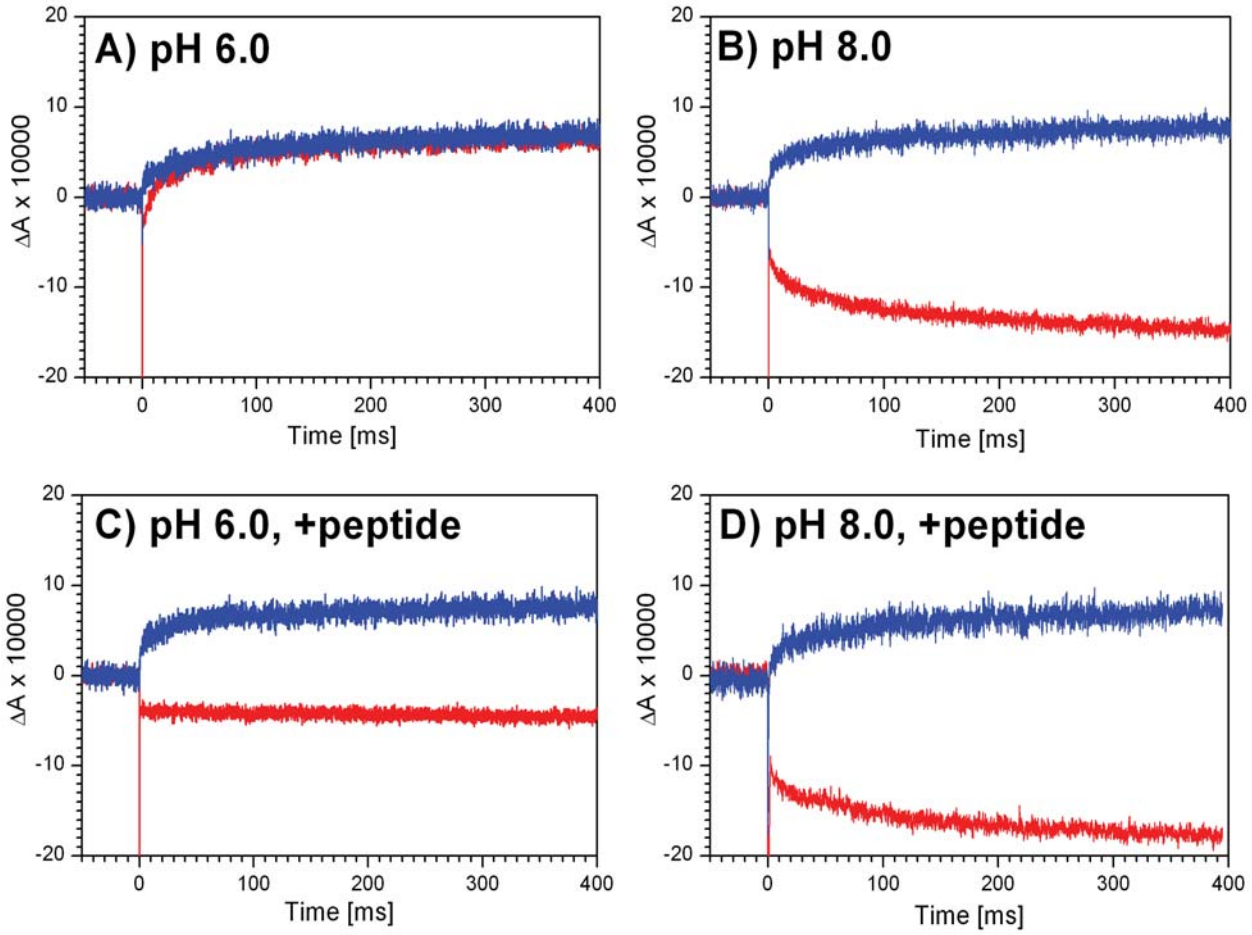

Fig. 40: *Typical flash photolysis experiment on rhodopsin crystals (rhodopsin concentration: 10 µM; BCP or CR, respectively: 50 µM) at 30 °C. Blue lines represent the formation of Meta-II (380 nm) and red lines the proton uptake (595 nm).* **A** *At acidic pH a clear proton uptake is observable.* **B** *At basic pH the proton uptake turns into a proton release.* **C** *In presence of high affinity $G_t\alpha$ derived peptide (ILENLKDCGLF) the proton uptake disappears.* **D** *At acidic pH the high affinity $G_t\alpha$ peptide leads to an even stronger proton release.*

There are two observations that are not self-evident for rhodopsin crystals: Firstly, a clear proton uptake indicative of the formation of Meta-IIb·H^+ can be detected. Therefore the active rhodopsin form is established. Secondly, the high affinity $G_t\alpha$-derived peptide has the same influence on the proton uptake as described for the DM environement (see 3.6.2), decreasing the proton uptake as far as even a proton release.

3.1.8 Activation energies

From the Arrhenius plots shown in Fig. 35 and Fig. 39 the activation energies for the different steps were deduced using the slope in the Arrhenius plot as in equation XXXVI on page 66. The results are shown in Table 5.

	Activation energies [kJ/mol] :							
	MII formation		TM6 mov. & H^+Uptake		H8 movement		N-Signal	
Conditions	E_A	+/-	E_A	+/-	E_A	+/-	E_A	+/-
Rho in DM	136,2	7,1	61,6	5,4				
Rho in DM with spin label	125,4	8,1	66,9	6,3	28,7	19,8		
V227R1 in DM (with spin label)	115,9	12,9	80,7 73,5	4,9 13,4				
Rho in membranes	138,7	12,2	104,9	13,4			93,0	15,1
Rho in membranes with spin label	146,8	7,1	119,0	18,8	30,4	18,8	57,7	12,5
Rho in membranes, FTIR sandwich	140,6	2,3	148,5	5,9				
Rho in vesicles	146,3	16,3	124,4	18,8				

Table 5: *Activation energies deduced from the Arrhenius plots in Fig. 35 and Fig. 39 through linear fits. The different conditions are described in the left column. For completeness data for rhodopsin in FTIR 'sandwiches' (as described in 2.3.4) and in reconstituted vesicles (following the protocol in [Kusnetzow et al., 2006]) are also shown but not further interpreted in the text. The columns are colored as in the Arrhenius plots. The data for TM6 motion (in green script) and proton uptake are shown in the red column, as both processes were shown above to coincide kinetically. Cells in which data could not be obtained due to technical reasons are colored grey; if sufficient data was not collected they are left empty.*

The activation energies for Meta-II formation and the proton uptake in DM are consistent with earlier findings [Arnis and Hofmann, 1993]. Although the kinetics are slightly faster for the spin labeled system (spin labels at Cys^{140} and Cys^{316}) as shown in Fig. 35B, the activation energies do not differ significantly. As seen in the Arrhenius plot, the movement of H8 has different kinetics with a much lower activation energy. Unfortunately the standard deviation of the H8 activation energy is high (see the error) due to the large scattering of the data points. The recombinant rhodopsin spin labeled at position 227 has similar properties to the spin labeled native rhodopsin (C140R1/C316R1). Therefore the mutation does not seem to change these properties severely. As visible in the Arrhenius plot, the movement of TM6 (red column, green number) has almost the same activation energy as the proton uptake.

In membranes the activation energy of Meta-II formation is basically the same as in detergent, but the proton uptake has a much higher activation energy. Here the light scattering 'N-signal' can also be observed and has a similar activation energy as the proton uptake. Again the spin labeled system has similar properties as the non spin labeled system, and the movement of H8 has a much lower activation energy than Meta-II formation and the proton uptake.

The squeezing of membranes into a 'sandwich' between to BaF_2 panes as they are used for FTIR spectroscopy has an enormous impact on the activation energy for proton uptake: While Meta-II formation is similar to the membrane environment, the activation energy for the proton uptake is not different from the activation energy for Meta-II formation. Therefore the high density of membranes does have an impact on activation. The 'N-signal' could not be measured here.
Artificial vesicles were prepared following the protocol of KUSNETZOW and HUBBELL [Kusnetzow et al., 2006]. The vesicles were preformed, and then rhodopsin in octyl glucoside (OG) detergent was added without dissolving the vesicles, followed by removal of the detergent by dialysis. The kinetics of both Meta-II formation and the proton uptake are faster than in membranes, but the activation energies are comparable. Again a 'N-signal' could not be detected. Consequently the vesicles, which can also be prepared with mutant pigments, seem to replace the membranes reasonably well but do not show the same kinetic properties.

3.2 The ERY-Motif

As already stated in the introduction, the D(E)RY motif is a highly conserved motif in GPCRs and is supposed to play an important role during rhodopsin activation. Therefore I tried to elucidate its role during activation by examination of different mutational pigments in the ERY motif and the connected region in TM6 with different biophysical methods.

3.2.1 UV/visible Spectra

Pigments were produced by expression of opsin in COS-1 cells and reconstitution with 11-*cis*-retinal or 11-*cis*-9-demethyl-retinal, respectively (see chapter 2.1.3). UV/visible spectra were taken from purified pigments in DM solution (Fig. 41; the prefix 9-dm denotes pigments which contain 9-demethyl-retinal). For the dark state the 9-dm-wild type pigment (9-dm-WT) shows a λ_{max} shifted to 466 nm due to the missing methyl group at C-9 of retinal as observed earlier [Meyer et al., 2000]. 9-dm-retinal shifts the Meta-I/Meta-II equilibrium towards the inactive state and was used to enable the identification of mutants facilitating formation of Meta-II.
As insets the plots of the 466 nm peak after illumination are shown which represent the fraction of molecules with protonated SB against the pH. For native 9-dm-WT (first row, left) the inactive fraction is higher at basic pH. This pH dependence is reversed for the 9-dm-E134Q pigment as described previously (second row, left) [Meyer et al., 2000]. The 9-dm-R135L pigment (fourth row, left) shows the same reversed pH trend, while the 9-dm-R135K pigment (third row, left) does not feature any clear pH dependence at all.

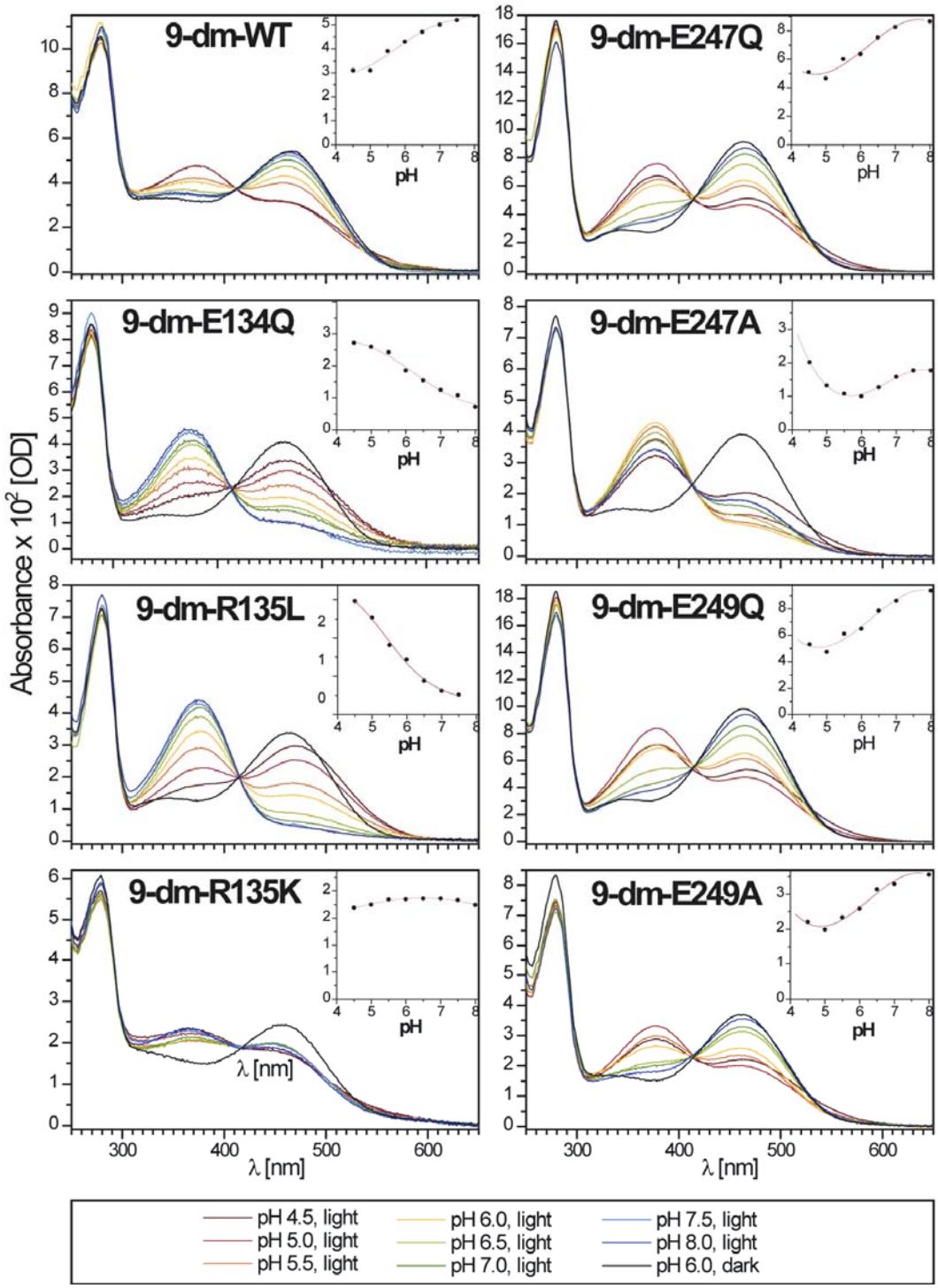

Fig. 41: *UV/vis spectra of the pH trends for the different mutants. The insets show the 466 nm band (= grund state for 9-dm-pigments) plotted against the pH. In WT rhodopsin (first row left) the active state (identified by the absorption at 380 nm) is favored at acidic pH. This is not changed by either the E247Q mutation (first row right) or any of the E249x mutations (third and fourth row right). At pH < 5 these mutants show an onset of Meta-II-PSB that reduces the amount of active species. The E134Q and the R135L mutations (second and third row left) both show a reversed pH dependence, while the R135K mutation (fourth row left) does not feature any explicit pH dependence. The E247A mutation (second row right) shows an overlay of a negative an a positive pH trend with the low point around pH 5.75.*

The E247Q mutation (first row, right) does not change the pH course of the 9-dm-pigment while the E247A mutation (second row, right) reveals an interesting behaviour: The pH trend has a minimum around pH 6.0 while the fraction of inactive molecules is higher for both more acidic and more alkaline pHs. This can be explained with a superposition of two opposite pH trends. The E249Q and E249A mutants (third and fourth row, right) do not show a changed pH dependence compared to 9-dm-wild type indicating that Glu^{249} does not play an important role for rhodopsin activation.

In all spectra at pH 5.0 and 4.5 a fraction of another photoproduct with an absorption maximum slightly shifted to the red compared to the dark state becomes visible. This species probably corresponds to Meta-II with a reprotonated schiff base (Meta-II-PSB) [Vogel et al., 2000]. In those spectra featuring an increased portion of Meta-II (9-dm-E134Q and 9-dm-R135L, as noted above), this product is already visible at higher pH and can easily be detected by the flank of the spectra being shifted to the right and looming out of the dark spectra.

3.2.2 FTIR Spectroscopy of the ERY motif mutations

Meta-II minus rhodopsin FTIR difference spectra of recombinant 9-dm-pigments in DM were recorded at pH 5.5 and 25 °C as shown in Fig. 42A. Meta-I minus rhodopsin difference spectra (Fig. 42B) were recorded at pH 7.5 and -10 °C. Spectra were normalized to the retinal marker band at 1238 cm^{-1} to create comparable band intensities.

The spectra of 9-dm-WT in Fig. 42A (red line) and B (dark blue line) clearly indicate the formation of Meta-II and Meta-I under the experimental conditions indicated in the figures. Similar observations were previously published [Vogel et al., 2000]. The spectra shown in Fig. 42A reveal that none of the mutations used for the experiments affect the formation of the Meta-II, since the typical Meta-II bands at 1713 $cm,^{-1}$, 1745 cm^{-1} and at 1768 cm^{-1} are present in all spectra.

The spectra shown in Fig. 42B were recorded under Meta-I conditions. In the spectra of the mutants the bands at 1538 cm^{-1}, 1201 cm^{-1} and the band doublet at 1728 cm^{-1} and at 1736 cm^{-1} indicate the formation of Meta-I. Compared to the 9-dm-WT (Fig. 42B, dark blue line), the spectra of the mutants 9-dm-E134Q (green line), 9-dm-R135L (light blue line) and 9-dm-E247A (lower magenta line) still display a fraction of Meta-II, as proofed by the residual Meta-II bands between 1800 cm^{-1} and 1700 cm^{-1} and at 1644 cm^{-1}.

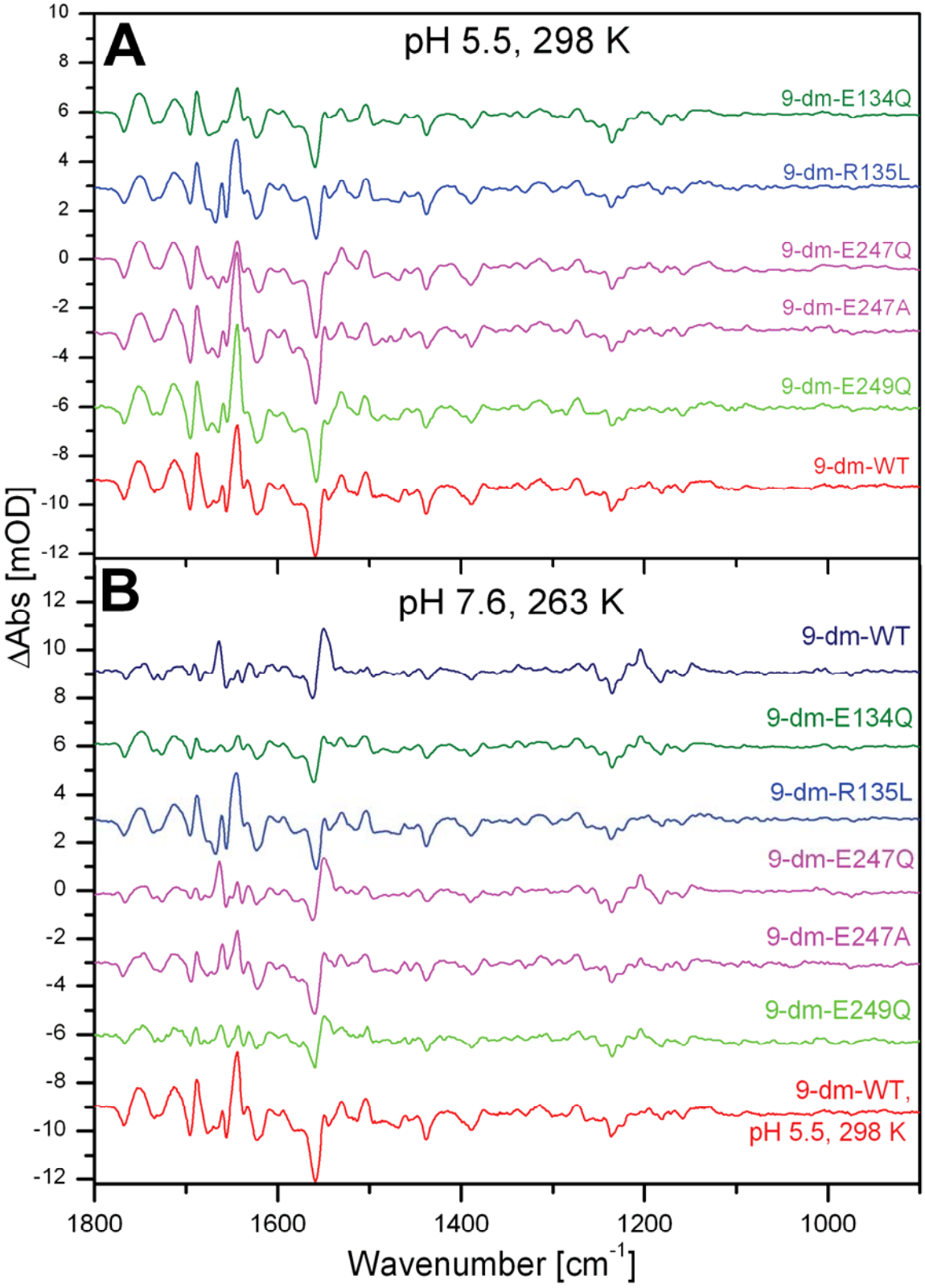

Fig. 42: *FTIR difference spectra (light minus dark) of purified pigments were recorded under two different conditions: At pH 5.5 and 25 °C (=298K) WT rhodopsin mainly forms Meta-II (last spectra in both panels), while at pH 7.6 and 263K it mainly forms Meta-I (first spectrum in* B*).* **A** *Under identical Meta-II conditions all mutants equally show Meta-II.* **B** *In contrast, under Meta-I conditions only the E249Q and the E247Q pigments show pure Meta-I, while the E134Q, R135L and E247Q pigments show fractions of Meta-II. For a detailed description of the marker bands see the text.*

3.2.3 Flash Photolysis Measurements

Flash photolysis was performed as described (see chapter 2.3.1) with pigments containing 11-*cis*-retinal. Bromocresol purple and cresol red were used as dyes to sense pH changes. An exemplary overlay of the 380-nm and the 595-nm curves for WT is shown in Fig. 43, the 380-nm graph showing the formation of Meta-II and the 595-nm curve showing the proton uptake from solution, which is slower and represents the formation of Meta-IIb [Arnis and Hofmann, 1993]. The proton uptake has been normalized to the amount of activated rhodopsin (R*) (measured at 380 nm, see 2.3.1).

The upper left panel shows the normal situation with WT rhodopsin: The proton uptake clearly lags behind Meta-II formation. For the R135K pigment (upper right panel) the amplitudes stay

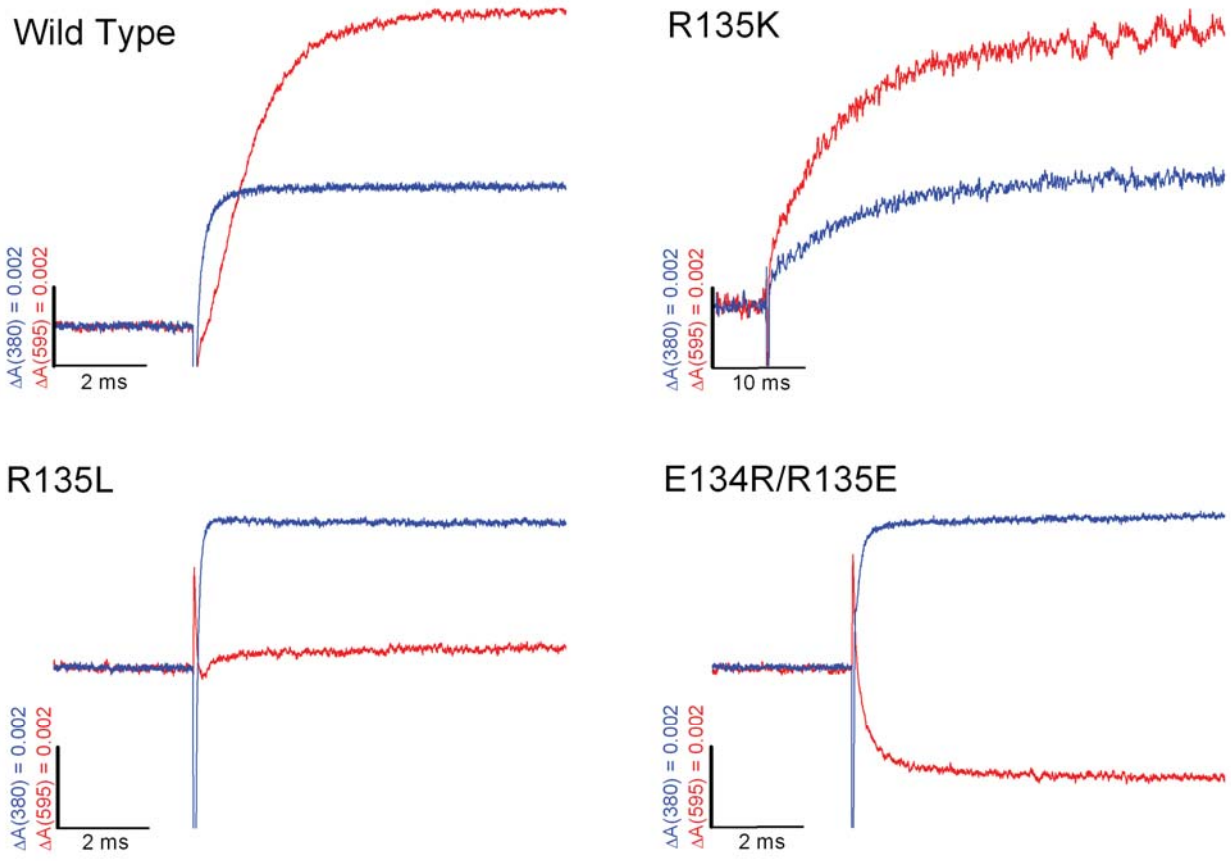

Fig. 43: *Flash photolysis experiments show the formation of Meta-II at 380 nm (blue traces) and the proton uptake at 595 nm (red traces). To make proton uptake visible, bromocresol purple was used as a pH dependent dye (see 2.3.1). WT rhodopsin (upper left panel) shows that Meta-II formation is faster than the proton uptake (= Meta-IIb formation). For the R135K pigment (upper right panel) the whole process is slowed down by one order of magnitude (please note the changed time scale), while for the R135L pigment (lower left panel) Meta-II formation is accelerated and the proton uptake is small. The E134R/R135E pigment (lower right panel) shows Meta-II kinetics similar to WT rhodopsin, but instead of proton uptake proton release is observed.*

the same, but the speed is decreased by one order of magnitude (note the modified timescale). In contrast to that, the R135L pigment (lower left panel) shows an accelerated formation of Meta-II but no more proton uptake. The E134R/R135E pigment (lower right panel) shows regular Meta-II formation but a proton release instead of a proton uptake.

In Fig. 44 a compilation of the final amplitudes for the proton uptake data is presented. WT rhodopsin shows an uptake of one proton at pH 5.5 which is lower at more basic pH and reverses itself into a slight proton release at pH 8.0. The pKa of the course is around 6.5.

The pigments E247Q (magenta squares), E249Q (light green squares) and E247A (magenta triangles) show a proton uptake course which does not differ significantly from that of WT rhodopsin. For the pigment R135K (blue squares) the pK might be slightly shifted to the acidic. The pigments E134Q (dark green squares), E134R/R135E (dark blue diamonds) and R135L (blue triangles) do not show any proton uptake at all, even at pH 5.5. In contrast to the R135L pigment

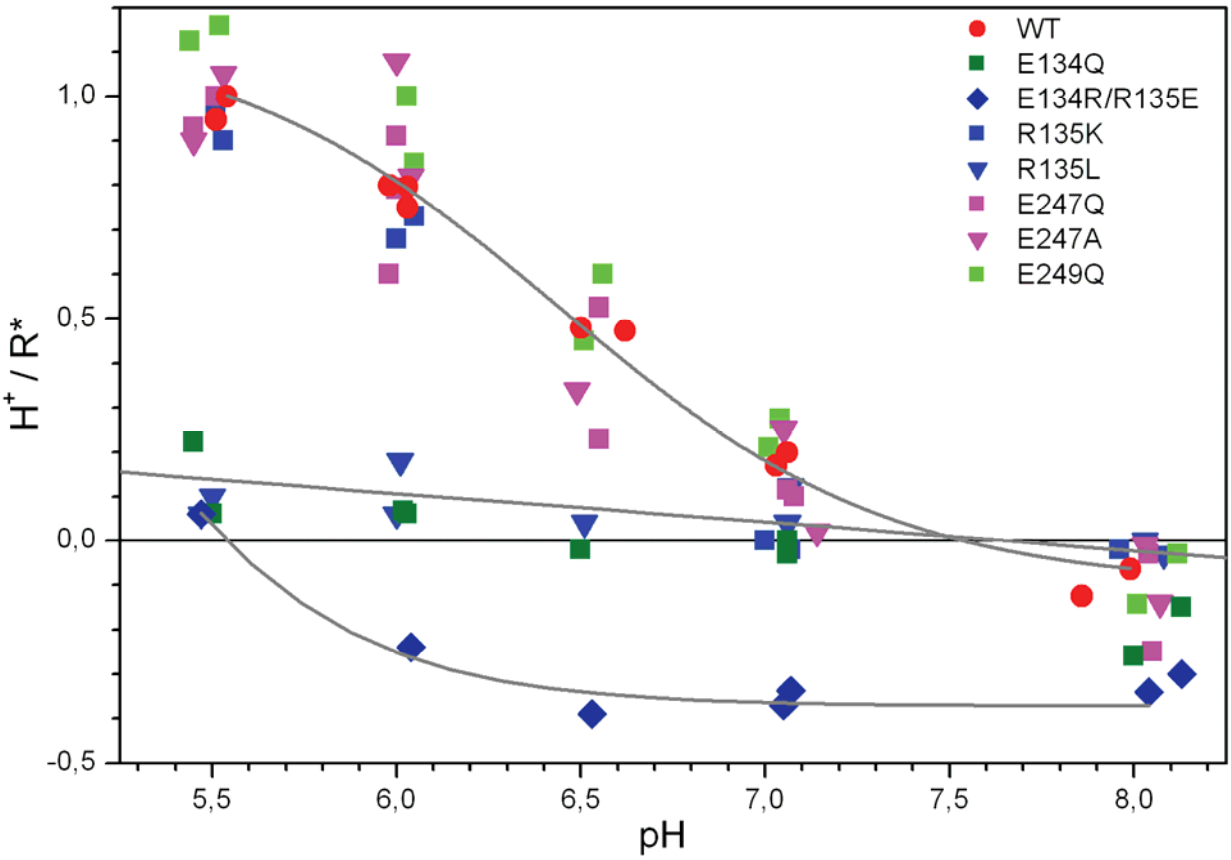

Fig. 44: *The plot shows the number of protons taken up per activated rhodopsin R* against the pH. The proton uptake signals were calibrated as described in 1.2.7. For WT rhodopsin as well as for the pigments R135K, E247Q, E247A and E249Q there is roughly one proton taken up at pH 5.5, and this goes down to 0 with rising pH. The pK is about 6.5. Both the E134Q and the R135L pigments do not feature any significant proton uptake at any pH. The E134R/R135E pigment shows a release of roughly 0.4 protons per activated rhodopsin at pH > 5.5.*

which does show neither uptake nor release of protons the E134R/R135E pigment shows a clear proton release (about 0.4 protons per activated rhodopsin molecule) at pH > 5.5. The E134Q pigment shows a similar proton release at pH > 7.5 as described earlier [Arnis et al., 1994].

3.2.4 EPR experiments

The mutations E135K, E135L and E134R/R135E were combined with the V227R1 mutation in order to label them with the R1 spin label (see 2.2.1) and obtain information about TM6 motion. The dark state spectra of the three mutations and V227R1 for comparison are shown in Fig. 45. The same spectra for the illuminated states are shown in Fig. 46. V227R1 without any additional mutation does not feature any pH dependence in either the dark or in the illuminated state (compare chapter 3.1.2 and especially Fig. 36, data not shown again here) [Knierim et al., 2007]. Spectra were taken at three different pH values to determine the influence of the proton concentration on the stabilization of TM6 in the dark state. For the E134R/R135E/V227R1 'charge re-

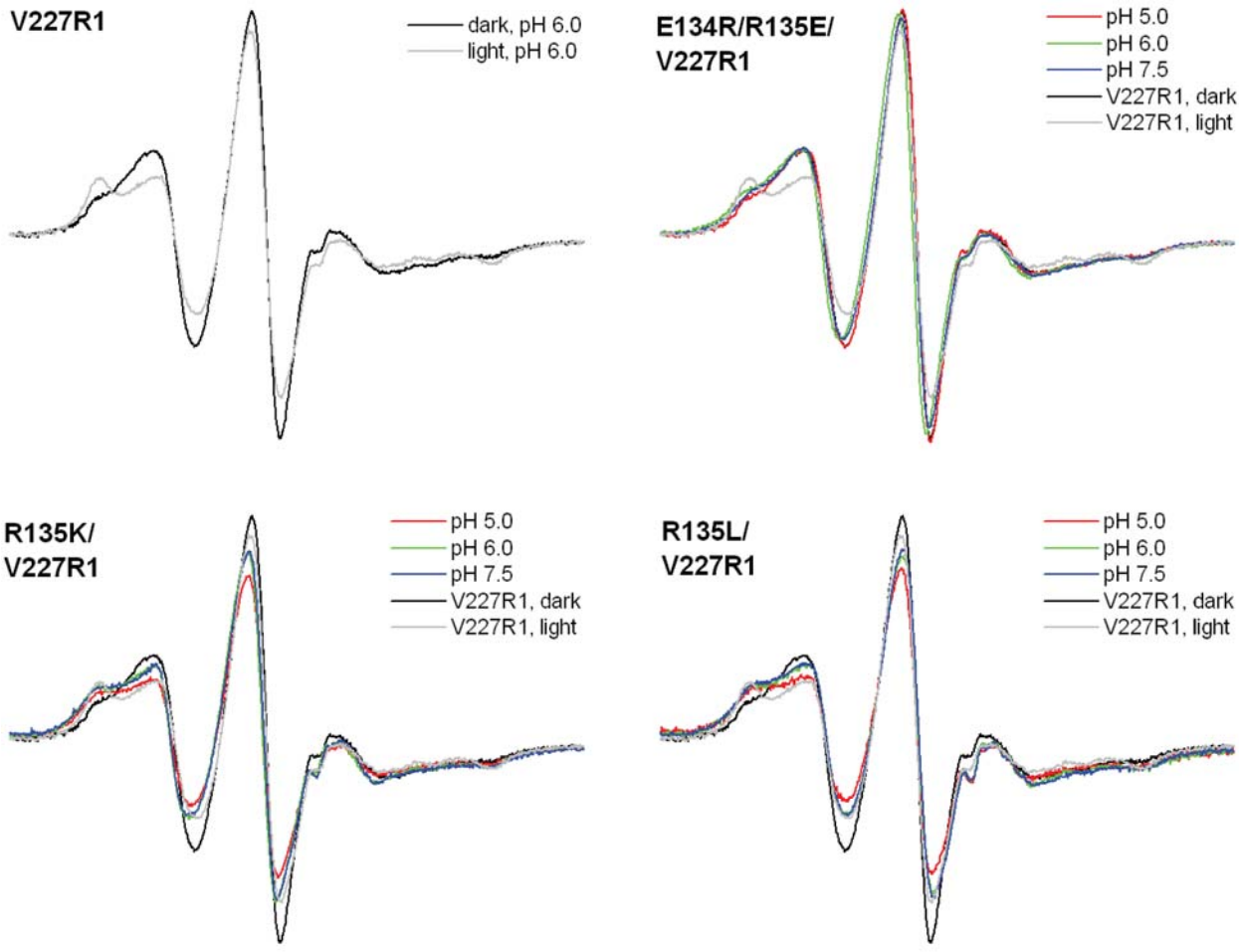

Fig. 45: *EPR spectra of the spin labeled pigments in the dark state at 25 °C. The three pH values are shown for every pigment, and V227R1, which did not undergo any change in line shape with pH, is drawn in every panel for comparison.*

versal' pigment the dark state is essentially the same as for the V227R1 pigment and pH independent. Although the inversion of Glu[134] and Arg[135] is supposed to be a severe disturbance of the structure in the ERY region it causes the least severe changes. In contrast, both the R135K/V227R1 and the R135L/V227R1 pigments show a spectrum in between the V227R1 dark and illuminated state. The effect is even higher at acidic pH for both pigments.

In the illuminated state the E134R/R135E/V227R1 'charge reversal' pigment again shows a small change. The spin label seems to be a little bit less immobilized compared to the pure V227R1 pigment. The pigments R135K/V227R1 and R135L/V227R1 also show an illuminated state similar to that of the pure V227R1 pigment but also with slight deviations in shape. None of the pigments features a distinct pH dependence in the illuminated state. Summing up these results, we see firstly, that both the R135x pigments show a constitutive activity in terms of TM6 movement in the dark, which is enhanced at acidic pH, and secondly all three mutations do not change the illuminated state much.

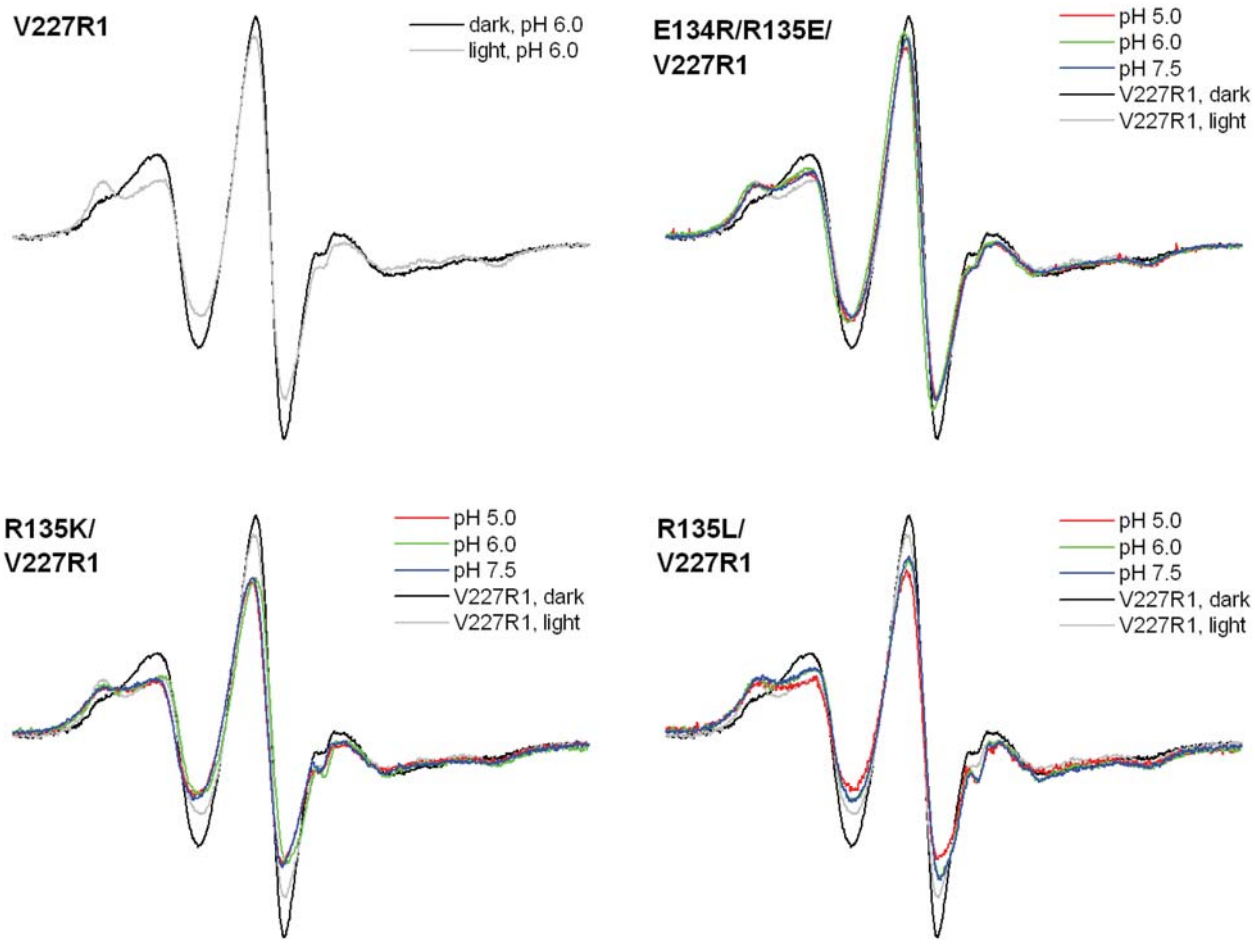

Fig. 46: *EPR spectra of the spin labeled pigments in the illuminated state at 25 °C. The three pH values are shown for every pigment, and V227R1, which did not undergo any change in line shape with pH, is drawn in every panel for comparison.*

At high temperatures the destabilizing effects on TM6 are more clearly visible than at room temperature. Therefore the spectra of the same pigments were also taken at 37 °C. The results are shown in Fig. 47. Again the E134R/R135K/V227R1 pigment features a similar dark state as V227R1, and the same is true for the illuminated state. In contrast to that, both the R135K/V227R1 and the R135L/V227R1 pigments show clear differences: Especially the dark state of both pigments is about half-way between the dark and the illuminated state of the V227R1 pigment. The illuminated spectra are similar to that of the V227R1 pigment but also have a slightly different shape: Instead of the two peaks in the low field region (left side) there is only one peak which does not feature a pronounced dip between them as the spectrum of the illuminated V227R1 pigment does.

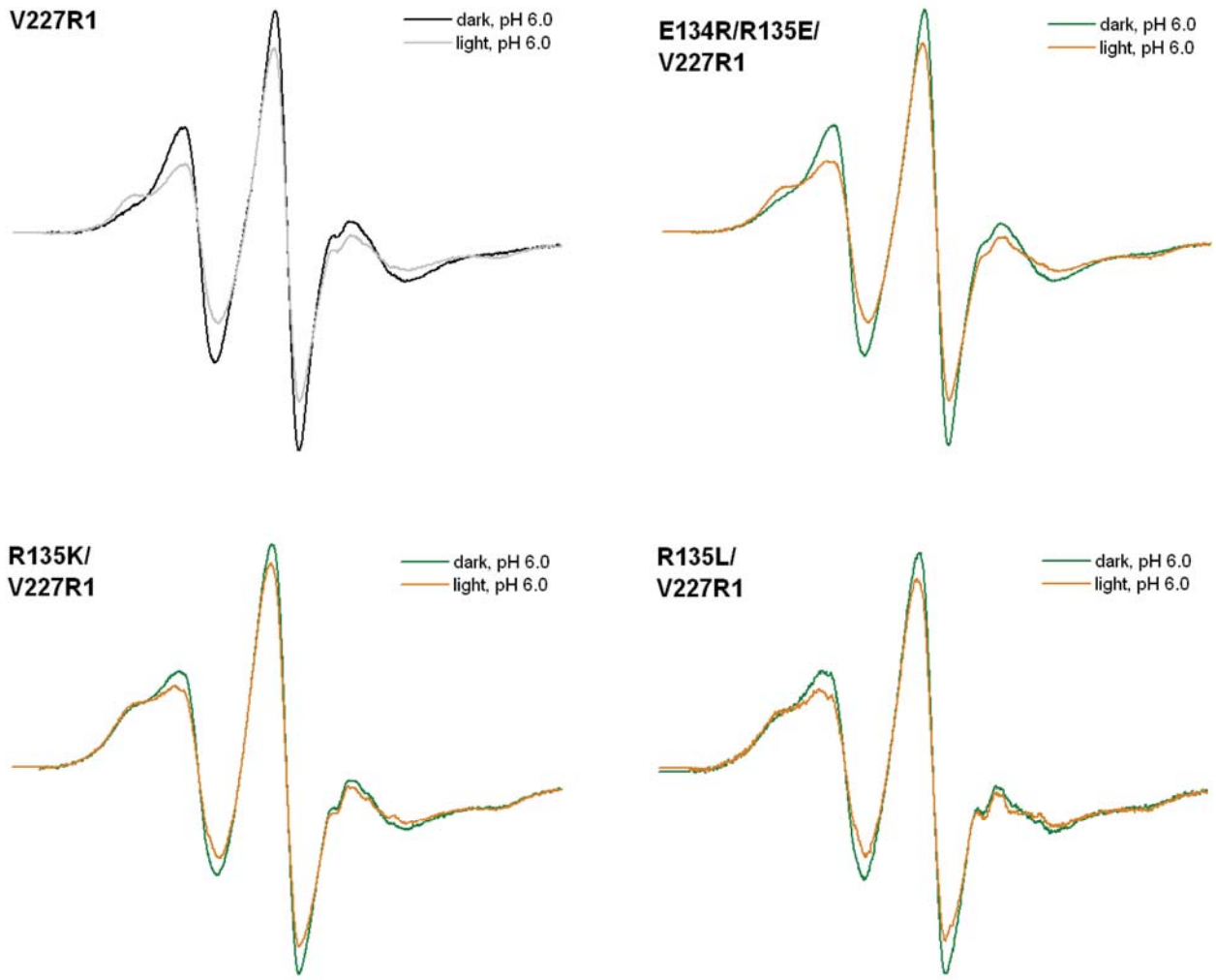

Fig. 47: *EPR spectra of the same pigments as in Fig. 45 and Fig. 46 at 37 °C and pH 6.0. The spectra of V227R1 (same temperature) are shown for comparison.*

3.2.5 G_t activation assay

The values of G_t activation determined through intrinsic Tryptophane flourescence (see 2.3.7) are shown in Fig. 48 for the different mutant pigments. Most pigments do not show a significant difference to WT rhodopsin. Only for the R135L pigment there is no activation visible at all, while the R135K pigment has a reduced activity. The activation is also totally cancelled out for the E134R/R135E 'charge reversal' pigment as reported previously [Franke et al., 1990].

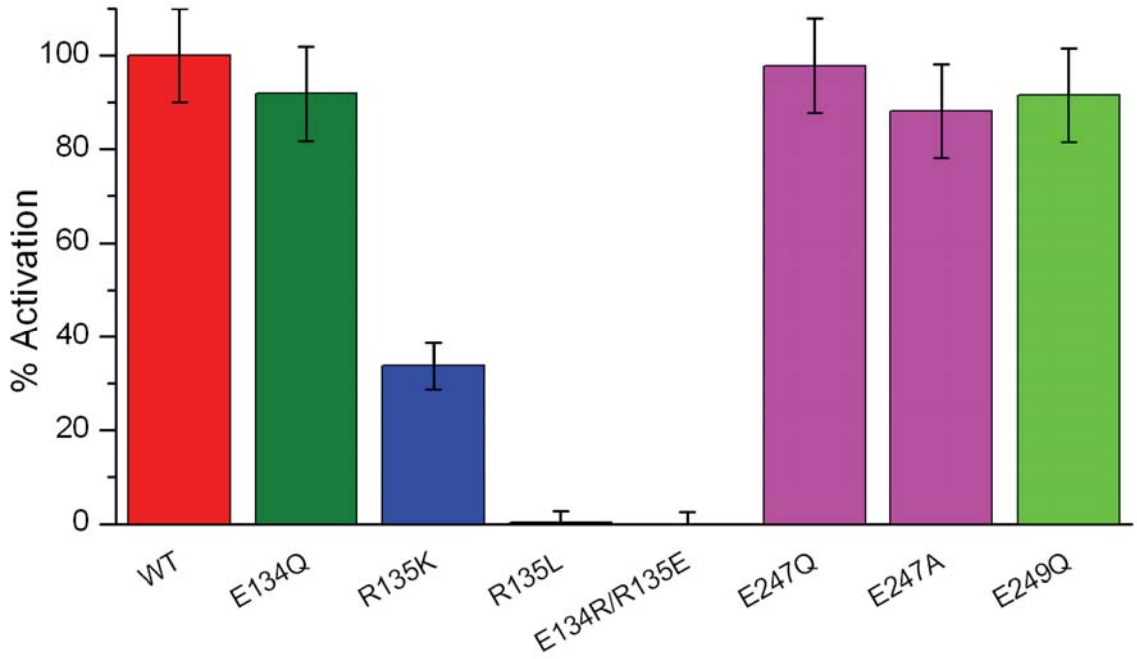

Fig. 48: *Fluorescence measurements using the GTPγS uptake as a benchmark for the activity of the pigments towards trasducin (G_t). The WT activation was set as 100 %. The pigments E134Q, E247Q and E249Q do not show a significant difference from wt rhodopsin, and the activity of the E247A pigment is only slightly reduced. The R135K pigment show only one third of the activation of wt rhodopsin, and both the R135L and the E134R/R135E pigments do not show any G_t activation at all.*

3.3 Other important regions for rhodopsin activation

To investigate the involvement of other regions than the ERY motif into rhodopsin activation, several mutants in the NPxxY$(x)_{5,6}$F motif, the retinal region and other regions that are supposed to be involved in activation were tested with the same techniques. The work on the NPxxY$(x)_{5,6}$F motif and on the mutations of helix 8 has been done together with OLAF FRITZE.

3.3.1 The NPxxY(x)$_{5,6}$F motif

The NPxxY(x)$_{5,6}$F motif in the transition region between TM7 and H8 has been investigated in a recent study [Fritze et al., 2003] and found to be a crucial region for the activation of rhodopsin. Therefore I investigated with OLAF FRITZE mutants which were characterized earlier [Fritze et al., 2003]. We used flash photolysis in the same way as for the ERY mutants (see chapter 3.2.3). The mutant pigments N302A, P303A, Y306A and F313A (all reconstituted with 11-*cis* retinal) were tested with flash photolysis (see 2.3.1).

Traces for the single Alanine replacements in the NPxxY(x)$_{5,6}$F motif are shown in Fig. 49. The rate of Meta-II formation stays unaffected, although Meta-II formation had been shown to be

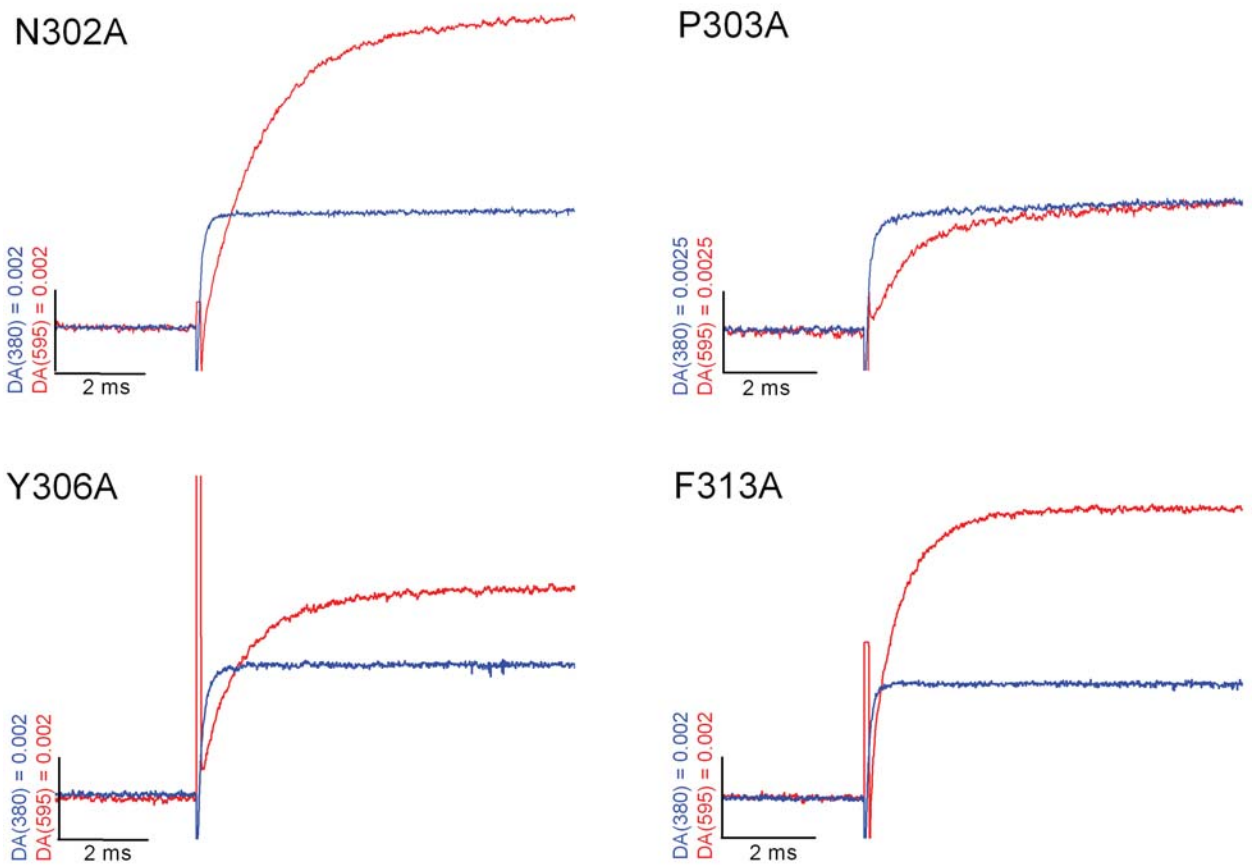

Fig. 49: *Flash photolysis experiments show the formation of Meta-II at 380 nm (blue traces) and the proton uptake at 595 nm (red traces), analog to Fig. 43 (for the ERY motif). For proton uptake bromocresol purple was used as a pH dependent dye (see chapter 1.2.1). All experiments were done at pH 6.0. N302A (upper left panel) shows – similar to WT rhodopsin (see Fig. 43, upper left panel) – Meta-II formation being faster than the proton uptake (= Meta-IIb·H^+ formation). For the P303A pigment (upper right panel) Meta-II formation stays unaffected, but the amplitude of the proton uptake is slightly reduced. For the Y306A pigment (lower left panel) Meta-II formation is unaffected, and the amplitude of the proton uptake is slightly reduced. The F313A pigment (lower right panel) shows the proton uptake amplitude as WT rhodopsin again, but the rate is slightly increased.*

facilitated with both the Y306A and the F313A pigments reconstituted with 9-dm retinal [Fritze et al., 2003]. Instead, a minor influence on the proton uptake is visible: For the P303A pigment (upper right panel) the amplitude is reduced by approximately 50 %, for the Y306A pigment (lower left panel) by approximately 25 %. The F313A pigment (lower right panel) shows a slightly increased proton uptake rate. For the P303A pigment another observation was made at all pH tested: Both Meta-II formation and proton uptake have a small, but reproducible slow component that continues to increase over a long time. Taken together these experiments show that there is at least some interplay between the NPxxY(x)$_{5,6}$F and the ERY region where the proton uptake has been shown to take place (see chapter 3.2.3).

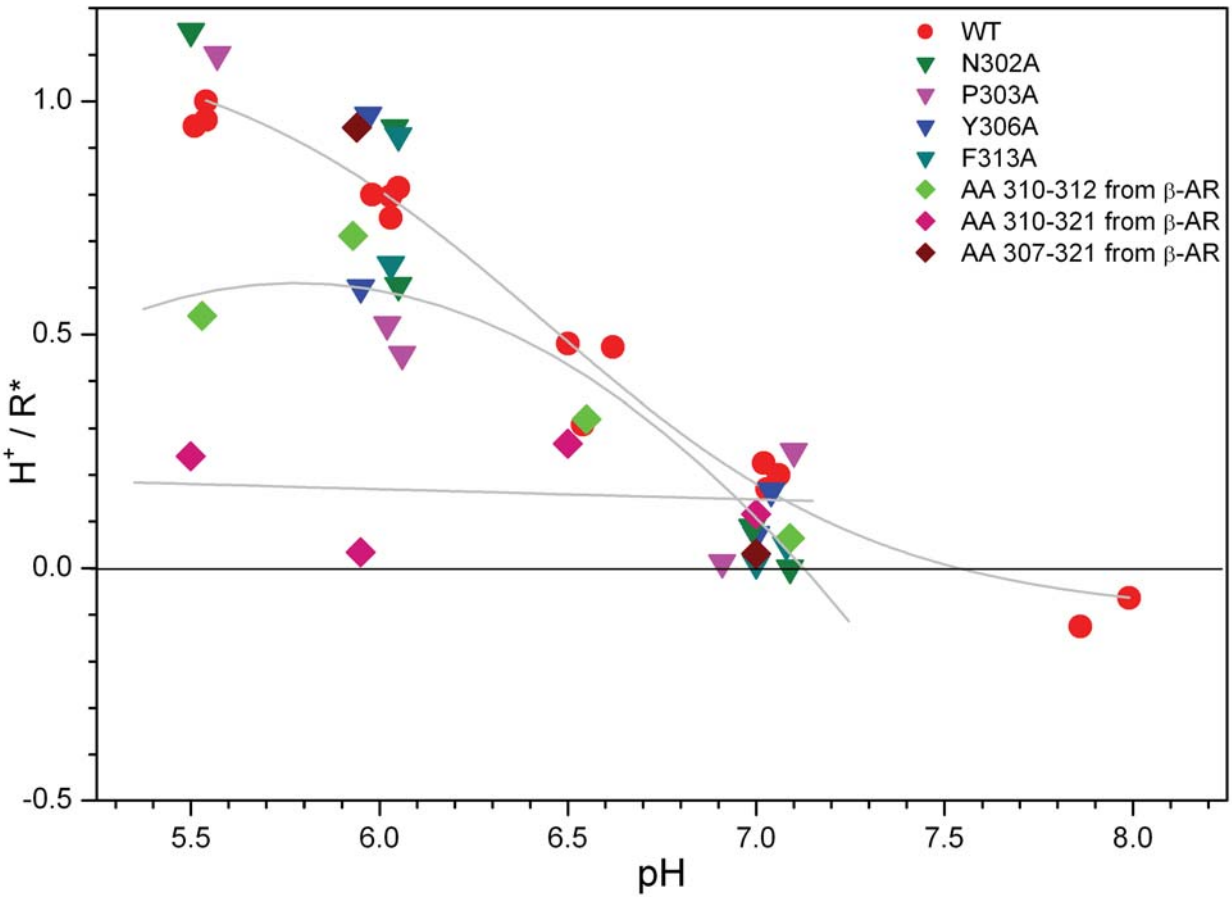

Fig. 50: *Plot showing the number of protons taken up per activated rhodopsin against the pH, comparable to Fig. 44 (for the ERY motif). Proton uptake signals were calibrated as described in 1.2.7. For WT rhodopsin as well as for the pigments Y306A, P303A, N302A, F313A, N73D and N73A roughly one proton is taken up at pH 5.5, decreasing to 0 with rising pH; the pK is about 6.5. Replacement of the whole region with the according sequence of the β_2-adrenoreceptor leads to attenuation of the proton uptake, if amino acids 310-312 are replaced (light green diamonds), or almost a circumvention of the proton uptake, if amino acids 310-321 are replaced (magenta diamonds). If the whole H8 region (amino acids 307-321) is replaced, the proton uptake can be restored (violet diamonds).*

	TM7					turn						helix 8								
	302	303	304	305	306	307	308	309	310	311	312	313	314	315	316	317	318	319	320	321
WT	N	P	V	I	Y	I	M	M	N	K	Q	F	R	n	C	M	V	T	T	L
N302A	A	P	V	I	Y	I	M	M	N	K	Q	F	R	n	C	M	V	T	T	L
P303A	N	A	V	I	Y	I	M	M	N	K	Q	F	R	n	C	M	V	T	T	L
Y306A	N	P	V	I	A	I	M	M	N	K	Q	F	R	n	C	M	V	T	T	L
F313A	N	P	V	I	Y	I	M	M	N	K	Q	A	R	n	C	M	V	T	T	L
AA 310-312 β-AR	N	P	V	I	Y	I	M	M	S	P	D	F	R	n	C	M	V	T	T	L
AA 310-321 β-AR	N	P	V	I	Y	I	M	M	S	P	D	F	R	I	A	F	Q	E	L	L
AA 307-321 β-AR	N	P	V	I	Y	C	-	R	S	P	D	F	R	I	A	F	Q	E	L	L

Table 6: *The mutants in the NPxxY(x)$_{5,6}$F region (chapter 3.3.1) and in the C-terminus (chapter 3.3.2). The native NPxxY(x)$_{5,6}$F motif is highlighted in green, and the single NPxxY(x)$_{5,6}$F mutations are highlighted in orange. The parts from the β_2-adrenergic receptor that replace the homologous sequence from rhodopsin are shaded in blue. Amino acid 308 is missing in the β_2-adrenergic receptor so that the turn between TM7 and helix 8 is one amino acid shorter.*

In Fig. 50 the total amount of protons taken up per activated rhodopsin molecule is plotted against the pH and partly relativises the observations. For the majority of the pigments the mutation in the NPxxY(x)$_{5,6}$F region did not dramatically change the proton uptake behaviour compared to WT rhodopsin (red points): As also shown in Fig. 49, the amplitude of the proton uptake is clearly reduced for P303A (magenta triangles) and slightly reduced for the Y306A pigment (blue triangles), but at pH 5.5 it is on the same level as WT rhodopsin (approx. one proton per activated rhodopsin molecule). Therefore the pK of the proton uptake obviously is shifted to a lower value for these pigments without dramatically changing the whole process.

3.3.2 Replacement of helix 8

To investigate the general mechanism of G protein activation in GPCRs helix 8 (H8) or parts of it have been removed in earlier studies [Osawa and Weiss, 1994; Weiss et al., 1994]. Replacement of H8 in rhodopsin with homologous sequences from the β_2-adrenergic receptor also were investigated [Ernst et al., 2000b; Kim et al., 2005; Marin et al., 2000]. All these mutant pigments have been shown before to express well in COS-1 cells and to reconstitute with 11-*cis* retinal. Only the last mutant in which amino acids 307-321 have been replaced with the homologous ones from the β_2-adrenergic receptor has an expression rate of only 20-25 % compared to WT rhodopsin.

These mutant pigments also show an influence on the proton uptake. The sequences of the different mutations used in chapters 3.3.1 and 3.3.2 are shown in Table 6. All these pigments have been prepared by OLAF FRITZE with whom I collaborated on this.

Flash photolysis measurements on the mutants are shown in Fig. 51. Replacement of amino acids 310 to 312 only (upper right panel) leads to a slight acceleration of the proton uptake. If amino acids 310-321 are replaced (lower left panel), there is no proton uptake detectable any longer, which means that it is either anticipated or cancelled out. If the whole region consisting of amino acids 307-321 is replaced (lower right panel), the proton uptake is totally restored.

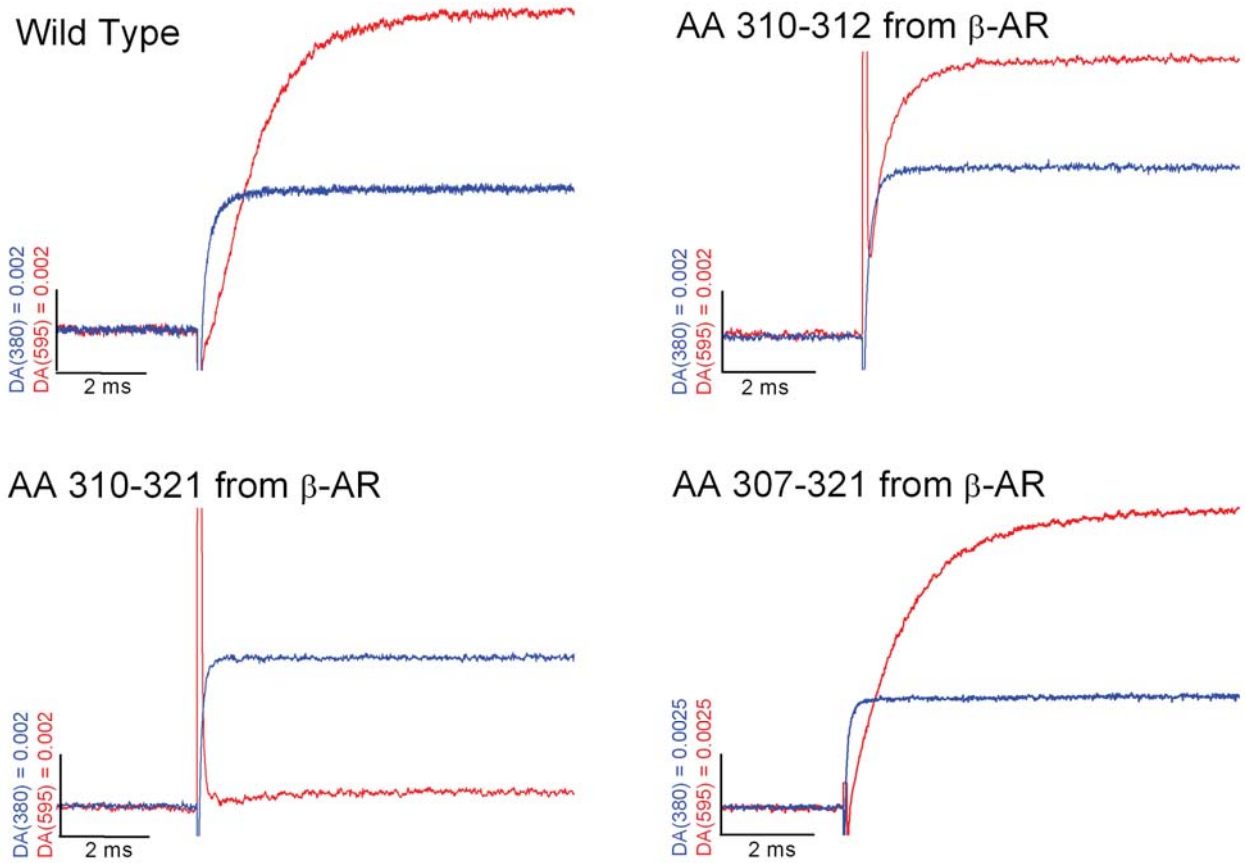

Fig. 51: *Flash photolysis experiments show the formation of Meta-II at 380 nm (blue traces) and the proton uptake at 595 nm (red traces), analogous to Fig. 49 (for the NPxxY(x)$_{5,6}$F mutant pigments). To make this proton uptake visible, bromocresol purple was used as a pH dependent dye (see chapter 1.2.1). All experiments were performed at pH 6.0. WT rhodopsin is plotted for comparison (upper left panel) and shows that Meta-II formation is faster than the proton uptake. For the pigment with amino acids 310-312 replaced by those from the β_2-adrenergic receptor (upper right panel) Meta-II formation stays unaffected, but the proton uptake becomes faster. For the pigment with amino acids 310-321 replaced by those from the β_2-adrenergic receptor (lower left panel) Meta-II formation again stays unaffected, but the proton uptake is not existent any longer. If the whole region (amino acids 307-32) is replaced by that from the β_2-adrenergic receptor (lower right panel) the proton uptake is restored as with WT rhodopsin.*

In Fig. 50 on page 89 the total amount of protons taken up per activated rhodopsin molecule is plotted against the pH. For the majority of the pigments the mutation in the NPxxY(x)$_{5,6}$F region did not dramatically change the proton uptake behaviour compared to WT rhodopsin (red points): The effect is clearer for the pigments with H8 replaced by the analogous region from the β_2-adrenergic receptor: If only amino acids 310-312 are replaced (green diamonds), the proton uptake is reduced by about 50 %. Replacement of amino acids 310-321 (pink diamonds) leads to almost no proton uptake any longer, as it is also visible in Fig. 51 (lower left panel). If amino acids 307-309 are replaced in addition to this (dark red diamonds), the proton uptake is restored to the level of WT rhodopsin.

3.3.3 Other protein regions involved in activation

Similar experiments as shown above for the ERY and the NPxxY(x)$_{5,6}$F mutant pigments were also carried out for pigments with other mutations in regions that are supposed to be involved in rhodopsin activation.

Fig. 52 shows typical flash photolysis traces. If His^{211} in TM5 is replaced with a sterically similar phenylalanine (H211F mutation, upper right panel), the amplitude of the proton uptake remains unaffected. Interestingly both Meta-II formation and the proton uptake are slowed down by approximately a factor of 50 (the time constant of Meta-II formation is 28 ms compared to 0.2 ms for WT rhodopsin; the time constant for proton uptake is 45 ms compared to 1 ms for WT). If His^{65} in the loop region between TM1 and TM2 is replaced with a Cysteine (H65C mutation, lower left panel), the proton uptake amplitude is reduced by about 50 %. The pigments, in which Asn^{73} in TM2 was changed to either Asparagine or Alanine or Asp^{83} in TM2 was contrarily changed to Asparagine, did not show any influence on Meta-II formation or proton uptake kinetics and amplitudes (data not shown here).

The E113Q pigment (lower right panel) has been shown to have a deprotonated Schiff base in the ground state, because Glu^{113} is – together with Glu^{181} – the counterion for the retinal Schiff base (Lys^{296}) [Ludeke et al., 2005; Martinez-Mayorga et al., 2006]. Because of this it is not possible to illuminate the pigment with green light, and therefore it was illuminated with blue light (380 – 480 nm). The traces are shown in Fig. 52, lower right panel. The Meta-II level is restored, after the flash, although the time in between is hard to judge due to a long flash artefact. Interestingly the proton uptake looks similar to WT rhodopsin. It is only slightly slower (please note the different time scale).

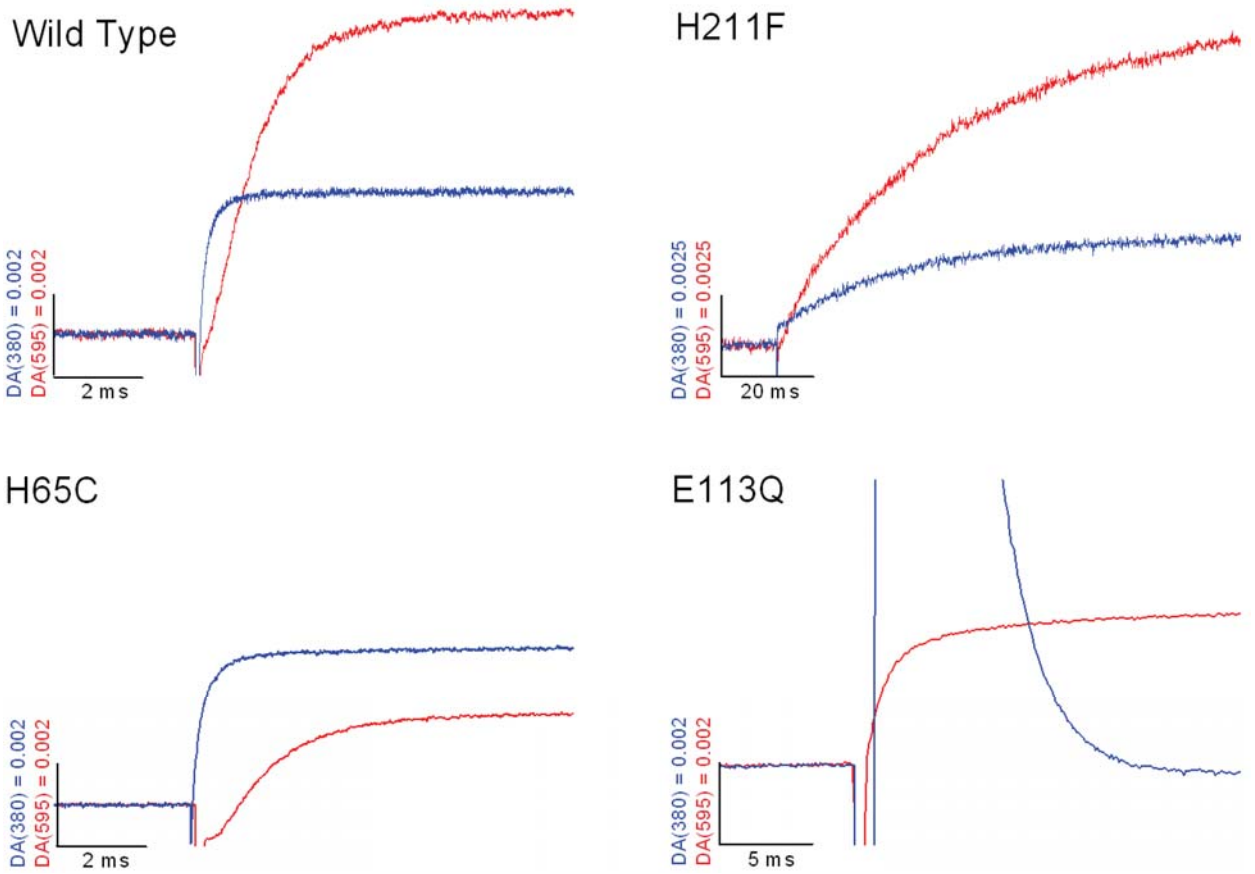

Fig. 52: *Flash photolysis experiments showing the formation of Meta-II at 380 nm (blue traces) and the proton uptake at 595 nm (red traces), analogous to Fig. 43 (for the ERY motif). To detect the proton uptake, bromocresol purple was used as a pH dependent dye (see chapter 1.2.1). All experiments were performed at pH 6.0. WT rhodopsin (upper left panel) shows Meta-II formation being faster than the proton uptake. For the H211F pigment (upper right panel) both Meta-II formation and proton uptake are slowed down extremely (please note the time scale!), although Meta-II formation still shows a very fast component (note the little jump at the point where the flash was applied). For the H65C pigment (lower left panel) Meta-II formation stays unaffected, but the proton uptake is reduced by about 50 %. The E113Q pigment (lower right panel) has an absorption maximum at 380 nm due to counterion replacement and therefore cannot be illuminated with green light. Due to the longer and stronger flash with blue light (380-480 nm filter) the Meta-II signal shows a long flash artefact but finally returns to the initial value. Interestingly the proton uptake is similar to the proton uptake for the WT pigment (please note the different time scale that was chosen to show the return of the Meta-II signal).*

In Fig. 53 again the number of protons taken up is plotted against the pH. As already shown in Fig. 52, the H65C pigment shows a reduced proton uptake, while the N73D, the N73A, and the D83N pigments did not show any influence. E113Q features – in spite of the already deprotonated Schiff base – a normal proton uptake as well, and the same is true for the H211F pigment, although it was shown to be a lot slower than WT rhodopsin (see Fig. 52, upper right panel).

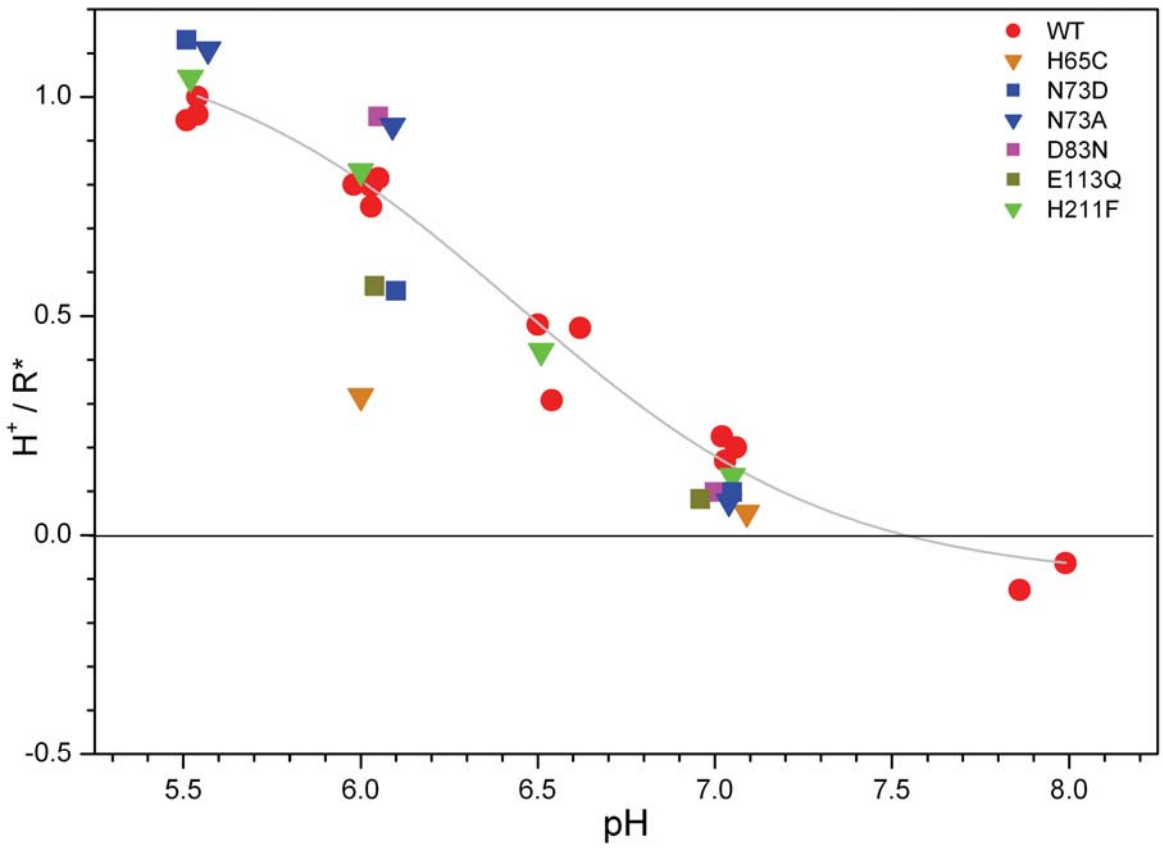

Fig. 53: *The plot shows the number of protons taken up per activated rhodopsin against the pH, comparable to Fig. 44 (for the ERY motif) and Fig. 50 (for the NPxxY(x)$_{5,6}$F motif). The proton uptake signals were calibrated as described in 1.2.7. For WT rhodopsin as well as for the pigments N73D, N73A, D83N, E113Q and H211F there is roughly one proton taken up at pH 5.5, and this decreases to 0 with rising pH. The pK is about 6.5. Only the H65C pigment shows a different behaviour: There is only roughly half the proton uptake compared to WT and the other similar pigments.*

3.4 Partial agonists: 9-demethyl and acyclic retinal

The influence of the partial agonists 9-demethyl retinal (Fig. 21) and acyclic retinal (Fig. 22) on rhodopsin activation has been discussed in detail before [Bartl et al., 2005; Knierim et al., 2007; Meyer et al., 2000]. In this work the focus on the partial agonists is how these affect the activation mechanism and stabilization of the dark state, respectively.

3.4.1 Lack of stabilization with acyclic retinal

To determine the importance of both the 9-methyl group and the β-ionone ring of the retinal for the stabilization of the rhodopsin dark state, the effect of the retinal analogs on TM6 motion in the dark state was tested. As shown before [Knierim et al., 2007], the dark state of the pigments

with the three different retinals does not differ at room temperature (data not shown here). Therefore the same experiment were performed at body temperature (37 °C), finding a distinct effect for the acyclic retinal (see Fig. 54): While the pigment with 9-dm retinal shows an dark state identical to that with 11-*cis* retinal, the dark state for the pigment with acyclic retinal shows a higher mobility for TM6 (mirrored in the increased mobility of the R1 side chain at position 250), which can be deduced from the narrower spectrum (see the dark blue line in Fig. 54).
The spectra of the illuminated pigments by contrast do not differ from what has been shown before: The spinlabel at position 250 and therewith TM6 gets more mobile during activation. For the 9-dm and acyclic pigments this effect is smaller, indicating that only a fraction of the molecules switches into the active state due to the partial agonism of both the 9-dm and the acyclic retinal. For the effect of partial agonism on TM6 motion please see my diploma thesis or the corresponding publication [Knierim et al., 2007].

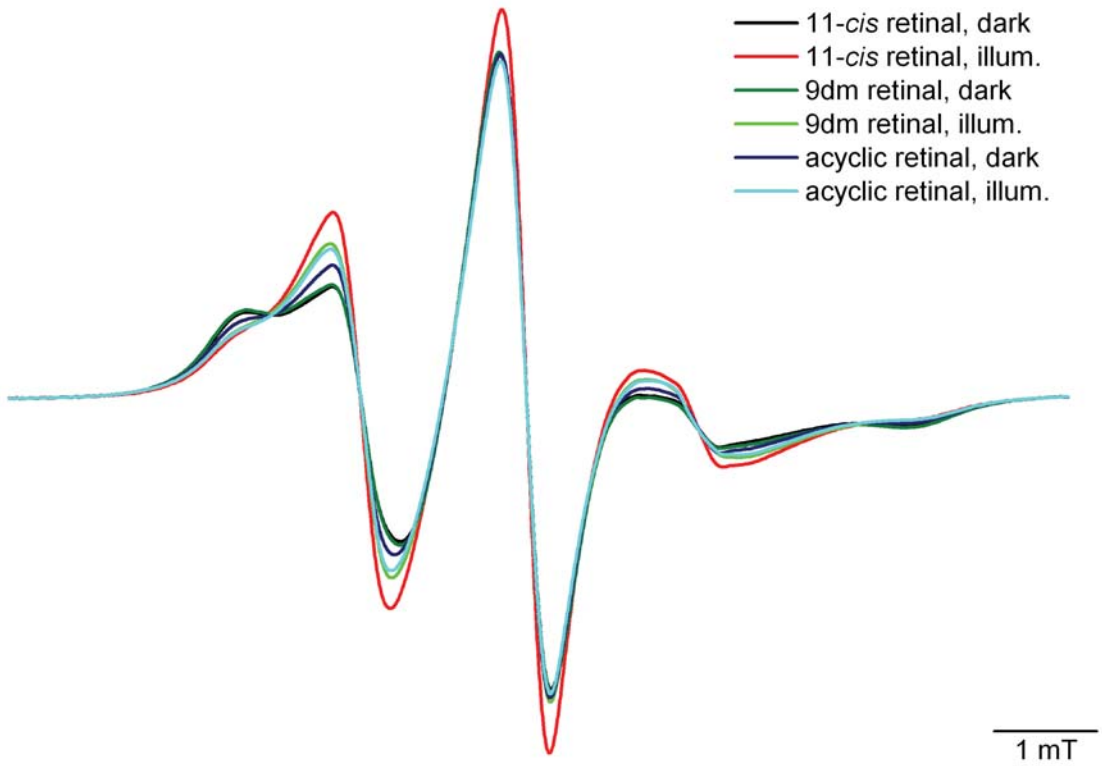

Fig. 54: *EPR spectra of the V250R1 pigment at 318 K with the three different retinals (see Fig. 20 - Fig. 22). For each pigment a spectrum of the dark state and of the illuminated, Meta-II similar state is shown. The pigment with native 11-*cis *retinal shows a distinct change from a less mobile dark state (black line) to a more mobile illuminated state (red line), indicating the outward movement of TM6. The pigment with 9-dm retinal has an identical dark state (dark green line), but a smaller fraction of the molecules passes into the illuminated state (light green line). The pigment with acyclic retinal shows a more mobile spectrum for the dark state already (dark blue line). This shows that the β-ionone ring is indeed important for stabilization of TM6. The illuminated state therefore does not differ from the illuminated state of the 9-dm pigment (light blue line).*

3.5 Blue light illumination: ground state and Meta-III

3.5.1 Reversion of rhodopsin into the ground state

In native disc membranes, illumination of Meta-II with blue light reverses Meta-II into Meta-III with a small percentage ground state [Bartl and Vogel, 2007; Ritter et al., 2007; Ritter et al., 2004].

I was interested in the effect of blue light on Meta-II in detergent solution. It turns out that Meta-II can indeed be reversed into the ground state, at least about a third of the molecules, if it is in a detergent environment. Fig. 55 shows typical absorption spectra of rhodopsin in DM environment: The ground state with the 500 nm absorption maximum (black line) is switched to the 380 nm absorbing Meta-II state upon activation with green light (red line). If the Meta-II state is then illuminated with blue light (400 nm) the resulting spectrum looks like a mixture of different

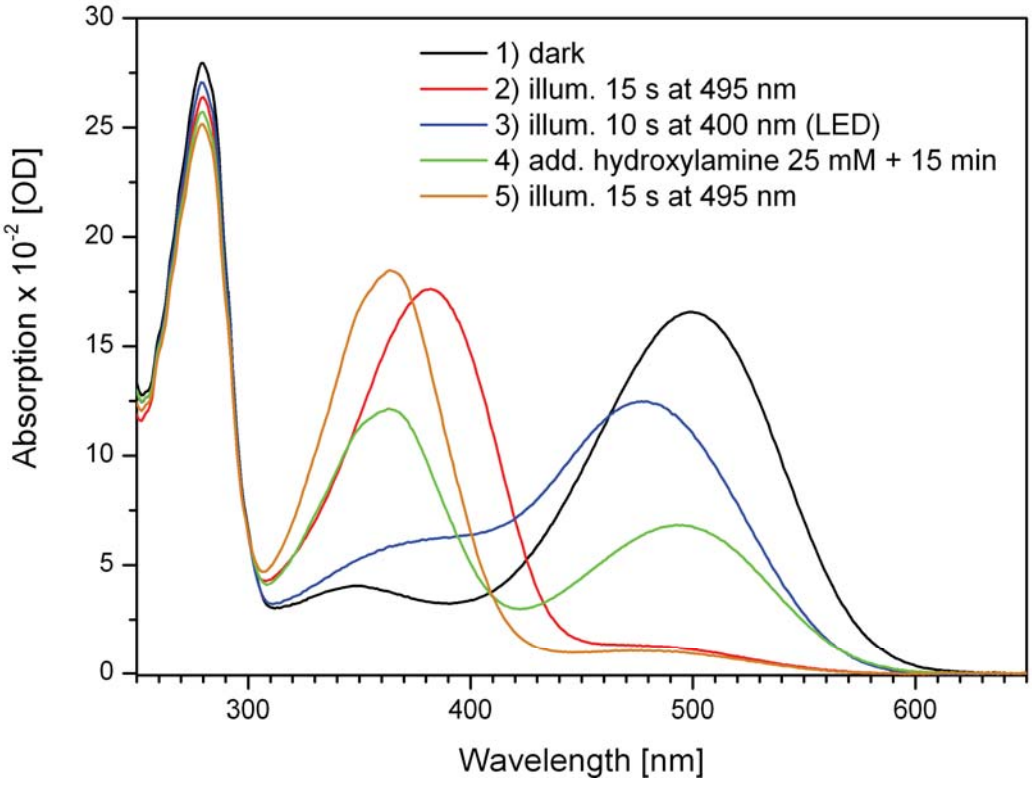

Fig. 55: *UV/vis spectra of rhodopsin in DM, first illuminated first with green light (495 nm, red line) and then with blue light (400 nm, blue line). The absorption maximum changes from 500 nm to 380 nm and then back to 478 nm, representing an overlay of different photoproducts. To determine the existence of rhodopsin in the ground state, hydroxylamine was then added to the sample (1 mM) and incubated for 15 min (green line). The restoration of a significant amount of 500 nm absorbing species proves the existence of intact Schiff base. The second illumination with green light (495 nm, orange line) shows that the product can still be illuminated.*

photoproducts (blue line) including the 500 nm absorbing ground state.

To test this mixture for the existence of rhodopsin ground state 1 mM hydroxylamine was added and incubated for 15 min. Hydroxylamine has been shown before to react selectively with a protonated Schiff base that connects the retinal to the protein [Hofmann et al., 1983; Sakmar et al., 1991]. The resulting spectrum showed – apart from the 365 nm absorbing retinal oxime – an articulate absorption maximum at 500 nm indicating that there is rhodopsin ground state formed upon blue light illumination. The same amount of ground state rhodopsin in the photoproduct mixture is also revealed if the solution is left at room temperature for several hours, because Meta-III decays into opsin and all-*trans* retinal unlike the ground state (data not shown).

To further investigate the formation of the ground state, a similar experiment was performed

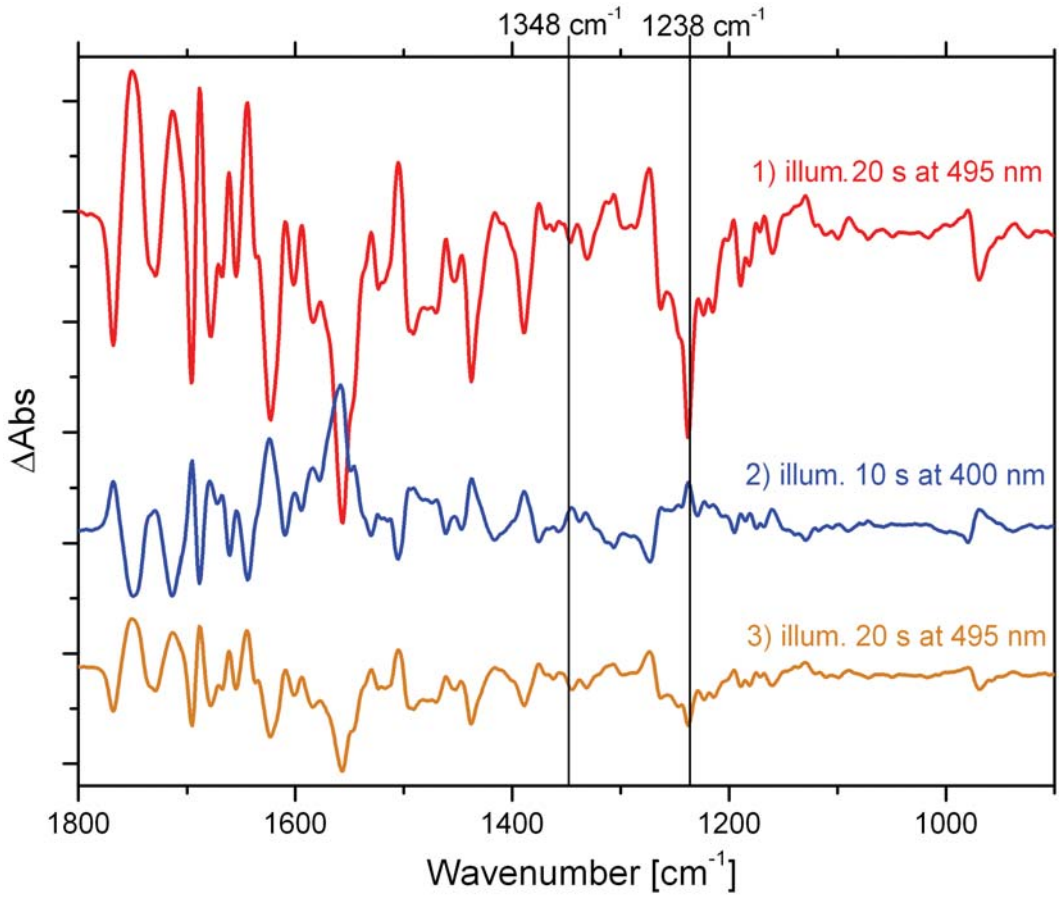

Fig. 56: *FTIR difference spectra of rhodopsin in DM, first illuminated with green light (495 nm, red line) and then with blue light (400 nm, blue line). The negative band at 1238 cm^{-1} indicating the isomerization of the 11-*cis *retinal to all-*trans *retinal is reverted into a positive band, while there is no huge 1348 cm^{-1} band which would show quantitative formation of Meta-III. This shows that 11-*cis *retinal is restored. To test this, the sample was again illuminated with green light (495 nm, orange line), showing the 1238 cm^{-1} band as a negative band again which shows the inverse isomerization of 11-*cis *to all-*trans *retinal.*

with FTIR spectroscopy. Rhodopsin in DM was dried onto a BaF_2 surface and then rehumidified as described (see chapter 2.3.4). The illumination with green light (495 nm) showed the known difference spectrum [Siebert, 1990]. The illumination with blue light did not show a clear positive 1348 cm^{-1} band indicative of Meta-III formation [Bartl et al., 2001; Ritter et al., 2004]. Instead it revealed positive 1238 cm^{-1} and 1206 cm^{-1} bands (small) which show that both 11-*cis* and 9-*cis* retinal are created, thus rhodopsin and isorhodopsin. A second illumination with 495 nm light reverts both bands to negative bands again which is another prove that 11-*cis* and a small fraction of 9-*cis* retinal have been present in the blue light illuminated state.

Finally the retinal extracted from the DM purified samples was directly analysed using HPLC (see chapter 2.2.10). As expected the ground state (black spectrum) shows mainly 11-*cis* retinal with a small fraction of all-*trans* retinal which is in equilibrium with 13-*cis* retinal [Ritter, 2006].

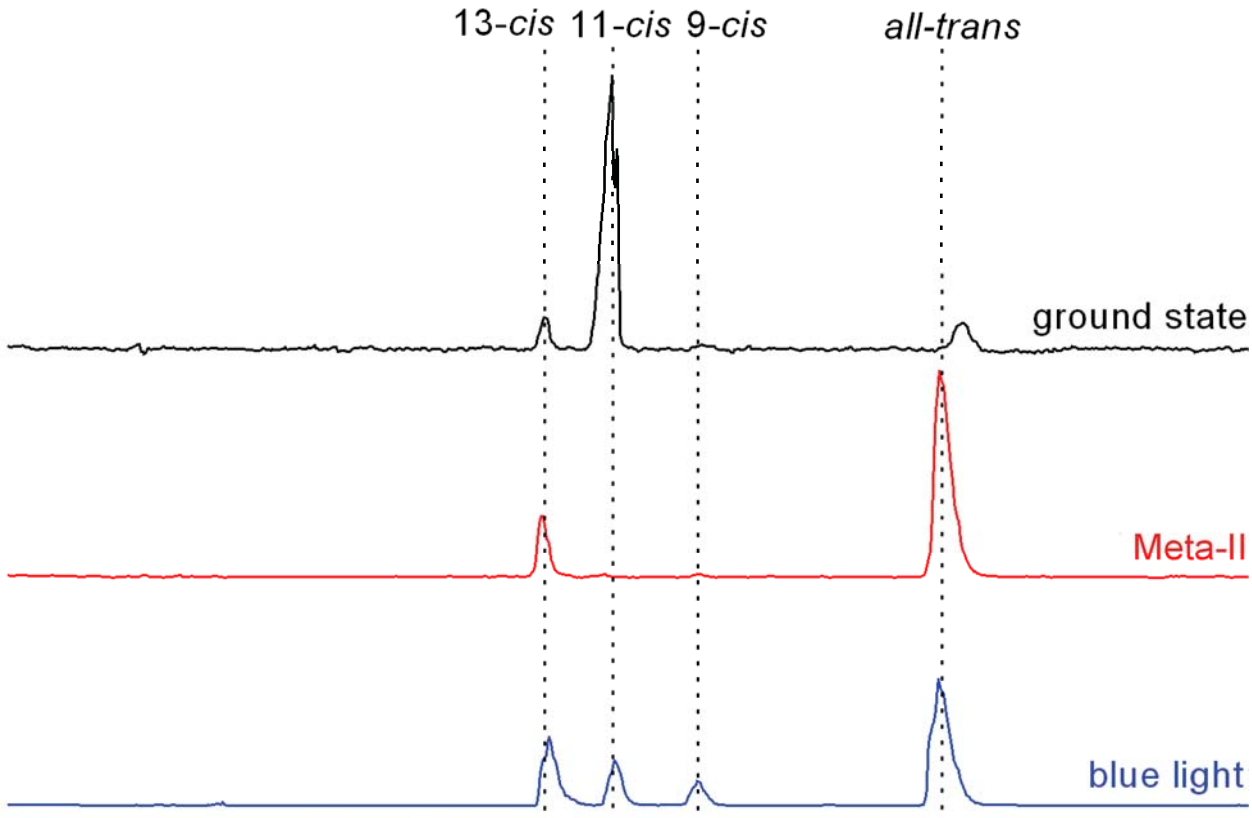

Fig. 57: *HPLC analysis of the retinal extracted from the rhodopsin samples. Rhodopsin in the ground state shows mainly 11-*cis *retinal (83 %) with a small onset of all-*trans *retinal (9 %) which always is in equilibrium with 13-*cis *retinal (7 %). The bleached rhodopsin in the Meta-II state only shows all-*trans *retinal (83 %), again in equilibrium with 13-*cis *retinal (16 %). Interestingly, apart from a big fraction of all-*trans *(56 %) and 13-*cis *retinal (23 %), the blue light state shows clear fractions of 11-*cis *retinal (14 %) and 9-*cis *retinal (8 %), showing that rhodopsin ground state has been recreated.*

This is probably due to the isomerization of retinal during the extraction process or a small fraction of decayed rhodopsin. The illuminated sample (red spectrum) shows only all-*trans* retinal which is again in equilibrium with 13-*cis* retinal.

After blue light illumination there is a mixture of all the different retinals. As deduced from the UV/vis and FTIR experiments there is indeed a significant fraction of 11-*cis* retinal (14 %) and 9-*cis* retinal (8 %), so rhodopsin and isorhodopsin are actually recreated from Meta-II.

3.5.2 Examination of the environmental influence on restoration of the ground state

As described in the previous chapter the restoration of the ground state has only been observed in DM. Does it also work in other environments?

In Fig. 58 a typical blue light illumination experiment is shown for rhodopsin purified in octyl glucoside (OG) – analog to Fig. 55 with DM. As the spectra show, rhodopsin is quantitatively

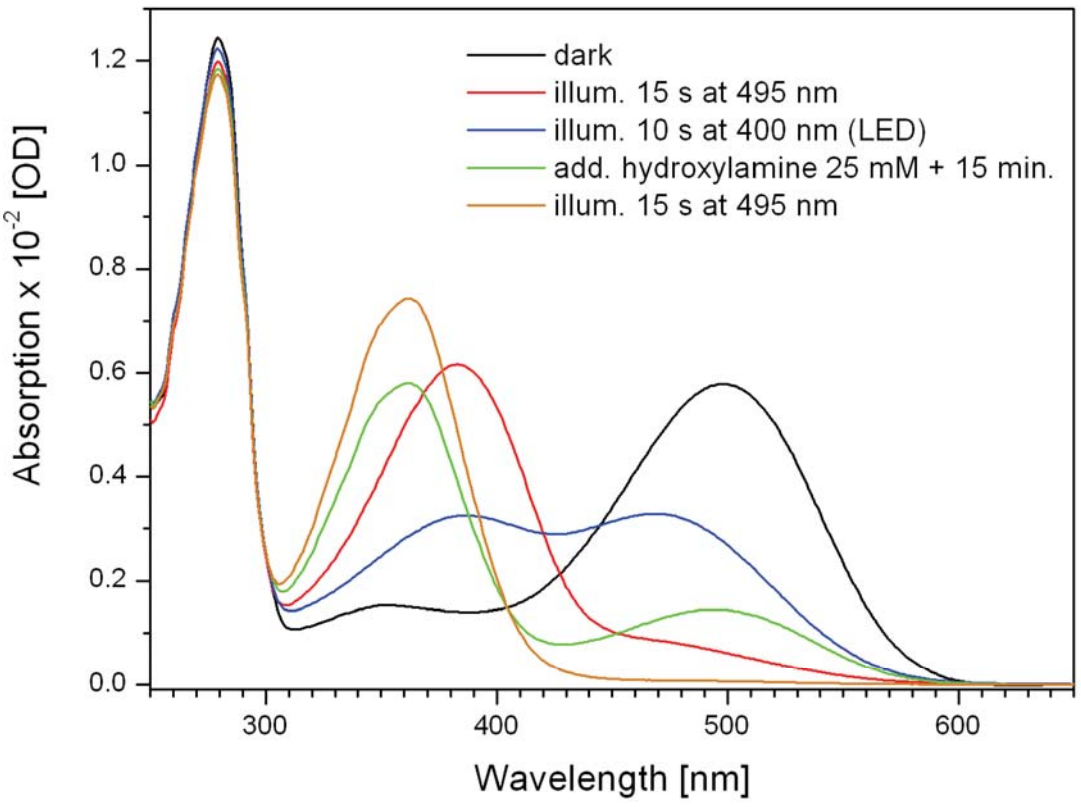

Fig. 58: *UV/visible spectra of rhodopsin in OG (pH 6.0, 25 °C), first illuminated with green light (495 nm, red line) and then with blue light (400 nm, blue line). The absorption maximum changes from 500 nm to 380 nm and then back to 478 nm, representing an overlay of different photoproducts. To determine the existence of rhodopsin in the ground state, hydroxylamine (1 mM) was added to the sample afterwards and incubated for 15 min (green line). The remaining fraction of 500 nm absorbing species proves the existence of intact Schiff base. The second illumination with green light (495 nm, orange line) proves that the product can still be reverted to Meta-II.*

converted into Meta-II. However, upon blue light illumination there is a smaller 470 nm peak than in DM. The addition of hydroxylamine as described above shows that only a small fraction (less than one third compared to DM) is switched back into the ground state.
In membranes blue light illumination has been examined excessively before [Bartl et al., 2001; Ritter et al., 2007; Ritter et al., 2004; Zimmermann et al., 2004]. My results underline their argument, no hydroxylamine stable species could be found in membranes (data not shown), so the restoration of the ground state seems to be an exclusive ability of the detergent system that also depends on the type of detergent used.

3.5.3 Effect of mutations on restoration of the ground state

Which role do certain protein regions play for the described restoration of the ground state?
I performed the same experiments as shown in Fig. 55 and Fig. 58 also with different mutant pigments at two different pH values (pH 5.5 and pH 7.5). The amount of restored ground state was determined by treating the samples with hydroxylamine as described above (see Fig. 55 and Fig. 58). The photoproducts with protonated Schiff base can be divided into a hydroxylamine sensitive and insensitive fraction. The latter one consists of the restored ground state (11-*cis* retinal) and Isorhodopsin (9-*cis* retinal). Both fractions were then related to the original ground state at 498 nm. The data is shown in Fig. 59.
Rhodopsin in DM as the reference system shows a ground state level of 40 % and 35 % of hydroxylamine instable products. Both amounts are independent of pH. Mutants in the Schiff base region were investigated: The mutant pigments F293L and F91L/F293L both have a ground state that is not stable against hydroxylamine because the Schiff base environment is changed by the mutations. Therefore the amount of restored ground state was determined by decay of the blue light illuminated sample for several hours. Both mutants showed the same level of ground state as rhodopsin in DM, but the level of hydroxylamine instable species was reduced.
The E134Q mutant and the R135L mutant in the ERY region that have already been examined above (see 3.2) were also tested. Both of them showed an interesting behaviour: While the amount of restored ground state is only slightly reduced, the amount of hydroxylamine instable becomes pH dependent for both pigments: The amount of the product is significantly smaller at basic pH than at acidic pH.
Mutants involving the E113Q mutation are constitutively active and therefore do not feature any 500 nm absorbing ground state at all. With both the E113Q/M257Y and the E113Q/M257Y/E134Q pigment no 500 nm absorbing ground state is recreated upon blue light illumination either, and the fraction of hydroxylamine instable species is on a normal level at pH 7.5. Interestingly, at pH

5.5 this level is down to zero for E113Q/M257Y and strongly increased for the triple mutant E113Q/M257Y/E134Q – once again showing an inverse pH dependence caused by the E134Q mutation (as in chapter 3.2.1).

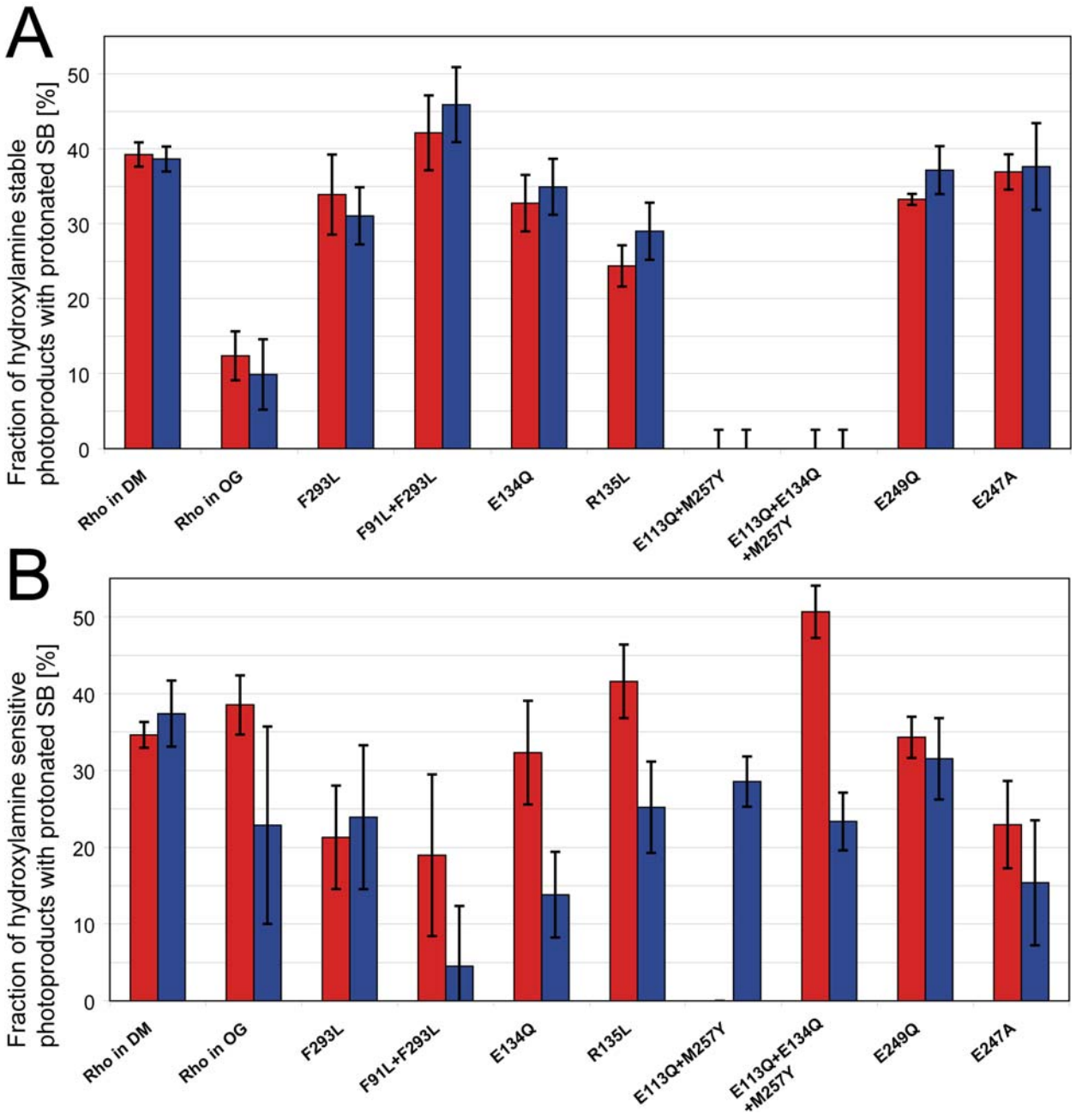

Fig. 59: *Restoration of hydroxylamine stable and instable species with protonated Schiff base from Meta-II by blue light illumination. Experiments were done at 25 °C. The red columns represent the percentage of the respective product at pH 5.5, the blue columns at pH 7.5. The data is deduced from experiments of the type shown in Fig. 55 and Fig. 58 by measuring the respective amplitudes and relating them to the level of the original ground state (498 nm), which was regarded as 100 %. The values shown here do not add up to 100 %, because a significant fraction stays in the Meta-II state upon blue light illumination.* **A** *The percentage of the species that is stable against hydroxylamine and is therefore assumed to represent the ground state.* **B** *The percentage of the species that is not stable against hydroxylamine and is therefore assumed to represent Meta-III.*

The side chains opposite of the ERY motif, Glu^{247} and Glu^{249} were also examined again (see 3.2): Both the E249Q and the E247A mutants did not show a significant change in the level of recreated ground state, and the level of hydroxylamine instable species was only slightly reduced (a little bit more for the E247A pigment) without any clear pH dependence.

3.5.4 Kinetics of Metarhodopsin-III and ground state formation

With the described flash photolysis setup not only the formation of Meta-II can be observed, but also its decomposition upon illumination of Meta-II with blue light. For this purpose a flash with a high output of UV light, equipped with a 380-450 nm filter is used (for a detailed description see 1.2.3). Because this is the same wavelength at which Meta-II decomposition is observed, the detector is saturated for several milliseconds resulting in a huge artefact.

Fig. 60 shows a typical experiment in a DM environment. Obviously the decomposition of Meta-II (blue trace) is faster than the proton release (red trace). The amplitudes are just opposite to the amplitudes observed for normal illumination with green light (compare for example Fig. 33A). Interestingly the order of the two processes remains the same: First the reprotonation of the Schiff base leading to the decrease of the 380 nm formation takes places and afterwards the proton release reaction out of the protein. Nevertheless, both processes are extremely slowed down compared to the normal illumination with green light: The reaction constant is 0.012 ms^{-1} for Meta-II decomposition and 0.007 ms^{-1} for proton release. This means that both processes are roughly a factor of 100 slower than Meta-II formation of proton uptake, respectively.

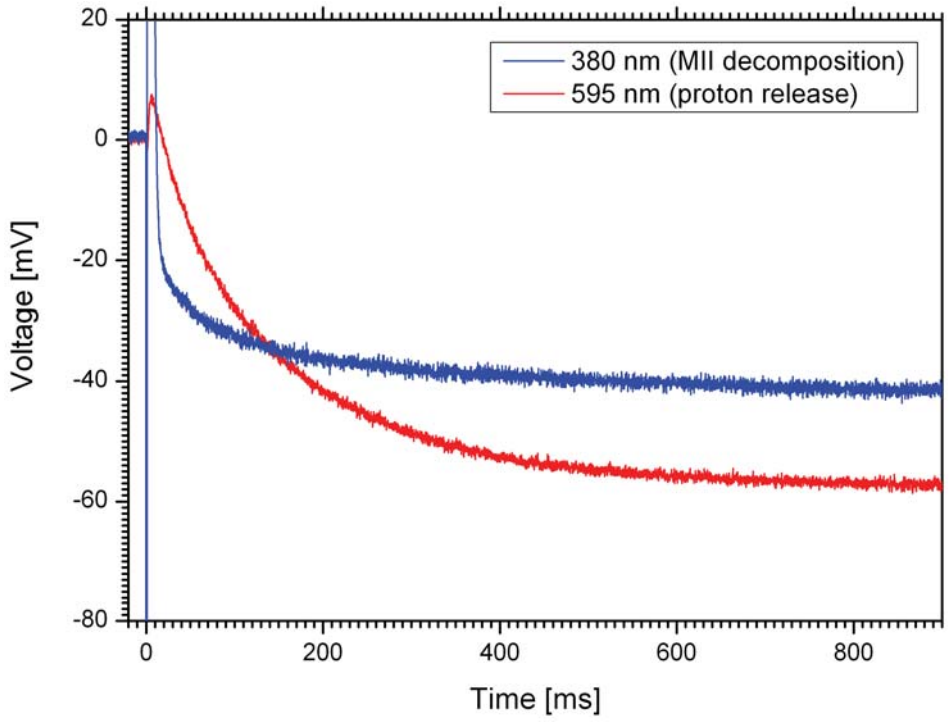

Fig. 60: *A typical flash photolysis experiment on rhodopsin in DM with blue light illumination at 20 °C and pH 6.0. Meta-II decomposition (blue line) is obviously faster than the proton release (red line).*

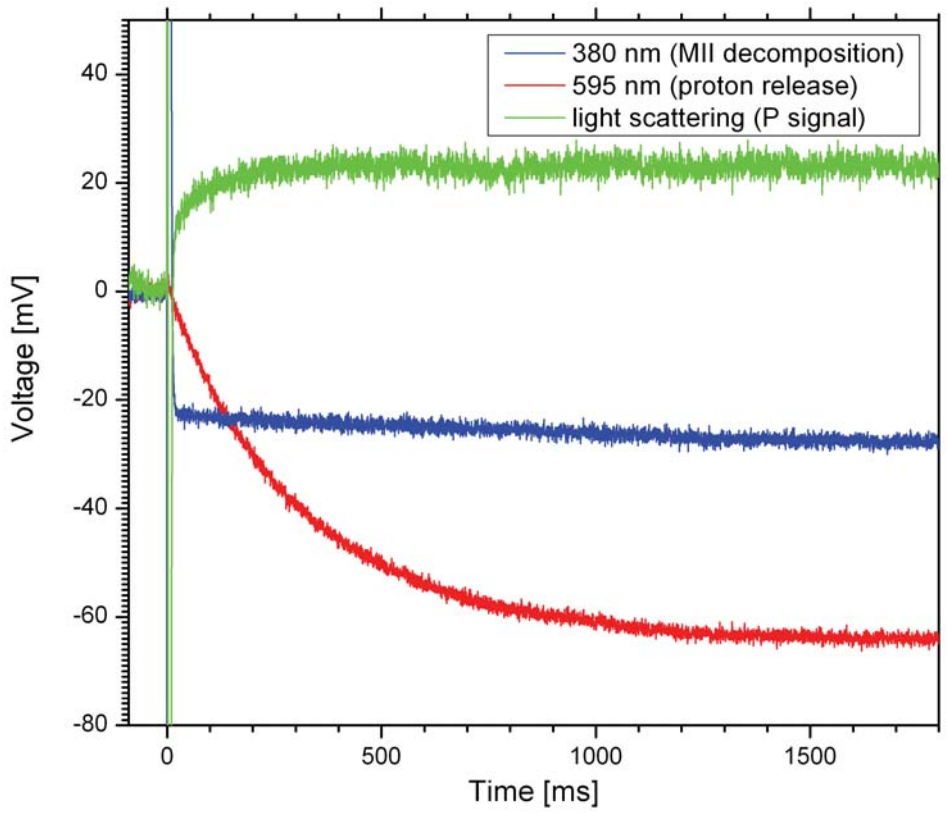

Fig. 61: *A typical flash photolysis experiment on WT rhodopsin in washed membranes with blue light illumination at 20 °C and pH 6.0. Meta-II decomposition (blue line) is clearly faster than the positive light scattering signal (green line) and the proton release (red line).*

A similar experiment in membranes is shown in Fig. 61. The basic findings are the same as for the DM environment: The amplitudes are comparable to those observed during normal activation with opposite algebraic sign – including the light scattering signal that can be additionally observed in membranes but not in DM. Again the order of the processes is reversed compared to the normal activation pathway: First, the deprotonation of the Schiff base (measured through the decrease at 380 nm) is observed, followed by the positive light scattering signal and the proton release (measured at 595 nm). Thus there is no severe difference between restoration of the ground state (in DM) and Meta-III formation (in membranes). Meta-II decomposition has a reaction constant of 0.2 ms^{-1} (this number has a high uncertainty due to the huge flash artefact) and therefore has comparable kinetics to Meta-II formation upon illumination with green light. The light scattering signal has a reaction constant of 0.01 ms^{-1}, which means that it is roughly a factor of 5 slower than the 'N-signal' during activation. The proton release has a reaction constant of 0.003 ms^{-1} and is therewith by roughly a factor of 10 slower than the proton uptake during activation.

Therefore the comparison of the kinetics between activation with green flashes and deactivation with blue flashes is different depending on the environment: In detergent both processes are slowed down by roughly two orders of magnitude while the processes develop inconsistently in membranes.

	Activation energies [kJ/mol]:							
	MII decompos.		H^+ Release		H8 movement		N-Signal	
Conditions	E_A	+/-	E_A	+/-	E_A	+/-	E_A	+/-
Rho in membranes, blue flash			82,1	8,2			107,8	12,6
Rho in membranes with SL, blue fl.			81,3	3,8			94,8	6,1
Rho in membranes, sandw., bl. fl.			125,4	15,0				
Rho in vesicles, blue flash			74,5	3,4				

Table 7: *Activation energies deduced from the Arrhenius plots through linear fits as in Table 5. The different conditions are described in the left column. For completeness data for rhodopsin in FTIR sandwiches (squeezing the membrane sample between to BaF_2 panes as described in 2.3.4) and in reconstituted vesicles (following the protocol in [Kusnetzow et al., 2006]) are also shown. The columns are colored as in the Arrhenius plots for easier visibility. Cells in which data cannot be obtained due to technical reasons are colored grey; if data was not collected they are left empty. The kinetics of Meta-II decomposition could not be obtained, because they are overlapped by a long flash artefact.*

As for the activation data the kinetics for the membrane data is assembled into an Arrhenius plot and the activation energies are derived from the slope in this plot (for an explanation see 2.4.5). The results are shown in Table 7 (with the same coloring and labeling as in Table 5 for the activation data). Reliable data for the decomposition of Meta-II could not be observed, because the flash artefact was usually too long to resolve the kinetics.

Similar to what has been stated for the activation data (see chapter 3.1.8) washed membranes with and without spinlabel have comparable activation energies, but the dried 'sandwich' membranes between two BaF_2 panes (for a description see chapters 2.3.4 and 3.1.8) have a higher activation energy for the proton release. For the activation process also a higher activation energy with the 'sandwich' sample was observed (see Table 5).

3.5.5 Influence of mutations in the ERY motif, helix 8 and other protonable groups

I tested the same mutant pigments as shown above also with blue light illumination, and the same general principle also holds here: Generally Schiff base deprotonation and proton uptake were reverted upon blue light illumination (see chapters 3.2.3 and 3.3.1).

In Fig. 62 the effect of blue light illumination is depicted for the ERY-region mutant pigments. WT is shown in the upper left panel for comparison. The pigment R135K (first row right) shows a reduced proton release, and the pigment R135L (second row left) even shows a proton uptake,

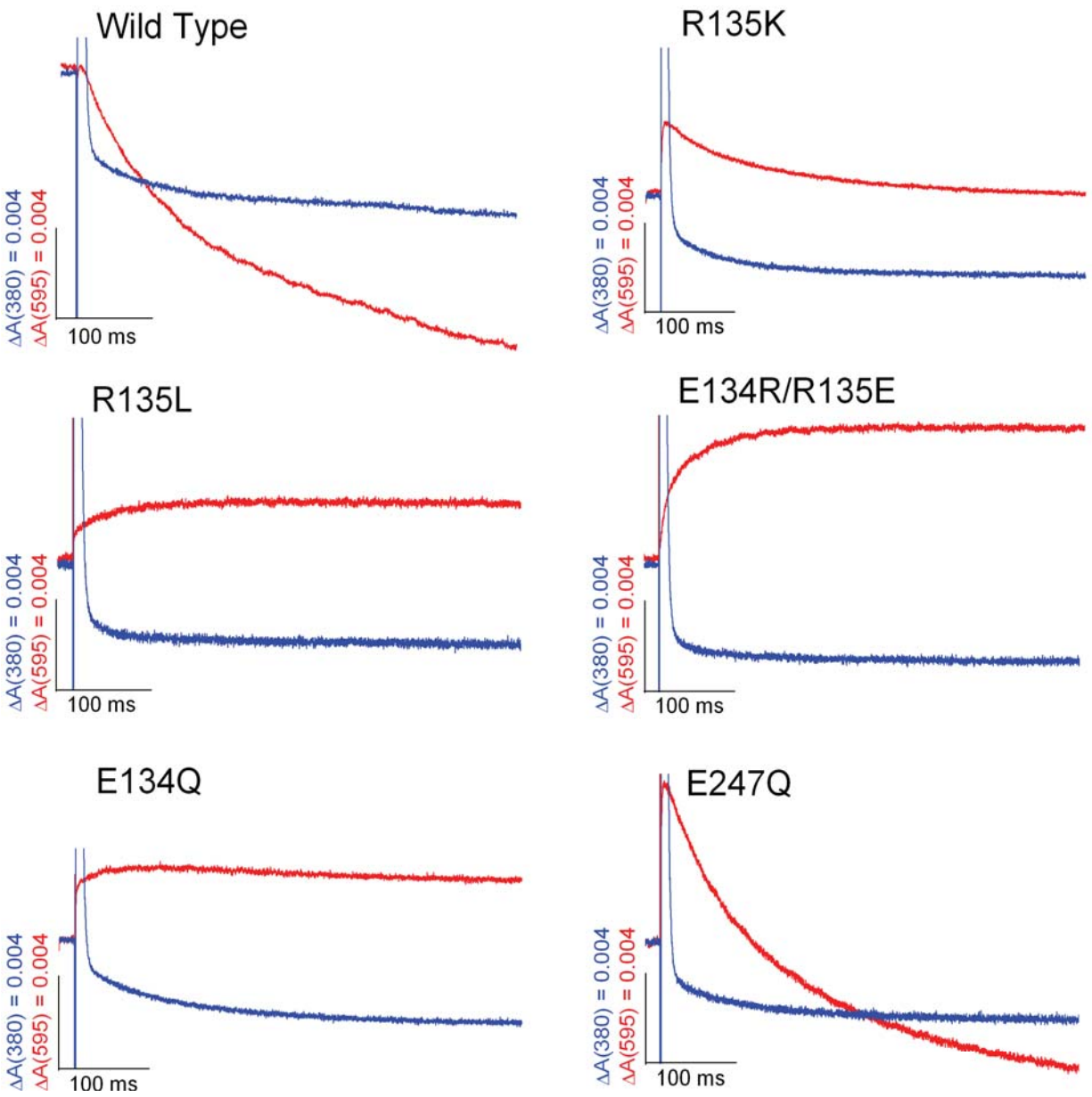

Fig. 62: *Flash photolysis experiments at pH 6.0 and 20 °C showing the decomposition of Meta-II at 380 nm (blue traces) and the proton release or uptake, respectively, at 595 nm (red traces). Bromocresol purple was used as a pH dependent dye (see 2.3.1). WT rhodopsin (upper left panel) shows Meta-II decomposition being faster than proton uptake. For R135K (upper right panel) the proton release is much smaller in amplitude but with similar kinetics. With R135L (middle left panel) there is a proton uptake instead of a proton release, and Meta-II decomposition is slightly accelerated. E134R/R135E (middle right panel) shows a proton release, similar to E134Q (lower left panel). The E247Q pigment (lower right panel) does not show any change compared with WT rhodopsin. Positive jumps of the proton signal are due to additional formation of Meta-II.*

while the Meta-II decomposition is faster here than with WT. E134R/R135E (second row right) shows the strongest proton uptake upon blue light illumination, corresponding to the proton release observed during normal activation.

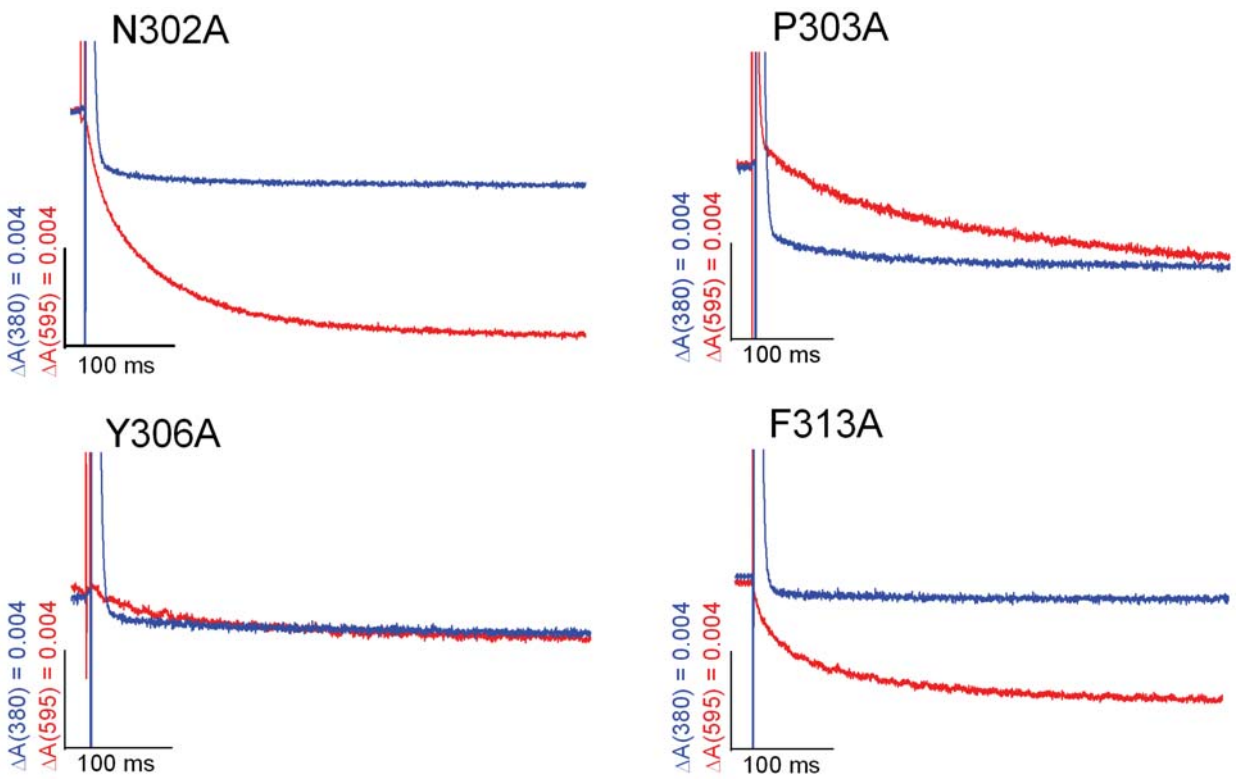

Fig. 63: *Flash photolysis experiments showing the decomposition of Meta-II at 380 nm (blue traces) and the proton release at 595 nm (red traces). To measure the proton signal, bromocresol purple was used as a pH dependent dye (see 2.3.1). The pigment N302A (upper left panel) shows a Meta-II decomposition faster than the proton uptake. For the P303A pigment (upper right panel) the proton release is smaller and slightly slower. Y302 A (lower left panel) only features very little Meta-II decomposition and proton release, and F313A also shows only very little Meta-II decomposition but a bigger proton release. Positive jumps of the proton signal are due to additional formation of Meta-II.*

The E134Q pigment (third row left) also features a proton uptake but with a tendency of a slow proton release afterwards. The E247Q pigment (third row right) – as seen with the flash photolysis experiments on the activation process – does not show any significant difference to WT.

The NPxxY$(x)_{5,6}$F mutant pigments (see Fig. 63) reveal some interesting behaviour: The N302A pigment shows a faster Meta-II decomposition compared to WT rhodopsin (compare to Fig. 62, upper left panel) and only a proton release without the fast intermediate proton uptake seen for WT. The P303A pigment behaves similar but features a slowed down proton release and a smaller proton release amplitude. The Y306A pigment shows a reduced Meta-II decomposition and also little proton release. This is similar to F313A which also features a reduced Meta-II decomposition but has a higher albeit still reduced proton release.

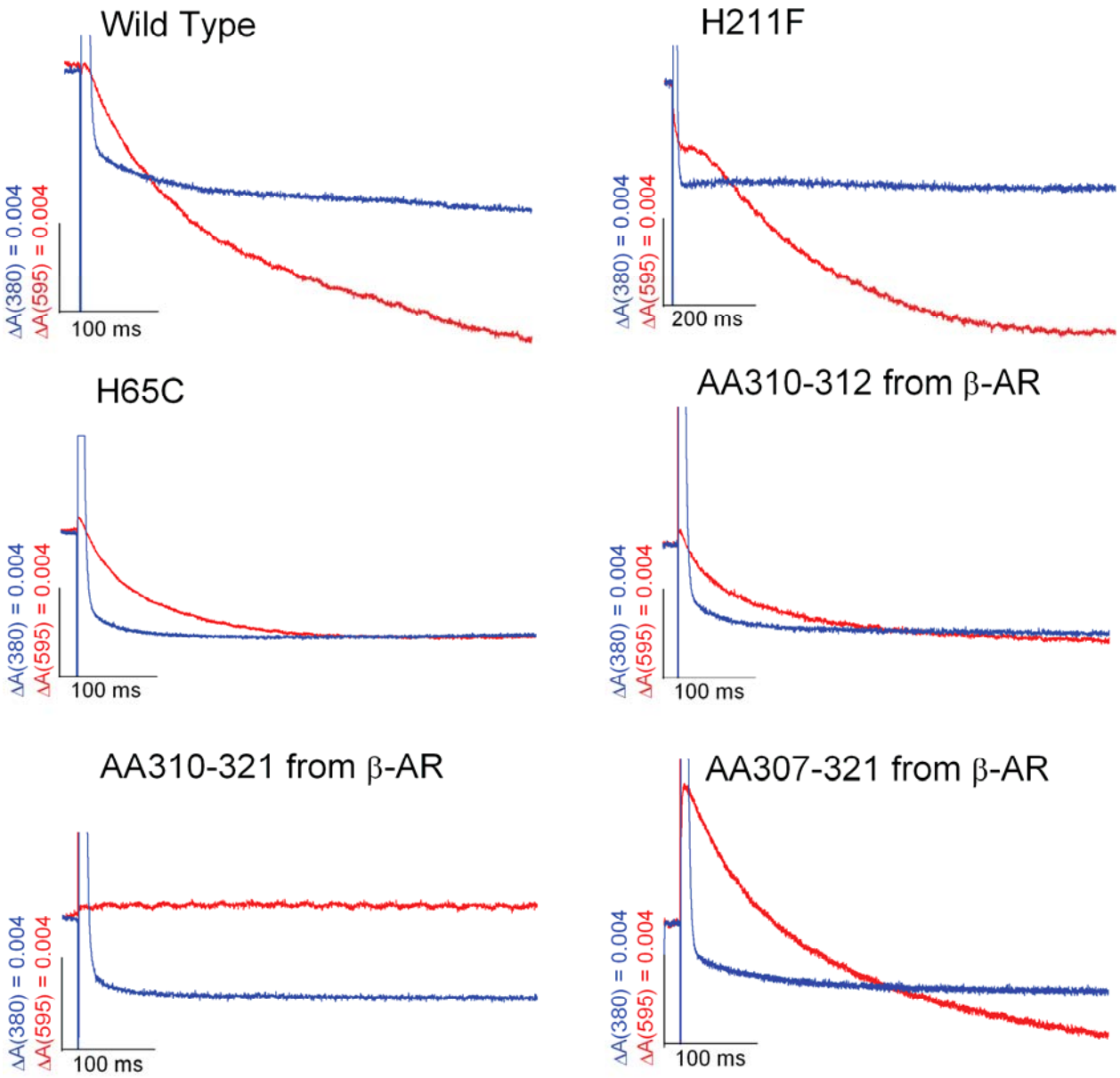

Fig. 64: *Flash photolysis experiments show the decomposition of Meta-II at 380 nm (blue traces) and the proton release at 595 nm (red traces). To measure the proton uptake, bromocresol purple was used as a pH dependent dye (see 2.3.1). WT rhodopsin (upper left panel) shows Meta-II decomposition being faster than proton release. For H211F (upper right panel) Meta-II decomposition is faster and proton uptake slower with a plateau at the beginning. H65C (middle left panel) features less proton release than WT. If amino acids 310-312 are replaced with the homologuos sequence from the β_2-AR (middle right panel) there is less proton release, while Meta-II decomposition is uninfluenced. The pigment with amino acids 310-321 replaced with the homologous sequence from the β_2-AR (lower left panel) shows no proton release at all, and that with amino acids 307-312 from the β_2-AR (lower right panel) the same behaviour like WT. Apparent fast positive protonation signals (e.g. lower right panel) result from additional Meta-II formation upon illumination. The samples were totally bleached prior to blue light illumination (see chapter 2.3.1), but the measuring light at 380 nm already induces a certain recreation of the ground state.*

The influence of other potentially protonable sites is shown in Fig. 64. H211F (upper right panel) undergoes a fast Meta-II decomposition compared to WT rhodopsin, but the proton release instead has slow kinetics and an interesting shape: There is first a plateau, which is also reproducible at different pH values. Only after approx. 50 ms the proton release starts. The proton release itself is by a factor of roughly 2 slower than WT rhodopsin.
The H65C pigment (middle left panel) features kinetics similar to WT, but the amplitude of proton release is reduced by roughly 50 %. This corresponds to the finding that the proton uptake during activation of H65C is also reduced by roughly 50 % (see Fig. 52, lower left panel).
In the other panels of Fig. 64 the same flash photolysis experiments with blue light are shown with the mutant pigments introduced in chapter 3.3.2 (for the sequences see Table 6 on page 90): A certain part of H8 is replaced with the homologous sequences from the β_2-adrenergic receptor. If only amino acids 310-312 are replaced (middle right panel), the effect is a reduction of the proton release. If the whole region is replaced, namely amino acids 310-321, (lower left panel) the result is a total abortion of the proton uptake. If only three more neighbouring amino acids are replaced with the homologous sequence from the β_2-adrenoreceptor, resulting in replacement of amino acids 307-321, (lower right panel) the behaviour of the pigment is exactly the same as with WT: Meta-II formation is not influenced and the proton release is back to the level and kinetics of WT. All these findings correspond well to the findings of flash photolysis experiments on the ground state (see chapter 3.3.2), again only with the opposite algebraic sign.
The mutant pigments N73D and N73A have been tested with the same flash photolysis assay as well and did not show any differences to WT rhodopsin (data not shown).

3.6 Peptide binding to Meta-II subspecies

Peptides are used in this study to elucidate the influence of the subunits of the G protein transducin (G_t) on rhodopsin. The sequences of the peptides are shown in Table 4 (page 56).
Peptides were tested with flash photolysis. While the kinetics and amplitude of Meta-II formation stay unaffected (data not shown), the proton uptake is reduced down to the release of half a proton per activated rhodopsin molecule. All experiments were done with WT rhodopsin in DM.

3.6.1 Peptides analogous to $G_t\alpha$

The titration with native $G_t\alpha$(340-350) peptide (sequence NH_2-IKENLKDCGLF-COOH) is shown in Fig. 65: The proton uptake is roughly one proton per activated rhodopsin if no peptide

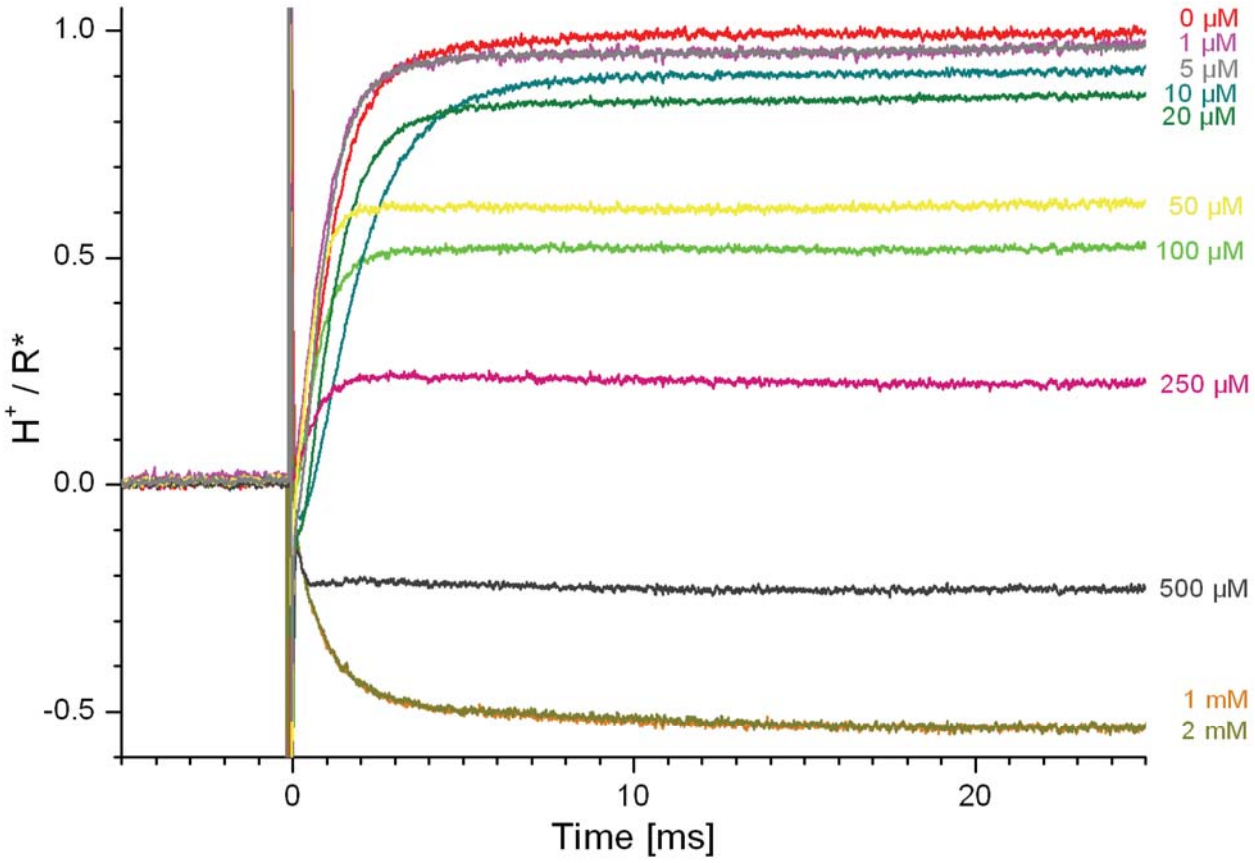

Fig. 65: *Titration of native $G_t\alpha$(340-350) peptide to rhodopsin (10 µM) observed with flash photolysis. Only the proton uptake data (595 nm absorption of bromocresol purple) is shown. The formation of Meta-II stays unaffected under all conditions (data not shown). The calculation of protons taken up per activated rhodopsin was done as described above (see chapter 1.2.7). The native $G_t\alpha$(340-350) peptide reduces the proton uptake until about half a proton per activated rhodopsin is released at concentrations above 1 mM.*

is present – as has been shown above. With increasing amounts of peptide, this number is reduced while the kinetics stay the same. Above 300 µM there are protons released instead of taken up. The maximal proton release is 0.5 protons per activated rhodopsin above a peptide concentration of 1 mM.

The kinetics and amplitude of Meta-II formation stay the same even at high concentrations of $G_t\alpha$(340-350) peptide (data not shown).

The same experiment for the $G_t\alpha$(340-350)L349A peptide (sequence NH_2-IKENLKDCG**A**F-COOH), where one Leucine side chain close to the C terminus is replaced by an Alanine, is shown in Fig. 66. It has been proven before that this peptide does not bind to rhodopsin [Bartl et al., 2000]. The comparison with the native $G_t\alpha$ peptide as in Fig. 65 (shown as light blue traces in Fig. 66) shows a much smaller decrease of the proton uptake for the nonbinding peptide. Again the kinetics and amplitude of Meta-II formation stay unaffected (data not shown).

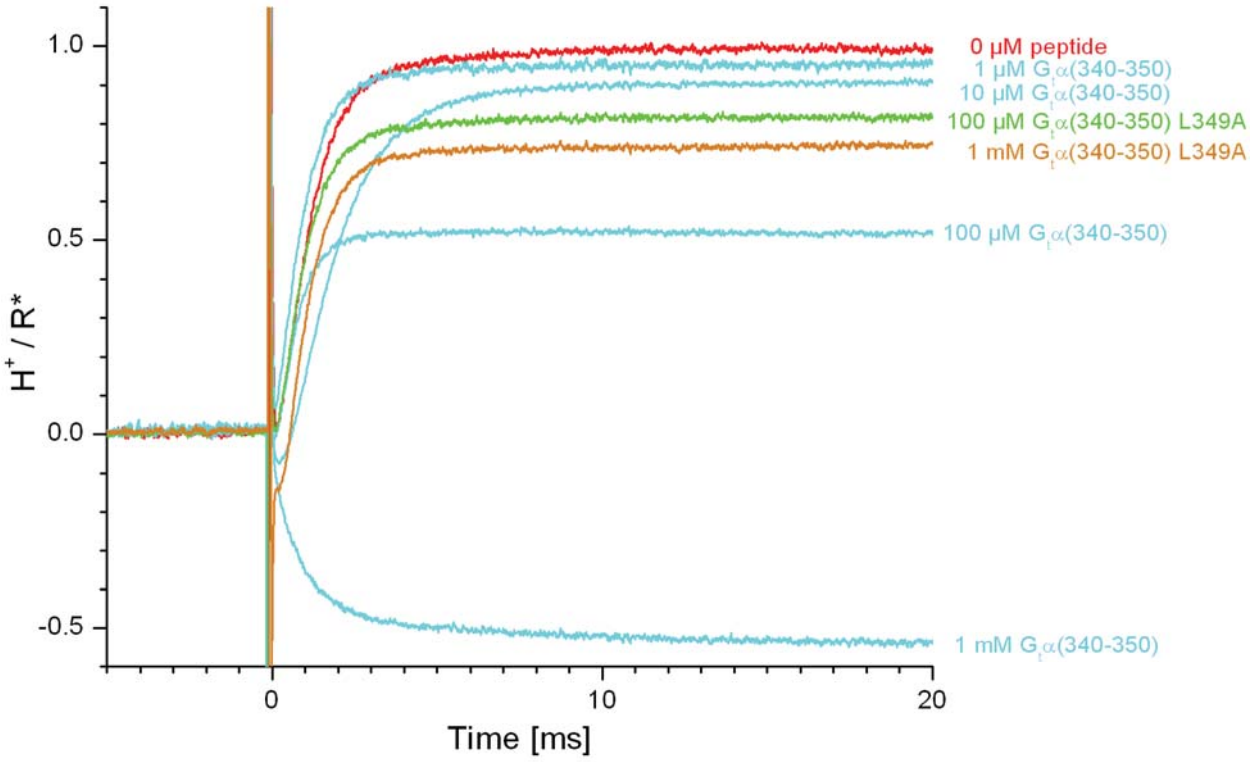

Fig. 66: *Titration with nonbinding $G_t\alpha$(340-350) L349A peptide to rhodopsin (10 µM) observed with flash photolysis. Only the proton uptake data (595 nm absorption of bromocresol purple) is shown. The formation of Meta-II stays unaffected under all conditions (data not shown). The calculation of protons taken up per activated rhodopsin was done as described above (see chapter 1.2.7). The proton uptake is only slightly reduced even at high peptide concentrations (down to 0.75 H^+/R* at 1 mM). The titration with native $G_t\alpha$(340-350) peptide is shown in light blue for comparison.*

This shows that the effect of the decreasing proton uptake is specific to the binding of the peptide. However the proton uptake does decrease even for the nonbinding peptide. This is due to the fact that the peptides themselves have a buffering effect at high concentrations. Thus this has to be taken into account for all peptides.

3.6.2 High affinity analogs of $G_t\alpha$

There are several $G_t\alpha$ peptide analogs known that have a much higher affinity towards rhodopsin than native $G_t\alpha$(340-350) peptide [Herrmann et al., 2004; Martin et al., 1996]. These peptides have in common that Lys^{341} at the N-terminus of the peptide is replaced with a Leucine.

The 'classic' high-affinity $G_t\alpha$ derived $G_t\alpha$(340-350) HAA peptide has the sequence NH_2-**VLED**LK**S**CGLF-COOH [Martin et al., 1996]. A new high affinity $G_t\alpha$ derived peptide $G_t\alpha$(340-350) HAA with the sequence NH_2-I**L**ENLKDCGLF-COOH has recently been discov-

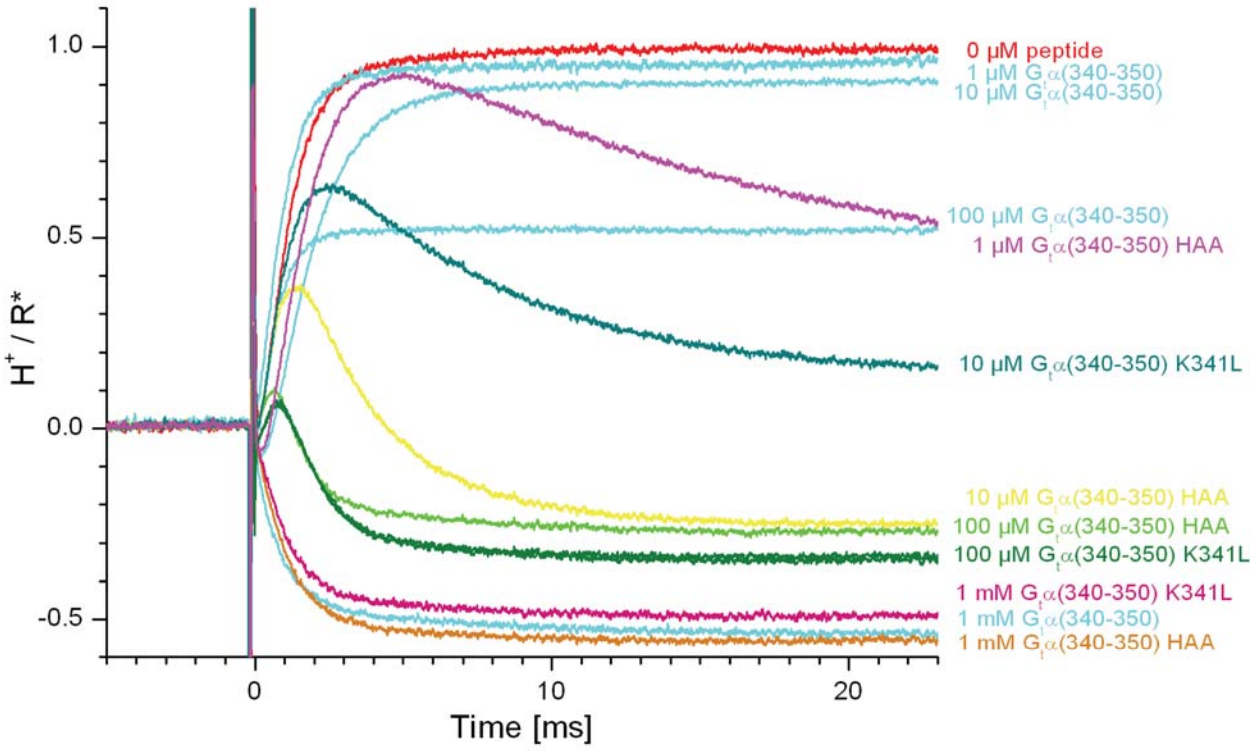

Fig. 67: *Titration with high affinity $G_t\alpha$ peptides to rhodopsin (10 µM) observed with flash photolysis. Two different high affinity peptides were tested as described in the text. Only the proton uptake data (595 nm absorption of bromocresol purple) is shown. The formation of Meta-II stays unaffected under all conditions (data not shown). The calculation of protons taken up per activated rhodopsin was done as described above (see chapter 1.2.7). The proton uptake is rapidly reduced with increasing peptide concentration. The titration with native $G_t\alpha$(340-350) peptide is shown in light blue for comparison.*

ered [Herrmann et al., 2004] and shown to have the same behaviour like the classic high-affinity peptide with only one amino acid replacement instead of four.

The titration for both high affinity $G_t\alpha$ derived peptides is shown in Fig. 67. With both peptides one observes a transient proton uptake, consistent with slower binding of peptide which allows the proton to be taken up before the peptide has a chance to bind. The effect of the transient binding will be dicussed later (see chapter 4.3.1). Both high affinity $G_t\alpha$ derived peptides behave similarly and only have a slightly shifted K_D. At high concentrations there is – like for the native $G_t\alpha$(340-350) peptide – a proton release of 0.5 protons per activated rhodopsin molecule.

Another $G_t\alpha$(340-350) HAA derived peptide with the 'classic' high affinity sequence but without Lys^{345} has a similar effect, shown in Fig. 68. Its sequence is NH_2-**VL**E**D**L**AS**CGLF-COOH. The same transient signal is visible, and the dependence on concentration is similar to the two other high affinity $G_t\alpha$ derived peptides shown above. Again there is a proton release of up to 0.5 protons per activated rhodopsin molecule at high peptide concentration.

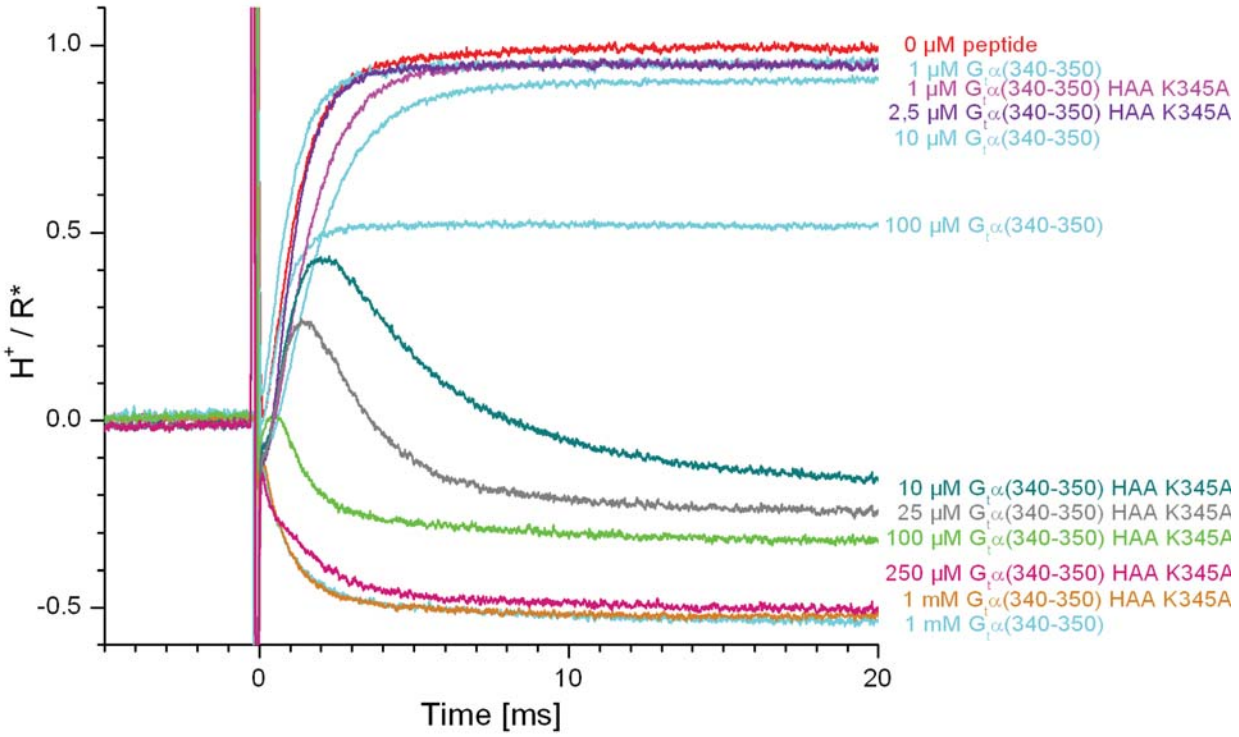

Fig. 68: *Titration with Lysine-free $G_t\alpha$(340-350) K345A peptide to rhodopsin (10 µM) observed with flash photolysis. The effect is similar to that of the high affinty peptides (Fig. 67). Only the proton uptake data (595 nm absorption of bromocresol purple) is shown. The formation of Meta-II stays unaffected under all conditions (data not shown). The calculation of protons taken up per activated rhodopsin was done as described above (see chapter 1.2.7). The proton uptake is rapidly reduced with increasing peptide concentration. The titration with native $G_t\alpha$(340-350) peptide is shown in light blue for comparison.*

3.6.3 C-terminal peptides derived from to $G_t\gamma$

Peptides derived from the $G_t\gamma$ C-Terminus have been investigated in the same way. The amino acid sequence of both these peptides is NH_2-DKNPFKELKGGC-$CONH_2$, identical to native $G_t\gamma$(60-71). One variant of the peptide has the native farnesyl group attached to the peptide (at the C-terminal Cysteine), the other one does not feature this farnesyl group. The titrations are shown in Fig. 69.

For the farnesylated $G_t\gamma$(60-71) peptide at low concentrations the effect is similar to the native $G_t\alpha$(340-350) peptide. However, at higher concentrations of farnesylated $G_t\gamma$(60-71) peptide results in a prevention of the proton uptake but not in a proton release like the native $G_t\alpha$ peptide. The kinetics of the proton uptake just as kinetics and amplitude of Meta-II formation again stay unaffected (data not shown).

The unfarnesylated $G_t\gamma$(60-71) peptide only has a small effect on the proton uptake, comparable

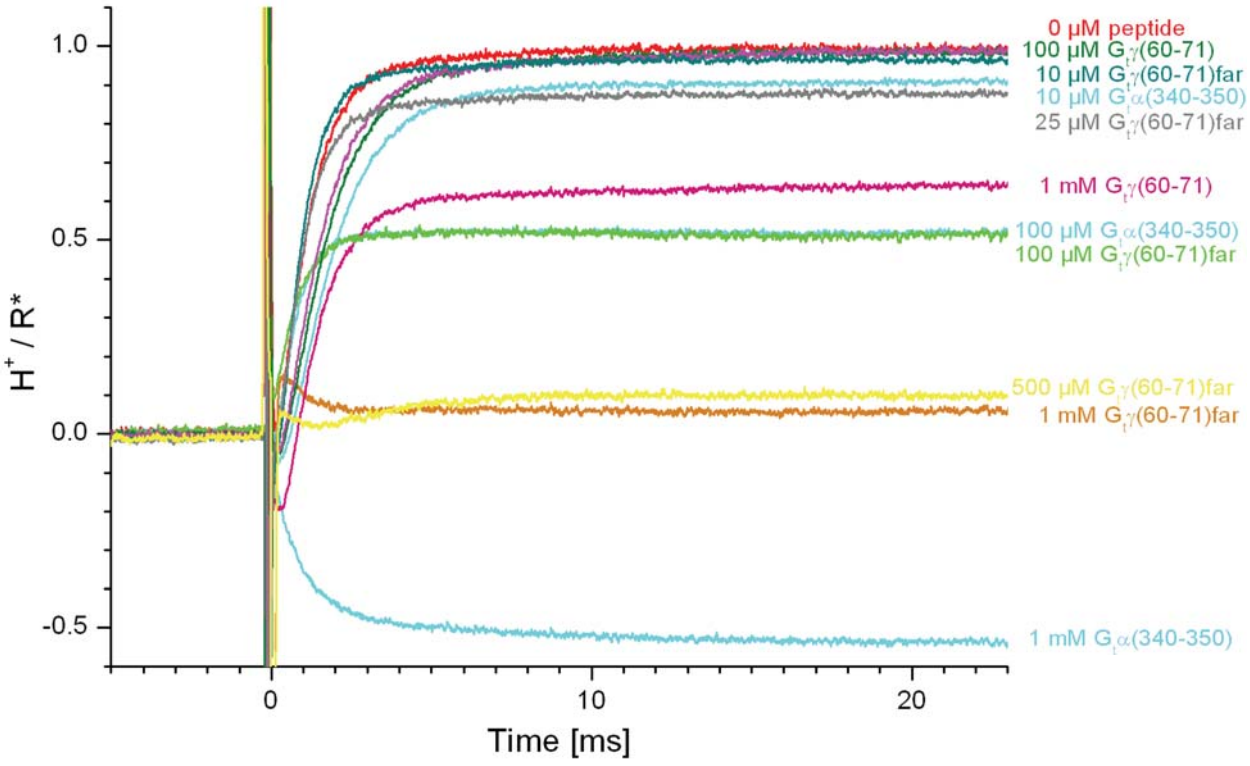

Fig. 69: *Titration with $G_t\gamma$ peptides to rhodopsin (10 µM) observed with flash photolysis. Only the proton uptake data (595 nm absorption of bromocresol purple) is shown. The effect is similar to that of the native $G_t\alpha$(340-350) peptide (shown in light blue for comparison) apart from high concentrations where the $G_t\gamma$(60-71)far peptide results in a proton uptake/release of 0 H^+/R*. The formation of Meta-II stays unaffected under all conditions (data not shown). The calculation of protons taken up per activated rhodopsin was done as described above (see chapter 1.2.7).*

to the nonbinding $G_t\alpha$ peptide (see Fig. 66). Therefore we can also assume no binding to rhodopsin either [Herrmann et al., 2004] and only a small buffering effect.

3.6.4 Subsumption of the data

Fig. 70 shows a plot of the protons taken up per activated rhodopsin molecule against the peptide concentration. Four different kinds of peptides can be distinguished: The two nonbinding peptides show a buffering effect only (upper right corner), the native $G_t\alpha(340\text{-}350)$ peptide starts at 1 H^+/R^* at acidic pH and goes down to -0.5 H^+/R^*, the high affinity peptides also start at 1 H^+/R^* at acidic pH and only go down at lower concentrations already while the farnesylated $G_t\gamma(60\text{-}71)$ peptide goes down to 0 H^+/R^* with a rate similar to native $G_t\alpha(340\text{-}350)$.

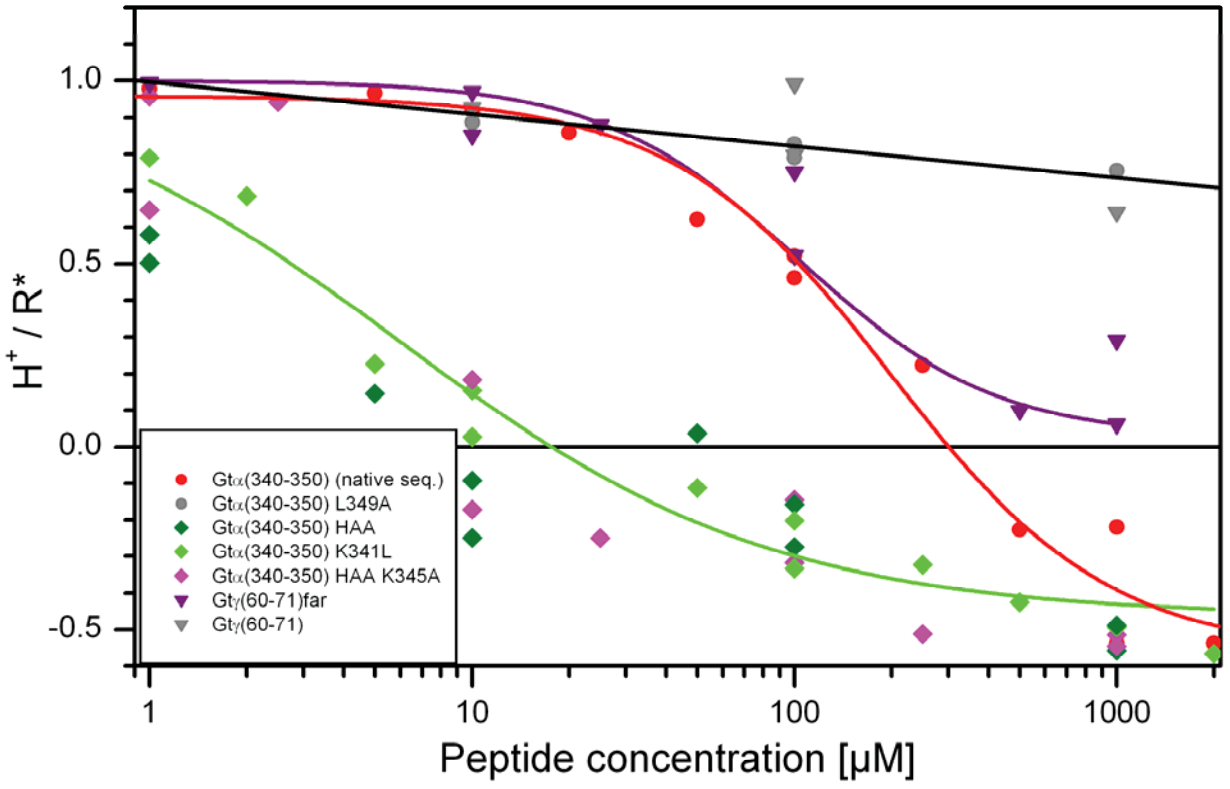

Fig. 70: *Binding of peptides to rhodopsin observed with flash photolysis. The data points are the amplitudes of proton uptake signals (deduced from the traces in Fig. 65 to Fig. 69). The temperature was 20 °C and the pH 6.0. The plot of the proton uptake against peptide concentration reveals the different behaviour of the three high affinity $G_t\alpha$ derived peptides (green diamonds: 'classic' high affinity $G_t\alpha$ derived peptide, light green diamonds: high affinity $G_t\alpha(340\text{-}350)$ K341L peptide, magenta diamonds: $G_t\alpha(340\text{-}350)$ HAA K345A) compared to the native $G_t\alpha(340\text{-}350)$ peptide (red circles). The farnesylated $G_t\gamma(60\text{-}71)$ peptide (violet triangles) behaves similar to the native $G_t\alpha(340\text{-}350)$ peptide but does not lead to a proton release but only to zero proton uptake. The nonbinding $G_t\alpha(340\text{-}350)$ L349A peptide (grey circles) and the unfarnesylated $G_t\gamma(60\text{-}71)$ peptide (grey triangles) only show a small buffering effect but do not bind to rhodopsin at all.*

3.6.5 Influence of peptides on the blue light effect

I also tested the influence of the peptides shown above on the Meta-II decomposition as described in chapter 3.5.4. The totally bleached sample was illuminated with blue flashes (380 – 480 nm). The plot of the protons released or taken up, respectively, is shown in Fig. 71.

As shown above for WT rhodopsin in different environments and the pigments with mutations in the ERY motif (see chapters 3.5.4 and 3.5.5), the traces observed during normal activation are reverted. Consequently the plot shown in Fig. 71 looks like a mirror image of the plot shown in Fig. 70: The native $G_t\alpha(340\text{-}350)$ peptide shows a proton release of one proton per activated

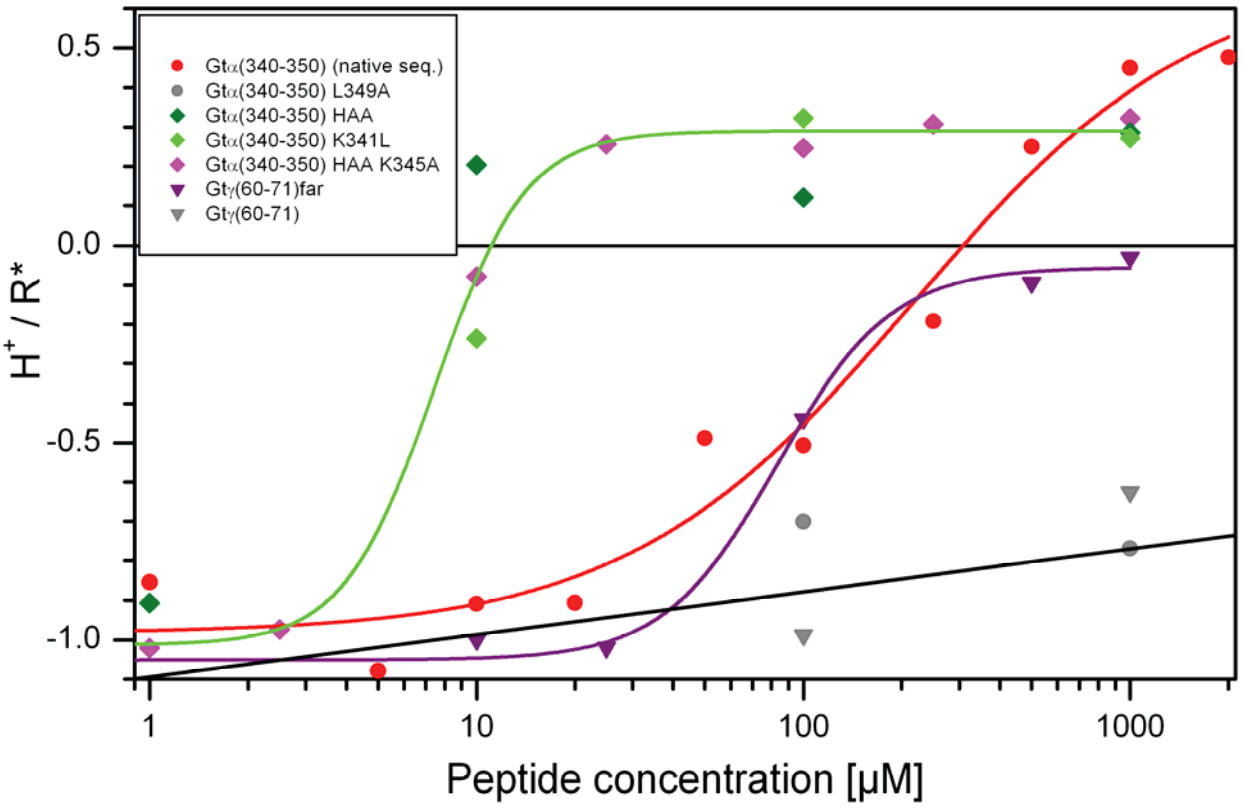

Fig. 71: *Binding of peptides to rhodopsin observed with flash photolysis with blue flashes applied to Meta-II. The data points are the amplitudes of proton release or uptake signals (comparable to Fig. 70 for Meta-II formation). The temperature was 20 °C and the pH 6.0. The decomposition of Meta-II stays unaffected under all conditions (data not shown). The plot of the proton release against peptide concentration reveals the different behavior of the three high affinity $G_t\alpha$ derived peptides (green diamonds: 'classic' $G_t\alpha(340\text{-}350)$ HAA peptide, light green diamonds: $G_t\alpha(340\text{-}350)$ K341L (see Methods in [Herrmann et al., 2004]), magenta diamonds: $G_t\alpha(340\text{-}350)$ K345A) compared to the native $G_t\alpha(340\text{-}350)$ peptide (red circles). The farnesylated $G_t\gamma(60\text{-}71)$ peptide (violet triangles) behaves similar to the native $G_t\alpha(340\text{-}350)$ peptide but does not lead to a proton uptake but only to zero proton release at high concentrations. The nonbonding $G_t\alpha(340\text{-}350)$ L349A peptide (grey circles) and the unfarnesylated $G_t\gamma(60\text{-}71)$ peptide (grey triangles) only show a small buffering effect but do not bind to rhodopsin at all.*

rhodopsin molecule at low concentrations. This release is reverted into a proton uptake of 0.5 protons per activated rhodopsin at high peptide concentration. A similar behaviour is also observed for the three high affinity $G_t\alpha$ derived peptides, but here the effect can already be seen at a much lower concentration. The farnesylated $G_t\gamma(60\text{-}71)$ peptide has a similar effect, but only leads to a proton release of zero instead of a proton uptake at high concentrations. Both the non-binding $G_t\alpha(340\text{-}350)$ L349A peptide and the unfarnesylated $G_t\gamma(60\text{-}71)$ peptide do not show any clear effect except for a buffering effect at high concentrations.

3.6.6 Quantification of peptide binding

The final amplitude of the proton uptake is plotted against the peptide concentration in Fig. 70. To deduce an equilibrium constant for the reaction, the data points have been matched with the following equation which has been deduced in 2.4.4 (eq. XXXIV), complemented with a second component without depletion (= second term):

$$[P] = 1 - \frac{\left(K_{d,1} + [A]_t + [B]_t\right) - \sqrt{\left(K_{d,1} + [A]_t + [B]_t\right)^2 - 4 \cdot [A]_t \cdot [B]_t}}{2} - \frac{[A]_t \cdot [B]_t}{K_{d,2} + [B]_t} \quad \text{(XXXIX)}$$

[P] represents the concentration of the formed rhodopsin+peptide complex; $[A]_t$ is the total rhodopsin concentration and $[B]_t$ is the total peptide concentration. The equilibrium constants $K_{d,1}$ and $K_{d,2}$ can be obtained through the above equation. $K_{d,2}$ is only needed for the high affinity $G_t\alpha(340\text{-}350)$ K341L peptide, because it features a very low $K_{d,1}$ for the amplitude 1 to 0 and obviously has another component for the amplitude 0 to -0.6 with $K_{d,2}$. For the native $G_t\alpha(340\text{-}350)$ and $G_t\gamma(60\text{-}71)$ peptides the second term can be removed. The results are shown in Table 8 and fit well to data that was obtained before with different methods [Herrmann et al., 2004].

Peptide	Sequence	$K_{d,1}$	$K_{d,2}$
native $G_t\alpha(340\text{-}350)$	NH_2-IKENLKDCGLF-COOH	268.8 µM	-
high affinity $G_t\alpha(340\text{-}350)$	NH_2-I**L**ENLKDCGLF-COOH	1.81 µM	160 µM
native $G_t\gamma(60\text{-}71)$	NH_2-DKNPFKELKGGC-$CONH_2$ (far)	123.3 µM	-

Table 8: *Equilibrium constants obtained from the plot in Fig. 70 using equation XXXVII.*

3.6.7 Peptides with changed amino acid sequences

It is an interesting question where the proton release found for all $G_t\alpha$ derived peptides (see 3.6.1 - 3.6.4) originates from. Therefore $G_t\alpha(340\text{-}350)$ derivatives in which certain amino acids were replaced by neutral amino acids (for the complete peptide sequences see Table 4) were tested

with the same assay used before. The results of these experiments are shown in Fig. 72. Again the formation of Meta-II was not affected by any of the peptides (data not shown).

The peptide without any Glutamate residue ($G_t\alpha$(340-350)E342N) is represented by orange circles. It shows basically the same behaviour as native $G_t\alpha$(340-350) peptide, although the proton release seems to be slightly smaller. The peptide with the D346M replacement ($G_t\alpha$(340-350) D346M) is represented by pink circles. It seems to have a slightly higher affinity than the native $G_t\alpha$(340-350) peptide but also shows a proton release of 0.5 protons per activated rhodopsin molecule at high concentrations. The peptide with the Cys^{347} replaced by an alpha amino butyric acid group ($G_t\alpha$(340-350)C347Abu) is represented by light blue circles and also features a higher affinity but the same proton release at high concentrations.

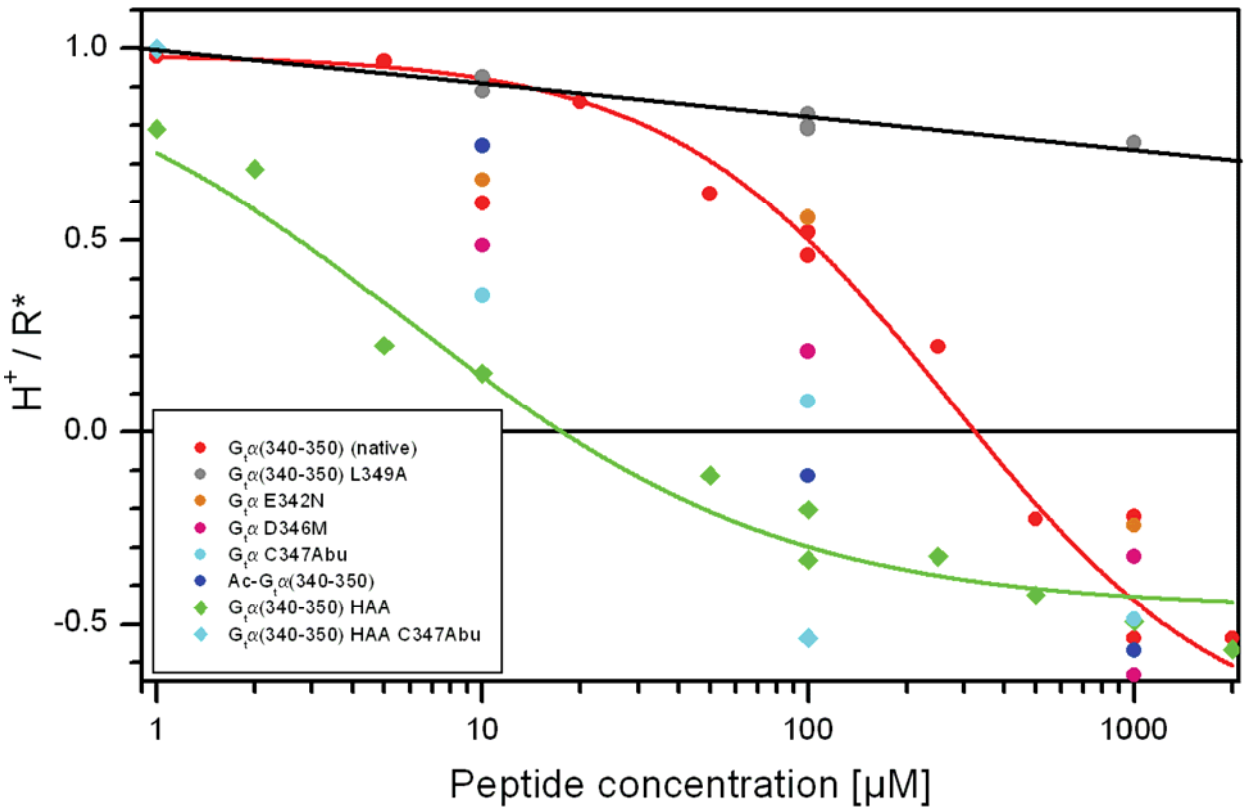

Fig. 72: *Binding of peptides with different amino acid substitutions to rhodopsin observed with flash photolysis. The data points are the amplitudes of proton uptake signals. All experiments were performed at 20 °C and pH 6.0. Native $G_t\alpha$(340-350) peptide (red circles) and $G_t\alpha$(340-350) HAA peptide (green diamonds) are shown for reference. A $G_t\alpha$ derived peptide without a Glutamate (orange circles) does not show any difference to native $G_t\alpha$(340-350), while a $G_t\alpha$ derived peptide without an Aspartate (pink circles) shows a slightly higher affinity. Both $G_t\alpha$ derived peptide and the equivalent HAA analog without a Cysteine have an increased affinity, too. The Ac-$G_t\alpha$(340-350) peptide with an acetylated N-terminus has an increased affinity as well.*

The same peptide with the C247Abu replacement was also tested as a high affinity analog ($G_t\alpha$(340-350) HAA C347Abu, light blue diamonds). Again this peptide has a higher affinity than the $G_t\alpha$(340-350) HAA peptide but leads to the same proton release at high concentrations. If the N-terminus of the HAA $G_t\alpha$ peptide is altered by acetylation (Ac-$G_t\alpha$(340-350) K341L) the peptide has a lower affinity but again shows the same proton release.

3.6.8 Peptide binding to ERY mutants

Because it seems likely that peptides bind to the highly conserved D(E)RY region (for more experiments on this region see chapter 3.2), some of the pigments with mutations in this region

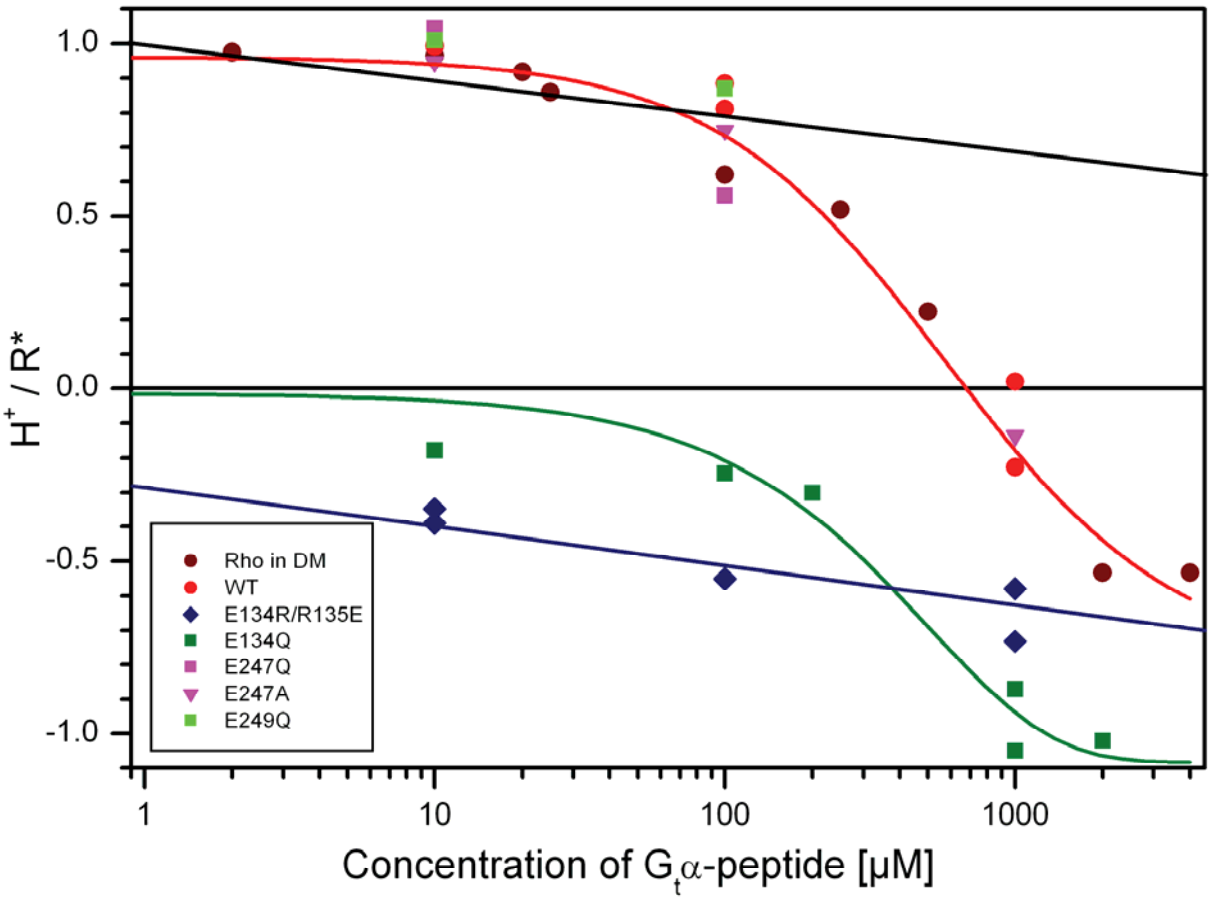

Fig. 73: *Binding of peptides to rhodopsin and mutant pigments observed with flash photolysis. The data points are the amplitudes of proton uptake signals. All pigments have been treated with the same concentration of native $G_t\alpha$(340-350) peptide, pH is 6.0 (unbuffered) and temperature 20 °C. WT rhodopsin (red circles) shows the same behaviour as purified rhodopsin in DM (dark red circles). Also the same behaviour is observable for the pigments E247Q (magenta squares), E247A (magenta triangles), and E247Q (light green squares). The pigment E134Q (dark green squares) features an increasing proton release until roughly one proton at 1 mM peptide concentration, while E134R/R135E (blue diamonds) shows a maximal proton release around 0.5 protons at 1 mM peptide concentration.*

were tested with peptide binding in the same flash photolysis assay used above. As demonstrated in chapter 3.2.3, the E134Q pigment does not undergo any significant proton uptake, and the E134R/R135E 'charge reversal' pigment even features a proton release at pH > 6, while the other pigments exhibit the same proton uptake as WT (see Fig. 44).

Fig. 73 contains the data of proton uptake / release in presence of increasing concentrations of $G_t\alpha$(340-350) peptide. The formation of Meta-II stays unaffected under all conditions (data not shown). The reference system for the recombinant expressed pigments is WT rhodopsin (red points), but rhodopsin in DM (dark red points) is plotted as well for comparison, and obviously they do not differ from each other. Only the pigments with mutations in the ERY motif feature a special behaviour: Starting from zero proton uptake or release, the pigment E134Q (green squares) shows an increasing proton release with titration of the peptide, reaching about 1 proton at 1 mM peptide concentration. With the E134R/R135E 'charge reversal' pigment (blue diamonds) the proton release shows an only slightly increasing proton release. From the number of data points and due to the small changes it cannot be distinguished if these decreases are linear or sigmoidal. The pigments E247Q (magenta squares), E247A (magenta triangles) and E249Q (light green squares) do not show any significant changes compared to WT rhodopsin.

3.6.9 Influence of peptide binding on helix motion

It is not clear yet to which exact rhodopsin conformation G_t can bind. Therefore spin labeled rhodopsin was tested both with native $G_t\alpha$(340-350) and native $G_t\gamma$(60-71) peptide. The spin labeled mutant pigment V227R1 was again used and likewise spin labeled WT rhodopsin with spin labels at Cys^{140} and Cys^{316}. A flash photolysis experiment (analog to chapters 3.6.1 to3.6.3) to show the binding of the peptide to the V227R1 pigment as well as to the spin labeled WT is shown in Fig. 74. Apart from a slight kinetic difference due to the spin label in position 227 both pigments behave just as WT: They show a proton release of roughly half a proton per activated molecule if 1 mM $G_t\alpha$(340-350) HAA peptide is present. Thus we can deduce from these experiments that the peptide indeed does bind to both spin labeled WT rhodopsin and the spin labeled mutant pigment V227R1.

The EPR spectra are shown in Fig. 75, black spectra representing the dark states and red spectra the illuminated states. Spectra of V227R1 are shown in the left column, those of the spin labeled WT in the right column.

Without any peptide the spectra for V227R1 and C140R1/C316R1 are observed (first row, identical to the spectra in Fig. 32A). If native $G_t\alpha$(340-350) peptide is added in a high concentration (1 mM) both spectra are essentially uninfluenced (second row) – both for the V227R1 pigment

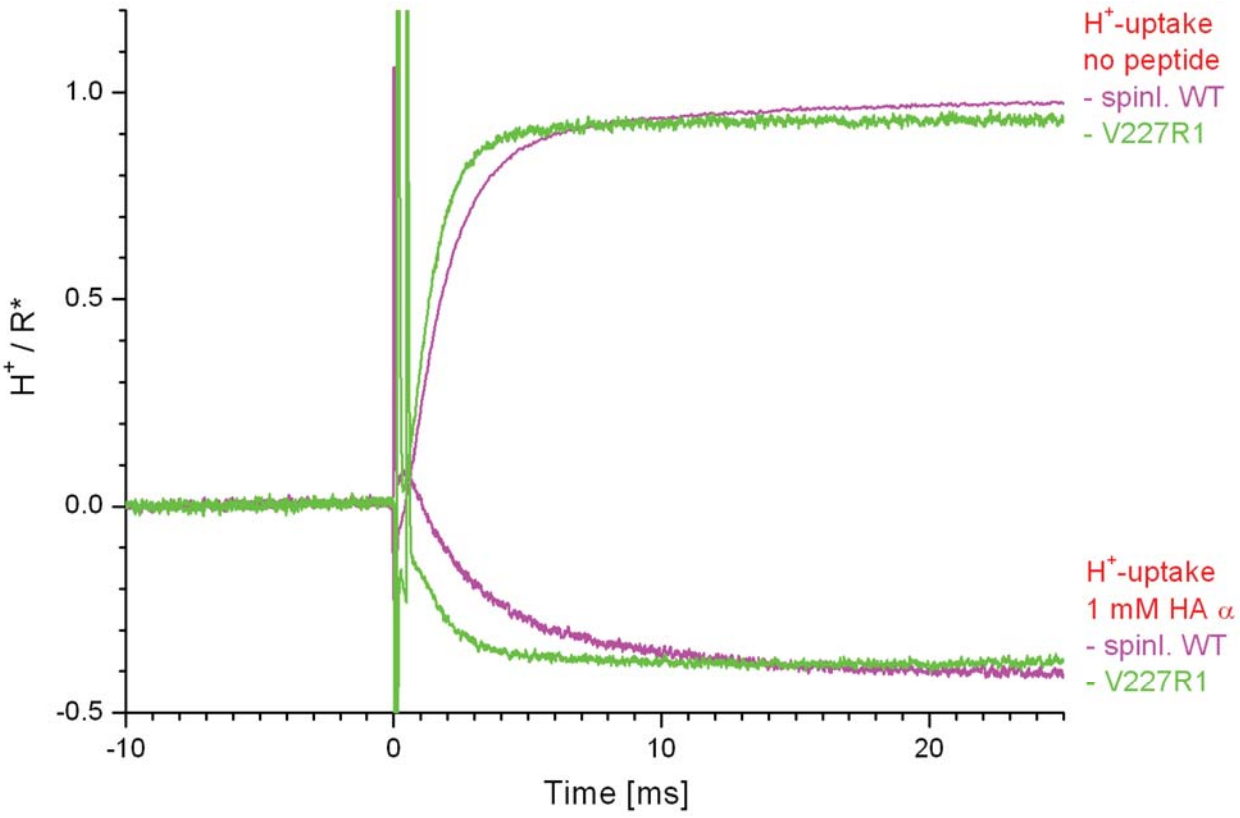

Fig. 74: *Binding of $G_t\alpha(340–350)$ HAA peptide to spinlabeled rhodopsin WT (10 µM) and V227R1 (5 µM) observed with flash photolysis. Only the proton uptake data (with 50 µM BCP as pH dependent dye) are shown, while the Meta-II traces are all identical (data not shown). Both samples show the same behaviour as unlabeled WT: Proton uptake of 1 proton per activated rhodopsin molecule without peptide and release of 0.5 protons per activated rhodopsin at 1 mM peptide concentration. The kinetics of the V227R1 pigment are slightly faster.*

and for WT rhodopsin. The same result is found if native $G_t\gamma$(60-71)far peptide is added in a high concentration (1 mM, third row). Thus both peptides do not seem to influence the motion of TM6 or H8.

Interestingly the dark state for the V227R1 pigment is slightly more immobilized if either of the two pigments is bound. This can be seen in the low field peak (left side) being a bit less sharp for the black spectra with either peptide. This may indicate that the spin label in the 227 position is hindered by either a slightly more outward tilted TM6 or by a different environment of the spin label. As there is no obvious reason for a different position of TM6, this could point to the fact that the peptide at least partly binds to the dark state thereby immobilizing the spin label in the 227 position. It was proposed that G_t binds to the inactive dark state of rhodopsin [Dell'Orco et al., 2007; Fanelli and Dell'Orco, 2005; Morizumi et al., 2003].

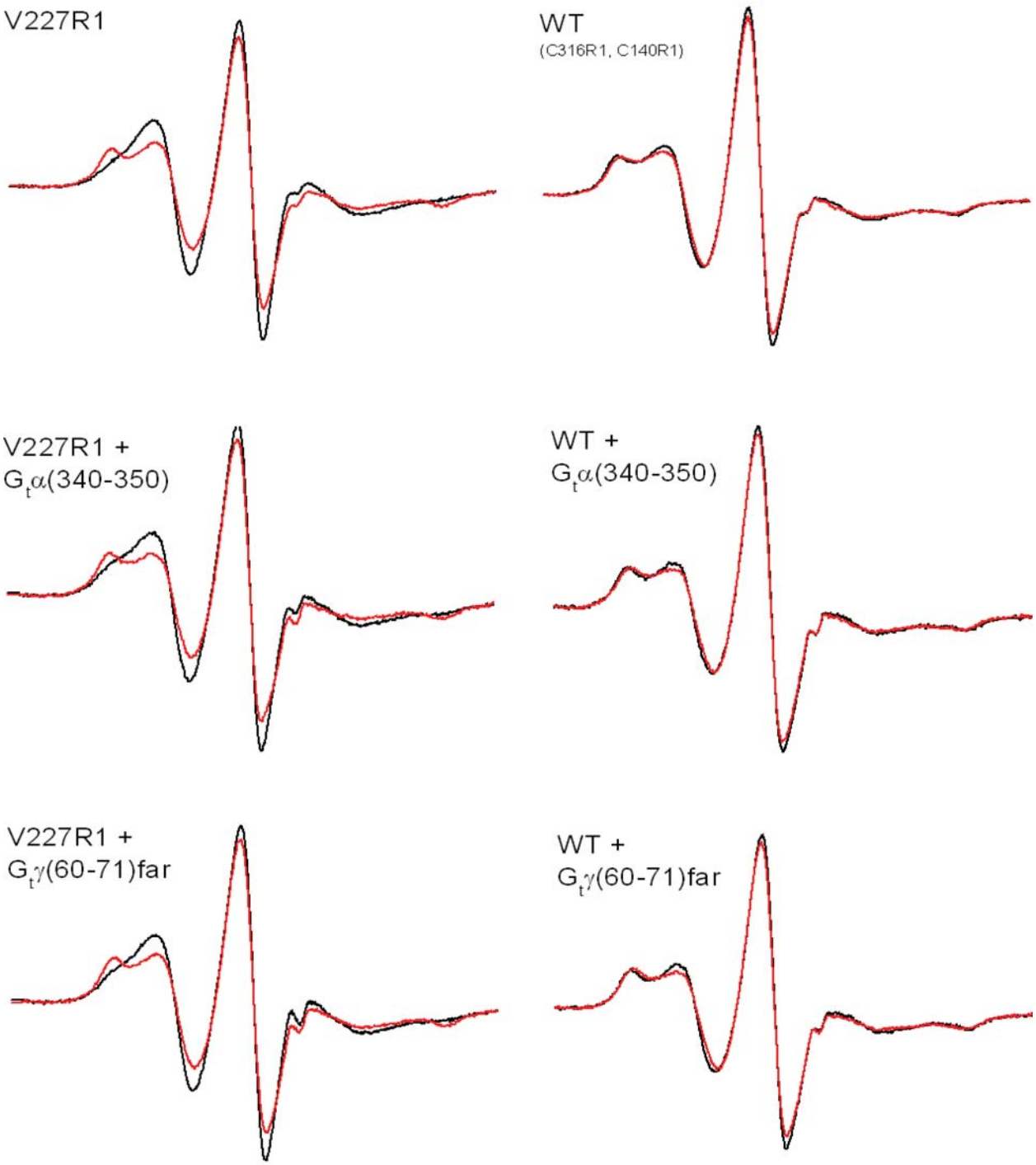

Fig. 75: *EPR spectra of rhodopsin with high affinity $G_t\alpha$(340-350) and $G_t\gamma$(60-71)far peptides. The pigment V227R1 (left column) and spin labeled WT rhodopsin with spin labels at positions 140 and 316 (right column) were examined. Spectra of the dark state are shown in black, those after 15 s illumination with an orange light (> 515 nm) filter are shown in red. In the first line the spectra for pure rhodopsin without peptide are shown as reference. In the second line the spectra of the same pigments with 1 mM native $G_t\alpha$(340-350) peptide are shown and in the third line those of the pigments with 1 mM $G_t\gamma$(60-71)far peptide (for the complete peptide sequences see Table 4 on page 56).*

3.7 G-protein binding to rhodopsin

Although G_t derived peptides (see chapter 3.6) are a good model system for G protein binding, some effects can only be seen through binding of the native G_t to rhodopsin in its native lipid environment. All experiments shown here were performed like this and under conditions of almost 100 % Meta-II formation: pH 6.0 and 25 °C. Therefore no effect of G_t binding on Meta-II formation ('extra Meta-II' [Schleicher et al., 1989]) was observed. Instead of washed membranes differently prepared disc membranes were used here [Smith et al., 1975]. These have been shown to be osmotically intact disc membrane vesicles and feature a homogeneous size distribution. This makes them well suited for G_t binding studies. Flash photolysis experiments were done, and G_t binding was observed with light scattering in the same experiment.

3.7.1 Uptake of additional protons

As shown before there is a second proton taken up per each activated rhodopsin molecule in the presence of G_t [Schleicher and Hofmann, 1985]. This has been tested with titration of G_t to osmotically intact disks (see Fig. 76), and these findings are reproduced: In the presence of G_t in a 1:1 ratio towards rhodopsin (red trace) there is a second proton taken up for each activated rhodopsin molecule in addition to the proton that is already taken up in the absence of G_t. But in addition to this proton, there is a third proton taken up very slowly – with a half life time of roughly one second.

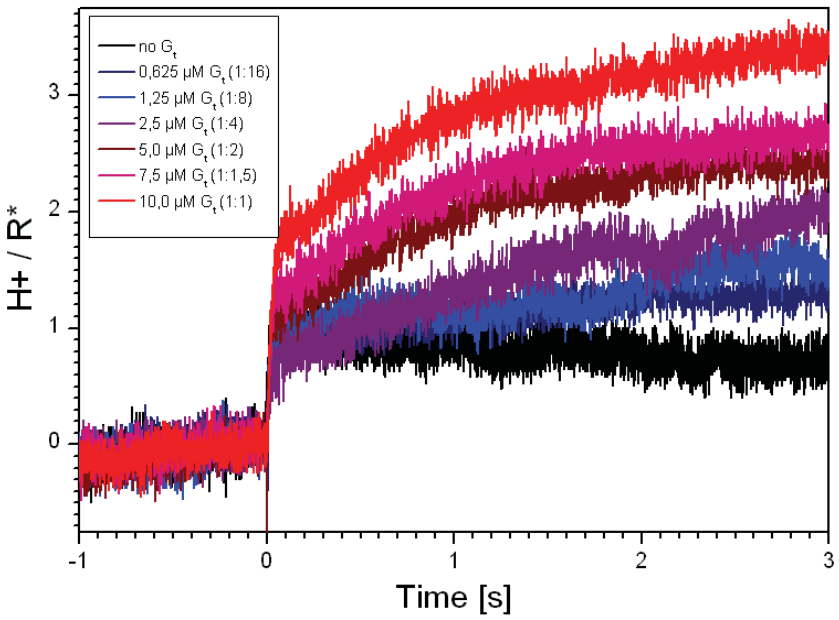

Fig. 76: *Influence of G_t on the proton uptake. The experiment was performed with osmotically intact discs at pH 6.0 and 25 °C to ensure full Meta-II formation. Without G_t there is roughly one proton taken up per activated rhodopsin. With increasing G_t formation there is an additional proton taken up on the fast time scale, and a third proton gets taken up on a very slow time scale.*

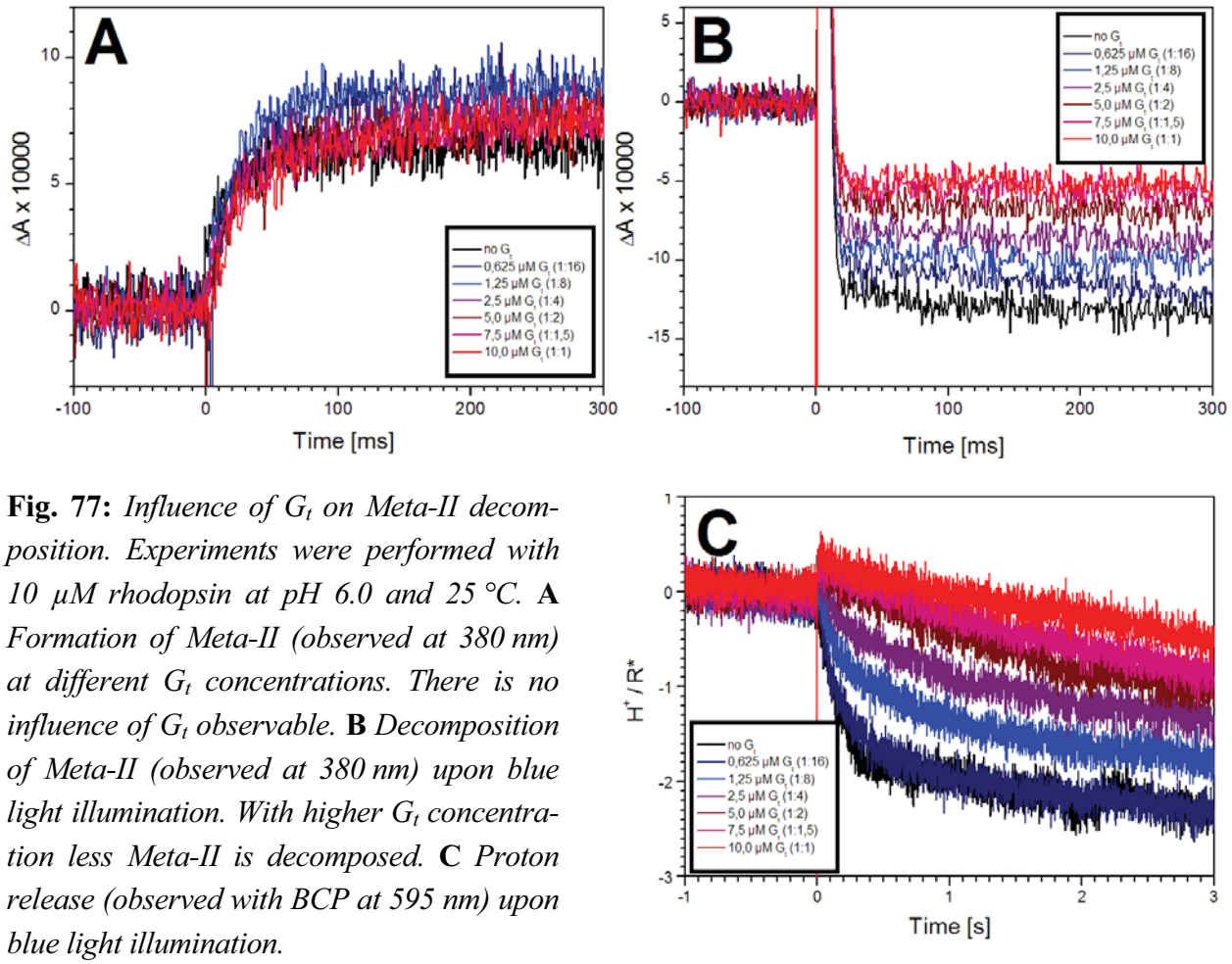

Fig. 77: *Influence of G_t on Meta-II decomposition. Experiments were performed with 10 µM rhodopsin at pH 6.0 and 25 °C.* **A** *Formation of Meta-II (observed at 380 nm) at different G_t concentrations. There is no influence of G_t observable.* **B** *Decomposition of Meta-II (observed at 380 nm) upon blue light illumination. With higher G_t concentration less Meta-II is decomposed.* **C** *Proton release (observed with BCP at 595 nm) upon blue light illumination.*

3.7.2 Influence of G_t on Meta-II decomposition

As mentioned above, there is no effect on Meta-II formation of the different G_t concentrations, because Meta-II is quantitatively formed already without G_t due to the environment conditions. This is shown in Fig. 77A where the formation of Meta-II is plotted for different G_t concentrations without showing any significant difference.

Nevertheless, Meta-II is stabilized upon binding of G_t as shown in Fig. 77B: Blue flashes were applied to fully bleached samples of the same G_t concentrations as in Fig. 77A. The result is as follows: With increasing G_t concentration less Meta-II is decomposed, which implies that G_t stabilizes the active Meta-II conformation. The same effect is consequently also mirrored in the decrease of the proton release by the same percentage upon blue light illumination (Fig. 77C).

3.8 Role of Lipids in rhodopsin activation

The environment of rhodopsin plays an important role for its activation – in a membrane environment the behaviour is totally different from a detergent (in this study mostly DM) environment. Therefore the effect of the phospholipids POPE, POPC and POPS (for the structures see Fig. 30 on page 57) which are naturally found in disc membranes on rhodopsin activation was investigated.

Flash photolysis measurements were performed with DM solubilized samples to which lipid suspension in H_2O were added (see chapter 2.2.8).

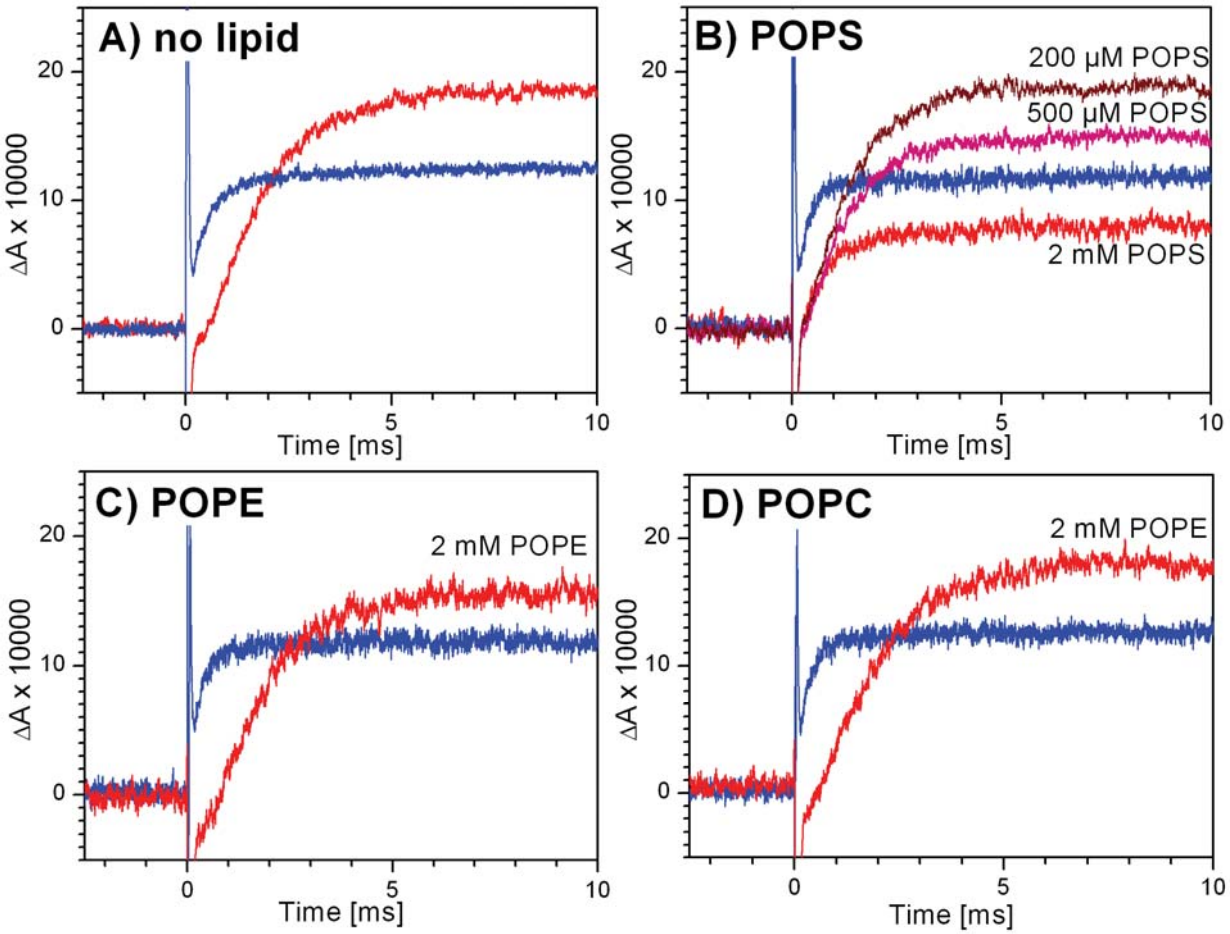

Fig. 78: *Flash photolysis experiments on rhodopsin in DM with lipids added. All experiments were performed at pH 6.0 and 20 °C with 5 µM rhodopsin; 50 µM BCP as pH-dependent dye was present. The traces are corrected for the rhodopsin effect (see 2.3.1). Blue traces represent the formation of Meta-II observed at 380 nm and red traces the proton uptake observed at 595 nm.* **A** *Reference experiment of rhodopsin without lipid.* **B** *POPS leads to a decrease of the proton uptake with increasing lipid concentration, while Meta-II stays unaffected (only one trace shown in blue for 2 mM POPS).* **C** *Even at high POPE concentration there is no significant effect observable.* **D** *POPC does not show a significant effect at high concentration either.*

3.8.1 Addition of lipids to DM samples

To find out if lipids directly interact with rhodopsin, flash photolysis experiments with rhodopsin solubilized in DM and lipids added to this system were investigated. This model system was chosen because lipids were removed in the purified rhodopsin (see chapter 2.2.6) and thus lipids can be added to the sample in a defined manner without distortion by other lipids that are already present in the sample.

Experiments with lipids added are shown in Fig. 78. With POPS (panel B) there is an effect only on the proton uptake but not on Meta-II formation observable: The kinetics stay unaffected, but the amplitude of the proton uptake is decreased with increasing POPS concentration. This might be an effect of the POPS on rhodopsin, but it could as well just be a buffering effect, because the serine group in the hydrophilic part of the protein is likely to buffer protons. Therefore another assay was applied to determine whether POPS has a specific effect on rhodopsin or not. Both POPE and POPC (panels C and D) do not show a significant effect on either proton uptake or Meta-II formation.

3.8.2 Addition of lipids to DM samples with peptide

To further test the effect of POPS shown above, the effect of POPS on rhodopsin with $G_t\alpha$(340-350) HAA peptide was investigated. In Fig. 79 flash photolysis data of rhodopsin with a constant concentration of $G_t\alpha$(340-350) HAA peptide is shown (for the peptide sequence see Table 4 on page 56). Only the proton uptake traces are shown because formation of Meta-II again stays unaffected (data not shown).

Without any lipid, a proton release is observed as shown before (see chapter 3.6.2). POPS is titrated to this sample, and this results in a decrease of the proton release. At concentrations above roughly 50 µM POPS we can see a proton uptake instead of a release. This proton uptake increases further with additional POPS concentration, saturating at about 75 % of the proton uptake which is observable without any peptide (only with POPS to take the buffering effect into account). Interestingly even at high POPS concentrations the traces still retain a small proton release effect (the traces move downwards again) which is slower than the proton uptake and gets smaller at higher concentrations. This points to an overlay of two processes – a fast proton uptake and a slower proton release.

The shown effect is again specific to POPS: Even with high concentrations of either POPE or POPC no significant change except for a small buffering effect is observable if the same assay is applied (data not shown).

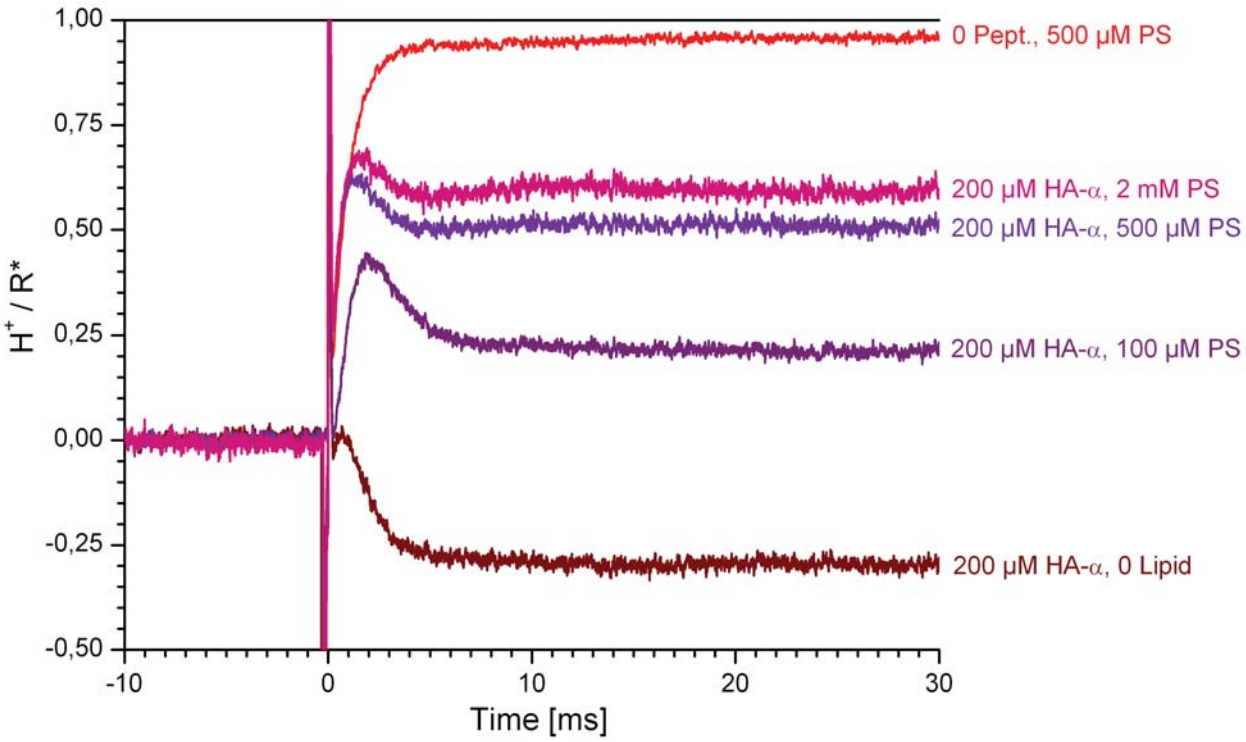

Fig. 79: *Flash photolysis experiments on rhodopsin with a constant concentration of high affinity $G_t\alpha$ peptide and increasing concentrations of PS. Experiments were done at pH 6.25 and 20 °C, the rhodopsin concentration is 10 µM. Only the proton uptake traces (595 nm) are shown and are slightly scaled for constant Meta-II formation. Meta-II data (380 nm) are not shown, because the traces are identical except for a slight deceleration at high PS concentration. The red line is for reference and is measured without peptide but with 500 µM PS. The brown line represents the pure effect of the $G_t\alpha$(340-350) HAA peptide without lipid: a proton release of roughly 0.3 protons per activated rhodopsin. With increasing PS concentration (traces in the middle) the proton release is reversed into a proton uptake again.*

3.8.3 Crosslinking between rhodopsin and POPS

In order to determine the place where POPS interacts with rhodopsin, I tried to crosslink the lipid to rhodopsin. The crosslinking reaction was performed with EDC as described in chapter 2.2.9.

A comparison of the proton uptake by DM solubilized rhodopsin under different conditions is shown in Fig. 80. Meta-II formation was again not influenced so that the data is not shown here. For reference rhodopsin without lipids and without EDC crosslinking is shown (red trace). If the sample without lipid is treated with EDC the proton uptake is slightly reduced (violet trace). A similar behaviour is observable if rhodopsin is treated with EDC in the same manner after addition of either POPE (cyan trace) or POPC (green trace). In contrast, addition of POPS to rhodopsin and crosslinking with EDC leads to an almost total abortion of the proton uptake (orange trace).

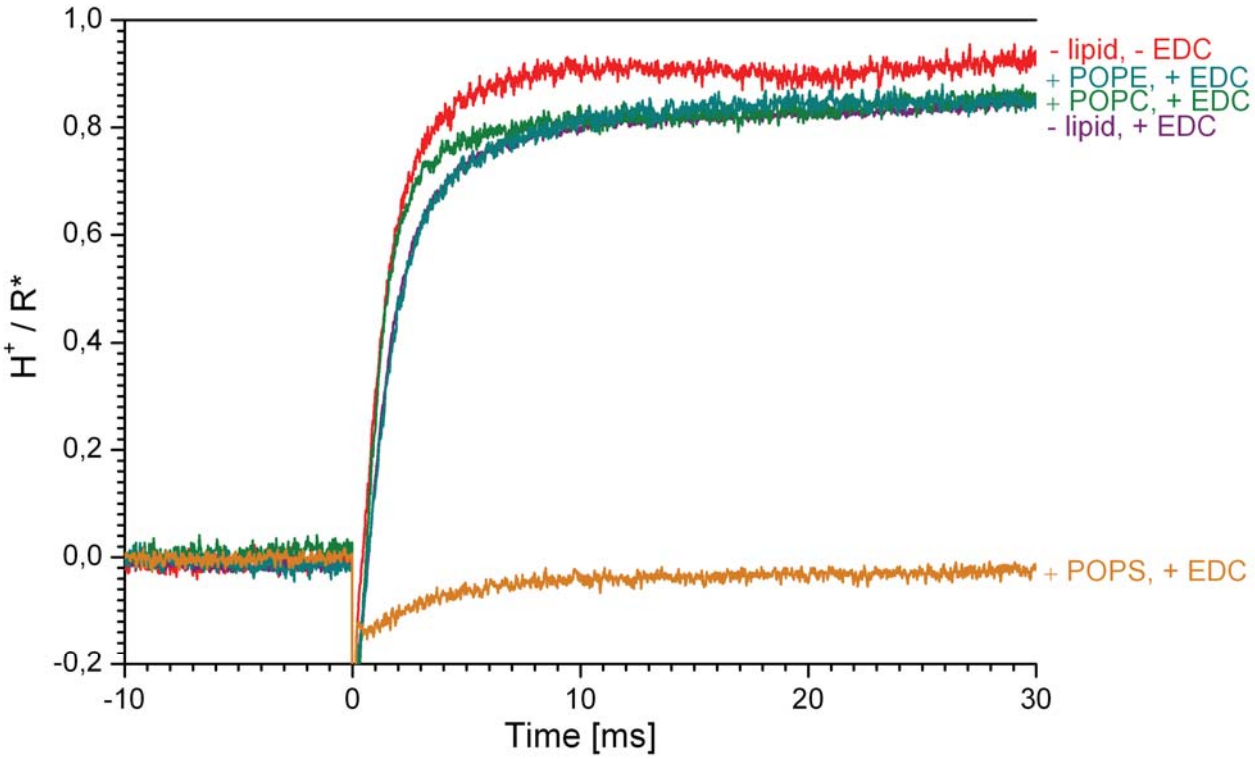

Fig. 80: *Flash photolysis experiments on rhodopsin treated with EDC after addition of different lipids. Experiments were performed at pH 6.25 and 20 °C, the rhodopsin concentration is 5 µM, the BCP concentration 50 µM. Only the proton uptake traces (595 nm) are shown and are slightly scaled for Meta-II formation. Meta-II data (380 nm) are not shown, because the traces are independent of lipid and/or EDC. The red line is the proton uptake for rhodopsin without lipid and without EDC. The violet trace represents an identical sample treated with EDC. The dark cyan trace shows the proton uptake for rhodopsin with POPE added and treated with EDC. The dark green trace shows an identical sample with POPC. The proton uptake for rhodopsin with POPS and cross-linked with EDC is drawn in orange showing almost total abortion of the proton uptake.*

Fig. 81: *Flash photolysis experiments of the same samples as in Fig. 80 with blue light illumination of the active states. Again proton uptake is shown only, mirroring the same effects as formation of Meta-II.*

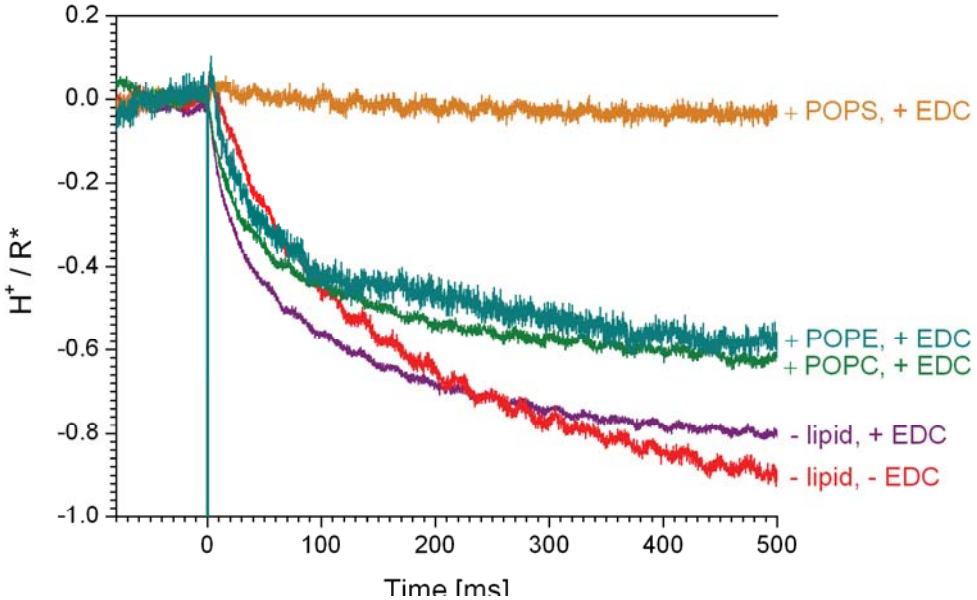

The same samples have been investigated with blue light illumination of the active states (as established in chapter 3.5.4). Fig. 81 shows the proton release signals. They mirror the same effect as the proton uptake shown in Fig. 80: Analogous to the proton uptake, the proton release for the cross-linked sample including POPS and peptide the proton release is cancelled out. The traces for Meta-II decomposition are not shown because they are identical.
Thus we can conclude that either only POPS is cross-linked to rhodopsin through the described EDC assay or only cross-linking of POPS but not of the other lipids leads to the described effect.

3.8.4 Addition of lipids to ERY mutant pigments

Both $G_t\alpha$(340-350) peptide and POPS have shown an interesting competing effect (chapter 3.8.2), and they are both supposed to bind in the conserved ERY region. Therefore the experiments shown in chapter 3.8.2 were repeated with two established mutant pigments which feature mutations in the ERY region: E134Q and R135L (more data on these pigments in chapter 3.2).
In Fig. 82 the proton uptake traces for the E134Q mutant pigment with a constant concentration

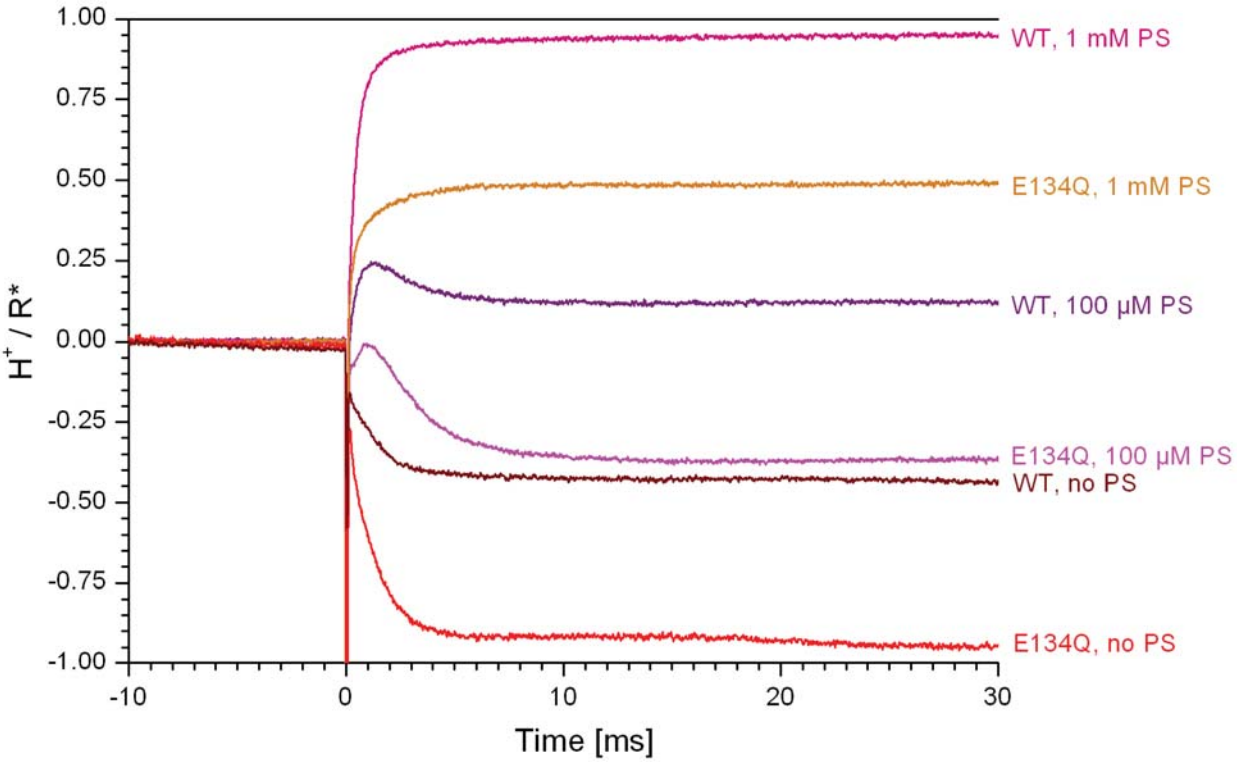

Fig. 82: *Flash photolysis experiments on the pigment E134Q in the presence of $G_t\alpha$(340-350) HAA peptide and POPS. Experiments were done at pH 6.25 and 20 °C, the rhodopsin concentration is 10 µM and the BCP concentration 50 µM. 200 µM $G_t\alpha$(340-350) HAA peptide is present in all samples. Only the proton uptake traces (595 nm) are shown and are slightly scaled for constant Meta-II formation. Meta-II data (380 nm) are not shown, because the traces are identical except for a slight deceleration at high POPS concentration.*

of 200 µM $G_t\alpha$(340-350) HAA peptide and different POPS concentrations are shown. Addition of peptide and POPS again does not influence the formation of Meta-II (data not shown).

The E134Q pigment shows a constant downshift of the proton uptake traces by roughly half a proton per activated rhodopsin at the three observed POPS concentrations, if the same POPS concentration is compared between WT and mutant pigment. Like observed with WT rhodopsin (see chapter 3.8.2) which is shown in Fig. 82 for comparison there is a proton release if only the peptide is present, and with increasing POPS concentration this proton release is converted into a proton uptake.

Fig. 83 shows comparable proton uptake traces for the mutant pigment R135L. Again Meta-II formation is not influenced by peptide and/or POPS (data not shown). The proton uptake traces with the R135L pigment are not influenced by addition of POPS even at high concentration – the proton uptake stays around 0 protons per activated rhodopsin molecule, only showing a small transient positive signal. This transient signal can again be understood as pointing towards an overlay between a faster positive and a slower negative signal which cancel out each other, lead-

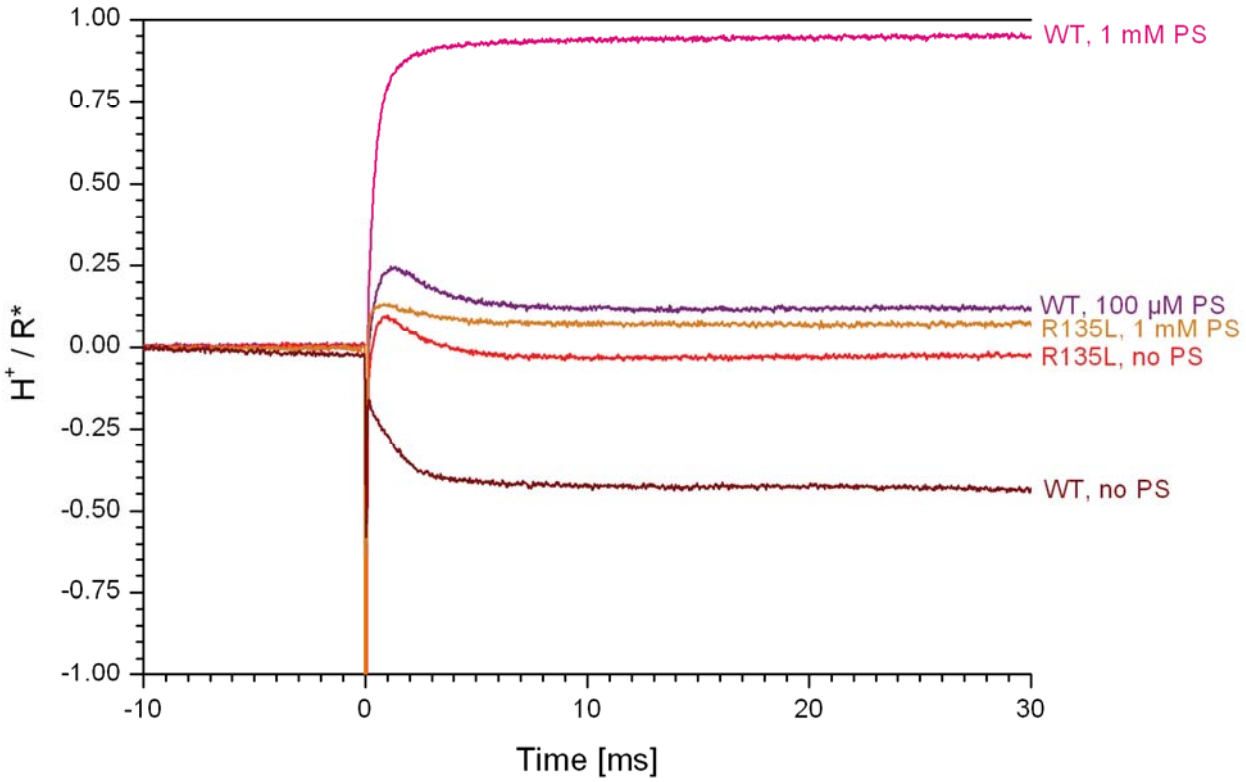

Fig. 83: *Flash photolysis experiments on the pigment R135L with $G_t\alpha$(340-350) HAA peptide and POPS. Experiments were done at pH 6.25 and 20 °C, the rhodopsin concentration is 10 µM and the BCP concentration 50 µM. 200 µM $G_t\alpha$(340-350) HAA peptide is present in all samples. Only the proton uptake traces (595 nm) are shown and are slightly scaled for constant Meta-II formation. Meta-II data (380 nm) is not shown, because the traces are identical except for a slight deceleration at high POPS concentration.*

ing to the proton uptake around zero. Thus neither peptide nor POPS have an influence on the proton uptake into the R135L pigment. The slight upward shift at 1 mM POPS concentration is probably caused by buffering of POPS.

4 Discussion

How does the activation of rhodopsin proceed? Although it may take some more years to ultimately answer this question, I can evolve a better understanding based on the data presented in the previous chapters.

4.1 Sequence of the main activation steps

The aim of this first chapter is to elucidate the sequence of the different activation steps. It is important to answer this question first in order to be able to understand the other experiments based on these activation steps. The question of the sequence of the activation steps has been investigated through the kinetic experiments at different temperatures shown in chapter 3.1.

4.1.1 TM6 motion occurs after Meta-II formation and simultaneously with proton uptake

The data in Fig. 34 show that the TM6 movement reflected in the EPR change of the spin label at position 227 is characteristically delayed with respect to retinal Schiff base deprotonation, which marks the transition to Meta-II. Its kinetics are very similar if not identical to those of the proton uptake.

The Arrhenius representation of the kinetic data (Fig. 35) reveals that at sufficiently low temperature, TM6 motion adopts the kinetics of Meta-II formation. This can be interpreted as Meta-II formation being the rate limiting step at those temperatures. At higher temperature, both steps display their own kinetics, which follow straight lines in the Arrhenius representation. The activation energies are 116 $\frac{kJ}{mol}$ for the formation of Meta-II and 74 $\frac{kJ}{mol}$ for TM6 motion (V227R1) at temperatures above 5 °C. Thus we can conclude that TM6 motion does not coincide with Meta-II formation.

By contrast to SB deprotonation, proton uptake coincides kinetically with TM6 movement. The activation energies are similar if not identical (81 and 74 $\frac{kJ}{mol}$ - the difference is within the error, see Table 5). Either TM6 motion or proton uptake are therefore rate limiting, with the respective other reaction occurring on a faster time scale.

The protonation has been proposed before to occur at or close to the D(E)RY motif [Arnis et al., 1994] (for a detailed discussion of this region see chapter 4.2.3). One obvious model would be that proton uptake induces the breakage of the D(E)RY network, which allows TM6 to move.

This model has been proposed before to be a general principle of GPCR activation [Ballesteros et al., 2001]. The other possibility is that TM6 is allowed to move first thereby opening the cleft in the vicinity of the D(E)RY motif. This would dramatically change the environment of the D(E)RY from hydrophobic to hydrophilic and consequently allow protonation of Glu^{134} or the cluster it is involved in. The kinetic data so far leave open whether TM6 motion is cause or consequence of proton uptake.

4.1.2 Proton uptake is a consequence of TM6 motion

As Fig. 36 shows, TM6 motion occurs with its full maximum amplitude at pH > 7. At this pH proton uptake does virtually not occur. This proves the proton uptake reaction to be a consequence of helix motion rather than its necessary precursor.

Proton uptake [Arnis and Hofmann, 1993] and FTIR data from rhodopsin mutants have shown that proton uptake can only occur if rhodopsin contains a protonable group at position 134. Therefore the likely acceptor for the proton is Glu^{134} or the cluster to which it belongs, similar to the situation in bacteriorhodopsin (with Asp^{94} as the relevant residue) [Garczarek and Gerwert, 2006]. Protonation occurs with a pK of ca. 6.5, the previously identified pK of proton uptake which fits to the pK shown in Fig. 36. The shift of the pK from 4.2, which is the pK of an isolated Glutamate residue, to a higher value ("forced protonation") is completely explained by the influence of neighbouring groups, which by their interaction enhance the free energy of the protonation and increase the pK [Buczylko et al., 1996; Hofmann, 1999].

Upon outward motion of TM6 (indicated by the brown arrow in Fig. 2) the D(E)RY motif, which has close contact to TM6 in the ground state, gets exposed to water. This change from an environment protected from water to a water exposed environment would elegantly explain why Glu^{134} or the cluster it is involved in gets protonated. However, the role of this protonation is not clear so far but further discussed in chapter 4.2.

4.1.3 H8 configuration change happens in a later step

A further new outcome of these studies is that the changes monitored in the EPR spectrum with the spin label 316R1 are slower than those related to TM6 motion (Fig. 34 and Fig. 35C). If this change displayed the dependence of proton uptake on pH (see Fig. 36), this would suggest that H8 changes as a late consequence of proton uptake. I was not successful in getting pH dependent data for H8 motion with EPR spectroscopy, because the absolute change of the spin label mobility is rather small (compare Fig. 32A, left side). Therefore I could not reliably dissolve

intermediate states between the dark and the illuminated state. Instead I chose an approach with Alexa-594 as a fluorescent dye in this case (description in chapter 2.2.5).

The fluorescent dye at position 227, monitoring TM6 motion, did not show a pH dependence (Fig. 37), consistent with the EPR data (Fig. 36). The fluorescent dye at position 316 did not show any pH dependence either which argues against the H8 configuration change being a late consequence of proton uptake. However in an earlier study by IMAMOTO et al. [Imamoto et al., 2000] a pH dependent behaviour was found ([Imamoto et al., 2000], Fig. 4), but this is probably explained by an effect on the Meta-I/Meta-II equilibrium, because these experiments were performed in membranes while I worked with samples in DM, which prevents Meta-I formation and therefore results in complete Meta-II formation.

As a consequence of the lacking pH dependence of the H8 change it is unlikely that the signal observable at H8 propagates through a sequence of TM6 movement, proton uptake and 'lateral' transmission to H8, explaining the late occurrence of the H8 change. This signal pathway could only be held up by assuming that the H8 change is directly coupled to TM6 motion without the proton uptake into the ERY. The second possibility is signal propagation directly from the chromophore region to H8. From the data presented here we cannot decide if the motion of H8 is an independent step.

What exactly is the cause of the observed EPR and fluorescence change at position 316? It seems likely that H8 performs a lateral movement during the activation process leading to a different environment due to neighbouring groups, which is sensed by the spin label. However, a complete disintegration of the helix structure as proposed by KRISHNA and SAKMAR [Krishna et al., 2002] is also possible. The role of the region for the rhodopsin activation process is discussed in detail in chapters 4.2.4 and 4.2.5

4.1.4 Synopsis of the activation steps and their potential relevance

According to the data presented above, a consistent scheme of rhodopsin activation would contain the following time ordered sequence of events: Retinal isomerization first leads to small relocations of several amino acid side chains (Meta-I, see e.g. [Ruprecht et al., 2004]) and eventually to the deprotonation of the SB, which marks the transition from Meta-I to Meta-IIa. It has been shown that SB deprotonation *per se* does not activate the receptor [Fahmy et al., 1995]. Only protonation of the complex counterion (in the native structure made up by Glu^{113} and Glu^{181} [Ludeke et al., 2005]) drives the activation process one further step. If this protonation step was delayed (which is not known) it could fit to the kinetics of TM6 motion. Then SB de-

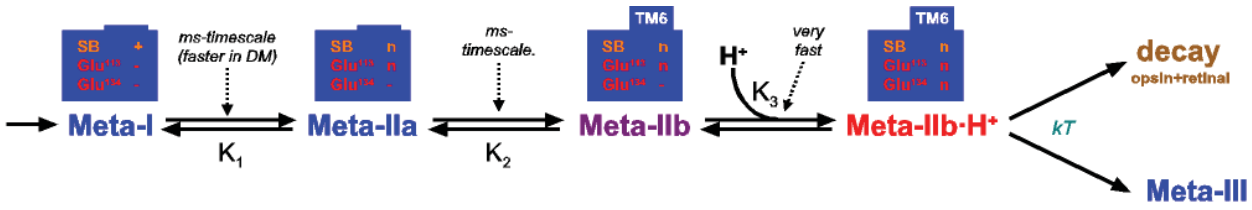

Fig. 84: *Scheme of the late photoproducts for rhodopsin corresponding to the old scheme in Fig. 4. '+' means a positively charged residue, '-' a negatively charged residue and 'n' an uncharged residue at the respective location. 'Glu^{134}' symbolizes the cluster around Glu^{134} where the proton is taken up in the last step. The outward rigid body motion of TM6 is symbolized by the blue bar. Residues change their charge state by proton uptake or release, respectively. Meta-IIb and/or Meta-IIb·H$^+$ are capable of catalyzing the GDP/GTP exchange in G_t.*

protonation would lead to Meta-IIa and protonation of Glu^{113}/Glu^{181} would lead to Meta-IIb. Different hypotheses on the cause of the time delay are discussed in chapter 4.5. Whatever, the outward motion of TM6 happens in a later step, the transition from Meta-IIa to Meta-IIb. This movement then changes the environment of the D(E)RY motif and enables immediate protonation of a protonable group in the D(E)RY region. These steps are depicted in the scheme in Fig. 84.

The product which we label Meta-IIb·H$^+$ now is the same which has been named Meta-IIb so far [Arnis and Hofmann, 1993]. As depicted in Fig. 84, we now have coupled equilibria between at least four late photoproducts (additional transitions might occur, which we cannot detect with the methods applied here). If the linear scheme applies, these equilibria all have the same apparent pK, but the amplitudes are likely to be different due to different equilibrium constants K_x. This means, that the amount of one or several neighbouring products might be dependent on the pH (with a common pK), while other products either accumulate or deplete over the whole pH range (with slight changes in amount which are not detectable experimentally). In detergent, the Meta-I/Meta-II equilibrium is almost 100 % on the Meta-II side. The equilibrium between Meta-IIa and Meta-IIb is also shifted to the right side, and the equilibrium between Meta-IIb and Meta-IIb·H$^+$ obviously has a pK around 6.5 in DM (see Fig. 36). Therefore under the detergent conditions examined here only the transition between Meta-IIb and Meta-IIb·H$^+$ has to be taken into account. Interestingly, in membranes the pK of the equilibria is shifted to the basic side, as we can deduce from the known Meta-I/Meta-II equilibrium [Hoffmann et al., 1978; Matthews et al., 1963; Parkes and Liebman, 1984].

The motion of H8 is an additional step whose relevance is not clear yet. Both the ERY motif and the H8 region are likely to be G_t binding sites (discussed in chapter 4.2). Thus a probable interpretation is that both sites are involved in the proposed sequential fit mechanism of G_t activation [Herrmann et al., 2004]. This aspect will be further discussed in chapter 4.3.2.

A recent crystal structure of a rhodopsin photoproduct which has been claimed to be in the G_t activating state showed no movement of either TM3 or TM6 compared to the dark state [Salom et al., 2006]. Looking at the photoproducts introduced above, it is likely that these crystals are trapped in the Meta-IIa state where TM6 motion has not occurred. The reason for the trapping is probably the dense packing of the molecules in the crystals not allowing this outward motion of TM6. However, the authors have reported that the photoproduct formed in the crystals activates G_t after dissolving the crystal. It is most likely that the protein can proceed from the formerly trapped Meta-IIa state towards Meta-IIb and -IIb·H^+ upon dissolving the crystal, thus explaining the ability to activate G_t. In contrast to this, the 2D crystals characterized here (see chapter 3.1.7) have the potential to reveal a structure of the active Meta-IIb·H^+ state because they have been shown to take up protons upon photoactivation (see chapter 3.1.7), but the work on the structure is not completed yet.

4.2 Role of the ERY motif and the NPxxY(x)$_{5,6}$F motif

The crystal structure of rhodopsin [Palczewski et al., 2000] revealed that both the ERY and the NPxxY(x)$_{5,6}$F regions involve dark state stabilizing hydrogen bonded networks. The NPxxY(x)$_{5,6}$F region has been examined in a recent study [Fritze et al., 2003]. The ERY region considered here is another constraint that keeps rhodopsin in the ground state and is broken during the activation process, but it also fulfils a second role in the activation of G_t. The motif occurs as a DRY sequence in many receptors and is therefore labeled D(E)RY if its general role in GPCRs is meant.

4.2.1 Effect of mutations in the ERY region

The ERY motif (see Fig. 85) has been discussed before as one of the important constraints keeping the rhodopsin structure and especially TM6 in the dark state [Li et al., 2004; Teller et al., 2001]. An 'ionic lock' which is broken during activation was also proposed for the β_2-adrenergic receptor (the respective residues in the β_2-AR are Asp^{130}, Arg^{131} and Glu^{268}) [Ballesteros et al., 2001]. As I will explicate below, this is only a part of the truth, because the ERY motif plays a

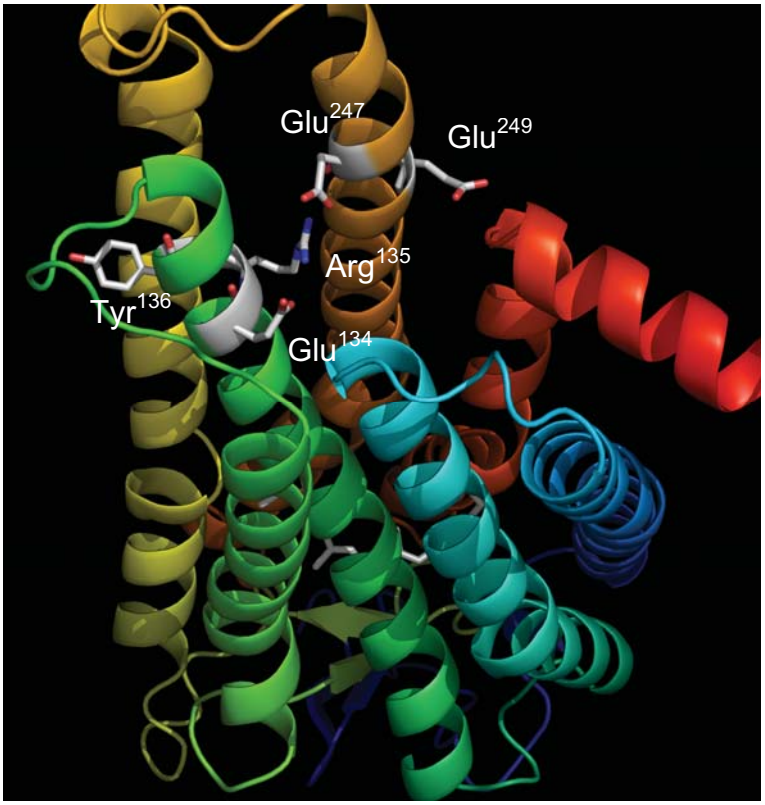

Fig. 85: *The ERY motif composed of the residues Glu[134], Arg[135] and Tyr[136] is located at the cytoplasmic end of TM3. Besides the salt bridge between Glu[134] and Arg[135] there is an interaction between Arg[135] and Glu[247] in TM6.*

double role: It helps to stabilize TM6 in the inward state and it is involved in formation of the receptor state capable of G_t activation. Both roles have been proposed for the D(E)RY motif in GPCRs in general, but only one of them in each group of GPCRs [Rovati et al., 2007]. Nevertheless there is no reason why the ERY motif in rhodopsin should not fulfil both roles, and the data suggest that this is indeed the case as explained below.

How is the ERY motif involved in stabilization of the dark state? The region is shown in Fig. 85. The different crystal structures [Li et al., 2004; Palczewski et al., 2000; Teller et al., 2001] agree that there is a salt bridge between Glu[134] and Arg[135] and a further interaction between Arg[135] and Glu[247] connecting TM3 and TM6. This interaction is claimed to be either a salt bridge (in the case of a negatively charged Glu[247]) or a hydrogen bond (for an uncharged Glu[247]). I will argue below why it is likely that it actually is a hydrogen bond. Additional interactions between TM3 and TM6 are the proposed van-der-Waals interactions of Arg[135] with Val[250], Thr[251] and Val[254]. The importance of the Arg[135]-Thr[251] interaction has been underlined by a recent study [Ramon et al., 2007]. This whole network seems to be intact in the Meta-I state [Ruprecht et al., 2004]. However it needs to be broken during formation of the active state to enable the outward motion of TM6 [Farrens et al., 1996; Kusnetzow et al., 2006] (see also chapter 4.1).

Glu[134]: The mutation of Glu[134] to Glutamine (E134Q mutation) anticipates protonation on this residue or another protonable group in the cluster (see the missing protonation in Fig. 44, green squares and [Arnis et al., 1994]) thereby facilitating the Meta-IIb·H^+ state [Knierim et al., 2007; Meyer et al., 2000]. This mutation also induces a movement of TM3 thus showing that the struc-

tural changes on TM3 and the protonation state of Glu^{134} are closely connected [Kim et al., 1997]. Computer simulations support this finding by showing that Glu^{134} is in a region which is highly sensitive to changes in the microenvironment and that it can easily change its protonation state [Periole et al., 2004]. A recent study even claims that two protons are taken up per activated rhodopsin [Lewis et al., 2006], but this finding is not in agreement with my data, since I find a maximum of one proton per activated rhodopsin molecule (see Fig. 44, red circles).

As shown in chapter 3.2, the E134Q mutant pigment cancels out the proton uptake, reverts the pH dependence observed with 9-dm retinal and shows a stronger formation of Meta-II with 9-dm retinal under Meta-I conditions.

My interpretation of these findings is that the Glutamine instead of a Glutamate in position 134 abolishes the salt bridge which is normally present between the negatively charged Glu^{134} and the positively charged Arg^{135} and which probably aligns Arg^{135} for the interaction with Glu^{247}. Due to this missing stabilizing salt bridge the interaction between Arg^{135} and Glu^{247} together with the Van-der-Waals contacts of Arg^{135} with Val^{250}, Thr^{251} and Val^{254} [Li et al., 2004] are weakened. This destabilizes the interaction between TM3 and TM6 so that TM6 can move outward much easier. But the remaining interactions along with the interaction between the retinal β-ionone ring and Trp^{265} are still strong enough to well stabilize the inward position of TM6 until the formation of Meta-II [Kim et al., 1997], because otherwise constitutive activity of the retinal bound pigment would occur. Due to this destabilization effect the equilibrium is shifted towards the active state, as can be seen with UV/vis and FTIR spectroscopy of pigments containing 9-dm retinal, which normally favors the Meta-I state (see Fig. 41, second row left, and Fig. 42, green line). The anticipation of the protonation therefore shifts the equilibrium towards the Meta-IIb·H^+ state.

During the normal activation mechanism the salt bridge between Glu^{134} and Arg^{135} could be broken in a slightly different way: It is likely that there is an internal water molecule close to the ERY motif, located between TM3 and TM6 [Saam et al., 2002]. Thus the proton is not necessarily taken up by Glu^{134} alone but into the cluster composed out of Glu^{134}, Arg^{135} and the mentioned water molecule – or alternatively a lipid molecule in the same place (see chapter 4.4.2). This would explain why no protonation change of Glu^{134} is observable with FTIR spectroscopy (see Fig. 42) which should be the case if the proton is taken up by Glu^{134} directly.

The unchanged activity of the pigment E134Q towards rhodopsin (see Fig. 48) although the ERY motif is likely to be a G_t binding site shows that Glutamine replaces Glutamate well in matters of the binding site. Earlier studies even reported a slight hyperactivity of the E134Q mutant

pigment towards G_t [Fahmy and Sakmar, 1993] and revealed that the E134Q mutant shows constitutive activity in the pure opsin state, i.e. without any retinal [Buczylko et al., 1996]. The report of a 10 % G_t activation (relative to WT in the illuminated state) of E134Q in the dark but retinal bound state already [Ramon et al., 2007] suggesting a severe perturbation of the structure is in conflict with the other cited studies and could thus be an artefact of the used assay (measurement through radioactive GTPγ^{35}S).

Arg^{135}: Mutant pigments with a replaced Arg^{135} have also been examined before, finding that mutants behave normal in terms of absorption spectra but do not activate G_t [Min et al., 1993]. This finding agrees with my data (see Fig. 48) but probably depends on the environment in which the mutant pigment is examined, as the same mutants reconstituted in vesicles have shown G_t activation [Shi et al., 1998]. This can be interpreted such that the ERY region is extremely sensitive to the environment which agrees with molecular modeling of the region, placing the motif right at the lipid-water interface [Periole et al., 2004].

The effect of replacing Arg^{135}, which is positively charged in the ground state, with the neutral amino acid Leucine (R135L mutation) is similar to the E134Q replacement: The salt bridge between Glu^{134} and Arg^{135} is broken thus rupturing one of the important constraints stabilizing the ground state. This can be deduced from the absorption spectra and the FTIR spectra for the 9-dm-R135L pigment both showing a higher fraction of Meta-II than 9-dm-WT under the same conditions (see Fig. 41, third row left, and Fig. 42, blue line).

As the proton uptake measurements show, the lack of interaction of the mutated Leu^{135} with Glu^{134} leads to the cancellation of the proton uptake, also just like the E134Q mutation (see Fig. 43, lower left panel, and Fig. 44, blue squares). This is further supported by the finding that there is, in contrast to WT, a proton uptake instead of a proton release detectable if either of the two activated mutants is illuminated with blue light ($\lambda < 430$ nm, see Fig. 62, second and third rows left). Obviously the protonable cluster including Glu^{134} and possibly a water molecule is already protonated in the dark state due to the missing negative charge on residue 135. Therefore the inward position of TM6 is not stabilized as in the native state because the hydrogen bond between Arg^{135} and Glu^{247} is consequently missing, while the weaker van-der-Waals interactions between Leu^{135} and Val^{250}, Thr^{251} and Val^{254} as well as other constraints holding TM6 might still be present. However, this destabilizing effect seems to be more severe than that of the E134Q mutation as a slightly increased mobility of TM6 in the dark state can be observed with the R135Q pigment [Kim et al., 1997] and as well with the R135L pigment (see Fig. 45).

For the 9-dm-R135L pigment, the active state, which in 9-dm-WT is favoured at acidic pH, is already observed at basic pH (see Fig. 41), thereby showing that the effect of the E134Q mutation and the R135L mutation onto this equilibrium is similar. The species occuring at acidic pH has been identified as Meta-II with a reprotonated Schiff base showing a λ_{max} = 480 nm in the UV/visible spectra (see Fig. 41, second row and fourth row right) [Meyer et al., 2000; Vogel et al., 2000]. This reprotonated species is favored at acidic pH, resulting in a pH trend with a negative slope. Such a pH trend is only visible with the E134Q and the R135L pigments because they do not feature the pH trend with a positive slope resulting from normal protonation of the Glu^{134} cluster. This protonation is a stronger effect than reprotonation of the SB and therefore cancels it out in WT and all other pigments with the normal proton uptake cluster (for a detailed discussion see [Knierim et al., 2007]).

Interestingly, the R135L mutant features no G_t activation (see Fig. 48) in DM (also reported in [Acharya and Karnik, 1996; Franke et al., 1992; Min et al., 1993]) while it was reported to have nearly normal activation in a membrane environment [Cohen et al., 1993; Shi et al., 1998]. This can be understood as another hint that the ERY motif is extremely sensitive to the environment. Depending on the presence of lipids or DM instead, the mutated ELY motif seems to have different structures either enabling G_t to bind or not.

If Arg^{135} is mutated to Lysine (R135K mutation), so that the side chain still has an ε-amino group featuring a positive charge, there seems to be an intermediate situation: The absorption spectra show no articulate dependence from the pH in either direction. This can be interpreted such that the Lysine at this position can still form a salt bridge with Glu^{134}, but the protonation equilibrium of the cluster composed of Glu^{134}, Arg^{135} and the potential water molecule is shifted. The stabilizing bond to Glu^{247} is also changed due to the different chemical situation given by the single amino group. The decreased activity of the pigment R135K (see Fig. 48) is probably explained by the changed chemical situation as well: Lysine still enables G_t to bind to the mutated EKY motif, but changes the binding affinity.

Interestingly, the kinetics of Meta-II formation are clearly faster for the R135L pigment (not so for the E134Q pigment!) and they are slower (including the proton uptake which is followed by Meta-II formation) for the R135K pigment (see Fig. 43). This indicates that the ERY motif is connected to the Schiff base region. The occurrence of a hydrogen bonded network has been discussed in chapter 4.2.6. Thereby changes in the ERY region can affect the kinetics of Meta-IIa formation. This also substantiates the role of Arg^{135} as the key position of the whole ERY motif, because a single amino acid substitution at this position can affect the kinetics of the

whole activation process. As stated above, the R135L mutation inhibits the stabilizing network between the ERY and TM6. The lack of one of the stabilizing links lowers the activation energy and could thus explain the faster kinetics, while the R135K mutation leads to a different sterical situation that obviously is responsible for slower activation kinetics.

As the EPR experiments show (see chapter 3.2.4) TM6 seems to have a higher flexibility in the ground state of both the R135K and the R135L mutant pigments. Interestingly, such a behaviour has not been found for the E134Q mutant pigment [Kim et al., 1997]. Again, this stresses the role of Arg^{135} as the linchpin of the whole network that causes perturbations in the protein if it is replaced by another amino acid. In contrast to the mutation of Glu^{134}, the replacement of Arg^{135} leads to lack of all the connections between TM3 and TM6 which are described above. This enables an increased flexibility of TM6 in the dark state already. How is the even higher TM6 flexibility of the R135x pigments at acidic pH (see Fig. 45) explained? Due to the protonation upon pH decrease in the absence of the normally occuring Glu^{134}-Arg^{135} salt bridge there is probably a repulsion between Glu^{134} and residues on TM6 (possibly Glu^{247} being involved) accounting for the increase in outward TM6 motion. The illuminated state in contrast is not seriously changed by any of the Arg^{135} mutations (see Fig. 46) since the network is broken in this state anyway. Therefore the lack of G_t activation may be explained by a direct binding of G_t to the ERY motif. This is also supported by further evidence discussed in chapter 4.3.

Another result stressing the extraordinary importance of Arg^{135} is the reduced restoration of rhodopsin ground state reproduction upon blue light illumination in DM with the R135L pigment (see Fig. 59A). If the ground state is less stabilized (as has been shown for the R135L pigment above), there is also consequently a smaller amount of ground state formed in photo equilibrium. Also interestingly, the amount of hydroxylamine sensitive product that is formed with both the E134Q and the R135L pigments upon blue light illumination is clearly lower at basic pH – another pH dependence for these two mutants which is inverse to WT.

The flash photolysis traces observed upon blue light illumination of the Meta-II state of both pigments (see Fig. 62) are basically slowed down mirror images of the flash photolysis traces measured during normal activation (Fig. 43): The pigments E134Q and R135L feature a small proton uptake, corresponding to the release during activation, while WT shows a release, corresponding to the uptake during activation. Similarly, the pigment R135K shows a reduced proton release upon blue light illumination. Therefore we can assume that the more or less disturbed ground states or corresponding Meta-III states of the pigments with similar properties are recreated upon blue light illumination.

A pigment in which Glu^{134} and Arg^{135} are exchanged (E134R/R135E mutation) had been examined before showing that Meta-II was formed spectroscopically but G_t activation was abolished [Franke et al., 1990]. These findings are reproduced in this study (Fig. 43, Fig. 48), and the most striking result is the fact that for this pigment there is a fast proton release instead of a proton uptake at pH > 5.5 (this is consistent with a study by LEWIS et al. that was published parallel to my work [Lewis et al., 2006]). This finding can be interpreted in two ways: 1) There is a salt bridge between Arg^{134} and Glu^{135} which forms upon light activation, assuming Glu^{135} to be protonated in the ground state and getting deprotonated upon light activation explaining the proton release. 2) The other explanation is formation of a Glu-Glu pairing [Flocco and Mowbray, 1995] between Glu^{135} and Glu^{247} upon light activation due to deprotonation of either of the two Glutamate residues. With either of the two explanations the dark state looks similar to WT in terms of TM6 position (see Fig. 45), even at high temperature (see Fig. 47). Upon illumination, TM6 can move, but could be fixed in a slightly different position than WT rhodopsin (see Fig. 46). This position could be unfavorable for the activation of G_t, but the effect onto the ERY as a G_t binding site that is destroyed by swapping of the two residues is probably more important.
The role of the third ERY residue, Tyr^{136}, which has not been examined here, is probably formation of a hydrophobic cluster that helps stabilizing Meta-II [Ishiguro et al., 2004] by protecting the cluster from water and therewith the Glu^{134} cluster from premature protonation. In addition to that, Tyr^{136} is connected to Glu^{225} in TM5, an interaction which stabilizes the position of TM3 and TM5 to each other [Stenkamp et al., 2005].

4.2.2 Effect of mutations in TM6

Glu^{247}: Mutation of Glu^{247} to Glutamine (E247Q mutation) does change neither the absorption nor the FTIR spectra compared to 9-dm-WT (see Fig. 41, first row right, and Fig. 42B, upper magenta line). This can be explained such that the protonation state of Glu^{247} (interpreting the E247Q mutation as anticipation of a protonation, because Glu and Gln are similar in size) does not have a feedback onto the ERY and the Schiff base region.
The situation is different if Glu^{247} is mutated to Alanine (E247A mutation) so that it cannot form a hydrogen bond to Arg^{135}: The pH trend from the absorption spectra (see Fig. 41, second row right) shows both the effect of 9-dm-Meta-II being favored at acidic pH like for 9-dm-WT and the effect of 9-dm-Meta-II being strongly favored at basic pH like for the 9-dm-E134Q and 9-dm-R135L pigments (due to formation of Meta-II-PSB at acidic pH). The superposition of both effects leads to the shown course with an activation maximum around pH 6.0. The FTIR

data (Fig. 42B, lower magenta line) supports this finding by showing a significant fraction of 9-dm-Meta-II under Meta-I conditions compared to 9-dm-WT. This proportion is even higher than the fraction of 9-dm-Meta-II under the same conditions obtained with the 9-dm-R135L and the 9-dm-E134Q pigments. The UV/vis spectra show a bigger 9-dm-Meta-II fraction than these two pigments, too (at pH 6, Fig. 41, second row right). From this it can be concluded that the Glu^{247} residue is important for stabilization of the dark state by formation of the hydrogen bond to Arg^{135} although the effect cannot be seen with the E247Q mutation due to the steric change being only small.

The flash photolysis data show that Meta-II formation and the proton uptake are not affected by either the E247A or the E247Q mutation (see Fig. 44, magenta symbols). This is not surprising, as the proton uptake into the Glu^{134} cluster is not influenced by Glu^{247} which directly interacts with Arg^{135} only. Furthermore the stabilization between TM3 and TM6 is not completely cancelled out by mutation of Glu^{247} to Alanine. This is because the van-der-Waals interactions between Arg^{135} and Val^{250}, Thr^{251} and Val^{254} are still present. The G_t activation is not changed (see Fig. 48) suggesting that Glu^{247} is not involved in G_t binding. This is in contrast to the report of a 20 % G_t activation (relative to WT in the illuminated state) of the E247A pigment and 15 % of the E247Q pigment in the dark state and hyperactivity in the illuminated state (130 % for E247A) [Ramon et al., 2007]. This would suggest a severe perturbation of the structure, but as explained above the finding is contrary to all other studies and could be an artefact of the used assay (measurement through radioactive $GTP\gamma^{35}S$).

Glu^{249}: Mutation of Glu^{249} to either Glutamine or Alanine does not induce any change in both the absorption and the FTIR spectra (see Fig. 41, third and fourth row right, and Fig. 42B, light green line). The same is true for the examination of the E249Q mutant with flash photolysis (Fig. 44, light green squares). Therefore I conclude that this residue is not involved in interaction between TM3 and TM6. This finding is supported by the rhodopsin structure showing Glu^{249} facing away from the ERY-region (see Fig. 85 and [Li et al., 2004]). Is it possible that Glu^{249} therefore stabilizes Meta-IIb with TM6 in the outward state? This suggestion can be shown to be wrong either, as the blue light illumination of the active state is not affected by the mutation (see Fig. 59) and the activity towards G_t is not affected (see Fig. 48).

4.2.3 The ERY motif during activation

The ERY-motif in rhodopsin seems to be one of the important constraints holding rhodopsin in the dark state until it gets illuminated and the constraints are consequently broken. It has been

speculated before that there might be a salt bridge or a hydrogen bond between Arg^{135} and Glu^{247} which connects TM3 and TM6 thereby keeping TM6 in its inward position. In addition to that there are van-der-Waals interactions of Arg^{135} with Val^{250}, Thr^{251} and Val^{254} further stabilizing the TM6 inward position [Li et al., 2004]. This interpretation agrees well with the findings of a similar network of interactions among $Asp^{3.49}$, $Arg^{3.50}$ and $Glu^{6.30}$ (called 'ionic lock') observed in the β_2-adrenergic receptor, maintaining the helices TM3 and TM6 immobilized in the inactive state and being broken upon activation [Ballesteros et al., 2001]. These constraints are broken with a time delay after Meta-II formation (the cause of the delay is discussed in chapter chapter 4.5). This allows the outward motion of TM6 forming the active conformation and consequently enabling protonation of the Glu^{134} cluster.

The rhodopsin structures show a close proximity between Arg^{135} and Glu^{247} in the rhodopsin ground state, but it is not clear if the described interaction between Arg^{135} and Glu^{247} is a hydrogen bond (as proposed by TELLER et al. [Teller et al., 2001]) or a salt bridge (as proposed by ISHIGURO et al. [Ishiguro et al., 2004]). The data presented here argues for the existence of a hydrogen bond, because the mutation experiments (chapter 3.2) did not show any changes with the E247Q mutation. Glutamate could obviously be replaced by Glutamine without any change in function, but a (neutral) Glutamine cannot form a salt bridge with Arginine. The importance of the residue in position 247 is nevertheless underlined by the destabilization of the ground state through the E247A mutation; thus the most likely explanation is a hydrogen bond between Arg^{135} and Glu^{247}. Molecular dynamics simulations further showed that Glu^{247} is also connected to Lys^{141} in TM3 through another hydrogen bond [Fritze et al., 2003], and a further connection between Glu^{134} and Arg^{147}, which has not been examined here, is also proposed [Kong and Karplus, 2007].

The shown interactions are not the only constraints keeping TM6 in the inward position: There is a direct interaction of TM6 with the β-ionone ring of the retinal at side chain Trp^{265} [Li et al., 2004] which seems to be important for stabilization of the dark state as well, but in contrast to the Arg^{135}-Glu^{247} interaction it is broken in Meta-I already [Ruprecht et al., 2004]. Therewith breaking of the described network around the cytoplasmic part of TM6 is the last constraint that keeps TM6 in the dark state until Meta-IIa.

Glu^{134} is negatively charged in the dark state up to Meta-IIb. It is connected to Arg^{135} through a salt bridge [Li et al., 2004; Teller et al., 2001]. During activation the Glu^{134} cluster gets protonated, which marks the transition from Meta-IIb to Meta-IIb·H^+ (for the discussion see chapter 4.1). This effect is facilitated by change of the Glu^{134} residue from a hydrophobic to a hydro-

philic environment due to the motion of TM6. It is suggested to be the only residue in the whole rhodopsin molecule being that close to the lipid-water interface [Periole et al., 2004].

It is even possible that the whole structure of the cytoplasmic part of TM3 is changed upon proton uptake. There are hints from a FTIR and fluorescence study with peptides analogous to TM3, that this part of TM3 gets unstructured upon proton uptake [Madathil et al., 2006]. If this is also true for rhodopsin and not only for the isolated helix, it might explain the role of the proton uptake, as the structural change around the ERY motif would not only expose but also structurally form the G_t binding site.

Independent of the occurrence of this helix unstructuring process, the ERY motif obviously is a G_t binding site, as has been claimed for rhodopsin [Franke et al., 1990; Franke et al., 1992] and other GPCRs [Favre et al., 2005]. Therefore the protonation of the cluster could play a role for the G_t activation process, especially with respect to the sequential G_t activation process [Herrmann et al., 2004] that could involve both the unprotonated Meta-IIb and the protonated Meta-IIb·H^+ form. This suggestion is supported by the report that the protonation of Glu^{134} can be forced by the binding of G_t to Meta-II [Fahmy et al., 2000]. This would imply that the binding of G_t has an influence on the equilibrium between Meta-IIb and Meta-IIb·H^+. Both Meta-II subspecies could be involved in the G_t activation process. This aspect is discussed in detail in chapter 4.3.2.

It remains to be elucidated how the ERY motif is connected to other functionally relevant regions in the rhodopsin molecule and how the signal propagates from the retinal binding pocket, where the initial activation steps happen, to the ERY motif.

4.2.4 The NPxxY(x)$_{5,6}$F and helix 8 region

The NPxxY(x)$_{5,6}$F motif is composed of the amino acids Asn^{302}, Pro^{303} and Tyr^{306} in TM7 and Phe^{313} in H8. It is important for the formation of the kink between TM7 and H8 (see Fig. 86).

Asn^{302} has been shown to be connected to Asp^{83} and Phe^{261} through a water molecule [Okada et al., 2002; Teller et al., 2001]. Nevertheless a mutation of this residue to a neutral Alanine does not change the Meta-I/Meta-II equilibrium [Fritze et al., 2003]. In the Thyrotropin receptor the analogous Asparagine ($Asn^{7.49}$ according to the GPCR helix.residue numbering) has been claimed to act as a molecular switch that interacts with different residues in TM6 and TM2 before and after activation. Mutation of the residue even leads to constitutive activity [Urizar et al., 2005].

Pro^{303} is likely to be involved in structural rearrangements upon Meta-II formation [Fritze et al., 2003]. This is supported by experiments and MD simulations showing the flexing of TM7 at Pro^{303} in order to satisfy the hydrophobic mismatch in the membrane, because the helix would be too long without this flexing [Yeagle et al., 2007]. Thus its role could be similar to Pro^{267} in TM6 which also enables flexibility in the helix and acts as a hinge for TM6 motion in the activation process. A general role for Prolines as such hinges around which flexing of helices commonly occurs was proposed [Bright and Sansom, 2003; Yeagle et al., 2007].

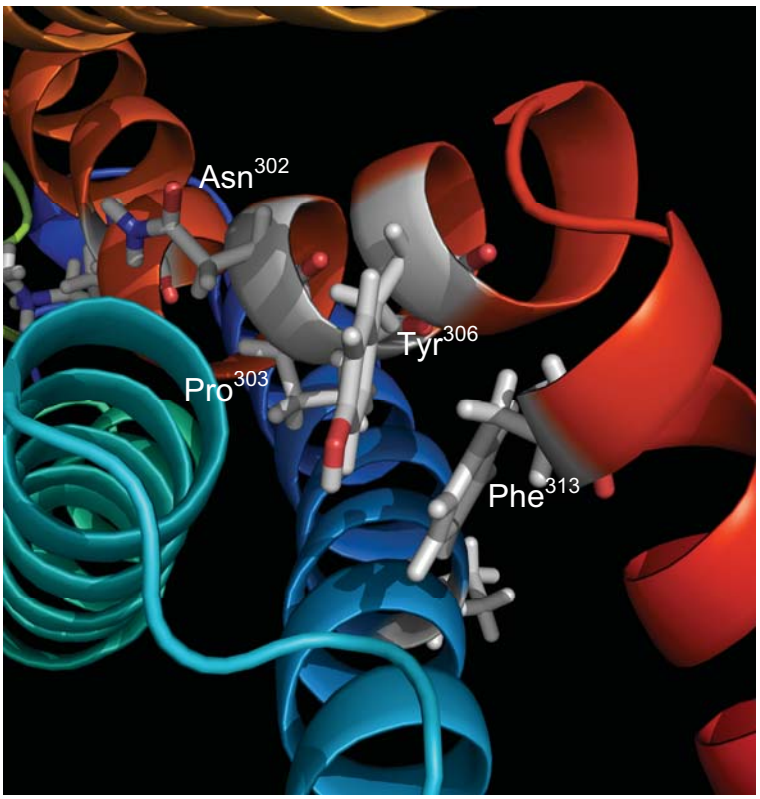

Fig. 86: *The NPxxY(x)$_{5,6}$F motif is located at the cytoplasmic end of TM7 and consists of Asn^{302}, Pro^{303} and Tyr^{306}. Tyr^{306} interacts with Phe^{313} in H8 [Fritze et al., 2003].*

Tyr^{306} *and Phe*^{313} have been shown to interact with each other, which is another constraint keeping rhodopsin in the dark state: If this interaction is broken, the Meta-I/Meta-II equilibrium is shifted towards Meta-II, and if the two residues are locked by a disulfide bond, Meta-II cannot be formed [Fritze et al., 2003]. In the serotonin 5HT2C receptor certain replacements of the Tyrosine residue (Tyr$^{7.53}$ in this case) even have been shown to lead to different grades of constitutive activity [Prioleau et al., 2002]. This suggests that the interaction between Tyr^{306} and Phe^{313} is part of an important switch during rhodopsin activation. Tyr^{306} is further connected to Asn^{73} in TM2 through a hydrogen bond which is suggested to align Tyr^{306} for proper interaction with Phe^{313} [Fritze et al., 2003; Okada et al., 2002].

Thus the NPxxY(x)$_{5,6}$F region is like the D(E)RY region involved in Meta-II formation, and both regions also appear to interplay [Fritze et al., 2003; Kim et al., 1997], which is further discussed below. Like the ERY region the NPxxY(x)$_{5,6}$F region is also likely to be part of a G_t binding site [Fritze et al., 2003].

The changes observed with the NPxxY(x)$_{5,6}$F mutant pigments in this study (see chapter 3.3.1) are generally small. From the data presented it is obvious that the NPxxY(x)$_{5,6}$F region is not directly involved in proton uptake, because the effects observable with flash photolysis are not as dramatic as those of mutations in the D(E)RY region: Unlike those in the D(E)RY region, there are only slight effects on the amplitude of the proton uptake rather than a total prevention or even a proton release (see Fig. 49 and Fig. 50).

The only observable direct effect on the proton uptake is a slight deviation of the pH dependence for the P303A mutant pigment, although not very strong (see Fig. 49, upper right panel). Why does only the P303A pigment show an effect? As noted above, Pro^{303} is the most important residue in TM7 in terms of structure, because the whole shape of the helix changes if this putative hinge point is missing. In contrast, the N302A mutation does not affect the structure of TM7 (nevertheless it probably has an impact on the connected residues, but this is not detected here). The mutations Y306A and F313A probably have an impact on the connection between TM7 and H8, but this is not detected in the proton uptake in the D(E)RY region or Meta-II formation either. It is important to keep in mind that the effects observed on Meta-II formation [Fritze et al., 2003] were only obtained if 9-dm retinal was used to prevent quantitative Meta-II formation so that other equilibria become visible, while 11-*cis* retinal leading to full Meta-II formation in DM was used in this study.

If complete parts of the NPxxY(x)$_{5,6}$F / H8 region are replaced instead of single amino acids (see chapter 3.3.2) the effect is much more severe: The exchange of three amino acids already leads to an acceleration and attenuation of the proton uptake (see Fig. 51, upper right panel), and upon replacement of the whole H8 the proton uptake is totally abolished (see Fig. 51, lower left panel), but can interestingly be restored if the kink region between TM7 and H8 is replaced with the accordant residues, too (see Fig. 51, lower right panel). The result is a hybrid built out of rhodopsin with a H8 from the β_2-adrenergic receptor which functions like normal rhodopsin in terms of Meta-II formation and proton uptake.

The results from blue light illumination of the NPxxY(x)$_{5,6}$F mutant pigments (see Fig. 63) showed an interesting behaviour: While the blue flash experiments looked like mirror images for the D(E)RY mutant pigments in terms of amplitude of Meta-II and proton release (compare Fig. 62), this is not true for the NPxxY(x)$_{5,6}$F mutant pigments: Both the Y306A and the F313A pigments show minimal Meta-II decomposition. This can be interpreted such that the Meta-II state with these pigments features severe perturbations compared to the WT Meta-II state. H8 might be in a different position due to the change in the important 306-313 interaction which prevents

decomposition of Meta-II to Meta-III or the ground state. This is also supported by the finding that both mutants have severely reduced activity towards G_t [Fritze et al., 2003]. The effect of the P303A mutation can also be explained similarly: The changed hinge in this position leads to a different position of H8 – in this case resulting in a reduced proton release upon blue light illumination (see Fig. 63, upper right panel) and in hyperactivity towards G_t [Fritze et al., 2003].
For the mutant pigments with complete parts of H8 being replaced, blue light illumination of the Meta-II state (see Fig. 64) again results in mirror images of the activation experiments in terms of amplitude (compare Fig. 51): Proton release is reduced for the pigment with amino acids 310-312 being replaced – analoguos to proton uptake during activation; proton release is totally cancelled out for the pigment with amino acids 310-321 being replaced; and proton uptake is completely restored if the whole region consisting of amino acids 307-321 is replaced with those from the β_2-adrenergic receptor.
How could the NPxxY$(x)_{5,6}$F motif and H8 be connected to the D(E)RY motif? HUBBELL et al. suggested that the C-terminal tail interacts with residues 324 to 330 of H8 blocking this region from the environment [Hubbell et al., 2003] and possibly from interaction with G_t in the dark state, while the same tail might also have a weak interaction with TM6. Furthermore an interaction between Glu^{249} in TM6 and Met^{309} between the NPxxY$(x)_{5,6}$F motif is suggested [Palczewski, 2006]. Another suggested interaction between both regions is that of the NPxxY$(x)_{5,6}$F with Met^{257} in TM6 [Han et al., 1998]. Either of those interactions could be the explanation for a link between the D(E)RY / TM6 and the NPxxY$(x)_{5,6}$F / H8 regions, as the data have shown.

4.2.5 The NPxxY$(x)_{5,6}$F and helix 8 during activation

As proposed before, the NPxxY$(x)_{5,6}$F motif is likely to be a G_t binding site [Ernst et al., 2000b; Fritze et al., 2003]. Several studies on different GPCRs have shown that mutations in this region lead to lack of G_t activation, although G_t can still bind to the pigments: In the CB1 cannaboid receptor there is a Leucine residue instead of a Phenylalanin in the NPxxY$(x)_{5,6}$F motif (position 7.60). If it is mutated to Phenylalanin, it does not activate the G protein [Anavi-Goffer et al., 2007]. A similar study with the 5-HT2A receptor also showed alteration of the binding preferences, in this case upon replacement of the Asparagine (N376D mutation) [Johnson et al., 2006]. The same effect has been shown for the cholecystokinin B receptor, where the replacement of the Asn^{391} also affected G protein (G_q) activation, but not binding. Thus the NPxxY$(x)_{5,6}$F sequence seems to govern the specificity for G protein binding also in other GPCRs.

What exactly is the origin of the environment change detected with a spinlabel or a fluorescent label attached to Cys^{316}? Again the comparison with other GPCRs can give some hints: A current model claims that H8 moves sideward towards TM6 along the membrane surface during activation. The replacement of the Tyrosine with a Phenylalanine (mutant Y7.53F) in the serotonin 5HT2C receptor has been observed showing a lack of activation, while the additional replacement of the Phenylalanine with a neutral Alanine (double mutant Y7.53F/F7.60A) restores activity, most likely because the motion of H8 is hindered by the interaction of the two Phenylalanines in the single mutant but again enabled by the double mutation [Prioleau et al., 2002]. The putative hinge of this motion is the conserved Proline residue (Pro^{303} in rhodopsin). This H8 motion agrees well with earlier SDSL studies although they were interpreted differently at that time due to lack of knowledge about the existence of H8 [Altenbach et al., 1999]. It is further supported by the finding that the region (amino acids 304 - 311) is exposed to the cytoplasm upon formation of Meta-II [Abdulaev and Ridge, 1998]. The high mobility in this region involving movements of both TM2 relative to H8 and TM7 relative to TM1 is also stressed by EPR distance measurements [Altenbach et al., 2001a; Altenbach et al., 2001b].

Two studies even claim a partial loss in secondary structure of H8 during activation [Krishna et al., 2002; Lehmann et al., 2007], which is supported by a distance increase between residues Asn^{310} and Cys^{316} upon illumination [Altenbach et al., 2001b]. KRISHNA et al. have reported that H8 can easily be dissolved upon environment changes (H8 can only be formed as a helix in presence of PS) and suggested, that H8 acts as a conformational switch that could even assume a helical or a looplike conformation depending on illumination [Krishna et al., 2002]. If this loss in structure upon illumination is a real effect, it would equally well account for the differences detected with EPR experiments and would also well explain the formation of a G_t binding site in this region upon illumination. Such a peripheral helix like H8 could even serve to detect changes in the physical properties of the membrane [Krishna et al., 2002], a capability assigned to 'amphitropic proteins' [Johnson and Cornell, 1999].

As our kinetic EPR data showed, the motion at H8 happens later than the outward motion of TM6. I assume that it is necessary for the proper formation of the G_t binding site at the $NPxxY(x)_{5,6}F$ motif. The potential role of the $NPxxY(x)_{5,6}F$ motif and H8 motion for the sequential fit mechanism of G_t activation is further discussed in 4.3.2.

4.2.6 Other residues and their role during activation

In this study also side chains that play a role during rhodopsin activation apart from the D(E)RY and the NPxxY(x)$_{5,6}$F / H8 regions have been examined. Some of these residues feature an interesting behaviour that can help us to understand the interplay between the different rhodopsin regions involved in activation. An enlargement of the potentially interesting side chains in the loop between TM1 and TM2 and in TM2 is shown in Fig. 87.

His^{65} is located in the cytoplasmic loop between TM1 and TM2. It is oriented towards H8. Replacement of His^{65} with a Cysteine (H65C mutation) had no influence on Meta-II formation, but the proton uptake is reduced by roughly 50 % (Fig. 52, lower left panel), which is also mirrored in the reduced proton release upon blue light illumination of the Meta-II state (Fig. 64, middle left panel). Obviously His^{65} is connected to the D(E)RY region, where the proton uptake has been suggested to take place (see chapter 4.2.3). Direct contact of His^{65} with Cys^{316} was reported, especially if there is a spin label attached to this side chain increasing its size [Kusnetzow et al., 2006]. SDSL experiments in the region (including spin labels in position 65) have revealed a distance increase both between TM2 and H8 and between TM1 and TM7 [Altenbach et al., 2001a; Altenbach et al., 2001b]. Thus His^{65} is in a region that is critical for structural rearrangements. An interaction with a part of the C terminus (Asp^{330} and Asp^{331}) has also been proposed [Li et al., 2004]. It is not even clear if His^{65} has a special role in terms of interaction with other residues, as it is – in contrast to the other residues in the TM1-TM2 loop – not highly conserved [Li et al., 2004]. Thus the measured effect is probably just due to the influence onto the mentioned rearrangements in that region and can distort those in a way similar to the P303A mutation.

Asn^{73}: Mutations of the Residue Asn^{73}, located at the cytoplasmic end of TM2 (see Fig. 87), have not shown any significant effect in the experiments performed here (see Fig. 53, blue symbols) – independent of the mutation to either Alanine (N73A) or Aspartate (N73D). This is in contrast to this residue being conserved in vertebrate visual pigments and its hydrogen bond with Tyr^{306} in the NPxxY(x)$_{5,6}$F motif [Li et al., 2004; Pogozheva et al., 1997]. Asn^{73} is further connected to an internal water molecule (‘Wat-4’) [Okada et al., 2002]. I assume that Asn^{73} does stabilize the NPxxY(x)$_{5,6}$F region, but the lack of an effect onto Meta-II formation and proton uptake can be explained by the small effect that the neutralisation mutation of Tyr^{306} itself had, so that the mutation of a residue which is connected to Tyr^{306} also has a small effect only.

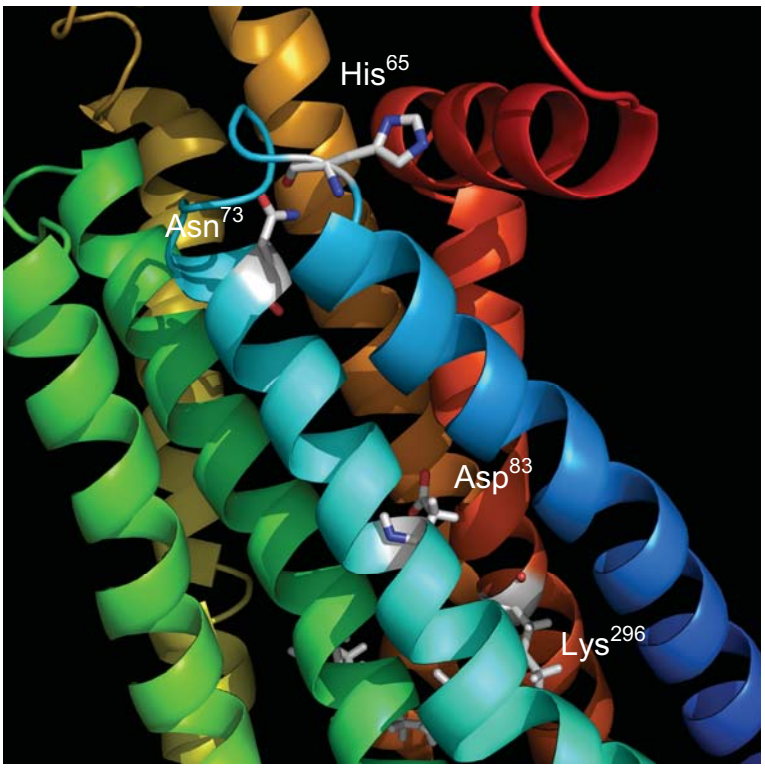

Fig. 87: *The positions of the potentially interesting side chains in and around TM2.*

Asp^{83}: Another key residue which is also highly conserved (even in red and green cone opsins [Nathans, 1990]) is Asp^{83}, which is located in the middle of TM2 (see Fig. 87) and has been shown to be connected to Asn^{302} in the NPxxY(x)$_{5,6}$F motif via a water molecule ('Wat-1b') [Lehmann et al., 2007; Okada et al., 2002; Teller et al., 2001] and directly to Asn^{55} in TM1 [Li et al., 2004], stabilizing the packing of TM1, TM2 and TM7 in the dark state (the Asn^{55}-Asp^{83}-pair is sometimes referred to as the 'N-D-pair'). This role is stressed by investigations on the Thethyrotropin-releasing hormone receptor which showed total deactivation if the homologous Asp residue was mutated to a non hydrogen-binding one [Perlman et al., 1997]. Asp^{83} is also connected to the Schiff base – probably through Gly^{120} and a water molecule as mediators [Nagata et al., 1998]. The existence of this connection is stressed by observations that the interaction of the hydrogen bonding network around Asp^{83} is modulated by Glu^{181} [Ludeke et al., 2005]. FTIR studies on Asp^{83} have shown that it is protonated both in the dark and in the active state [Fahmy et al., 1993].

However, mutation of Asp^{83} to Asparagine (D83N mutation) and examination of this pigment with flash photolysis has not shown any effect (see Fig. 53, magenta squares). Thus I can – similarly to Asn^{73} – conclude, that the effect of mutations of Asp^{83} is not observable through Meta-II formation or proton uptake in the D(E)RY region. This is not surprising, as mutation of the residue Asn^{302}, which it is connected to, did not show any effect either (see chapter 4.2.4). Nevertheless the described network is important for stabilization of the NPxxY(x)$_{5,6}$F region keeping it in the closed state and has recently been proposed to be an important threshold against background noise in rhodopsin [Kong and Karplus, 2007].

His^{211}: The residue His^{211} is located in the middle of TM5 (see Fig. 88). It has been shown to be important for the formation of Meta-II (there is no Meta-II formation upon mutation to Phenylalanine or Cysteine) [Weitz and Nathans, 1992]. His^{211} and Glu^{122} together play the role of mediators in the interaction between TM3 and TM5 [Beck et al., 1998; Patel et al., 2004]. They are connected through a hydrogen bond [Lewis et al., 2006], which has the structure of a triangle between His^{211}, Glu^{122} and Trp^{126} [Li et al., 2004; Schlegel et al., 2005]. The region has also been identified as a binding region for Zn^{2+} ions [Stojanovic et al., 2004], but it is not clear if this is of physiological importance. Glu^{122} has been shown to be important for the opsin-shift [Sakmar et al., 1989] and to interact with the β-ionone ring of the retinal [Vogel et al., 2005]. An interaction between Glu^{122} and the above examined Asp^{83} has been proposed but challenged by another study [Lehmann et al., 2007].

Mutation of His^{211} to a neutral Phenylalanine (H211F mutation) resulted in an extreme deceleration of both Meta-II formation and proton uptake (see Fig. 52, upper right panel) but leaves the amplitudes unaffected. Similar results of slow Meta-II formation have been obtained in a study that was published recently and were attributed to a long lived Lumi intermediate for the mutant (however, the authors claim a proton release upon illumination, which I cannot reproduce) [Lewis et al., 2006].

A different but also interesting behaviour is observable in the respective traces during blue light illumination of the Meta-II state (see Fig. 64, upper right panel): Meta-II degradation happens much faster than observed with WT, indicating that the Meta-II state is less efficiently stabilized. In contrast, the proton release is slowed down and shows an initial lag phase before it starts. Obviously His^{211} is involved in kinetic tuning of the activation process. This is not surprising looking at the above described interactions of the residue with the retinal.

How is His^{211} connected to the D(E)RY region? A recent study claims Glu^{134} to be connected with Glu^{122} and His^{211}, probably through the conserved residue His^{152} [Lewis et al., 2006]. This would explain the contact to the D(E)RY region and therefore the influence of His^{211} onto proton uptake, while the interactions mentioned above (the triangle with Glu^{122}, Trp^{126} and the proximity to the retinal β-ionone ring) explain the impact the mutation has on the kinetics of Meta-II formation. The whole network taken together is the proposed propagation pathway of the activation signal from the retinal region to the D(E)RY motif [Lewis et al., 2006], which the H211F mutation affects.

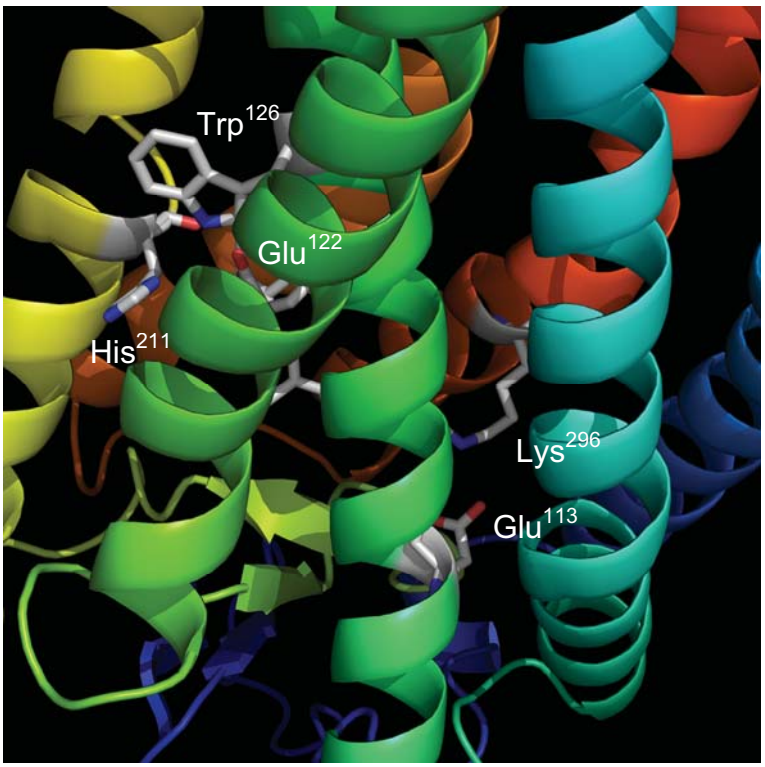

Fig. 88: *The positions of the potentially interesting side chains in the retinal region.*

Glu^{113} is located in the extracellular region of TM3 (see Fig. 88) and is part of the complex counterion that stabilizes the protonated form of the Schiff base formed by Lys^{296} in the rhodopsin dark state [Ludeke et al., 2005; Martinez-Mayorga et al., 2006]. The residue is in close proximity to an internal water molecule ('Wat-2b') which connects it to the retinal, to Cys^{187} and to Phe^{91} [Okada et al., 2002]. If the Glutamate is mutated to a neutral Glutamine (E113Q), the protein can adopt an unprotonated Schiff base in the ground state already with a pK around 6 [Sakmar et al., 1991]. In pure opsin without retinal this mutant is constitutively active [Robinson et al., 1992]. Only if combined with other mutations it can also constitutively activate rhodopsin [Kim et al., 2004]. I tested the same mutant pigment with flash photolysis here. The Schiff base was obviously already non-protonated (due to the DM environment shifting the pK), because no further formation of 380 nm absorbing species was observed upon illumination with green light. Therefore the pigment was illuminated with blue light (see Fig. 52, lower right panel), and upon illumination proton uptake with similar kinetics like WT was observed, while the 380 nm absorption indicative of non-protonated Schiff base returned to the initial value.

My understanding of these findings is that the E113Q mutation indeed anticipates the active state around Glu^{113} but not in the regions at the extracellular surface. Thus the proton uptake in the D(E)RY region has not occurred in spite of the mutation as long as the pigment is not illuminated. Consequently, the changes in the protonation state of residues in the SB region are necessary, but not sufficient for activation of the protein, but other processes have to occur in the retinal region. These processes can probably only be caused by isomerization of the retinal (the interactions between the retinal and TM6 are discussed above).

4.3 G_t binding to rhodopsin

The mechanisms of G_t binding to rhodopsin and subsequent G_t activation are still under discussion. While there is some evidence for G_t binding to rhodopsin dimers or even higher oligomers [Fotiadis et al., 2006; Fotiadis et al., 2003; Jastrzebska et al., 2006], it has been shown that the G_t subunits $G_t\beta\gamma$ and $G_t\alpha$ interact with activated rhodopsin in a sequential manner [Herrmann et al., 2004]. Actually, a recent study revealed that monomeric rhodopsin in solution can activate G_t at a high rate [Ernst et al., 2007].

In this chapter I want to shine some more light onto the interaction of the G_t subunits with activated rhodopsin.

4.3.1 Proton uptake and peptides

Peptides have been shown to mimic different parts of G_t [Hamm et al., 1988]. In this study well-established peptides mimicking the $G_t\alpha$ and $G_t\gamma$ C-termini have been employed (see chapter 3.6). These peptides obviously bind to Meta-IIb / Meta-IIb·H^+, both states with TM6 in the outward position or at least one of these. This can be deduced from the SDSL experiments with peptides (Fig. 75, left row) showing that TM6 stays in the outward position upon peptide binding. As peptides have been shown to stabilize the Meta-II state, the so-called Extra Meta-II [Emeis et al., 1982; Kohl and Hofmann, 1987; Schleicher et al., 1989], we can assume that they do not only bind to but also stabilize the outward position of TM6. This is further supported by an FTIR study that found the characteristic bands for fully formed Meta-II upon binding of either $G_t\alpha$(340-350) or $G_t\gamma$(60-71) to Meta-I [Bartl et al., 2000], but not upon addition of the nonbinding peptides ($G_t\alpha$(340-350) L349A or $G_t\gamma$(60-71) without farnesyl). Also in agreement with this is the finding that binding of G_t holoprotein stabilizes the Meta-IIb·H^+ state, because both Meta-II degradation and proton release upon blue light illumination of the active state were blocked if G_t was present (see Fig. 77B and C). In addition to that, the position of H8 is not influenced by binding of $G_t\alpha$(340-350) HAA or $G_t\gamma$(60-71) either (Fig. 75, right row).

Binding of sufficiently high concentrations of the peptides tested here leads to the release of up to 0.5 protons per activated rhodopsin molecule (Fig. 70) in contrast to a proton being taken up into rhodopsin in absence of peptides, as discussed above (chapters 4.1 and 4.2). Obviously this proton uptake is reversed by the presence of peptides. Only those peptides known to be unable to bind to rhodopsin [Bartl et al., 2000] do not lead to this proton release (Fig. 70, grey symbols).

The proton release effect is best seen with the high affinity $G_t\alpha$ analogs (Fig. 67), which bind slowly enough to allow accumulation of the protonated state so that a transient protonation is seen. While the rising proton uptake phase retains the same kinetics for all peptide concentrations, the falling phase gets faster if more peptide is present. This is in agreement with a bimolecular reaction between the active receptor and the peptide. We can conclude that proton uptake and release occur on the constant background of TM6 in the active outward position. Of course, these data only reflect *net* proton uptake and release. Thus we cannot decide whether the released proton comes from the site to which it was taken up before or whether the released proton originates from a different site, although the former possibility seems more likely. In addition to that there are two proton release sites needed to fully explain the data, because at high concentrations of all binding $G_t\alpha$(340-350) analogs the net effect is a release of roughly half a proton per activated rhodopsin molecule (Fig. 70), which can even add up to one proton per activated rhodopsin in case of the E134Q mutation (Fig. 73).

The analysis of the protonation amplitude upon G_t binding (see chapter 3.6.6) revealed two processes for high affinity $G_t\alpha$(340-350) K341L peptide which show a difference in K_d of roughly a factor 10 (K_ds are given in Table 8). The amplitude of the first process ($K_{d,1}$ = 1.81 µM) is 1 H^+/R*, while the amplitude of the second process ($K_{d,2}$ = 160 µM) is 0.5 H^+/R*. Therefore the two processes correspond to the re-release of one proton and release of 0.5 additional protons. It is likely that the same holds true for the $G_t\alpha$(340-350) peptide, but in this case only one K_d was obtained in the analysis, because the two K_ds are on the same order of magnitude (K_d = 270 µM) if we assume a $K_{d,2}$ similar to the one for $G_t\alpha$(340-350) HAA. Thus they could not be distinguished. The two clearly different K_ds observed for $G_t\alpha$(340-350) K341L with the respective amplitudes argue for two different processes being responsible for the re-release of 1 H^+/R* and the release of the additional 0.5 H^+/R*.

The farnesylated peptide from the C-terminus of the $G_t\gamma$-subunit was similarly effective in proton release as native $G_t\alpha$-derived peptide (see Fig. 70). The K_d obtained for the $G_t\gamma$(60-71) peptide (K_d = 123,3 µM) is on the same order of magnitude as the K_d for $G_t\alpha$(340-350) peptide and $K_{d,2}$ for the $G_t\alpha$(340-350) K341L peptide. This corresponds to similar shapes in the plots (Fig. 70 and Fig. 71) and indicates that the proton re-release reaction (with the amplitude 1 H^+/R*) is similar for both peptides. Remarkably, high $G_t\gamma$(60-71) concentration brought the protonation level back to the baseline and not to a negative level of ca. 0.5 H^+ per activated rhodopsin molecule, as seen with the G_t-α derived peptides. Such fractional net proton uptake has been discussed before and explained by a pH dependent reaction enthalpy [Parkes and Liebman, 1984]. Obviously the bind-

ing of peptides $G_t\alpha$(340-350) and $G_t\gamma$(60-71), although there are a lot of similarities, has indeed a different impact onto the receptor.

The proton release effect does not depend on the chemical nature of the peptide. All three high affinity $G_t\alpha$ analog peptides, namely $G_t\alpha$(340-350) HAA, $G_t\alpha$(340-350) HAA K345A, $G_t\alpha$(340-350) K341L (see Fig. 70) and – less pronounced – Ac-$G_t\alpha$(340-350) and $G_t\alpha$(340-350) C347S (see Fig. 72) display a similarly enhanced effect, shifting the competition curve by more than one order of magnitude to the left compared to native $G_t\alpha$(340-350) peptide. This is seen irrespective of their sequence, e.g. whether it contains a Lysine or Glutamate (as potential proton release group) or not (for the exact sequences of all peptides see Table 4).

To test the other amino acids in the peptide as potential proton release groups, peptides with single amino acid substitutions have been observed (see Fig. 72). If either Aspartate (D346M replacement) or Cysteine (C347Abu replacement) were removed from the protein, the affinity was also increased – for the Cysteine replacement on the high affinity analog (HAA) peptide even above the normal HAA level. The affinity was also increased for the Ac-$G_t\alpha$(340-350) peptide with the N-terminus altered by acetylation (this is in agreement with a recent study [Herrmann et al., 2006b]). Taken together, all the peptides analogous to $G_t\alpha$(340-350) show a net proton release at high concentrations.

If Glu^{342} in the peptide was replaced ($G_t\alpha$(340-350) E342N), the affinity is unchanged, but the proton release is smaller than normal (roughly 0.25 H^+/R*, see Fig. 72). This effect is small but reproducible and could be a hint to an interaction of the Glutamate in the peptide with a group in the receptor that is involved in the proton release reaction (possibly in the ERY motif).

Therefore we can conclude that the proton release does not originate from the peptide itself but from the receptor. Obviously the peptide sequence does influence the proton uptake and release reactions, but the proton release does not happen in the peptide and is consequently caused by the receptor.

Interestingly, a net proton release of roughly 0.5 protons per activated rhodopsin molecule is not only observed for the shown peptides but also for the E134R/R135E 'charge reversal' mutant pigment and as well for other pigments, but here only at basic pH (see Fig. 44). Most interestingly, the proton release can even increase to one proton per activated rhodopsin molecule, if the E134Q pigment, which shows zero proton uptake or release without any peptide (pH 6), is illuminated in presence of peptides (Fig. 73). In this case the fractional character of the proton release seems to have vanished. We can only speculate how this proton release is caused, and it is not clear whether the proton release caused by the presence of peptides and that caused by muta-

tions in the ERY motif and / or basic pH are identical. One possible candidate for proton release would be Glu^{247}. However, there is also a proton release observed at basic pH if Glu^{247} is mutated to either Glutamine or even Alanine (Fig. 44), which cannot release protons. Another possible candidate is Arg^{135} (which is in the 134 position in case of the 'charge reversal' pigment). This is supported by the finding that both the R135K and R135L mutant pigments which do not feature Arg^{135} do not show any proton release in the plots even at basic pH (Fig. 44). So far Arginine residues have not been regarded as candidates for proton exchange reactions due to the high pK_a of the guanidine group (around 13) which would normally lead to the assumption that the residue can only occur in its protonated form. However, recent investigations show that Arginine residues can effectively take part in proton transfer reactions, especially in proximity of a carboxylate (which would be Glu^{134} here) and if they are solvent accessible (which is true for Meta-IIb and Meta-IIb·H^+) [Guillen Schlippe and Hedstrom, 2005]. Arg^{94} in proteorhodopsin has analogously been proposed as a proton donor [Braiman, 2007].

4.3.2 Sequential G_t activation mechanism

The above shown proton uptake experiments with peptides allow some insights into the activation of G_t. Experiments on G_t activation in membranes have shown that G_t activation is pH dependent and might therefore be connected to proton uptake and release reactions in the receptor [Kisselev et al., 1999]. This could be explained through the two Meta-II substates with outward tilted TM6, Meta-IIb and Meta-IIb·H^+, representing the catalytically active conformations which are employed by G_t for sequential interaction of its key binding sites to enable GDP → GTP exchange [Herrmann et al., 2004; Herrmann et al., 2006b]. This idea is supported by findings from FTIR studies that Aspartate or Glutamate (possibly Glu^{134}) protonation is involved in $G_t\alpha$ binding [Fahmy, 1998] and as well in G_t holoprotein binding [Fahmy et al., 2000].

From peptide studies with FTIR it could be excluded that either $G_t\alpha$(340-350) or $G_t\gamma$(60-71) binds to rhodopsin intermediates prior to Meta-IIb [Bartl et al., 2000] – consistent with the finding that TM6 stays in the outward state upon binding of either peptide (Fig. 75) (but contrary to MD simulations that suggest docking of G_t to the rhodopsin to occur in the dark state already [Fanelli and Dell'Orco, 2005] and that $G_t\alpha$(340-350) binds also to inactive rhodopsin [Dratz et al., 1993]). Thus the rhodopsin states we have to take into account for G_t binding and activation are Meta-IIb, Meta-IIb·H^+ and their possible further substates, if they exist. Interestingly, an FTIR study found specific bands in the amide I and amide II regions upon binding of $G_t\alpha$ and $G_t\gamma$ C-terminal peptides, which also slightly differ in shape between binding of $G_t\alpha$(340-350)

and $G_t\gamma$(60-71) peptide [Bartl et al., 2000]. These bands are characteristic for changes in secondary structure, which could occur either in the peptides themselves or possibly in the receptor. Accordingly, this could be a hint that there are some structural differences between the rhodopsin states that bind $G_t\alpha$(340-350) and $G_t\gamma$(60-71), respectively. A more recent study also claims that changes are induced at both the peptide and the receptor itself upon peptide binding to the receptor [Vogel et al., 2007]. This is supported by a study that presents a G_t activation mechanism involving an induced fit [Yeagle and Albert, 2003]. It is proposed that upon binding of $G_t\beta\gamma$ a conformational change in the G_t holoprotein occurs which then exposes the $G_t\alpha$ C-terminus [Herrmann et al., 2004; Nanoff et al., 2005].

Both peptides, $G_t\alpha$(340-350) and $G_t\gamma$(60-71), seem to interact with the D(E)RY motif or at least to influence it by binding in its vicinity, as the proton uptake experiments with both peptides showed (see chapter 4.3.1). For the $G_t\gamma$(60-71) peptide this interaction could be an at least mainly hydrophobic interaction of the farnesyl group with rhodopsin, because the effect on the proton uptake (as well as binding in general [Bartl et al., 2000; Herrmann et al., 2006b]) is not observable if the peptide lacks the farnesyl group (see Fig. 70, grey triangles). It is important to note that this necessity of the farnesyl group has been observed in detergent and might not be true in membranes. This indicates that the farnesyl group is necessary for interaction with rhodopsin and not mainly with the membrane, although this might be an additional effect. Obviously the other interactions between G_t and the receptor are not sufficient for binding. Interestingly, for the G_t holoprotein in membranes the farnesyl group can be functionally replaced by the myristoyl group [Herrmann et al., 2004] having the same hydrophobic effect.

How could the interaction of G_t with the D(E)RY motif of the receptor and its surroundings work? The opening of a hydrophobic cleft upon outward motion of TM6 was deduced from fluorescence experiments, although the binding into this cleft was only examined for the $G_t\alpha$ C-terminus [Janz and Farrens, 2004]. For the $G_t\alpha$ C-terminus the interaction partners have been proposed: Lys^{345} and Asp^{346} of $G_t\alpha$ might interact with Glu^{134} and Arg^{135} of the receptor [Slusarz and Ciarkowski, 2004; Yeagle and Albert, 2003], and additionally the peptide also interacts with H8 [Ernst et al., 2000b; Marin et al., 2000], possibly Lys^{345} of $G_t\alpha$ with Phe^{313} of Meta-II [Ciarkowski et al., 2005] or Cys^{347} of $G_t\alpha$ with Tyr^{306}, Asn^{310} and Phe^{313} of Meta-II [Slusarz and Ciarkowski, 2004] (interestingly, the same authors propose contradictory interactions, which nourishes the impression that these modelling studies are only suggestions). The necessity of the Glu^{134}-Arg^{135} pair for G_t activation has been shown [Franke et al., 1990; Franke et al., 1992]. Furthermore binding of the $G_t\alpha$ C-terminus has been observed in the cleft created by the outward

moved TM6 (residues Cys^{140}, Lys^{141} and Phe^{228} have been shown to be in proximity using a fluorescence technique) [Janz and Farrens, 2004]. Other receptor sites important for G_t activation (but not further assigned to $G_t\alpha$ or $G_t\gamma$) are Lys^{248} [Franke et al., 1988] and compatibly regions 244-249 [Franke et al., 1992] and 237-249 [Ernst et al., 1995] in the highly flexible TM5-TM6 loop. This variety of interactions might explain the fact that almost any amino acid in $G_t\alpha$(340-350) – except for Leu^{349} – can be replaced without losing its ability to bind to the activated receptor, as there are still enough remaining interactions.

The different effects of both peptides onto the proton uptake – namely proton release at high concentrations for $G_t\alpha$(340-350) and zero proton uptake at the same concentrations with $G_t\gamma$(60-71) – could be assigned to these different binding modes of interactions dominated by hydrophobicity and by charge, respectively. In addition to that, the peptides, although they have a lot of common interaction sites, probably do not interact with exactly the same receptor sites, as their sequence has hardly any similarities (see Table 4).

Taking these evidences together, a sequential activation mechanism as proposed recently [Herrmann et al., 2004] could possibly involve the following steps: The initial affinity between rhodopsin and G_t is probably caused by a hydrophobic interaction with low specificity originating from the myristoyl group at $G_t\alpha$ and the farnesyl group in $G_t\gamma$ (both groups have been shown to be able to replace each other) [Herrmann et al., 2004; Herrmann et al., 2006a]. Thus $G_t\gamma$ of the G_t holoprotein binds to the receptor which is most likely in the Meta-IIb·H^+ state at least at acidic pH (without peptide being present the receptor undergoes full proton uptake at acidic pH, as discussed in 4.1). This leads to a rearrangement in G_t and possibly in the receptor as well. Besides, the interaction of $G_t\gamma$ with the D(E)RY motif leads to deprotonation of the Glu^{134} cluster. As a consequence of the rearrangement in the G_t subunits, the previously buried C-terminus of $G_t\alpha$ becomes exposed, while the γ subunit leaves the binding site to which it was (probably only weakly) bound before. This step might also be facilitated by a change of the receptor structure. Hence $G_t\alpha$ can bind to the receptor which could have switched its conformation in parallel. This second interaction then leads to GDP $\rightarrow$ GTP exchange, in which helix α5 in $G_t\alpha$ [Marin et al., 2002; Oldham et al., 2006] and the so called 'switch II' region [Mazzoni and Hamm, 1993; Mazzoni et al., 1991] are involved, and therewith leads to activation of G_t.

This activation scheme still leaves two questions open:

1. Does only G_t undergo structural changes during this sequential fit mechanism or does the receptor (which is likely) do the same? The latter possibility is supported by a further peptide binding study claiming that $G_t\alpha$(340-350) and $G_t\gamma$(60-71) bind to different receptor con-

formations, although the iso-spectral Meta-II subspecies could not be further characterized [Downs et al., 2006]. Another hint are the structural changes found between the FTIR spectra with both peptides bound to Meta-II [Bartl et al., 2000; Vogel et al., 2007]. If this change in the receptor does occur:

2. Which are the rhodopsin substates required for G_t activation? As pointed out above, they both feature TM6 in the outward state. Do the substates correspond to Meta-IIb and Meta-IIb·H^+, differing in their protonation state and maybe additional features? Based on the findings that the changes in the NPxxY$(x)_{5,6}$F region can – if they are severe – affect the proton uptake in the D(E)RY region (for a detailed discussion see chapters 4.2.4 and 4.2.5) a concerted switch in the D(E)RY and the NPxxY$(x)_{5,6}$F / H8 regions is possible and might be involved in the sequential G_t activation mechanism.

   The possibilities for the sequential fit mechanism between G_t and the receptor are outlined in Table 9. The possibility proposed by KISSELEV et al. [Kisselev et al., 1999], namely sequential binding to Meta-IIa and Meta-IIb (now named Meta-IIb·H^+) seems unlikely (as already stated in their paper) regarding the results in the work at hand, because both the $G_t\gamma$(60-71) and the $G_t\alpha$(340-350) peptides bind to receptor states featuring the outward tilted TM6 (Fig. 75) and Meta-IIa features TM6 in the inward position (chapter 4.1).

	Proposed by:	Interaction site 1	Interaction site 2
G_t	KISSELEV et al. [Kisselev et al., 1999]	$G_t\alpha$ / $G_t\beta\gamma$ (order not clear)	
	HERMANN et al. [Herrmann et al., 2004]	$G_t\beta\gamma$	$G_t\alpha$ C-terminus
Receptor	KISSELEV et al. [Kisselev et al., 1999]	Meta-IIa	Meta-IIb
	KNIERIM et al. (this work), possibility 1	Meta-IIb	Meta-IIb·H^+
	KNIERIM et al. (this work), possibility 2	Meta-IIb/·H^+ with H8 in position a	Meta-IIb/·H^+ with H8 in position b

Table 9: *Possible mechanisms of the sequential fit between G_t and activated receptor.*

The activation in membranes is approximately 10 fold faster than activation in detergent. This finding might be sufficiently explained by less degrees of freedom of G_t in the membrane compared to detergent solution [Ernst et al., 2007] due to its hydrophobic groups at $G_t\alpha$ and $G_t\gamma$ (see above) that anchor G_t in the membrane. However, we cannot exclude a different activation mechanism in detergent and in membranes, although this is not likely. The sequential activation

mechanism might be further complicated by different substates of the binding sites in G_t as proposed recently [Herrmann et al., 2006b], but this is not further discussed here.
Another issue which is hard to solve is the uptake of a second proton [Schleicher and Hofmann, 1985] and even a third, slower proton upon binding of G_t holoprotein to the activated receptor (see Fig. 76), which is in contrast to the proton re-release upon peptide binding. Obviously there are further proton exchange reactions that occur during or as a consequence of activation, which might be assigned to processes in G_t and to the activity of the GTPase (representing the slow process on a s timescale, see Fig. 76).

4.4 Role of the lipid environment for rhodopsin activation

The lipid environment is important for rhodopsin and its activation mechanism. This is obvious from the comparison of the behaviour of rhodopsin in DM and in membranes showing severe differences (for example obvious in the comparison of the Arrhenius plots of the activation steps in Fig. 35 and Fig. 39). Apart from the general influence of the ROS membrane which has a special lipid composition [Borggreven et al., 1970; Grossfield et al., 2006b], specific interactions between rhodopsin and lipids have been proposed [Fahmy et al., 2000; Madathil et al., 2006]. Besides, the rhodopsin crystal structures also contain lipids interacting with the rhodopsin molecules in different positions [Li et al., 2004; Palczewski et al., 2000].

4.4.1 Unspecific influence of the lipid environment

The presence of the membrane puts rhodopsin into a more constrained environment compared to detergent. This accounts for the observed effects such as general slowing down of the activation kinetics (chapter 3.1.6) and the impossibility to recreate significant amounts of ground state from the Meta-II state (chapter 3.5.2). It is suggested, that the slowing down of the kinetics is comparable to the effect of the mutation H211F (see 4.2.6) and similar mutations which can be understood to put similar constraints onto the protein [Lewis et al., 2006].
The Arrhenius plots of rhodopsin activation in DM and in membranes are shown in Fig. 35 and Fig. 39, respectively. The effect of the membrane environment is a deceleration of all processes and disappearance of the kinetic differences between formation of Meta-IIa and Meta-IIb. While the activation energy of Meta-IIa formation – independent of the slowing down – stays the same (compare the slopes in Fig. 35 and Fig. 39, represented in the E_As in Table 5), the activation energy of the proton uptake (which is connected to TM6 motion as pointed out in 4.1.2) is raised to

roughly the same level as Meta-IIa formation in membranes (see Table 5). Thus in membranes the formation of Meta-IIa seems to be the main rate limiting step for formation of the active receptor conformation, while TM6 motion is the rate limiting step in DM. Although the activation steps can hardly be distinguished kinetically in membranes, the DM experiments substantiate the model that Meta-II formation, TM6 motion and consequent proton uptake are actually different steps, and they still are distinguishable in membranes as well (see Fig. 39).

Looking at the effect of the lipid environment on illumination of the fully bleached Meta-II state with blue light (see chapter 3.5.4), an opposite effect becomes obvious: While the proton rerelease is equally slow in both DM and membrane environment, the degradation of Meta-II (represented by the decreasing 380 nm absorption) is also slow in the DM environment (only roughly a factor 3 faster than proton release at 20 °C), but fast in membranes (see Fig. 60 and Fig. 61). Thus the kinetic difference between both processes is small in DM and big in membranes during blue light induced formation of Meta-III and ground state (only in DM), while it is big in DM and small in membranes for Meta-II formation. This is also connected to the amplitude of TM6 motion in membranes being smaller than in DM environment [Kusnetzow et al., 2006], which enables more flexibility of TM6.

Interestingly, the velocity and activation energy of H8 motion, which has been shown to happen in a later step (discussed in 4.1.3), stays similar between DM and the membrane (Fig. 35 and Fig. 39, E_As in Table 5). This is a surprising result, as H8 is amphiphatic and exactly at the membrane surface, and its C-terminal end is anchored in the membrane through two palmitoylated Cysteine residues (Cys^{322} and Cys^{323}). The kinetics of this motion are consequently not governed by the environment but mainly by the internal restrictions such as Pro^{303} and the kink stabilizing interaction between Tyr^{306} and Phe^{313} (the motion is discussed in 4.2.5).

How do lipids influence the rhodopsin activation mechanism? Several studies have shown how the lipid environment can effectively influence the activation of rhodopsin by changing the mechanical properties of the membrane. BOTELHO et al. argue, that the activation of rhodopsin is influenced by lipids which stabilize different lipid phases [Botelho et al., 2002; Botelho et al., 2006], whereas both Phosphatidylserine (PS) and Phosphatidylethanolamine (PE) together with polyunsaturated fatty acids are needed for full Meta-II formation [Niu and Mitchell, 2005; Wang et al., 2002]. Through the hydrophobic matching of lipids with the nonpolar interface of rhodopsin, receptor and membrane influence each other [Huber et al., 2004]. A chain length of 20 C atoms was found as optimal environment for rhodopsin stabilization, and rhodopsin is believed to form oligomers due to hydrophobic forces in the membrane [Botelho et al., 2006]. Also, the

unsaturation of lipids and cholesterol have effects on the stability of rhodopsin [Grossfield et al., 2006a; Grossfield et al., 2006b].

These studies on lipid environments and the enormous impact that different environments can have on rhodopsin shed a light on the effect that total absence of lipids in the detergent environment has. The impact of DM environment compared to vesicles onto different regions has been investigated with SDSL, and severe differences were found as well [Kusnetzow et al., 2006]. Thus it seems surprising that rhodopsin still behaves so similar in detergent and membranes in terms of activation. This importance of the environment also explains why nobody succeeded in forming artificial vesicles so far which show the same properties as native membranes (e.g. compare the activation energies in Table 5), because it appears impossible to artificially create a similar lipid composition. Besides, it seems all the more more surprising that it is possible to get the fully active Meta-IIb state in a 2D crystal (as shown in chapter 3.1.7), which puts rhodopsin into an even stronger restricted environment.

4.4.2 Specific rhodopsin-lipid interactions

In addition to these unspecific effects of the membrane environment discussed above, I propose here a specific interaction between rhodopsin and the membrane lipid Phosphatidylserine (although the experiments were performed with POPS I only abbreviate PS due to the fact that the phosphatidylserine headgroup is supposed to be the important determinant widely independent of the fatty acids).

Apart from the work at hand some hints point to an interaction between PS and rhodopsin: A recent study suggests a specific interaction between PS and rhodopsin without naming certain sites [Soubias et al., 2006b]. Several studies showed an increase of Meta-II formation in the presence of PS [Gibson and Brown, 1993; Wang et al., 2002; Wiedmann et al., 1988]. An influence of lipid headgroups on G_t activation was also found [Alves et al., 2005; Wang et al., 2002]. In addition to that, PS (in contrast to other lipids) becomes more extractable from bleached ROS compared to dark adapted ROS, which is another hint to a specific rhodopsin-PS interaction in dark adapted rhodopsin [Hessel et al., 2003]. Interestingly, some GPCRs such as the cannaboid receptor can bind lipid substances as effectors (2-arachidonylglycerol and arachidonoylethanolamide in case of the cannaboid receptor) [Devane et al., 1992; Sugiura et al., 1995], proving the general possibility of such lipid-protein interacting sites in GPCRs.

An interaction between the lipid headgroup and the D(E)RY motif was implied before: FAHMY et al. proposed that a specific interaction of Glu^{134} with lipid headgroups might be important for

G_t binding and activation [Fahmy et al., 2000]. Furthermore, the lack of a lipid was detected for the E134Q replacement in an FTIR study on a peptide analogous to TM3 (the use of different lipid compositions for the experiments did not change the effect, but these lipid compositions all contained PS). It is suggested that the C-terminus of TM3 is moved towards the lipid headgroups in the membrane during activation and that the D(E)RY motif acts as a conserved proton-dependent hydrophobicity switch with a pK between 5.5 and 6.0 [Madathil et al., 2006].

I propose here a specific interaction between the D(E)RY motif and the Serine headgroup of PS, such that the amino group of Serine interacts with the carboxyl group of Glu^{134} and the (deprotonated) carboxyl group of Serine interacts with the guanidine group of Arg^{135}. This double salt bridge would then replace the direct salt bridge between Glu^{134} and Arg^{135} [Li et al., 2004]. A proposition how the interaction could look like is drawn in Fig. 89, although this is only a sketch and not a molecular dynamics simulation.

This idea of an interaction between PS and the D(E)RY motif is supported by the finding that the proton uptake (which was assigned to Glu^{134} or the cluster it is included in) was totally abolished if POPS was cross-linked to rhodopsin through EDC (see Fig. 80). I interpret this experiment such that the described ionic interactions of Glu^{134} and Arg^{135} with PS are converted to covalent bonds upon cross-linking (see the reaction in Fig. 31), resulting in the impossibility to take up protons to Glu^{134}. This effect was exclusive to PS only, indicating a specific interaction with the Serine headgroup.

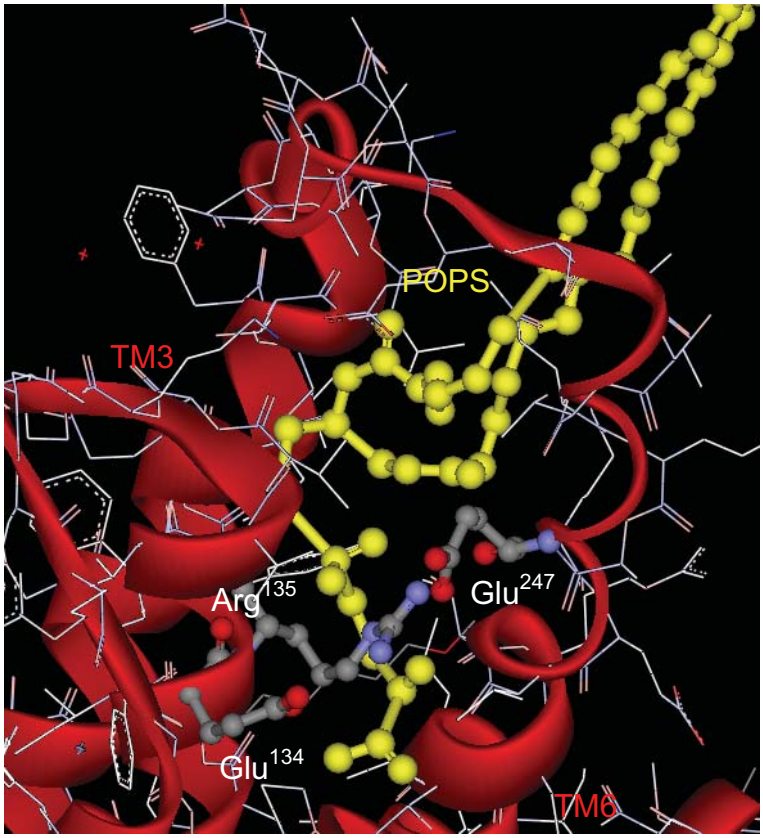

Fig. 89: *Proposition of the POPS embedding into the cleft between TM6 and TM3. POPS is drawn in yellow, and its headgroup could interact with Glu^{134} and Arg^{135} of the highly conserved D(E)RY motif. The other side chains are drawn as thin lines. Please note that this structure is no MD simulation (created with Accelrys DS-ViewerPro 5.0).*

How can we explain the flash photolysis experiments with POPS and peptides (chapter 3.8.2) on this background? When the receptor gets activated, TM6 consequently moves outward (formation of Meta-IIb) and opens the binding site for the peptide (for a detailed discussion see 4.3.2). Therefore the peptide binds to the receptor and competes against the PS molecule that consequently leaves its binding site at Glu^{134} and Arg^{135}. But why is the proton release observable

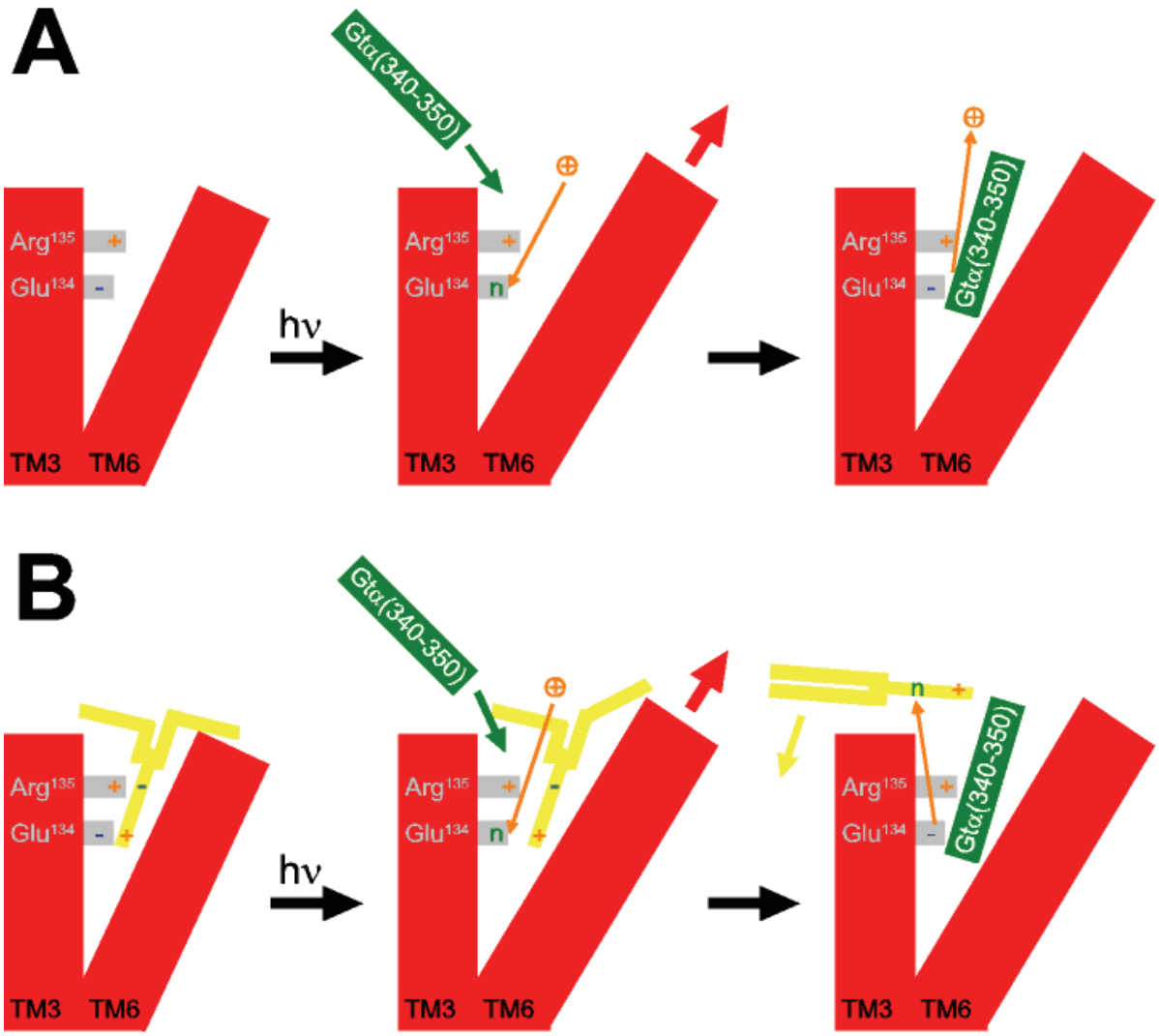

Fig. 90: *Proposed scheme for the competition between peptide and receptor-bound PS, explaining the experiments in chapter 3.8.2. Positively charged groups are symbolized with an orange '+', negatively charged groups with a blue '-' and neutral ones with a green 'n'.* **A** *The binding of peptide (green) in absence of PS. A proton (orange) is taken up upon formation of Meta-IIb·H^+ and re-released when the peptide binds.* **B** *The same situation in presence of PS (yellow). The proton is taken up as well, but the re-release is not detected, because the proton is taken up into the previously bound PS molecule in order to neutralize the hydroxyl group (symbolized by the blue '-' and green 'n').*

upon peptide binding to rhodopsin not visible with increasing PS concentrations? I propose that the PS molecule takes up this proton in order to neutralize the carboxyl group when it leaves the protein so that the *net* proton release is zero. The process is depicted schematically in Fig. 90.
Interestingly, a specific interaction between rhodopsin and PS has also been suggested to occur at H8, the short membrane peripheral helix at the C-terminal end of the receptor, which may even loose its loop structure if PS is not present in the membrane [Krishna et al., 2002]. Thus even two specific PS interaction sites might exist in rhodopsin. Similarly, specific sites for interaction with another lipid, docosahexaenoic acid (DHA) have also been reported [Grossfield et al., 2006b; Soubias et al., 2006a].

4.4.3 Rhodopsin size change

Near infrared light scattering signals that occur upon rhodopsin activation have been examined for a long time [Hofmann and Reichert, 1985; Hofmann et al., 1981; Hofmann et al., 1976; Hofmann and Emeis, 1981; Kühn et al., 1981; Uhl et al., 1985; Uhl et al., 1977; Uhl et al., 1980]. The negative 'N-signal' has been shown to be proportional to rhodopsin bleaching [Hofmann et al., 1976]. Interestingly, this light scattering signal has roughly the same kinetics as the proton uptake during rhodopsin activation (see Fig. 39), which on its part has been shown to happen immediately upon outward motion of TM6 (see Fig. 35). The activation energies of proton uptake and the 'N-signal' are also similar (see Table 5). Therefore the 'N-signal' could be caused mainly by outward motion of TM6. This is further supported by the fact that the negative signal converts into a positive one if Meta-II is illuminated with blue light (shown in Fig. 61), which would correspond to TM6 moving into the inward position like in the ground state again.
How could such a relatively small rigid body helix motion of 5-8 Å [Hubbell et al., 2003] cause such a macroscopically detectable light scattering change? Upon activation, rhodopsin undergoes a volume increase or an increase in the asymmetry of the shape, which means a lateral expansion of rhodopsin in the membrane [Attwood and Gutfreund, 1980; Lamola et al., 1974; Mielke et al., 2002a]. Meta-II was also suggested to have a bigger hydrophobic thickness than Meta-I and the rhodopsin ground state, which would result in a thickening of the lipid bilayer upon Meta-II formation in order to match this increased hydrophobic length [Botelho et al., 2002]. This effect is probably related to Meta-IIb formation, that is the outward motion of TM6. The related increase of the hydrophobic thickness could have an influence on the curvature of the lipid bilayer [Botelho et al., 2006]. This is supported by the finding that, conversely, a high density of rhodopsin molecules in 2D crystal arrays [Ruprecht et al., 2004; Szundi et al., 2006; Vogel et al.,

2004b] or even in 3D crystals [Okada et al., 2002] prevents formation of Meta-II or at least of Meta-IIb [Salom et al., 2006], which also is likely to be an effect of hindered TM6 motion.
An additional effect might explain the coupling between TM6 motion and the change in shape of the disc membrane: HUBBELL and coworkers presented the hypothesis, that rhodopsin molecules are interconnected through the disc as 'tail to tail' dimers [Hubbell et al., 2003], although this idea is contested. This would elegantly explain how the disc vesicles can retain their shape and be only 16 nm thin. At the same time it would explain how a change of the molecule shape could instantly lead to a change of the disc shape.
Therefore a relatively small event like the motion of TM6 possibly together with the other motions (i.e. H 8 movement) could trigger a change in shape of a whole disc membrane. I propose that this is the way how the 'N-signal' is caused.
Upon blue light illumination of the active state, the positive light scattering signal is, although slower than Meta-II deformation, clearly faster than proton release (see Fig. 61). Does this mean that TM6 inward motion and proton release are uncoupled? Or is the hypothesis of the 'N-signal' representing the helix motion wrong? As pointed out in chapter 4.1.2, proton uptake is a consequence rather than the cause of TM6 motion. Therefore it is not surprising, that the same order holds true in the mechanism of Meta-III formation. It has been shown in a kinetic FTIR study on formation of Meta-III that the structural changes (represented by the Amide-I band at 1643 cm^{-1}, which has a half lifetime of 1350 ms at 10 °C and pH 6) occur prior to the internal hydrogen bonding rearrangements (i.e. the cluster around Asp^{83} and Glu^{122}, represented by the band at 1748 cm^{-1} with a half lifetime of 1700 ms) [Ritter et al., 2007]. Unfortunately the authors make no statement about the proton release from the ERY cluster. However, based on their findings and their proposed deactivation scheme ([Ritter et al., 2007], scheme 1) it seems reasonable that the inward motion of TM6 happens first and is then ensued by the rearrangements of the hydrogen bonding networks and consequently proton release from the cluster around Glu^{134}. Therefore these data support the hypothesis of the 'N-signal' representing the motion of TM6, even though the proton release is slower than the positive light scattering signal upon blue light illumination.

4.4.4 Reversion of Meta-II into the ground state

Obviously the lipid environment also influences the blue light induced decomposition of Meta-II into Meta-III and rhodopsin ground state, respectively. As consistently shown in chapter 3.5.1 by UV/vis, FTIR and HPLC analysis, the rhodopsin ground state can be restored in a detergent environment. This implies that the asserted impossibility to recreate significant amounts of ground

state from Meta-II [Bartl et al., 2001; Ritter et al., 2007; Ritter et al., 2004; Zimmermann et al., 2004] does only apply to the membrane environment but not to detergent environments.

Although a detergent environment must be regarded an artificial environment for rhodopsin which is undoubtedly very different from the native membrane environment, we can learn from this finding how important the ROS lipid environment is for the Meta-II state. Interestingly, different detergents even lead to different levels of ground state recreation (see Fig. 58).

How can this different behaviour of rhodopsin in membrane and detergent environment be explained? In a recent paper on blue light induced Meta-III, RITTER et al. propose that upon blue light illumination of Meta-II or alternatively thermal decay the retinal experiences a 'second switch' which is responsible for the 15-*syn-anti* instead of the 11-*trans-cis* isomerization of the bound retinal [Ritter et al., 2004]. This 'second switch' could function through TM6 which has a higher flexibility in detergent [Kusnetzow et al., 2006] and could easily affect the retinal through Trp^{265} and other interactions, thereby explaining the dependence on the environment.

Some mutations, especially in the D(E)RY motif, also have an influence on the amount of ground state reformation, and the creation of Meta-III species is pH dependent in contrast to WT (see Fig. 59B). This could be explained by TM6, which interacts with the D(E)RY motif through Glu^{247}, Val^{250}, Thr^{251} and Val^{254}, and / or TM3 directly being involved in this 'second switch'.

It was suggested that Meta-III is formed thermally via Meta-I [Soubias et al., 2006b; Vogel et al., 2004a; Zimmermann et al., 2004]. It is generally accepted that Meta-I is not formed in DM but the equilibrium is fully shifted towards Meta-II. Thus the question arises through which photoproduct the rhodopsin ground state is formed. According to the shifted equilibrium it is likely that it should be one of the Meta-II subforms.

4.5 Rhodopsin activation scheme

Based on the data and discussion in this work I propose a rhodopsin activation scheme which involves two parallel pathways: The signal is initiated in the retinal region upon uptake of a photon and then propagates to the D(E)RY region and to the NPxxY$(x)_{5,6}$F /H8 region parallel. Both these processes are necessary to create the G_t activating form or probably rather two receptor species needed for G_t activation [Downs et al., 2006].

This two-pathway-scheme is strongly supported by examinations of partly constitutively active mutants (G90D, E113Q, M257Y, A292E) which are in presence of retinal only completely constitutively active if they occur as double mutations (E113Q/M257Y, E113Q/M257N, E113Q/M257A) [Han et al., 1998; Kim et al., 2004]. The single mutations only cause a partly active conformation in certain rhodopsin regions (at least as long as the retinal is present in the protein – in pure opsin the whole protein has a higher flexibility and thus a bigger tendency to activate), indicating that they can only activate one of the activation pathways each.

The whole rhodopsin activation process starts through isomerization of the retinal from its 11-*cis* to the all-*trans* configuration (Fig. 3) upon illumination. This process leads to smaller rearrangements in the protein and hence to proton release from the Schiff base (SB) and consequent disruption of the SB-Glu^{113} salt bridge. It has been deduced from SDSL studies with constitutively active mutants, that protonation at Glu^{113} (quasi anticipated via E113Q mutation) is a cause of TM6 motion [Kim et al., 2004]. The signal probably propagates from the retinal region to the D(E)RY region via the hydrogen bonded network built of the residues Trp^{126}, Glu^{122}, His^{211} and His^{152} (for further discussion see 4.2.6). Furthermore, TM3 is also directly linked to the retinal through the residues Gly^{114}, Thr^{118} and Gly^{121}. This results in outward TM6 motion (discussed in chapter 4.1.1).

What causes the time delay between the incidents in the retinal region (represented by the Meta-II kinetics) and the outward TM6 motion (see the Arrhenius plot in Fig. 35)? Three factors might be mutually exclusively or collectively responsible for this:

1. After deprotonation of the SB a protonation of the complex counterion Glu^{113} and Glu^{181} has to occur, which is time-delayed.
2. The outward motion of TM6 itself might cause the time delay, because TM6 does not move immediately but only after additional restraints (e.g. in the D(E)RY region, see 4.2.3) have been broken.

3. The rearrangements of hydrogen bonds in the network Trp^{126}-Glu^{122}-His^{211}-His^{152}-D(E)RY might take some time to occur. The reason could be the necessity of the involved residues to find the right positions – analogous to the situation for proton transfer reactions [Gutman and Nachliel, 1990]. If this process is disrupted by an amino acid replacement in this chain (e.g. H211F as discussed in chapter 4.2.6), it gets even slower, which shows how important this signal propagation pathway is for the time regime of the activation mechanism.

TM6 is probably already partly loosened upon isomerization of the retinal because it interacts with the retinal through the residues Trp^{265} and Tyr^{268} [Patel et al., 2004]. Trp^{265} is only two residues away from Pro^{267}, the proposed hinge of TM6 motion, and its large indole side chain can thus act as a lever. How these interactions are changed if the retinal lacks the β-ionone ring, can be seen in the increased mobility of TM6 already in the dark state with acyclic retinal (see chapter 3.4.1). This increased flexibility may take some time to finally break the remaining constraints connecting TM6 with TM3 in the D(E)RY region (in detail discussed in chapter 4.2.3). Also the 9-methyl group (lack of this group leads to lack of activation [Meyer et al., 2000; Vogel et al., 2000] including TM6 motion [Knierim et al., 2007]) interacts with Tyr^{268} in TM6 and Thr^{118} in TM3 [Patel et al., 2004], although lack of this small group does not have direct consequences on TM6 mobility (see Fig. 54).

As a consequence of TM6 motion and the smaller motion of TM3, the proton uptake in the D(E)RY region can occur, because the region becomes accessible to water (discussed in chapter 4.1.2), while it was enclosed in a hydrophobic environment until Meta-IIb is formed. The PS molecule bound to the D(E)RY motif (see chapter 4.4.2) might be a further shield protecting this region from water molecules pouring into the protein. It would thereby stabilize the rhodopsin ground state. The result of the whole process is the exposure and possibly the formation of a G_t binding site located at the D(E)RY motif.

In parallel, the signal from the retinal region also propagates to the NPxxY$(x)_{5,6}$F / H8 region via TM7. The retinal interacts directly with TM7 through the Schiff base Lys^{296} which changes its protonation state when Meta-II is formed. Additionally there are hydrogen bonds between Asp^{83} (TM2, discussed in chapter 4.2.6) and Asn^{302} in the NPxxY$(x)_{5,6}$F motif and between Ala^{299} and Asn^{55} (TM1, also highly conserved) which are broken during activation [Patel et al., 2004]. The cytoplasmic parts of TM7 and H8 are fixed in their orientation to each other via the conserved residues Tyr^{306} and Phe^{313} (acting like a bracket, described in chapter 4.2.5). This whole part moves as a consequence of the hydrogen bond rearrangements with Pro^{303} as the hinge – analogous to Pro^{267} in TM6.

Additionally there is an interaction between the D(E)RY motif and the NPxxY$(x)_{5,6}$F motif. A mutation in TM6 (M257Y) has been shown to have an impact on the H8 region [Kim et al., 2004]. In the opposite direction, severe changes in the structure of H8 have an impact onto the D(E)RY-based proton uptake (see chapter 4.2.4). A possible candidate for this intramolecular signal pathway could be the proposed interaction between Glu^{249} and Met^{309} [Palczewski, 2006]. Thus, finally H8 can undergo its motion or even disintegrate the helix into a looplike structure [Krishna et al., 2002], which consequently exposes the second G_t binding site located at the NPxxY$(x)_{5,6}$F motif.

The described interaction between the D(E)RY and NPxxY$(x)_{5,6}$F regions might be just a part of the pathway forming the active receptor conformation, but it might as well be the mechanism how the switch between the two proposed Meta-II substates [Downs et al., 2006] involved in sequential fit of G_t works (discussed in detail in chapter 4.3.2).

What is the sense of such a complicated activation pathway with two parallel "arms"? And likewise, what is the sense of a sequential G_t activation mechanism? Both mechanisms – which could be interconnected as discussed above – could increase the fidelity of activation: The mechanism through two parallel, but equally necessary pathways avoids spontaneous activation while still maintaining the capability to be efficiently activated. If only one "arm" is spontaneously activated due to a disturbance, this is not sufficient to activate the whole receptor – and the spontaneous parallel activation of both "arms" is highly unlikely. Thus the proposed activation scheme might be one part of the answer solving the mystery how rhodopsin can on the one hand have such an extremely high stability in the dark state and on the other hand be activated by only one photon – a signal to noise ratio which is still without any technical counterpart and enables vision even under very low light conditions.

It is an interesting question how far a parallel two pathway mechanism like this can be found in other GPCRs as well and if it might be a general mechanism.

Bibliography

Abdulaev, N. G. and Ridge, K. D. (1998): Light-induced exposure of the cytoplasmic end of transmembrane helix seven in rhodopsin, *Proc. Natl. Acad. Sci. U.S.A.* **95** [22], 12854-12859.

Acharya, S. and Karnik, S. S. (1996): Modulation of GDP release from transducin by the conserved Glu134-Arg135 sequence in rhodopsin, *J. Biol. Chem.* **271** [41], 25406-11.

Altenbach, C.; Klein-Seetharaman, J.; Cai, K.; Khorana, H. G. and Hubbell, W. L. (2001a): Structure and Function in Rhodopsin: Mapping Light-Dependent Changes in Distance between Residue 316 in Helix 8 and Residues in the Sequence 60- 75, Covering the Cytoplasmic End of Helices TM1 and TM2 and Their Connection Loop CL1, *Biochemistry* **40** [51], 15493-15500.

Altenbach, C.; Cai, K.; Khorana, H. G. and Hubbell, W. L. (1999): Structural features and light-dependent changes in the sequence 306-322 extending from helix VII to the palmitoylation sites in rhodopsin: a site-directed spin-labeling study, *Biochemistry* **38** [25], 7931-7937.

Altenbach, C.; Cai, K.; Klein-Seetharaman, J.; Khorana, H. G. and Hubbell, W. L. (2001b): Structure and Function in Rhodopsin: Mapping Light-Dependent Changes in Distance between Residue 65 in Helix TM1 and Residues in the Sequence 306-319 at the Cytoplasmic End of Helix TM7 and in Helix H8, *Biochemistry* **40** [51], 15483-15492.

Altenbach, C.; Oh, K. J.; Trabanino, R. J.; Hideg, K. and Hubbell, W. L. (2001c): Estimation of inter-residue distances in spin labeled proteins at physiological temperatures: experimental strategies and practical limitations, *Biochemistry* **40** [51], 15471-82.

Alves, I. D.; Salgado, G. F.; Salamon, Z.; Brown, M. F.; Tollin, G. and Hruby, V. J. (2005): Phosphatidylethanolamine Enhances Rhodopsin Photoactivation and Transducin Binding in a Solid Supported Lipid Bilayer as Determined Using Plasmon-Waveguide Resonance Spectroscopy, *Biophys. J.* **88** [1], 198-210.

Anavi-Goffer, S.; Fleischer, D.; Hurst, D. P.; Lynch, D. L.; Barnett-Norris, J.; Shi, S.; Lewis, D. L.; Mukhopdhyay, S.; Howlett, A. C.; Reggio, P. H. and Abood, M. E. (2007): Helix 8 Leu in the CB1 cannabinoid receptor contributes to selective signal transduction mechanisms, *J. Biol. Chem.*

Arnis, S.; Fahmy, K.; Hofmann, K. P. and Sakmar, T. P. (1994): A conserved carboxylic acid group mediates light-dependent proton uptake and signaling by rhodopsin, *J. Biol. Chem.* **269** [39], 23879-23881.

Arnis, S. and Hofmann, K. P. (1993): Two different forms of metarhodopsin II: Schiff base deprotonation precedes proton uptake and signaling state, *Proc. Natl. Acad. Sci. U.S.A.* **90** [16], 7849-7853.

Arnis, S. and Hofmann, K. P. (1995): Photoregeneration of bovine rhodopsin from its signaling state, *Biochemistry* **34** [29], 9333-9340.

Attwood, P. V. and Gutfreund, H. (1980): The application of pressure relaxation to the study of the equilibrium between metarhodopsin I and II from bovine retinas, *FEBS Lett.* **119** [2], 323-326.

Ballesteros, J. A.; Jensen, A. D.; Liapakis, G.; Rasmussen, S.G.F.; Shi, L.; Gether, U. and Javitch, J.A. (2001): Activation of the beta 2-Adrenergic Receptor Involves Disruption of an Ionic Lock between the Cytoplasmic Ends of Transmembrane Segments 3 and 6, *J. Biol. Chem.* **276** [31], 29171-29177.

Bartl, F.; Ritter, E. and Hofmann, K. P. (2000): FTIR spectroscopy of complexes formed between metarhodopsin II and C- terminal peptides from the G-protein alpha- and gamma-subunits, *FEBS Lett.* **473** [2], 259-264.

Bartl, F. J.; Fritze, O.; Ritter, E.; Herrmann, R.; Kuksa, V.; Palczewski, K.; Hofmann, K. P. and Ernst, O. P. (2005): Partial agonism in a G protein-coupled receptor: Role of the retinal ring structure in rhodopsin activation, *J. Biol. Chem.* **280**, 34259-34267.

Bartl, F. J.; Ritter, E. and Hofmann, K. P. (2001): Signaling States of Rhodopsin. Absorption of light in active metarhodopsin II generates an all-trans-retinal bound inactive state, *J. Biol. Chem.* **276** [32], 30161-30166.

Bartl, F. J. and Vogel, R. (2007): Structural and functional properties of metarhodopsin III: Recent spectroscopic studies on deactivation pathways of rhodopsin, *Phys. Chem. Chem. Phys.* **9** [14], 1648-58.

Baylor, D. A.; Lamb, T. D. and Yau, K. W. (1979): Responses of retinal rods to single photons, *J. Physiol.* **288**, 613-634.

Beck, M.; Sakmar, T. P. and Siebert, F. (1998): Spectroscopic evidence for interaction between transmembrane helices 3 and 5 in rhodopsin, *Biochemistry* **37** [20], 7630-7639.

Borggreven, J. M.; Daemen, F. J. and Bonting, S. L. (1970): Biochemical aspects of the visual process. VI. The lipid composition of native and hexane-extracted cattle rod outer segments, *Biochim. Biophys. Acta* **202** [2], 374-381.

Borhan, B.; Souto, M. L.; Imai, H.; Shichida, Y. and Nakanishi, K. (2000): Movement of retinal along the visual transduction path, *Science* **288** [5474], 2209-2212.

Botelho, A. V.; Gibson, N. J.; Thurmond, R. L.; Wang, Y. and Brown, M. F. (2002): Conformational energetics of rhodopsin modulated by nonlamellar-forming lipids, *Biochemistry* **41** [20], 6354-6368.

Botelho, A. V.; Huber, T.; Sakmar, T. P. and Brown, M. F. (2006): Curvature and hydrophobic forces drive oligomerization and modulate activity of rhodopsin in membranes, *Biophys. J.* **91** [12], 4464-77.

Braiman, M. (2007): Conservation of Mechanism in Archaeal and Bacterial Ion-pumping Rhodopsins, Biophysical Society 2007, Baltimore.

Bright, J. N. and Sansom, Mark S. P. (2003): The flixing/twirling helix: exploring the flexibility about molecular hinges formed by proline and glycine motifs in transmembrane helices, *J. Phys. Chem.* **107**, 627-6363.

Buczyłko, J.; Saari, J. C.; Crouch, R. K. and Palczewski, K. (1996): Mechanisms of opsin activation, *J. Biol. Chem.* **271** [34], 20621-20630.

Budil, D. E.; Lee, S.; Saxena, S.; Freed, J. H. (1996): Nonlinear least-squares analysis of slow-motion EPR spectra in one and two dimensions using a modified Levenberg-Marquardt-algorithm, *J. Magn. Reson.* **A 120**, 155-189.

Burns, M. E. and Arshavsky, V. Y. (2005): Beyond Counting Photons: Trials and Trends in Vertebrate Visual Transduction, *Neuron* **48** [3], 387-401.

Chabre, M. and Worcester, D. L. (1982): X-ray and neutron diffraction of retinal rod outer segments, *Methods Enzymol.* **81**, 593-604.

Chen, Y. S. and Hubbell, W. L. (1978): Reactions of the sulfhydryl groups of membrane-bound bovine rhodopsin, *Membr. Biochem.* **1** [1-2], 107-130.

Ciarkowski, J.; Witt, M. and Słusarz, R. (2005): A hypothesis for GPCR activation, *J. Mol. Model. (Online)* **11** [4-5], 407-15.

Cohen, G. B.; Oprian, D. D. and Robinson, P. R. (1992): Mechanism of activation and inactivation of opsin: role of Glu113 and Lys296, *Biochemistry* **31** [50], 12592-12601.

Cohen, G. B.; Yang, T.; Robinson, P. R. and Oprian, D. D. (1993): Constitutive activation of opsin: influence of charge at position 134 and size at position 296, *Biochemistry* **32** [23], 6111-6115.

Dell'Orco, D.; Seeber, M. and Fanelli, F. (2007): Monomeric dark rhodopsin holds the molecular determinants for transducin recognition: insights from computational analysis, *FEBS Lett* **581** [5], 944-8.

Devane, W. A.; Hanus, L.; Breuer, A.; Pertwee, R. G.; Stevenson, L. A.; Griffin, G.; Gibson, D.; Mandelbaum, A.; Etinger, A. and Mechoulam, R. (1992): Isolation and structure of a brain constituent that binds to the cannabinoid receptor, *Science* **258** [5090], 1946-9.

Dolph, P. J.; Ranganathan, R.; Colley, N. J.; Hardy, R. W.; Socolich, M. and Zuker, C. S. (1993): Arrestin function in inactivation of G protein-coupled receptor rhodopsin in vivo, *Science* **260** [5116], 1910-1916.

Downs, M. A.; Arimoto, R.; Marshall, G. R. and Kisselev, O. G. (2006): G-protein alpha and beta-gamma subunits interact with conformationally distinct signaling states of rhodopsin, *Vision Res.* **46** [27], 4442-8.

Dratz, E. A.; Furstenau, J. E.; Lambert, C. G.; Thireault, D. L.; Rarick, H.; Schepers, T.; Pakhlevaniants, S. and Hamm, H. E. (1993): NMR structure of a receptor-bound G-protein peptide [published erratum appears in Nature 1997 Nov 27;390(6658):424], *Nature* **363** [6426], 276-281.

Ebrey, T. G. (1968): The thermal decay of the intermediates of rhodopsin in situ, *Vision Res.* **8** [8], 965-982.

Emeis, D.; Kühn, H.; Reichert, J. and Hofmann, K. P. (1982): Complex formation between metarhodopsin II and GTP-binding protein in bovine photoreceptor membranes leads to a shift of the photoproduct equilibrium, *FEBS Lett.* **143** [1], 29-34.

Ernst, O. P.; Bieri, C.; Vogel, H. and Hofmann, K. P. (2000a): Intrinsic biophysical monitors of transducin activation: fluorescence, UV-visible spectroscopy, light scattering, and evanescent field techniques, *Methods Enzymol.* **315**, 471-489.

Ernst, O. P.; Gramse, V.; Kolbe, M.; Hofmann, K. P. and Heck, M. (2007): Monomeric G protein-coupled receptor rhodopsin in solution activates its G protein transducin at the diffusion limit, *Proc. Natl. Acad. Sci. U.S.A.* **104** [26], 10859-64.

Ernst, O. P.; Hofmann, K. P. and Sakmar, T. P. (1995): Characterization of rhodopsin mutants that bind transducin but fail to induce GTP nucleotide uptake. Classification of mutant pigments by fluorescence, nucleotide release, and flash-induced light-scattering assays, *J. Biol. Chem.* **270** [18], 10580-10586.

Ernst, O. P.; Meyer, C. K.; Marin, E. P.; Henklein, P.; Fu, W. Y.; Sakmar, T. P. and Hofmann, K. P. (2000b): Mutation of the fourth cytoplasmic loop of rhodopsin affects binding of transducin and peptides derived from the carboxyl-terminal sequences of transducin alpha and gamma subunits, *J. Biol. Chem.* **275** [3], 1937-1943.

Fahmy, K. (1998): Binding of transducin and transducin-derived peptides to rhodopsin studied by attenuated total reflection-fourier transform infrared difference spectroscopy, *Biophys. J.* **75**, 1306-1318.

Fahmy, K.; Jäger, F.; Beck, M.; Zvyaga, T. A.; Sakmar, T. P. and Siebert, F. (1993): Protonation states of membrane-embedded carboxylic acid groups in rhodopsin and metarhodopsin II: a Fourier-transform infrared spectroscopy study of site-directed mutants, *Proc. Natl. Acad. Sci. U.S.A.* **90** [21], 10206-10210.

Fahmy, K. and Sakmar, T. P. (1993): Regulation of the rhodopsin-transducin interaction by a highly conserved carboxylic acid group, *Biochemistry* **32** [28], 7229-7236.

Fahmy, K.; Sakmar, T. P. and Siebert, F. (2000): Transducin-dependent protonation of glutamic acid 134 in rhodopsin, *Biochemistry* **39** [34], 10607-10612.

Fahmy, K.; Siebert, F. and Sakmar, T. P. (1995): Photoactivated state of rhodopsin and how it can form, *Biophys. Chem.* **56** [1-2], 171-181.

Fanelli, F. and Dell'Orco, D. (2005): Rhodopsin activation follows precoupling with transducin: inferences from computational analysis, *Biochemistry* **44** [45], 14695-700.

Farahbakhsh, Z. T.; Hideg, K. and Hubbell, W. L. (1993): Photoactivated conformational changes in rhodopsin: a time-resolved spin label study, *Science* **262** [5138], 1416-1419.

Farrens, D. L.; Altenbach, C.; Yang, K.; Hubbell, W. L. and Khorana, H. G. (1996): Requirement of rigid-body motion of transmembrane helices for light activation of rhodopsin, *Science* **274** [5288], 768-770.

Farrens, D. L. and Khorana, H. G. (1995): Structure and function in rhodopsin. Measurement of the rate of metarhodopsin II decay by fluorescence spectroscopy, *J. Biol. Chem.* **270** [10], 5073-5076.

Favre, N.; Fanelli, F.; Missotten, M.; Nichols, A.; Wilson, J.; di Tiani, M.; Rommel, C. and Scheer, A. (2005): The DRY motif as a molecular switch of the human oxytocin receptor, *Biochemistry* **44** [30], 9990-10008.

Findlay, J. B.; Barclay, P. L.; Brett, M.; Davison, M.; Pappin, D. J. and Thompson, P. (1984): The structure of mammalian rod opsins, *Vision Res.* **24** [11], 1501-8.

Flocco, M. M. and Mowbray, S. L. (1995): Strange bedfellows: interactions between acidic sidechains in proteins, *J. Mol. Biol.* **254** [1], 96-105.

Fotiadis, D.; Jastrzebska, B.; Philippsen, A.; Muller, D. J.; Palczewski, K. and Engel, A. (2006): Structure of the rhodopsin dimer: a working model for G-protein-coupled receptors, *Curr. Opin. Struct. Biol.* **16** [2], 252-9.

Fotiadis, D.; Liang, Y.; Filipek, S.; Saperstein, D. A.; Engel, A. and Palczewski, K. (2003): Atomic-force microscopy: Rhodopsin dimers in native disc membranes, *Nature* **421** [6919], 127-8.

Franke, R. R.; König, B.; Sakmar, T. P.; Khorana, H. G. and Hofmann, K. P. (1990): Rhodopsin mutants that bind but fail to activate transducin, *Science* **250** [4977], 123-125.

Franke, R. R.; Sakmar, T. P.; Graham, R. M. and Khorana, H. G. (1992): Structure and function in rhodopsin. Studies of the interaction between the rhodopsin cytoplasmic domain and transducin, *J. Biol. Chem.* **267** [21], 14767-14774.

Franke, R. R.; Sakmar, T. P.; Oprian, D. D. and Khorana, H. G. (1988): A single amino acid substitution in rhodopsin (lysine 248-leucine) prevents activation of transducin, *J. Biol. Chem.* **263** [5], 2119-2122.

Fritze, O.; Filipek, S.; Kuksa, V.; Palczewski, K.; Hofmann, K. P. and Ernst, O. P. (2003): Role of the conserved NPxxY(x)5,6F motif in the rhodopsin ground state and during activation, *Proc. Natl. Acad. Sci. U.S.A.* **100** [5], 2290-2295.

Garczarek, F. and Gerwert, K. (2006): Functional waters in intraprotein proton transfer monitored by FTIR difference spectroscopy, *Nature* **439** [7072], 109-12.

Gibson, N. J. and Brown, M. F. (1993): Lipid headgroup and acyl chain composition modulate the MI-MII equilibrium of rhodopsin in recombinant membranes, *Biochemistry* **32** [9], 2438-2454.

Grossfield, A.; Feller, S. E. and Pitman, M. C. (2006a): Contribution of omega-3 fatty acids to the thermodynamics of membrane protein solvation, *J. Phys. Chem. B.* **110** [18], 8907-9.

Grossfield, A.; Feller, S. E. and Pitman, M. C. (2006b): A role for direct interactions in the modulation of rhodopsin by omega-3 polyunsaturated lipids, *Proc. Natl. Acad. Sci. U.S.A.* **103** [13], 4888-93.

Guillen Schlippe, Yollete V. and Hedstrom, Lizbeth (2005): A twisted base? The role of arginine in enzyme-catalyzed proton abstractions, *Arch. Biochem. Biophys* **433** [1], 266-278.

Gutman, M. and Nachliel, E. (1990): The dynamic aspects of proton transfer processes, *Biochim. Biophys. Acta* **1015**, 391-414.

Hamm, H. E.; Deretic, D.; Arendt, A.; Hargrave, P. A.; Koenig, B. and Hofmann, K. P. (1988): Site of G protein binding to rhodopsin mapped with synthetic peptides from the alpha subunit, *Science* **241** [4867], 832-835.

Han, M.; Smith, S. O. and Sakmar, T. P. (1998): Constitutive activation of opsin by mutation of methionine 257 on transmembrane helix 6, *Biochemistry* **37** [22], 8253-8261.

Heck, M. and Hofmann, K. P. (2001): Maximal rate and nucleotide dependence of rhodopsin catalyzed transducin activation: initial rate analysis based on a double displacement mechanism, *J. Biol. Chem.* **276** [13], 10000-10009.

Heck, M.; Pulvermüller, A. and Hofmann, K. P. (2000): Light scattering methods to monitor interactions between rhodopsin- containing membranes and soluble proteins, *Methods Enzymol.* **315**, 329-347.

Herrmann, R.; Heck, M.; Henklein, P.; Henklein, P.; Kleuss, C.; Hofmann, K. P. and Ernst, O. P. (2004): Sequence of interactions in receptor-G protein coupling, *J. Biol. Chem.* **279**, 24283-24290.

Herrmann, R.; Heck, M.; Henklein, P.; Hofmann, K. P. and Ernst, O. P. (2006a): Signal transfer from GPCRs to G proteins: role of the G alpha N-terminal region in rhodopsin-transducin coupling, *J. Biol. Chem.* **281** [40], 30234-41.

Herrmann, R.; Heck, M.; Henklein, P.; Kleuss, C.; Wray, V.; Hofmann, K. P. and Ernst, O. P. (2006b): Rhodopsin-transducin coupling: role of the Galpha C-terminus in nucleotide exchange catalysis, *Vision Res.* **46** [27], 4582-93.

Hessel, E.; Heck, M.; Müller, P.; Herrmann, A. and Hofmann, K. P. (2003): Signal transduction in the visual cascade involves specific lipid-protein interactions, *J. Biol. Chem.* **278**, 22853-22860.

Hoffmann, W.; Siebert, F.; Hofmann, K. P. and Kreutz, W. (1978): Two distinct rhodopsin molecules within the disc membrane of vertebrate rod outer segments, *Biochim. Biophys. Acta* **503** [3], 450-461.

Hofmann, K. P. and Reichert, J. (1985): Chemical probing of the light-induced interaction between rhodopsin and G-protein. Near-infrared light-scattering and sulfhydryl modifications, *J. Biol. Chem.* **260** [13], 7990-7995.

Hofmann, K. P.; Emeis, D. and Schnetkamp, P. P. (1983): Interplay between hydroxylamine, metarhodopsin II and GTP-binding protein in bovine photoreceptor membranes, *Biochim. Biophys. Acta* **725** [1], 60-70.

Hofmann, K. P. and Ernst, O. P. (2001): [To see from light – biophysics of visual signal transduction], *Zeitschrift für Medizinische Physik* **11** [4], 217-225.

Hofmann, K. P.; Schleicher, A.; Emeis, D. and Reichert, J. (1981): Light-induced axial and radial shrinkage effects and changes of the refractive index in isolated bovine rod outer segments and disc, *Biophys. Struct. Mech.* **8** [1-2], 67-93.

Hofmann, K. P.; Uhl, R.; Hoffmann, W. and Kreutz, W. (1976): Measurements on fast light-induced light-scattering and -absorption changes in outer segments of vertebrate light sensitive rod cells, *Biophys. Struct. Mech.* **2** [1], 61-77.

Hofmann, K. P. (1999): Signalling states of photoactivated rhodopsin., Rhodopsins and phototransduction, 224, 159-175, John Wiley & Sons, Chichester.

Hofmann, K. P. and Emeis, D. (1981): Comparative kinetic light-scattering and -absorption photometry, *Biophys. Struct. Mech.* **8**, 23-34.

Hubbell, W. L.; Altenbach, C.; Hubbell, C. M. and Khorana, H. G. (2003): Rhodopsin structure, dynamics, and activation: a perspective from crystallography, site-directed spin labeling, sulfhydryl reactivity, and disulfide cross-linking, *Adv. Protein Chem.* **63**, 243-90.

Hubbell, W. L.; Cafiso, D. S. and Altenbach, C. (2000): Identifying conformational changes with site-directed spin labeling, *Nature Structural Biology* **7** [9], 735739.

Huber, T.; Botelho, A. V.; Beyer, K. and Brown, M. F. (2004): Membrane model for the G-protein-coupled receptor rhodopsin: hydrophobic interface and dynamical structure, *Biophys. J.* **86** [4], 2078-100.

Humphries, G.M.K.; McConnell, H.M. (1982): Nitroxide Spin Labels, *In: Methods of Experimental Physics* **20**, 53-109.

Imai, H.; Kuwayama, S.; Onishi, A.; Morizumi, T.; Chisaka, O. and Shichida, Y. (2005): Molecular properties of rod and cone visual pigments from purified chicken cone pigments to mouse rhodopsin in situ, *Photochem Photobiol Sci* **4** [9], 667-74.

Imamoto, Y.; Kataoka, M.; Tokunaga, F. and Palczewski, K. (2000): Light-induced conformational changes of rhodopsin probed by fluorescent alexa594 immobilized on the cytoplasmic surface, *Biochemistry* **39** [49], 15225-15233.

Ishiguro, M.; Oyama, Y. and Hirano, T. (2004): Structural models of the photointermediates in the rhodopsin photocascade, lumirhodopsin, metarhodopsin I, and metarhodopsin II, *ChemBioChem* **5** [3], 298-310.

Jäger, F.; Fahmy, K.; Sakmar, T. P. and Siebert, F. (1994a): Identification of glutamic acid 113 as the Schiff base proton acceptor in the metarhodopsin II photointermediate of rhodopsin, *Biochemistry* **33** [36], 10878-10882.

Jäger, F.; Jäger, S.; Kräutle, O.; Friedman, N.; Sheves, M.; Hofmann, K. P. and Siebert, F. (1994b): Interactions of the beta-ionone ring with the protein in the visual pigment rhodopsin control the activation mechanism. An FTIR and fluorescence study on artificial vertebrate rhodopsins, *Biochemistry* **33** [23], 7389-7397.

Janko, K. and Reichert, J. (1987): Proton concentration jumps and generation of transmembrane pH-gradients by photolysis of 4-formyl-6-methoxy-3-nitrophenoxyacetic acid, *Biochim. Biophys. Acta* **905** [2], 409-16.

Janz, Jay M. and Farrens, David L. (2004): Rhodopsin activation exposes a key hydrophobic binding site forthe transducin alpha -subunit C-terminus, *J. Biol. Chem.* **279**, 29767-29773.

Jastrzebska, B.; Fotiadis, D.; Jang, G. F.; Stenkamp, R. E.; Engel, A. and Palczewski, K. (2006): Functional and structural characterization of rhodopsin oligomers, *J. Biol. Chem.* **281** [17], 11917-22.

Johnson, J. E. and Cornell, R. B. (1999): Amphitropic proteins: regulation by reversible membrane interactions (review), *Mol. Membr. Biol.* **16** [3], 217-35.

Johnson, M. S.; Robertson, D. N.; Holland, P. J.; Lutz, E. M. and Mitchell, R. (2006): Role of the conserved NPxxY motif of the 5-HT2A receptor in determining selective interaction with isoforms of ADP-ribosylation factor (ARF), *Cell Signal.* **18** [10], 1793-800.

Kim, J.-M.; Altenbach, C.; Kono, M.; Oprian, D. D.; Hubbell, W. L. and Khorana, H. G. (2004): Structural origins of constitutive activation in rhodopsin: Role of the K296/E113 salt bridge, *Proc. Natl. Acad. Sci. U.S.A.* **101** [34], 12508-12513.

Kim, J. M.; Altenbach, C.; Thurmond, R. L.; Khorana, H. G. and Hubbell, W. L. (1997): Structure and function in rhodopsin: rhodopsin mutants with a neutral amino acid at E134 have a partially activated conformation in the dark state, *Proc. Natl. Acad. Sci. U.S.A.* **94** [26], 14273-14278.

Kim, J. M.; Hwa, J.; Garriga, P.; Reeves, P. J.; Rajbhandary, U. L. and Khorana, H. G. (2005): Light-Driven Activation of beta(2)-Adrenergic Receptor Signaling by a Chimeric Rho-

dopsin Containing the beta(2)-Adrenergic Receptor Cytoplasmic Loops, *Biochemistry* **44** [7], 2284-92.

Kisselev, O. G.; Meyer, C. K.; Heck, M.; Ernst, O. P. and Hofmann, K. P. (1999): Signal transfer from rhodopsin to the G-protein: evidence for a two-site sequential fit mechanism., *Proc. Natl. Acad. Sci. U.S.A.* **96** [9], 4898-4903.

Knierim, B.; Hofmann, K. P.; Gärtner, W.; Hubbell, W. L. and Ernst, O. P. (2008): Rhodopsin and 9-demethyl retinal analog: Effect of a partial agonist on displacement of transmembrane helix 6 in class A GPCRs, *J. Biol. Chem.* **283** [8], 2967-2974.

Kohl, B. and Hofmann, K. P. (1987): Temperature dependence of G-protein activation in photoreceptor membranes. Transient extra metarhodopsin II on bovine disk membranes, *Biophys. J.* **52** [2], 271-277.

Kong, Y. and Karplus, M. (2007): The signaling pathway of rhodopsin, *Structure* **15** [5], 611-23.

Krishna, A. G.; Menon, S. T.; Terry, T. J. and Sakmar, T. P. (2002): Evidence that helix 8 of rhodopsin acts as a membrane-dependent conformational switch, *Biochemistry* **41** [26], 8298-309.

Kühn, H.; Bennett, N.; Michel Villaz, M. and Chabre, M. (1981): Interactions between photoexcited rhodopsin and GTP-binding protein: kinetic and stoichiometric analyses from light-scattering changes, *Proc. Natl. Acad. Sci. U.S.A.* **78** [11], 6873-6877.

Kuhn, H. and Wilden, U. (1982): Assay of phosphorylation of rhodopsin in vitro and in vivo, *Methods Enzymol.* **81**, 489-96.

Kusnetzow, A. K.; Altenbach, C. and Hubbell, W. L. (2006): Conformational states and dynamics of rhodopsin in micelles and bilayers, *Biochemistry* **45** [17], 5538-50.

Lamola, A. A.; Yamane, T. and Zipp, A. (1974): Effects of detergents and high pressures upon the metarhodopsin I--metarhodopsin II equilibrium, *Biochemistry* **13** [4], 738-745.

Langen, R.; Oh, K. J.; Cascio, D. and Hubbell, W. L. (2000): Crystal structures of spin labeled T4 lysozyme mutants: implications for the interpretation of EPR spectra in terms of structure, *Biochemistry* **39** [29], 8396-405.

Lehmann, N.; Alexiev, U. and Fahmy, K. (2007): Linkage between the intramembrane H-bond network around aspartic acid 83 and the cytosolic environment of helix 8 in photoactivated rhodopsin, *J. Mol. Biol.* **366** [4], 1129-41.

Lewis, J. W.; Szundi, I.; Kazmi, M. A.; Sakmar, T. P. and Kliger, D. S. (2006): Proton movement and photointermediate kinetics in rhodopsin mutants, *Biochemistry* **45** [17], 5430-9.

Li, J.; Edwards, P. C.; Burghammer, M.; Villa, C. and Schertler, G. F. (2004): Structure of bovine rhodopsin in a trigonal crystal form, *J. Mol. Biol.* **343** [5], 1409-38.

Ludeke, S.; Beck, M.; Yan, E. C.; Sakmar, T. P.; Siebert, F. and Vogel, R. (2005): The Role of Glu181 in the Photoactivation of Rhodopsin, *J. Mol. Biol.*

Madathil, S.; Furlinski, G. and Fahmy, K. (2006): Structure and pH sensitivity of the transmembrane segment 3 of rhodopsin, *Biopolymers* **82** [4], 329-33.

Marin, E. P.; Krishna, A. G. and Sakmar, T. P. (2002): Disruption of the alpha5 Helix of Transducin Impairs Rhodopsin- Catalyzed Nucleotide Exchange, *Biochemistry* **41** [22], 6988-6994.

Marin, E. P.; Krishna, A. G.; Zvyaga, T. A.; Isele, J.; Siebert, F. and Sakmar, T. P. (2000): The amino terminus of the fourth cytoplasmic loop of rhodopsin modulates rhodopsin-transducin interaction, *J. Biol. Chem.* **275** [3], 1930-1936.

Martin, E. L.; Rens-Domiano, S.; Schatz, P. J. and Hamm, H. E. (1996): Potent peptide analogues of a G protein receptor-binding region obtained with a combinatorial library, *J. Biol. Chem.* **271** [1], 361-6.

Martinez-Mayorga, K.; Pitman, M. C.; Grossfield, A.; Feller, S. E. and Brown, M. F. (2006): Retinal counterion switch mechanism in vision evaluated by molecular simulations, *J. Am. Chem. Soc.* **128** [51], 16502-3.

Matthews, R.G.; Hubbard, R.; Brown, P.K. and Wald, G. (1963): Tautomeric forms of metarhodopsin, *J. Gen. Physiol.* **47**, 215-240.

Mazzoni, M. R. and Hamm, H. E. (1993): Tryptophan207 is involved in the GTP-dependent conformational switch in the alpha subunit of the G protein transducin: chymotryptic digestion patterns of the GTP gamma S and GDP-bound forms, *J. Prot. Chem.* **12** [2], 215-221.

Mazzoni, M. R.; Malinski, J. A. and Hamm, H. E. (1991): Structural analysis of rod GTP-binding protein, Gt. Limited proteolytic digestion pattern of Gt with four proteases defines monoclonal antibody epitope, *J. Biol. Chem.* **266** [21], 14072-81.

Meyer, C. K.; Böhme, M.; Ockenfels, A.; Gärtner, W.; Hofmann, K. P. and Ernst, O. P. (2000): Signaling states of rhodopsin: Retinal provides a scaffold for activating proton transfer switches, *J. Biol. Chem.* **275**, 19713-19718.

Meyer, C. K. and Hofmann, K. P. (2000): Monitoring proton uptake from aqueous phase during rhodopsin activation, *Methods Enzymol.* **315**, 377-387.

Mielke, T.; Alexiev, U.; Glasel, M.; Otto, H. and Heyn, M. P. (2002a): Light-Induced Changes in the Structure and Accessibility of the Cytoplasmic Loops of Rhodopsin in the Activated M(II) State, *Biochemistry* **41** [25], 7875-7884.

Mielke, T.; Villa, C.; Edwards, P. C.; Schertler, G. F. and Heyn, M. P. (2002b): X-ray Diffraction of Heavy-atom Labelled Two-dimensional Crystals of Rhodopsin Identifies the Position of Cysteine 140 in Helix 3 and Cysteine 316 in Helix 8, *J. Mol. Biol.* **316** [3], 693-709.

Min, K. C.; Zvyaga, T. A.; Cypess, A. M. and Sakmar, T. P. (1993): Characterization of mutant rhodopsins responsible for autosomal dominant retinitis pigmentosa. Mutations on the cytoplasmic surface affect transducin activation, *J. Biol. Chem.* **268** [13], 9400-9404.

Mirzadegan, T.; Benko, G.; Filipek, S. and Palczewski, K. (2003): Sequence analyses of g-protein-coupled receptors: similarities to rhodopsin, *Biochemistry* **42** [14], 4310.

Morizumi, T.; Imai, H. and Shichida, Y. (2003): Two-Step Mechanism of Interaction of Rhodopsin Intermediates with the C-Terminal Region of the Transducin {alpha}-Subunit, *J. Biochem. (Tokyo)* **134** [2], 259-267.

Nagata, T.; Terakita, A.; Kandori, H.; Shichida, Y. and Maeda, A. (1998): The hydrogen-bonding network of water molecules and the peptide backbone in the region connecting Asp83, Gly120, and Glu113 in bovine rhodopsin, *Biochemistry* **37** [49], 17216-17222.

Nanoff, C.; Koppensteiner, R.; Yang, Q.; Fuerst, E.; Ahorn, H. and Freissmuth, M. (2005): The carboxyl terminus of the G{alpha}-subunit is the latch for triggered activation of heterotrimeric G proteins, *Mo.l Pharmacol.*, mol.105.016725.

Nathans, J. (1990): Determinants of visual pigment absorbance: identification of the retinylidene Schiff's base counterion in bovine rhodopsin, *Biochemistry* **29** [41], 9746-9752.

Niu, S. L. and Mitchell, D. C. (2005): Effect of Packing Density on Rhodopsin Stability and Function in Polyunsaturated Membranes, *Biophys. J.* **89** [3], 1833-1840.

Oesterhelt, D. and Stoeckenius, W. (1974): Isolation of the cell membrane of Halobacterium halobium and its fractionation into red and purple membrane, *Methods Enzymol.* **31** [Pt A], 667-78.

Oh, K. J.; Altenbach, C.; Collier, R. J. and Hubbell, W. L. (2000): Site-directed spin labeling of proteins. Applications to diphtheria toxin, *Methods Mol. Biol.* **145**, 147-69.

Okada, T.; Ernst, O.P.; Palczewski, K. and Hofmann, K.P. (2001): Activation of rhodopsin: New insights from structural and biochemical studies, *Trends Biochem. Sci.* **26**, 318-324.

Okada, T.; Fujiyoshi, Y.; Silow, M.; Navarro, J.; Landau, E. M. and Shichida, Y. (2002): Functional role of internal water molecules in rhodopsin revealed by x- ray crystallography, *Proc. Natl. Acad. Sci. U.S.A.*

Okada, T.; Sugihara, M.; Bondar, A. N.; Elstner, M.; Entel, P. and Buss, V. (2004): The retinal conformation and its environment in rhodopsin in light of a new 2.2 A crystal structure, *J. Mol. Biol.* **342** [2], 571-83.

Oldham, W. M.; Van Eps, N.; Preininger, A. M.; Hubbell, W. L. and Hamm, H. E. (2006): Mechanism of the receptor-catalyzed activation of heterotrimeric G proteins, *Nat. Struct. Mol. Biol.* **13** [9], 772-7.

Osawa, S. and Weiss, E. R. (1994): The carboxyl terminus of bovine rhodopsin is not required for G protein activation, *Mol. Pharmacol.* **46** [6], 1036-1040.

Palczewski, K. (2006): G protein-coupled receptor rhodopsin, *Annu. Rev. Biochem.* **75**, 743-67.

Palczewski, K.; Kumasaka, T.; Hori, T.; Behnke, C. A.; Motoshima, H.; Fox, B. A.; Le Trong, I.; Teller, D. C.; Okada, T.; Stenkamp, R. E.; Yamamoto, M. and Miyano, M. (2000): Crystal structure of rhodopsin: A G protein-coupled receptor, *Science* **289** [5480], 739-745.

Papac, D. I.; Thornburg, K. R.; Bullesbach, E. E.; Crouch, R. K. and Knapp, D. R. (1992): Palmitylation of a G-protein coupled receptor. Direct analysis by tandem mass spectrometry, *J. Biol. Chem.* **267** [24], 16889-16894.

Papermaster, D. S. and Dreyer, W. J. (1974): Rhodopsin content in the outer segment membranes of bovine and frog retinal rods, *Biochemistry* **13** [11], 2438-44.

Parkes, J. H. and Liebman, P. A. (1984): Temperature and pH dependence of the metarhodopsin I-metarhodopsin II kinetics and equilibria in bovine rod disk membrane suspensions, *Biochemistry* **23** [21], 5054-5061.

Patel, Ashish B.; Crocker, Evan; Eilers, Markus; Hirshfeld, Amiram; Sheves, Mordechai and Smith, Steven O. (2004): Coupling of retinal isomerization to the activation of rhodopsin, *Proc. Natl. Acad. Sci.*, 0402848101.

Periole, X.; Ceruso, M. A. and Mehler, E. L. (2004): Acid-base equilibria in rhodopsin: dependence of the protonation state of glu134 on its environment, *Biochemistry* **43** [22], 6858-64.

Perlman, J. H.; Colson, A. O.; Wang, W.; Bence, K.; Osman, R. and Gershengorn, M. C. (1997): Interactions between conserved residues in transmembrane helices 1, 2, and 7 of the thyrotropin-releasing hormone receptor, *J. Biol. Chem.* **272** [18], 11937-42.

Piasecki, W.; Froncisz, W. and Hubbell, W. L. (1998): A rectangular loop-gap resonator for EPR studies of aqueous samples, *J. Magn. Reson.* **134** [1], 36-43.

Pogozheva, I. D.; Lomize, A. L. and Mosberg, H. I. (1997): The transmembrane 7-alpha-bundle of rhodopsin: distance geometry calculations with hydrogen bonding constraints, *Biophys. J.* **72** [5], 1963-85.

Prioleau, C.; Visiers, I.; Ebersole, B. J.; Weinstein, H. and Sealfon, S. C. (2002): Conserved helix 7 tyrosine acts as a multistate conformational switch in the 5HT2C receptor. Identification of a novel "locked-on" phenotype and double revertant mutations, *J. Biol. Chem.* **277** [39], 36577-36584.

Ramon, E.; Cordomi, A.; Bosch, L.; Zernii, E. Y.; Senin, II; Manyosa, J.; Philippov, P. P.; Perez, J. J. and Garriga, P. (2007): Critical role of electrostatic interactions of amino acids at the cytoplasmic region of helices 3 and 6 in rhodopsin conformational properties and activation, *J. Biol. Chem.* **282** [19], 14272-82.

Resek, J. F.; Farahbakhsh, Z. T.; Hubbell, W. L. and Khorana, H. G. (1993): Formation of the meta II photointermediate is accompanied by conformational changes in the cytoplasmic surface of rhodopsin, *Biochemistry* **32** [45], 12025-12032.

Ritter, E. (2006): Lichtinduzierte Deaktivierung des Rhodopsins, PhD thesis, Math.-Nat. Fakultät I, Humboldt-University, Berlin.

Ritter, E.; Elgeti, M.; Hofmann, K. P. and Bartl, F. J. (2007): Deactivation and Proton Transfer in Light-induced Metarhodopsin II/Metarhodopsin III Conversion: A time-resolved Fourier Transform Infrared Spectroscopic Study, *J. Biol. Chem.* **282** [14], 10720-30.

Ritter, E.; Zimmermann, K.; Heck, M.; Hofmann, K. P. and Bartl, F. J. (2004): Transition of rhodopsin into the active metarhodopsin II state opens a new light induced pathway linked to Schiff base isomerization, *J. Biol. Chem.* **279**, 48102-11.

Robinson, P. R.; Cohen, G. B.; Zhukovsky, E. A. and Oprian, D. D. (1992): Constitutively active mutants of rhodopsin, *Neuron* **9** [4], 719-725.

Rodieck, R.W. (1998): The first steps in seeing, Sinauer Associated, Inc., Sunderland, Massachusetts.

Rovati, G. E.; Capra, V. and Neubig, R. R. (2007): The highly conserved DRY motif of class A G protein-coupled receptors: beyond the ground state, *Mol. Pharmacol.* **71** [4], 959-64.

Ruprecht, J. J.; Mielke, T.; Vogel, R.; Villa, C. and Schertler, G. F. (2004): Electron crystallography reveals the structure of metarhodopsin I, *EMBO J.* **23** [18], 3609-3620.

Saam, J.; Tajkhorshid, E.; Hayashi, S. and Schulten, K. (2002): Molecular dynamics investigation of primary photoinduced events in the activation of rhodopsin, *Biophys. J.* **83** [6], 3097-112.

Sakmar, T. P. ; Franke, R. R. and Khorana, H. G. (1989): Glutamic acid-113 serves as the retinylidene Schiff base counterion in bovine rhodopsin, *Proc. Natl. Acad. Sci. U.S.A.* **86** [21], 8309-8313.

Sakmar, T. P.; Franke, R. R. and Khorana, H. G. (1991): The role of the retinylidene Schiff base counterion in rhodopsin in determining wavelength absorbance and Schiff base pKa, *Proc. Natl. Acad. Sci. U.S.A.* **88** [8], 3079-3083.

Salom, D.; Lodowski, D. T.; Stenkamp, R. E.; Le Trong, I.; Golczak, M.; Jastrzebska, B.; Harris, T.; Ballesteros, J. A. and Palczewski, K. (2006): Crystal structure of a photoactivated deprotonated intermediate of rhodopsin, *Proc. Natl. Acad. Sci. U.S.A.* **103** [44], 16123-8.

Schertler, G. F.; Villa, C. and Henderson, R. (1993): Projection structure of rhodopsin, *Nature* **362** [6422], 770-772.

Schlegel, B.; Sippl, W. and Holtje, H. D. (2005): Molecular dynamics simulations of bovine rhodopsin: influence of protonation states and different membrane-mimicking environments, *J. Mo.l Model. (Online)* **12** [1], 49-64.

Schleicher, A. and Hofmann, K. P. (1983): Time-resolved angular dependent measurement of triggered light scattering changes in biological suspensions, *J. Biochem. Biophys. Methods* **8** [3], 227-37.

Schleicher, A. and Hofmann, K. P. (1985): Proton uptake by light induced interaction between rhodopsin and G-protein, *Zeitschrift fuer Naturforschung, C: Biosciences* **40** [5-6], 400-405.

Schleicher, A. and Hofmann, K. P. (1987): Kinetic study on the equilibrium between membrane-bound and free photoreceptor G-protein, *J. Membr. Biol.* **95** [3], 271-281.

Schleicher, A.; Kühn, H. and Hofmann, K. P. (1989): Kinetics, binding constant, and activation energy of the 48-kDa protein-rhodopsin complex by extra-metarhodopsin II, *Biochemistry* **28** [4], 1770-1775.

Schmidt, R. and Sapunov, V.N. (1982): Non-formal kinetics, in search for chemical reaction pathways, Verlag Chemie, Weinheim/Basel.

Shi, W.; Sports, C. D.; Raman, D.; Shirakawa, S.; Osawa, S. and Weiss, E. R. (1998): Rhodopsin arginine-135 mutants are phosphorylated by rhodopsin kinase and bind arrestin in the absence of 11-cis-retinal, *Biochemistry* **37** [14], 4869-74.

Shichi, H. and Somers, R. L. (1978): Light-dependent phosphorylation of rhodopsin. Purification and properties of rhodopsin kinase, *J. Biol. Chem.* **253** [19], 7040-6.

Shin, Y. K. and Hubbell, W. L. (1992): Determination of electrostatic potentials at biological interfaces using electron-electron double resonance, *Biophys. J.* **61** [6], 1443-53.

Siebert, F. (1990): Resonance Raman and infrared difference spectroscopy of retinal proteins, *Methods Enzymol.* **189**, 123-136.

Siebert, F. (1995): Application of FTIR spectroscopy to the investigation of dark structures and photoreactions of visual pigments, *Isr. J. Chem.* **35**, 309-323.

Słusarz, R. and Ciarkowski, J. (2004): Interaction of class A G protein-coupled receptors with G proteins, *Acta Biochim. Pol.* **51** [1], 129-36.

Smith, H. G. Jr.; Stubbs, G. W. and Litman, B. J. (1975): The isolation and purification of osmotically intact discs from retinal rod outer segments, *Exp. Eye Res.* **20** [3], 211-217.

Smyth, D. G.; Nagamatsu, A. and Fruton, J. S. (1960): Some Reactions of N-Ethylmaleimide, *J. Am. Chem. So.c* **82** [17], 4600-4604.

Soubias, O.; Polozov, I. V.; Teague, W. E.; Yeliseev, A. A. and Gawrisch, K. (2006a): Functional reconstitution of rhodopsin into tubular lipid bilayers supported by nanoporous media, *Biochemistry* **45** [51], 15583-90.

Soubias, O.; Teague, W. E. and Gawrisch, K. (2006b): Evidence for specificity in lipid-rhodopsin interactions, *J. Biol. Chem.* **281** [44], 33233-41.

Spooner, P. J.; Sharples, J. M.; Goodall, S. C.; Seedorf, H.; Verhoeven, M. A.; Lugtenburg, J.; Bovee-Geurts, P. H.; DeGrip, W. J. and Watts, A. (2003): Conformational Similarities in the beta-Ionone Ring Region of the Rhodopsin Chromophore in Its Ground State and af-

ter Photoactivation to the Metarhodopsin-I Intermediate, *Biochemistry* **42** [46], 13371-13378.

Stenkamp, R. E.; Teller, D. C. and Palczewski, K. (2002): Crystal Structure of Rhodopsin: A G-Protein-Coupled Receptor, *ChemBioChem* **3** [10], 963-967.

Stenkamp, R. E.; Teller, D. C. and Palczewski, K. (2005): Rhodopsin: a structural primer for g-protein coupled receptors, *Arch. Pharm. (Weinheim)* **338** [5-6], 209-16.

Stojanovic, A.; Stitham, J. and Hwa, J. (2004): Critical role of transmembrane segment zinc binding in the structure and function of rhodopsin, *J. Biol. Chem.* **279** [34], 35932-41.

Stryer, L. (1996): Biochemie, 4th. edition, Spektrum, Heidelberg/Berlin/Oxford.

Sugiura, T.; Kondo, S.; Sukagawa, A.; Nakane, S.; Shinoda, A.; Itoh, K.; Yamashita, A. and Waku, K. (1995): 2-Arachidonoylglycerol: a possible endogenous cannabinoid receptor ligand in brain, *Biochem. Biophys. Res. Commun.* **215** [1], 89-97.

Szundi, I.; Ruprecht, J. J.; Epps, J.; Villa, C.; Swartz, T. E.; Lewis, J. W.; Schertler, G. F. and Kliger, D. S. (2006): Rhodopsin photointermediates in two-dimensional crystals at physiological temperatures, *Biochemistry* **45** [15], 4974-82.

Teller, D. C.; Okada, T.; Behnke, C. A.; Palczewski, K. and Stenkamp, R. E. (2001): Advances in determination of a high-resolution three-dimensional structure of rhodopsin, a model of g-protein-coupled receptors (gpcrs)(,), *Biochemistry* **40** [26], 7761-7772.

Uhl, R.; Desel, H. and Wagner, R. (1985): Separation and characterisation of light scattering transients from rod outer segments of vertebrate photoreceptors: design and performance of a Multi Angle Flash Photolysis Apparatus (MAFPA), *J. Biochem. Biophys. Methods* **11** [1], 31-43.

Uhl, R.; Hofmann, K. P. and Kreutz, W. (1977): Measurement of fast light-induced disc shrinkage within bovine rod outer segments by means of a light-scattering transient, *Biochim. Biophy.s Acta* **469** [2], 113-122.

Uhl, R.; Kuras, P. V.; Anderson, K. and Abrahamson, E. W. (1980): A light scattering study on the ion permeabilities of dark-adapted bovine rod outer segment disk membranes, *Biochim. Biophy.s Acta* **601** [3], 462-477.

Urizar, E.; Claeysen, S.; Deupi, X.; Govaerts, C.; Costagliola, S.; Vassart, G. and Pardo, L. (2005): An Activation Switch in the Rhodopsin Family of G Protein-coupled Receptors: The Thyrotropin Receptor, *J. Biol. Chem.* **280** [17], 17135-17141.

Vogel, R.; Fan, G. B.; Sheves, M. and Siebert, F. (2000): The molecular origin of the inhibition of transducin activation in rhodopsin lacking the 9-methyl group of the retinal chromophore: a UV- Vis and FTIR spectroscopic study, *Biochemistry* **39** [30], 8895-8908.

Vogel, R.; Ludeke, S.; Radu, I.; Siebert, F. and Sheves, M. (2004a): Photoreactions of Metarhodopsin III, *Biochemistry* **43** [31], 10255-10264.

Vogel, R.; Martell, S.; Mahalingam, M.; Engelhard, M. and Siebert, F. (2007): Interaction of a G protein-coupled receptor with a G protein-derived peptide induces structural changes in both peptide and receptor: a Fourier-transform infrared study using isotopically labeled peptides, *J. Mol. Biol.* **366** [5], 1580-8.

Vogel, R.; Ruprecht, J.; Villa, C.; Mielke, T.; Schertler, G. F. and Siebert, F. (2004b): Rhodopsin photoproducts in 2D crystals, *J. Mol. Biol.* **338** [3], 597-609.

Vogel, R.; Siebert, F.; Ludeke, S.; Hirshfeld, A. and Sheves, M. (2005): Agonists and partial agonists of rhodopsin: retinals with ring modifications, *Biochemistry* **44** [38], 12914.

Vogel, R.; Siebert, F.; Mathias, G.; Tavan, P.; Fan, G. and Sheves, M. (2003): Deactivation of rhodopsin in the transition from the signaling state meta II to meta III involves a thermal isomerization of the retinal chromophore C[double bond]D, *Biochemistry* **42** [33], 9863-74.

Wang, Y.; Botelho, A. V.; Martinez, G. V. and Brown, M. F. (2002): Electrostatic properties of membrane lipids coupled to metarhodopsin II formation in visual transduction, *J. Am. Chem. So.c* **124** [26], 7690-7701.

Warshel, A., Barboy, N. (1982): Energy storage and reaction pathways in the first step of the vision process, *J. Am. Chem. Soc.* **104**, 1469-1476.

Weiss, E. R.; Osawa, S.; Shi, W. and Dickerson, C. D. (1994): Effects of carboxyl-terminal truncation on the stability and G protein-coupling activity of bovine rhodopsin, *Biochemistry* **33** [24], 7587-7593.

Weitz, C. J. and Nathans, J. (1992): Histidine residues regulate the transition of photoexcited rhodopsin to its active conformation, metarhodopsin II, *Neuron* **8** [3], 465-472.

Wiedmann, T. S.; Pates, R. D.; Beach, J. M.; Salmon, A. and Brown, M. F. (1988): Lipid-protein interactions mediate the photochemical function of rhodopsin, *Biochemistry* **27** [17], 6469-74.

Yeagle, P. L. and Albert, A. D. (2003): A conformational trigger for activation of a g protein by a g protein-coupled receptor, *Biochemistry* **42** [6], 1365-8.

Yeagle, P. L.; Bennett, M.; Lemaitre, V. and Watts, A. (2007): Transmembrane helices of membrane proteins may flex to satisfy hydrophobic mismatch, *Biochim. Biophys. Acta* **1768** [3], 530-7.

Zimmermann, K.; Ritter, E.; Bartl, F. J.; Hofmann, K. P. and Heck, M. (2004): Interaction with transducin depletes metarhodopsin III: A regulated retinal storage in visual signal transduction?, *J. Biol. Chem* **279**, 48112-9.

Curriculum vitae

Name:	Bernhard Knierim
Date of birth:	1.12.1978
Place of birth:	Bad Hersfeld, Germany
Marital status:	unmarried
Nationality:	German

School

1985 – 1989	Grundschule (Ernst-von-Harnack-Schule, Bad Hersfeld)
1989 – 1995	Förderstufe and Gymnasium (Gesamtschule Obersberg, Bad Hersfeld)
1995 – 1998	Gymnasiale Oberstufe (Modellschule Obersberg, Bad Hersfeld)
June 1998	Graduation (Abitur)
1998 – 1999	Alternative service with the WWF on Hallig Langeneß

University

1999 – 2001	Basic study period in biophysics at Humboldt-University, Berlin. Sponsorship by the German National Academic Foundation since 2000.
2001 – 2003	Main study period in biophysics at Humboldt-University, Berlin. Main subject: experimental biophysics; subsidiary subjects: theoretical biophysics and biochemistry.
April 2004	Diploma thesis („Activation Studies on Rhodopsin using EPR Spectroscopy“) at the Institute for Medical Physics and Biophysics (Charité Berlin) and the Jules Stein Eye Institute (University of California, Los Angeles); sponsored by the German National Academic Foundation. degree: Diploma
March 2008	PhD („Studies on the Late Rhodopsin Activation Steps“) supervised by Klaus P. Hofmann and Oliver Ernst at the Institute for Medical Physics and Biophysics (Charité Berlin) in collaboration with Wayne L. Hubbell at Jules Stein Eye Institute (University of California, Los Angeles); sponsorship by the Boehringer Ingelheim Foundation for Basic Research in Medicine and the German National Academic Foundation.

Hiermit erkläre ich gemäß §6 Abs. (3) der Promotionsordnung, dass ich diese Dissertation selbständig und nur unter Verwendung der angegebenen Hilfsmittel angefertigt habe. Alle Stellen, die dem Wortlaut oder dem Sinn nach anderen Werken entnommen sind, sind nach bestem Wissen und Gewissen durch Angabe der Quellen als Entlehnung kenntlich gemacht worden.
Ich habe mich weder anderwärts um einen Doktorgrad beworben noch besitze ich bisher einen Doktorgrad.
Die dem Promotionsverfahren zugrunde liegende Promotionsordnung vom 1.10.2002 ist mir bekannt.

Bernhard Knierim
Berlin, den 8. Oktober 2007